THE UNIVERSITY
of EDINBURGH

Role of budding morphology in pathogenesis and transmission of avian influenza A virus

Carina Liliete Brito Tomé da Conceição

Submitted for the degree of Doctor of Philosophy

The University of Edinburgh

2019

Acknowledgments

I would like to start by thanking Professor Paul Digard for the opportunity to do my PhD studies in his lab – I truly appreciated it. His guidance, support, motivation and endless knowledge of flu (and honestly pretty much everything science related) helped to see this project through and for that I am immensely grateful. I would also like to thank my secondary supervisor, Professor Lonneke Vervelde for her support, knowledge and bluntness, because sometimes I just needed someone to lay down the facts for me and for that I am truly grateful. I was also fortunate to have worked with Dr Sam Lycett, whose input was valuable to the completion of this project. Lastly, I would like to thank the Principal Career Development Scheme for funding my PhD studies.

Thank you to my placement year supervisor Dr Catarina Roma-Rodrigues for showing me, simply put, how to behave in a lab. I would also like to thank my Master's supervisor Dr Naomi Rankin for patiently putting an end to my doubts about doing a PhD.

I am also grateful to the Digard lab members that showed me the techniques I needed to get me started, particularly Drs Nikki Smith, Lita Murphy, Liliane Chung and Saira Hussain – thank you for your patience! Thank you to Dr Elly Gaunt for agreeing to help me with some experiments on the last week of my PhD - really made life easier! To Dr Samantha Ellis thank you for patiently showing me how to do cryo-sections of frozen trachea rings. One last thanks to Dr Helen Wise for always being at the distance of an email with valuable feedback.

I was very lucky to have worked alongside some incredible people. To the Digardians of the Galaxy – Anabel Clements, Mariya Goncheva, Becca Dewar, Matt Turntables, Seema Jasim and Rute Pinto – you made life so much easier! The Friday bars, the hot chocolate when things were not working, the pub trips, the Portuguese Easter tradition at Rute's and so much more. I am truly grateful as you all made this experience the best I could ever have asked for!

I could not go without saying a big thank you to my University friends from Portugal – Dr Anna Tolmatcheva, Silves Marise, Sofia Maria and Ricardo Ribeiro. Those 4 years in Lisbon in your company helped me grow as a person as it was the first time I was away from home. Anna, Silves and Sofia, thank you for the Kebab nights, the faculty parties, the funny TV show nights or just nights in with deep conversations. Those were some amazing moments that I will always be grateful for!

Lastly, I am extremely grateful to my family – brother Amílcar, sister-in-law São, nephew Rafael and niece Liliana. You stopped me from chickening out and encouraged me to pursue my dreams, wherever they would take me. I am also lucky to have an amazing grandma Maria Augusta that was a rock all the way through. I also had the pleasure to add Niall to my little family and he has been an endless source of support, love and cups of tea!

To my parents, even though you are no longer here to see what I have achieved, I hope that you would be proud.

Declaration

I declare that this thesis was composed by myself, that the work contained herein is my own except where explicitly stated otherwise in the text, and that this work has not been submitted for any other degree or professional qualification.

Carina Liliete Brito Tomé da Conceição

Contents

Acknowledgements ii

Declaration iii

Lay summary x

Abstract xii

List of figures and tables xv

Abbreviations xx

Chapter 1: Introduction to influenza A virus 1

1.1. Influenza A virus 1

1.1.1. Virus structure and composition 1

1.1.2. Genome organisation 5

1.2. Influenza epidemiology and clinical manifestations 8

1.3. Strategies to control influenza infection 10

1.4. Influenza A virus life cycle 12

1.4.1. Attachment and entry into the host cell 12

1.4.2. Import of vRNPs to the nucleus 14

1.4.3. Transcription and replication of the viral genome 15

1.4.4. Nuclear export of the vRNPs 17

1.4.5. Assembly and budding 18

1.5. Host range 22

1.5.1. Avian influenza 22

1.5.2. Host adaptation 24

1.5.3. Influenza epidemics and pandemics 27

1.6. Virion morphology of IAV 30

1.6.1. Viral determinants of virion morphology 31

1.6.1.1. M1 and M2 31
1.6.1.2. Other viral proteins 34
1.6.2. Cellular determinants of morphology 35
1.7. Functions associated with virion morphology of IAV 36
1.7.1. Escaping host barriers 36
1.7.2. Viral transmission 39
1.8. Aims of the study 40

Chapter 2: Characterisation of avian budding morphology *in vitro* 42
2.1. Introduction and aims 42
2.2. Results 43
2.2.1. Validation of plant lectin staining as a substitute for antibody stain in fully avian viruses 43
2.2.2. Segment 7 is the major determinant of budding morphology 50
2.2.3. Determination of the budding phenotype of IAVs through characterisation of PR8-based 7:1 reassortant viruses with segment 7s from avian strains 56
2.3. Discussion 72

Chapter 3: Identification of sequence polymorphisms in avian IAV M1 polypeptides correlating with different budding morphologies 78
3.1. Introduction and aims 78
3.2. Results 79
3.2.1. Identification of sequence polymorphisms in avian M1s 79
3.2.2. Correlating sequence polymorphisms in M1 with budding morphology of Dk/India and Dk/Tripura avian strains 80
3.2.3. Importance of position 169 in M1 of Ck/Pennsylvania strains 88

3.2.4. Assessing the importance of M1 position 234 in Ck/Italy and Dk/Netherlands strains 93
3.2.5. Statistical studies of the association of M1 sequence polymorphisms with budding morphology, genetic background and/or host species 98
3.2.6. Testing the importance of position 234 in another chicken virus 104
3.3. Discussion 112

Chapter 4: Functional characterisation of spherical and filamentous budding phenotypes *in vitro* and *in ovo* 122
4.1. Introduction and aims 122
4.2. Results....122
4.2.1. *In vitro* and *in ovo* characterisation of Dk/India and Dk/Tripura WT and M1-mutant viruses 122
4.2.2. *In vitro* and *in ovo* characterisation of Ck/Italy and Dk/Netherlands WT and M1-mutant viruses 132
4.2.3. Investigating the spherical and filamentous budding phenotypes of Ck/Pakistan strain *in vitro* and *in ovo* 140
4.3. Discussion 148

Chapter 5: *In vivo* studies with spherical and filamentous forms of an avian strain of IAV 152
5.1. Introduction and aims 152
5.2. Results....153
5.2.1. Shedding profiles of chickens infected with spherical or filamentous Ck/Pakistan viruses 153
5.2.2. Environmental sampling....160

5.2.3. Spherical and filamentous virus spread within the host and histopathology of respiratory tissues....160
5.3. Discussion....165

Chapter 6: Concluding remarks and future directions....171
6.1. Concluding remarks....171
6.2. Future directions....172
6.2.1. *In vitro* analysis....172
6.2.2. *In ovo* and *in vivo* studies....173

Chapter 7: Materials and methods....175
7.1. Materials....175
7.1.1. Antibodies and dyes....175
7.1.2. Oligonucleotides....176
7.1.3. Plasmids....179
7.1.4. Viruses and reverse genetics system....180
7.1.4.1. A/Puerto Rico/8/1934 (H1N1)....180
7.1.4.2. A/Udorn/1972 (H3N2)....182
7.1.4.3. A/mallard/Netherlands/10-Cam/1999 (H1N1)....182
7.1.4.4. A/chicken/Pakistan/UDL-01/2008 (H9N2)....183
7.1.5. Eukaryotic cells....183
7.1.6. Bacterial culture....184
7.2. Methods....184
7.2.1. Cell culture....184
7.2.1.1. Isolation of CEF cells....185
7.2.1.2. Culture of other primary cell types....186
7.2.2. Molecular techniques....186

7.2.2.1. Preparation of competent DH5α bacterial cells.....186
7.2.2.2. Preaparation of agar plates.....187
7.2.2.3. Transformation of competent DH5α bacterial cells.....187
7.2.2.4. Preparation of plasmid DNA.....187
7.2.2.5. Isolation of total RNA from allantoic fluid, cells, tissues and swabs.....188
7.2.2.6. Reverse transcription (RT).....189
7.2.2.7. Polymerase chain reaction (PCR).....189
7.2.2.8. Quantitative reverse transcription PCR (RT-qPCR).....189
7.2.2.9. Agarose gel electrophoresis.....190
7.2.2.10. Isolation of DNA fragments from agarose gels.....190
7.2.2.11. Purification of DNA segments.....191
7.2.2.12. Restriciton enzyme digestion.....191
7.2.2.13. Ligation of DNA fragments.....191
7.2.2.14. Sanger sequencing.....192
7.2.2.15. SDS-PAGE and Western Blotting.....192
7.2.3. Virus work.....193
7.2.3.1. Generation of P0 stocks.....193
7.2.3.2. Generation of P1 stocks.....194
7.2.3.3. Minigenome reconstitution assays.....195
7.2.3.4. Protein electrophoresis and western blotting analyses for the detection of M1 from Ck/Penn/1.....195
7.2.3.5. Generation of mutant viruses by site-directed mutagenesis of RG plasmids.....196
7.2.3.6. Growth of virus in embryonated chicken eggs.....198
7.2.3.7. Haemagglutination assays (HA spot).....198
7.2.3.8. Haemagglutination inhibition (HAI) assays.....198

7.2.3.9. Quantification of viral load by plaque assay....199
7.2.3.10. Embryonic lethality assays....200
7.2.3.11. Viral infections....200
7.2.3.12. Multicycle infections....200
7.2.3.13. Single cycle infections....201
7.2.4. Fluorescent imaging....201
7.2.4.1. Antibody staining....201
7.2.4.2. Lectin staining....203
7.2.4.3. Imaging....203
7.2.5. Study of *in ovo* pathology....204
7.2.6. *In vivo* experiments....204
7.2.6.1. Ethics statement....204
7.2.6.2. Biosecurity....205
7.2.6.3. *In vivo* viral infections....205
7.2.6.4. Tissue collection....205
7.2.6.5. Infectious virus isolation from infected tissues....206
7.2.6.6. Environmental sampling....206
7.2.7. Bioinformatics analysis....206
7.2.7.1. Structural modelling....207
7.2.7.2. Filamentous phenotype quantification....207
7.2.8. Statistical analysis....208

References 210

Lay summary

Influenza A virus (IAV) circulates in wild aquatic birds naturally, however, in some occasions, it can be spread to other hosts, such as chickens, ducks, horses, pigs, or humans. The infectious particle of IAV can display a range of shapes under the microscope, from small spherical particles to semi-long (designated bacilliform) or very long filamentous particles that are similar in appearance to a string of rope. In hosts such as humans or horses, it is common to find bacilliform or filamentous particles, which are lost when the virus is propagated repeatedly under laboratory conditions. Therefore, this suggests that the longer particles are necessary to ensure viral survival in those hosts. Furthermore, inside influenza particles lies the virus genetic material divided into 8 segments, which has previously been shown to contain a "signature" in segment 7 (M) that determines the shape of the infectious particle. Although these shapes of virus have been the focus of many studies since the late 1940s, to date there is still debate about their biological significance. Nonetheless, some studies have implied that filamentous particles play a role in host-to-host transmission. However, this is mainly known for mammalian hosts like humans or horses, yet IAV also infects birds, such as chickens, ducks or turkeys. Thus, knowing that IAV can spread from birds to animals and that the virus shape plays a role in host-to-host transmission, it is important to further explore the virus shape of avian-originated IAV. Therefore, the main aim of this study was to investigate the shape of IAV particles that come from avian hosts, determine if their segment 7 also possess the "signature" found in human and equine strains of IAV and, lastly, if avian-origin IAV are also filamentous, then investigate the biological significance of this shape in a natural influenza infection.

In this study we found that infectious particles of avian IAV display spherical and filamentous shapes, similar to what is observed in human and equine IAV. Furthermore, segment 7 was revealed to be very important in determining the virus shape, however the previous "signature" was not found in avian IAV. In fact, in avian viruses we identified a novel "signature" that set the shape of avian viruses available in the laboratory. Additionally, we also built pairs of otherwise identical viruses with spherical or filamentous shapes, and examined their replication in eggs, which revealed that those that produced spheres grew better than ones that produced filamentous particles. This explains why filamentous particles are lost upon growth

of viruses under laboratory conditions, as mentioned before. Lastly, to address the biological significance of the different shapes, we used an avian virus in which we could control particle shape to infect chickens and mimic a natural influenza infection. The filamentous virus was shed by the infected birds for longer periods of time, which also correlated with longer persistence within the host and in the environment. Therefore, this supports the hypothesis that filamentous particles are involved in host-to-host transmission. Overall, this study showed that filamentous particles are also common in avian strains of IAV and may have an enhanced transmissibility.

Abstract

Pleomorphism is a characteristic of influenza A virus (IAV), which can produce spherical particles of ~100 nm in diameter and filaments up to 30 µm in length. Laboratory-adapted strains mainly produce spherical virions, whereas clinical isolates of human and equine strains of IAV are mostly filamentous, thus suggesting that this latter virion morphology may be involved in viral fitness *in vivo*. Furthermore, M1 is known to be the main morphology determinant of mammalian strains of IAV, and a "filamentous signature" within its amino acid sequence has been shown to switch virus budding between spherical and filamentous phenotypes. Even though filamentous virions have been consistently detected in clinical isolates of human and equine IAV, their biological significance still remains unclear, although recent studies have implied a role in transmission.

In contrast, budding morphology of avian strains of IAV remains less well characterised with several unanswered questions, such as: (i) what is the predominant budding phenotype of avian IAV; (ii) is segment 7 also a major morphology determinant and, if so, is the mammalian "filamentous signature" present; and (iii) if avian IAVs do produce filamentous virions, what is their biological significance in this host? Therefore, the aim of this study was to answer these questions, starting with characterising the budding phenotype of 8 avian isolates by immunofluorescence assays (IF), which showed that avian isolates of IAV are as pleomorphic as mammalian isolates. Furthermore, using reverse genetics we identified avian segment 7 as the main determinant of budding morphology. Thus, in order to test a higher number of avian strains, complete nucleotide sequences of avian segment 7s available online were collected and organised into a phylogenetic tree, which was divided into clades (1 to 11) and fitted with segment 7s from avian strains available in the laboratory. For the clades with no representation, segment 7s were randomly selected, synthesised and cloned in a reverse genetics plasmid vector (pDUAL). Using this method, a total of 17 avian segment 7s were characterised as 7:1 reassortant viruses in the background of the laboratory strain A/PR/8/34 (PR8). Similar to mammalian segment 7s, avian segment 7s showed a pleomorphic budding phenotype in the PR8 backbone and some were able to produce filaments up to 10 µm in length. However, when sequence alignment was performed with the avian M1 amino acid sequences, grouped

according to budding phenotype, this showed that avian strains do not contain the same mammalian virus "filamentous signature". and, in fact, do not show a consistent pattern of amino acid alterations that would explain the different morphologies. However, by performing site-directed mutagenesis on closely related avian strains with opposite budding phenotypes, we identified M1 positions 59, 169 and 234 as morphology determinants. Furthermore, it was observed that chicken viruses were mainly spherical while duck viruses were predominantly filamentous. Bioinformatics coupled with statistical analysis led to the hypothesised identification of position 234 of M1 as a novel avian host species-dependent morphology determinant of IAV budding, as we observed that spherical chicken viruses mainly possessed isoleucine at this position while filamentous duck viruses had leucine. To test this, a spherical chicken virus (A/chicken/Pakistan/UDL-01/2008 H9N2 [Ck/Pakistan]) with isoleucine at position 234 of M1 was mutated to encode a leucine at this position. This resulted in conversion of a spherical chicken virus to a filamentous virus. Next, all the M1-mutant viruses and their WT counterparts were characterised *in vitro* and *in ovo*, showing that *in vitro,* spherical or filamentous morphologies were equally advantageous, whereas *in ovo* the spherical viruses showed a fitness advantage in some of the viruses characterised. Additionally, the ability to alternate the budding phenotype of Ck/Pakistan by a single amino acid change at position 234 of M1 provided the opportunity to determine the biological significance of filaments *in vivo*. Contact-infected birds with the filamentous mutant virus showed prolonged but similar higher-titre buccal shedding than the equivalent spherical virus. This observation correlated with the longer-lasting persistence of the filamentous virus in the environment and *in vivo*. Additionally, within the chicken host, spherical and filamentous morphologies replicated to comparable titre in the nasal tissues, but the filamentous virus showed a replication advantage in the tracheal tissues.

Overall, this study showed that avian IAVs are as pleomorphic as human and equine IAVs. It also showed that avian IAVs budding morphology is determined by segment 7 but that these do not follow the genetic determinants identified in mammalian strains as defining budding morphology. Instead, this study identified a novel position within M1 that was able to determine budding phenotype in an avian host species-dependent manner. Lastly, the *in vivo* data corroborated the hypothesis that filaments are associated with viral transmission, perhaps due

to their ability to readily cross the mucous barrier of the trachea when compared with the spherical-equivalent virus.

List of figures and tables

Chapter 1: Introduction to influenza A virus

Figure 1.1 Structure of the influenza virus.

Figure 1.2 The viral ribonucleoprotein complex packaged inside the virion.

Table 1.1 IAV gene products based on A/PR/8/34 (H1N1) strain.

Figure 1.3 Schematic representation of the virus life cycle.

Figure 1.4 Schematic representation of the proposed mechanism for assembly and budding of IAV.

Figure 1.5 IAV host range.

Figure 1.6 Schematic representation of domains within IAV M1 and M2 proteins.

Figure 1.7 Respiratory mucosal membrane.

Chapter 2: Characterisation of avian IAV budding morphology *in vitro*

Figure 2.1 Validation of plant lectin staining as an alternative to antibody staining.

Figure 2.2 Detection of infectivity of avian strains in MDCK cells.

Figure 2.3 Determination of the budding phenotype of avian IAV strains by IF.

Figure 2.4 Replication phenotypes of reassortant viruses between Dk/Netherlands and PR8.

Figure 2.5 Budding phenotypes of reassortant viruses between Dk/Netherlands and PR8.

Figure 2.6 Quantification of the budding phenotypes of reassortant viruses between Dk/Netherlands and PR8.

Figure 2.7 Phylogeny of viral matrix protein M1 from avian strains.

Table 2.1 IAV strains used in this study.

Figure 2.8 Replication phenotypes of PR8 7:1 reassortants with the selected avian M segments.

Figure 2.9 Budding phenotype of PR8 7:1 reassortant viruses in MDCK cells.

Figure 2.10 Quantification of the budding phenotypes of PR8 7:1 reassortant viruses.

Figure 2.11 Plaque phenotype of PR8 7:1 reassortant viruses and correlation with budding morphology.

Figure 2.12 Budding phenotype of PR8 7:1 reassortant viruses in chicken embryo fibroblast (CEF) and duck embryo fibroblast (DEF) cells.
Figure 2.13 Sequence alignment of the avian M1 proteins from viruses and/or segment 7s tested for budding morphology in this study.

Chapter 3: Identification of sequence polymorphisms in avian IAV M1 polypeptides correlating with different budding morphologies

Figure 3.1 M1 sequence alignments of closely related avian strains with opposite budding morphologies.
Figure 3.2 Replication fitness of WT and M1-mutant Dk/India and Dk/Tripura 7:1 reassortant viruses.
Figure 3.3 Budding phenotype of Dk/India and Dk/Tripura strains with WT or mutated M1 proteins.
Figure 3.4 Quantification of the budding phenotype of the PR8-based Dk/India and Dk/Tripura WT and M1-mutant viruses.
Figure 3.5 Plaque size of Dk/India and Dk/Tripura WT and M1-mutant 7:1 reassortant viruses and correlation with the % of filament-producing cells.
Figure 3.6 Replication fitness of Ck/Penn/1 and Ck/Penn/1370 strains with WT or mutated M1 at position 169.
Figure 3.7 Budding phenotype of 7:1 Ck/Pennsylvania reassortant strains with WT or mutated M1 at position 169.
Figure 3.8 Quantification of the budding phenotype of the Ck/Pennsylvania reassortant strains.
Figure 3.9 Replication fitness of Ck/Italy and Dk/Netherlands strains with WT and mutated M1 genes.
Figure 3.10 Budding phenotype of Ck/Italy and Dk/Netherlands strains with WT or M1 I234L mutations.
Figure 3.11 Quantification of the budding phenotype of Ck/Italy and Dk/Netherlands strains and correlation with plaque size.

Table 3.1 Summary of the budding morphology and segment 7 clade distribution of the virus strains used and corresponding clade distribution within the phylogenetic tree.

Table 3.2 Associations between M1 positions and budding morphology, genetic background and avian host.

Figure 3.12 Diversity of amino acids at M1 positions 59, 107, 144, 169 and 234 within IAV isolates from avian host species.

Figure 3.13 Fitness of PR8-based and fully avian viruses with WT and mutant Ck/Pakistan segment 7.

Figure 3.14 Budding phenotype of Ck/Pakistan WT and M1-I234L.

Figure 3.15 Quantification of the budding phenotype of viruses with the Ck/Pakistan M gene.

Figure 3.16 Predicted structures of Ck/Pakistan strain M1 with either isoleucine or leucine at position 234.

Figure 3.17 Predicted structures of Dk/India M1 with either isoleucine or methionine at position 59.

Figure 3.18 Predicted structure of Ck/Pakistan M1 with previously identified mammalian residues and the newly identified avian residues.

Chapter 4: Functional characterisation of spherical and filamentous budding phenotypes *in vitro* and *in ovo*

Figure 4.1 Growth characteristics of Dk/India and Dk/Tripura WT and M1-mutant viruses *in vitro* and *in ovo*.

Figure 4.2 Gross pathology of chicken embryos infected with Dk/India or Dk/Tripura WT and M1-mutant viruses at 48 h p.i..

Figure 4.3 Histopathology of chicken embryos infected with Dk/India or Dk/Tripura WT and M1-mutant viruses.

Figure 4.4 Characterisation of chicken embryo pathology following infection with Dk/India or Dk/Tripura WT and M1-mutant viruses.

Figure 4.5 Replication of Ck/Italy and Dk/Netherlands strains with WT or mutated M1 genes *in vitro* and *in ovo*.

Figure 4.6. Gross pathology of chicken embryos infected with Ck/Italy or Dk/Netherlands viruses.

Figure 4.7 Histopathology of chicken embryos infected with Ck/Italy or Dk/Netherlands viruses.

Figure 4.8 Embryo pathology and size following infection with Ck/Italy or Dk/Netherlands WT and M1-mutant viruses.

Figure 4.9 Viral fitness of Ck/Pakistan with WT or mutated M1 *in vitro* and *in ovo*.

Figure 4.10 Chicken embryo pathology following infection with Ck/Pakistan WT or M1-mutant viruses.

Figure 4.11 Embryo pathology following infection with Ck/Pakistan viruses.

Figure 4.12 Embryo viability upon infection with Ck/Pakistan viruses.

Chapter 5: *In vivo* studies with spherical and filamentous forms of an avian strain of IAV

Figure 5.1 Schematic representation of the *in vivo* study with spherical and filamentous forms of Ck/Pakistan avian strain.

Figure 5.2 Shedding profiles of Ck/Pakistan WT and M1-mutant viruses.

Table 5.1 Symptoms and survival rate of birds infected with the spherical WT or the filamentous mutant of Ck/Pakistan.

Figure 5.3 Environmental sampling of isolator units containing the infected chickens.

Figure 5.4 Detection of infectious virus and viral genome in tissues of chickens infected with WT or M1-mutant Ck/Pakistan viruses.

Figure 5.5 Representative histopathology of tracheal and lung tissues infected with the spherical WT or filamentous mutant of Ck/Pakistan.

Chapter 7: Materials and Methods

Table 7.1 Primary antibodies and antisera raised against IAV and cellular proteins.

Table 7.2 Plant lectins.

Table 7.3 Secondary antibodies.

Table 7.4 Fluorescent dyes.

Table 7.5 Sequencing primers.

Table 7.6 Site-directed mutagenesis primers.

Table 7.7 Primer and probe for RT-qPCR.

Table 7.8 Primers for cloning avian segment 7s into pDUAL.

Table 7.9 Plasmids used throughout the study.

Table 7.10 Reverse genetics system for PR8.

Table 7.11 Avian strains from which segment 7s were used in this study.

Table 7.12 Avian isolates used in this study.

Table 7.13 Reverse genetics system for Udorn.

Table 7.14 Reverse genetics system for Dk/Netherlands.

Table 7.15 Reverse genetics system for Ck/Pakistan.

Table 7.16 Eukaryotic cell lines.

Table 7.17 Bacterial culture media.

Figure 7.1 Minigenome reconstitution assay with Ck/Penn/1 and Ck/Penn/1370 M segment and PR8 RNP.

Figure 7.2 IF assays at different time points.

Figure 7.3 Example length measurements for filamentous bundles.

Abbreviations

cDNA	complementary DNA
CPE	cytopathic effect
cRNA	complementary RNA
DAPI	4',6-diamidino-2-phenylindole
DMSO	Dimethyl sulphoxide
dNTP	deoxyribonucleotide triphosphate
FDA	US Food and Drug administration
IAV	Influenza A virus
MOI	Multiplicity of infection
mRNA	messenger RNA
NEP/NS2	Nuclear export protein/Non-structural protein 2
PA	Polymerase acidic protein
PB1	Polymerase basic protein 1
PB2	Polymerase basic protein 2
PBS	Phosphate-buffered saline
PFU	Plaque forming unit
PHE	Public health England
p.i.	post infection
RIG-I	Retinoic Acid-Inducible Gene I
rSAP	Recombinant shrimp alkaline phosphatase
RNP	Ribonucleoprotein complex
SDS-PAGE	Sodium dodecyl sulphate polyacrylamide gel electrophoresis
vRNA	viral RNA
WHO	World health organisation
WT	Wild Type

Chapter 1: Introduction to influenza A virus

1.1. Influenza A virus

Influenza A virus (IAV) is an enveloped virus belonging to the *Orthomyxoviridae* family which also includes five other genera (influenza virus B, C and D, thogotovirus, quaranjavirus and isavirus) (ICTV, 2017). As typically seen within the *Orthomyxoviridae* family, IAV possesses a segmented single-stranded negative-sense RNA genome. The natural reservoir of IAV is wild aquatic birds (i.e. waterfowl, shorebirds); however, this zoonotic agent has a wide host range and can infect other avian species as well as mammalian hosts as described in more detail in section 1.5 (Webster, 1992).

1.1.1. Virus structure and composition

Pleomorphism is a characteristic of IAV particles, which translates into the production of three main forms of virions: spherical particles of ~ 100 nm in diameter; an intermediate form termed "bacilliform" with a smaller diameter and up to 300 nm in length; and filamentous particles that like bacilliforms, are between 80 and 100 nm in diameter but can be up to 30 µm in length (Calder et al., 2010; Cox et al., 1980; Mosley & Wickoff, 1946; Roberts & Compans, 1998; Vijayakrishnan et al., 2013) (Figure 1.1 A). The laboratory-adapted viruses that have been serially passaged in eggs or cells, e.g. A/Puerto Rico/8/1934 (PR8) or A/WSN/1933 (WSN), produce predominantly spherical particles although filamentous structures were also detected (Mosley, 1946). Conversely, filamentous viruses that produce both filaments and spheres with generally a large overrepresentation of the first, have been mainly detected in human and veterinary clinical isolates, with several reports showing that these elongated structures are usually lost following serial passage in eggs or cells (Chu et al., 1949; Elton et al., 2013; Seladi-Schulman et al., 2013). All forms of IAV are surrounded by a lipid bilayer originated from the host cell decorated with the viral glycoproteins haemagglutinin (HA) and neuraminidase (NA) (Palese & Shaw, 2007). HA is a homotrimeric protein that is produced as an HA0 precursor and cleaved by host proteases outside the cell into HA1 and HA2 subunits.

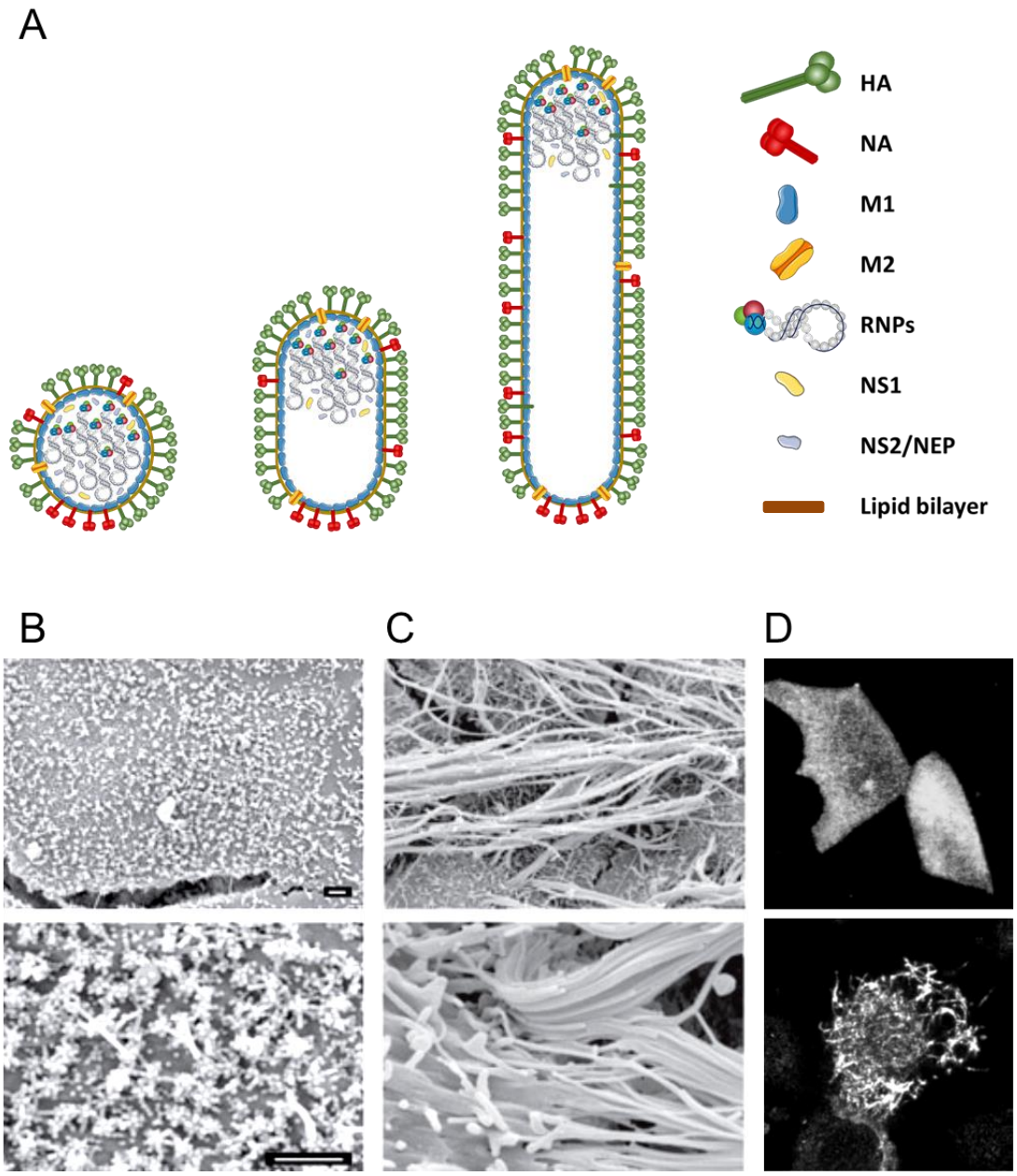

Figure 1.1 Structure of the influenza virus. (A) Schematic representations of spherical, bacilliform and filamentous influenza virions, respectively. Spherical virions are on average 100 nm in diameter, while filamentous virions extend many micrometres in length. The viral envelope (lipid-bilayer) originates from the host plasma membrane and its surface is decorated with the viral glycoproteins (HA and NA) and the M2 proton channel protein. The viral matrix protein M1 forms a protein layer underneath the virion that provides support and structure. The vRNA is encapsidated by viral proteins, forming the vRNPs, and packaged inside the virion by association with M1. NS2/NEP has also been found inside spherical virions. Cartoon drawn and kindly provided by Rute Pinto. (B) and (C) Scanning electron microscopy of MDCK cells infected with the spherical strain PR8 and the filamentous reassortant virus PR8 MUd. Scale bar 1 µm (Elton et al., 2013). (D) Immunofluorescent staining of surface HA of MDCK cells infected with the spherical strain WSN (top picture) or with the filamentous A/Udorn/1972 strain (bottom picture) (Elleman & Barclay, 2004).

This cleavage allows the exposure of the fusion peptide present in the HA2 subunit, which mediates the fusion of the viral and cellular membranes resulting in viral entry. On the other hand, NA is a tetrameric sialidase mainly involved in viral exit, facilitating clipping off the virus from the cell membrane (Palese & Ueda, 1974). IAV is further classified based on the antigenicity/sequence of the HA and NA glycoproteins. So far, there are 16 HA subtypes and 9 NA subtypes identified that have been isolated in waterfowl and other a variety of other species (Palese & Shaw, 2007). Additionally, more divergent and probably evolutionarily isolated H17N10 and H18N11 subtypes have been solely identified in bat isolates (Tong et al., 2012; Tong et al., 2013).

Anchored in the viral envelope is the proton ion channel protein M2, albeit to smaller amounts than the other structural proteins (Pinto et al., 1992). M2 is responsible for promoting the release of the vRNA into the host cell cytoplasm after membrane fusion but also plays a role in viral budding (Rossman & Lamb, 2011). Inside the IAV envelope, the viral matrix protein M1 forms a lattice underneath the lipid bilayer that supports the virion and it is known to be the main determinant of virion morphology (Gomez-Puertas et al., 2000; Sha & Luo, 1997). Within the virion, there are eight genome segments where, on average, for every 24 nucleotides of the single-stranded vRNA, one molecule of the nucleoprotein (NP) binds the phosphate backbone of the genome with high affinity and little apparent sequence specificity (Baudin et al.,1994; Ortega et al., 2000). Furthermore, several reports have shown that the NP-bound vRNA is arranged in a loose double helix structure while the RNA-dependent-RNA polymerase (RdRp) complex binds the 5' and 3' ends of the genome, holding the ends together in a panhandle structure as shown in figure 1.2 A (Baudin et al., 1994; Hsu et al., 1987). These RNA-protein complexes make up the viral ribonucleoprotein (vRNP) to which M1 binds via interactions with NP and the vRNA in a sequence-independent manner (Sha & Luo, 1997; Ye et al., 1989). Also found within the virion in much lower quantities are the viral NEP/NS2 and the non-structural protein 1 (NS1) (Hutchinson et al., 2014; Yasuda et al., 1993). Although what has just been described is the main structure and composition of IAV virions, subtle differences have been detected between spherical, bacilliform and filamentous particles.

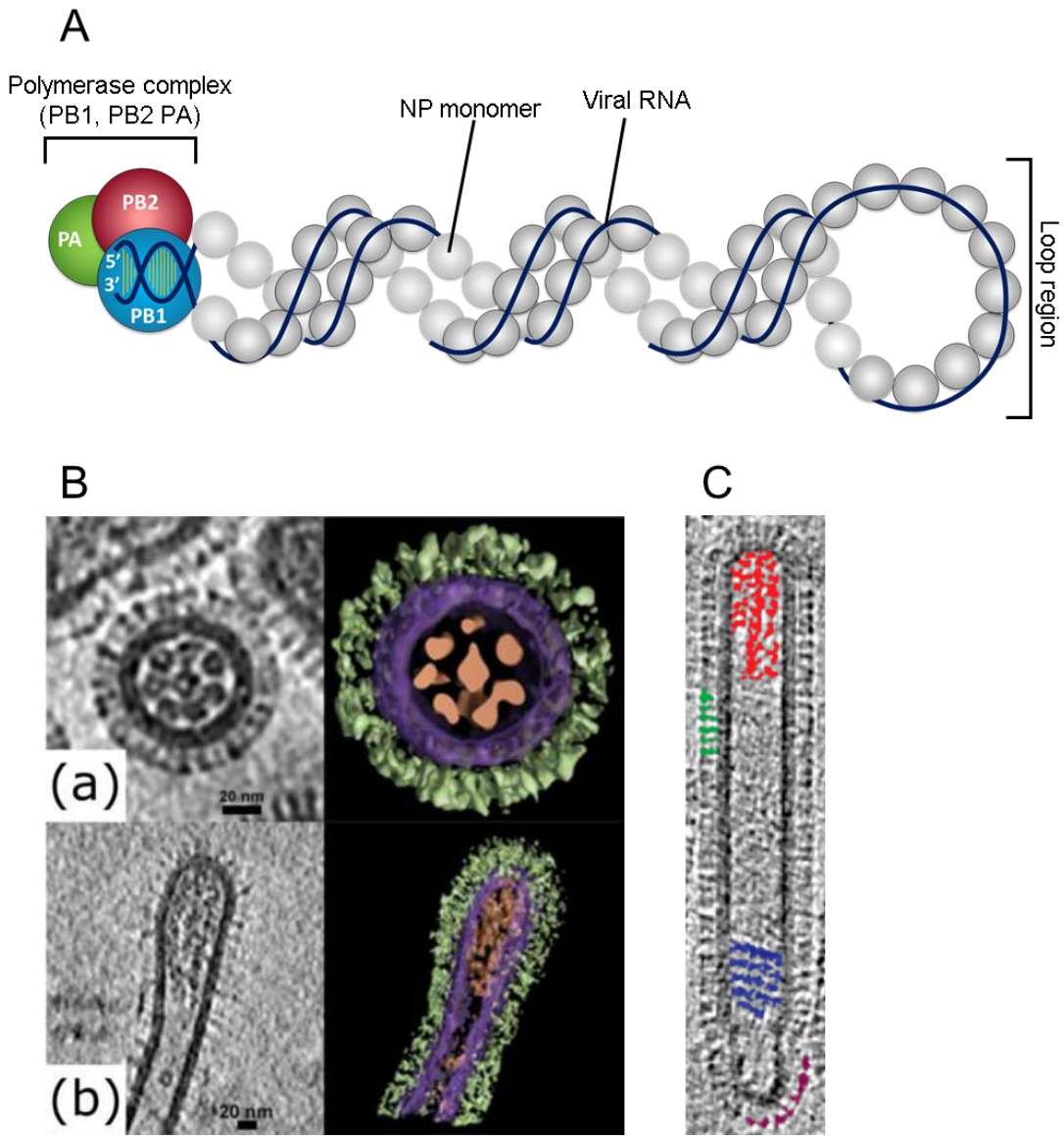

Figure 1.2 The viral ribonucleoprotein complex packaged inside the virion. (A) Schematic representation of a viral ribonucleoprotein (vRNP) complex. Each vRNP is composed of negative-sense single-stranded viral RNA coated by a NP monomer on average every 24 nucleotides. The 5' and 3' end of the vRNA show partial complementarity, which causes the vRNA to fold its ends. The viral polymerase complex (composed of PB1, PB2 and PA subunits) sits on this partially double-stranded structure. Cartoon drawn and kindly provided by Rute Pinto. (B) The eight vRNPs are packed into virus particles arranged in a "7+1" conformation; i.e., one vRNP is typically found at the centre surrounded by the other seven. This is more readily observed in spherical virions but is supposed to be the same in filamentous particles. Filamentous virions group the vRNPs at one end of the virion (taken from (Dadonaite et al., 2016)). (C) Tomogram section of a filamentous virion highlighting the vRNPs (red), the viral matrix layer formed by M1 (blue) and the viral glycoproteins HA (green) and NA (purple). Note the grouping of vRNPs at the opposite end to the NA clustering (taken from Calder et al., 2010).

For instance, all three forms pack the genome similarly, where one vRNP is at the centre and the other seven surrounding it in a parallel array; however the longer virus particles have all vRNPs in this 7+1 arrangement at the distal end of the particle (figure 1.2 B and C) (Calder et al., 2010; Vijayakrishnan et al., 2013). Additionally, cryo-electron microscopy showed that longer filaments often lack vRNPs and instead possess a fibrillar material of unknown origin (Vijayakrishnan et al., 2013). On the other hand, spherical particles have been shown to incorporate host proteins into their virions, such as annexins, tetraspanins, or cytoskeletal proteins (Berri et al., 2014; Hutchinson et al., 2014; Shaw et al., 2008). Their role during viral infection is still unclear; however, the host cellular components that make up spherical virions are dependent on host species the virus originated from (Hutchinson et al., 2014).

1.1.2. Genome organisation

The IAV genome is composed of eight RNA segments which encode for the main 12 viral proteins that are generally taken to be essential for viral replication outside of a laboratory setting. However, there are many more gene products encoded by the IAV genome which are summarised in table 1.1. The segment sizes vary between 0.89 Kb and 2.341 Kb, adding up to a total of 13.5 Kb (Palese & Shaw, 2007). All segments possess an antisense coding region flanked by short untranslated regions (UTRs), whose terminal regions are very conserved and show partial complementary.

To date, the IAV genome is known or is predicted to encode for up to 22 proteins, however, the relatively small size of the genome forces the virus to use several mechanisms in order to produce all these proteins. The main 12 viral proteins are generally products of unspliced mRNA transcripts, with the exception of two proteins (M2 and NEP) that arise from spliced mRNA transcripts (Palese & Shaw, 2007). In addition to splicing, IAV also employs ribosomal frameshifting and translation initiation from alternative start codons to maximize the use of its genome. For instance, segments 1, 2 and 3 primarily encode PB2, PB1 and PA viral proteins, respectively, which together form the RdRp complex (Blaas et al., 1982; Braam et al., 1983; Dias et al., 2009). These proteins are essential to viral replication; however, several

Table 1.1 IAV gene products based on A/PR/8/34 (H1N1) strain. *predicted proteins

Segment	Gene product(s)	Protein size (amino acid)	Reported function(s)
1	PB2	759	Subunit of the RdRp. Binds 5' cap on host cell mRNA
	PB2-S1	508	mRNA spliced product shown to inhibit RIG-I-signalling
2	PB1	757	Subunit of the trimeric RdRp. Catalyses nucleotide addition to produce viral RNA during transcription and replication
	PB1-F2	87	Product from an alternative start codon with IFN-antagonist and pro-apoptotic activity
	PB1-N40	718	Product from an alternative start codon with unknown function
3	PA	716	Subunit of the RdRp. Possesses endonuclease activity required for cap-snatching during viral mRNA transcription
	PA-X	152	Product of ribosomal frameshifting with host cell shut-off activity
	PA-N155	562	Product from an alternative start codon with unknown function
	PA-N182	535	Product from an alternative start codon with unknown function
4	HA	565	Viral glycoprotein involved in receptor binding, viral entry and budding
5	NP	498	Encapsidates vRNA, co-factor of RdRp activity and required for vRNP export from the nucleus
6	NA	454	Sialidase activity for viral exit and mucous clearance
7	M1	252	Structural protein that functions in vRNP nuclear export, virus budding, assembly and morphogenesis
	M2	97	Ion channel protein involved in uncoating of vRNPs and virus assembly and budding
	M3*	9	Spliced mRNA product of unknown function
	M42	99	Splice variant of M2 function
	M4*	54	Spliced mRNA product of unknown function
8	NS1	230	Primary function as an IFN-antagonist
	NS2/NEP	121	Spliced mRNA product involved in vRNP export from the nucleus
	NS3	187	Spliced mRNA product of unknown function
	tNS1	216	Products from alternative start codons with IRF inhibition activity
	NSP*	150/152	Protein expression not detected.

studies have reported the expression of other viral proteins from these segments that are not essential but play complementary roles in viral infection. These latter products are therefore termed accessory proteins. Segment 1 has been shown to encode a shorter form of PB2, designated PB2-S1, derived from spliced mRNA (Yamayoshi et al., 2016). This protein was mainly expressed in pre-2009 human H1N1 strains and was identified as an inhibitor of RIG-I-signalling. By contrast, segment 2 has several start codons, including several flanked by a strong Kozak signal, which make these prime sites for alternative translation initiation events (Wise et al., 2011). So far two polypeptides have been identified: one from the fifth AUG codon, (in frame 1, in frame with PB1) named PB1-N40 and another from the fourth AUG codon (in frame 2), designated PB1-F2 (Varga et al., 2012; Wise et al., 2009). Although the function of PB1-N40 is still uncertain, PB1-F2 has been shown to inhibit the interferon response in infected cells and induce apoptosis (Varga et al., 2012). Segment 3 not only encodes PA but due to ribosomal frameshifting it also produces the PA-X polypeptide, which has the endonuclease domain from PA and a C-terminus translated from the +1 reading frame of PA mRNA (Firth et al., 2012). PA-X was shown to have host cell shut-off activity by destroying the cellular mRNA transcripts (Jagger et al., 2012). Similarly to segment 2, segment 3 mRNA also has other internal start codons that were recently shown to produce two N-terminally truncated forms of PA: PA-N155 and PA-N182 (Muramoto et al., 2013). PA-N155 is expressed from the eleventh AUG codon, while PA-N182 is expressed from the thirteenth AUG codon, both in frame with PA. Although the function of these polypeptides is yet to be established, the authors suggested a role during the replication cycle of IAV, as mutants lacking these truncated forms of PA showed growth attenuation and lower pathogenicity *in vivo*. While segments 4 (HA), 5 (NP) and 6 (NA) only encode for one single protein each from an unspliced mRNA, the smaller segments of the IAV genome (segments 7 and 8) rely on splicing to produce essential and accessory proteins (Palese & Shaw, 2007). Segment 7 produces an unspliced mRNA 1 and three spliced transcripts named mRNA 2, 3 and 4 (Dubois et al., 2014). M1 is the product of mRNA 1, while M2 is translated from mRNA 2. The protein encoded by mRNA 3 has not yet been detected in the context of infection; however the product of this mRNA was shown to be preferred by the cellular splicing machinery, delaying the production of mRNA 2 (M2) until the viral RdRp complex is relatively abundant, as the binding of the viral polymerase complex blocks the splice donor site of mRNA 3 (Shih et al.,

1995). Similarly to M3, the M4 protein (from mRNA 4) has yet to be detected, however, it was reported by Shih et al. that mRNA 4 is produced as abundantly as mRNA 2 by the A/WSN/33 strain regardless of host species (Shih et al., 1998). More recently, the expression of the accessory protein M42, which can functionally replace M2, was also identified from mRNA4, but only in a small minority of IAV strains (Wise et al., 2012). Lastly, segment 8 encodes an unspliced mRNA that gives rise to NS1, which acts as an interferon antagonist, and a spliced mRNA that encodes for the other essential protein – NS2, now known as NEP – required for export of vRNPs from the nucleus (Hale et al., 2008; Lamb & Choppin & Tamm, 1979; O'Neill et al., 1998). Both NS2 and NEP are encoded from open reading frames (ORF) in the positive sense. However Zhirnov et al. reported the presence of an ORF in the negative sense genome that is predicted to encode for a transmembrane-like protein, which the authors called NSP (Zhirnov et al., 2007). The mechanism of expression and function of this protein has yet to defined, but peptides derived from it can be detected by the immune system of infected animals (Hickman et al., 2018). Another spliced mRNA transcript of segment 8 was identified following adaption of a human strain of IAV within a mouse host, which produced a polypeptide that the authors named NS3, with a currently unknown function (Selman et al., 2012). The latest and the last gene products identified from segment 8 are truncated products of NS1 expressed by alternative translation initiation from two downstream start codons, that give rise to N-terminally truncated forms of NS1 that have been shown to inhibit activation of the interferon regulatory factor 3 and interferon β in the PR8 strain of IAV (Kuo et al., 2016).

1.2. Influenza epidemiology and clinical manifestations

Influenza viruses are the causative agent of seasonal epidemics, which are estimated to cause severe illness in 3-5 million people and the death of 290,000 – 650,000 people every year (Iuliano et al., 2018). The term 'seasonal' derives from the fact that these epidemics mainly occur in the winter months, which can be explained from the findings of studies that have reported that virus transmission is greater at low temperatures and low humidity levels (Lowen et al., 2007; Schaffer et al., 1976). The mechanism by which zoonotic influenza viruses are transmitted to humans remains unclear; however there is evidence supporting airborne

transmission or direct contact with infected animals (Beigel et al., 2005; Brankston et al., 2007). The onset of influenza infection in humans is largely characterised by cough, headache, fever and malaise, which can last for several days. In children, elderly and immunocompromised individuals these symptoms can aggravate and cause severe illness (WHO, 2018b). Moreover, IAVs have also been responsible for sporadic pandemics over the last 100 years, which will be addressed later on in this chapter.

Currently, H1N1, H2N2 and H3N2 are the only subtypes reported to have achieved consistent circulation in humans and are thus the types responsible for seasonal epidemics (Petrova & Russell, 2018). Although influenza viruses have been circulating in the human population since at least the early 1900s, they are still a major health concern for two main reasons: their fast-evolving RNA genome, and the segmented nature of it. The error-prone viral RNA polymerase shows deficient proofreading activity, resulting in mutations throughout the viral genome; importantly, mutations in the viral antigens (HA and NA) usually result in a virus that is no longer recognised by the host humoral immune response that protects them from re-infection (Palese & Shaw, 2007). This is termed antigenic drift and is the main reason seasonal epidemics occur frequently and typically with mild symptoms. On the other hand, genome segmentation can result in antigenic shift. This occurs when two or more strains infect the same host cell, which promotes the exchange of genetic material or genome reassortment, thus resulting in a virus that is a mixture of the parental strains. This phenomenon is more alarming because the resulting virus possesses a new HA on its surface (but not always a new NA) that have not yet circulated in the human population, therefore has the potential to cause a pandemic (Webster et al., 1992). However, not all pandemics result from antigenic shift, in fact, the first recorded human pandemic is thought to have occurred due to adaptation of an avian strain of IAV to human hosts, which will be addressed in more detail in section 1.5.3 (Taubenberger et al., 2005).

1.3. Strategies to control influenza infection

Currently, vaccination is the primary preventive measure to control seasonal influenza, but due to their long period of manufacturing (minimum of 6 months), pandemic preparedness is primarily dependent on antivirals (Petrova & Russell, 2018). Currently, there are three types of vaccines licensed for use in the human population: live-attenuated virus, recombinant viral HA or inactivated virus (Krammer et al., 2018). These vaccines contain the antigens from at least three circulating influenza strains: two IAV subtypes (2009 pandemic H1N1 and H3N2) and one IBV subtype (Victoria or Yamagata lineages). In recent years however, the circulation of another influenza B virus has given rise to a quadrivalent vaccine (Krammer et al., 2018). The most used vaccine is the inactivated influenza vaccine, which induces a neutralising antibody response against HA epitopes, therefore eliciting a protective humoral immune response (Osterholm et al., 2012). However, the main epitopes targeted by neutralising antibodies are present in the receptor binding domain of HA, which differ quite drastically between HA subtypes, thus reducing vaccine efficacy to one specific subtype (Wiley & Skehel, 1987).

Although preventive vaccination has proved effective against seasonal influenza, the sudden emergence of a new HA subtype renders the vaccine useless; therefore antiviral drugs are used to provide a quick response to tackle influenza infection. There are two main classes of antivirals approved by the FDA and PHE for the treatment of influenza, which are neuraminidase inhibitors (NAIs) and M2 ion channel blockers. NAIs target the enzymatic activity of NA during viral exit, resulting in aggregation of progeny virions at the surface of the cell and, consequently, a reduction in the efficiency of viral spread (Colman, 1994; Palese & Ueda, 1974). Currently, there 3 main drugs approved within this class: oseltamivir (Tamiflu), zanamivir (Relenza) and peramivir (Rapivab) (Alame et al., 2016). The other class of antivirals, the adamantanes, target the ion channel activity of the M2 protein, which is responsible for acidifying the interior of the virion to promote dissociation of the genome from the viral envelope. Therefore these antivirals prevent the release of the RNA genome into the cytoplasm of the host cell, stopping the virus life cycle at the entry point (Cady et al., 2010; Pinto et al., 1992). However, this class of antivirals have been rendered largely ineffective towards influenza infection, with

almost half of available IAV protein sequences showing amino acid mutations in M2 known to confer resistance to adamantanes. Dong et al. showed that IAV subtypes currently circulating in human (H1 and H3) or poultry (H5, H7 and H9) populations were more prone to develop resistance (Dong et al., 2015). For instance, the seasonal H1N1 subtype before 2009 was reasonably resistant to adamantanes and even when the 2009 pandemic H1N1 replaced the seasonal H1N1, the latter proved to be resistant to M2 ion channel blockers as well. On the other hand, H3N2 subtypes showed varied frequency of resistant viruses over the last two decades (Dong et al., 2015). Resistant viruses were also observed within H5N1, H7 and H9N2 IAV subtypes, with an increase in frequency in more recent years. Therefore, the most widely used antivirals rely heavily on NAIs. However, resistant viruses have been already isolated, for example, the seasonal H1N1 viruses were completely resistant to NAIs by 2009 and the 2009 pandemic H1N1 viruses were able to develop resistance rapidly after NAI treatment, in contrast to H3N2 subtypes which remained relatively sensitive to NAIs (McKimm-Breschkin, 2013). Furthermore, there are also compounds being developed and in clinical trials to target host factors that are required during influenza infection (Yen, 2016). Overall, continued research is needed to develop novel antivirals to tackle future influenza outbreaks.

The current strategies to control avian influenza spread within domestic poultry are characterised by inclusion and exclusion biosecurity measures, although mass vaccination was recently reported as a success in China (Swayne, 2008). Inclusion biosecurity practices are a combination of measures employed to contain an infection within a certain area, which include quarantine, improved hygiene, disinfection of fomites and removal of infected animals within the flock. Conversely, exclusion biosecurity practices are used to protect naïve birds from infected birds with avian influenza, which include confinement of birds indoors during the bird migration season, therefore preventing the contact between domestic poultry and wild birds. Unlike in the case of human influenza, the use of vaccines in domestic poultry has stagnated over the years due to a combination of overuse without updating the vaccine composition, resulting in the emergence of variants that were able to evade the immune response elicited by the vaccine (Capua & Marangon, 2006). The currently used vaccines are oil-emulsified inactivated whole IAV or live vectored (using fowl pox as a vector) with low pathogenic avian IAV (LPAI) field

outbreak strains. These are predominantly used in countries with endemic highly pathogenic avian influenza (HPAI), such as Pakistan, China or Mexico and also in developing countries, but require subcutaneous or intramuscular administration with re-administration every 2-3 years to account for virus evolution, making them labour intensive and costly (Capua & Marangon, 2006; Swayne et al., 2014). Another measure to control avian influenza is the surveillance of wild birds and domestic poultry, as this gives information on the diversity, evolution and spread of avian influenza strains, thus providing information on the pandemic potential of avian IAVs (Verhagen et al., 2015).

1.4. Influenza A virus life cycle

IAV primarily targets epithelial cells of the respiratory or intestinal epithelia, as described later on. Influenza viruses have the particularity of replicating their nucleic acid in the nucleus and their life cycle can be divided into the following stages: attachment, entry and uncoating of the viral genome; import of the vRNPs to nucleus; replication and transcription; export of the vRNPs from the nucleus into the cytoplasm and, lastly, assembly at the plasma membrane and budding. In tissue culture, this life cycle takes between 8 and 10 hours to complete and a diagrammatic representation is shown in figure 1.3 (Gaush & Smith, 1968).

1.4.1. Attachment and entry into the host cell

The first step of IAV infection is the binding of HA to the host cell surface. The main cellular receptor for IAV is N-acetylneuraminic acid or sialic acid (SA), which is commonly found in N- or O-linked oligosaccharides of glycoproteins and glycolipids, attached to the underlying galactose via α2,3 or α2,6 linkages (Johnson et al., 1964; Ohuchi et al., 1997). HA binding to the SA receptor is of low affinity, but the multiple HA molecules present in the virion provide a high-avidity attachment to the host cell surface (Sauter et al., 1989). HA exists as a trimeric protein with a globular head formed by the N-terminal domain of HA1 and a stalk region at the C-terminus mainly formed by the HA2 subunit, which anchors the protein to the surface of the virion (Palese & Shaw, 2007). HA is synthesised in the rough endoplasmic reticulum (ER) and glycosylated in the Golgi network to form the precursor, HA0, composed of the two subunits:

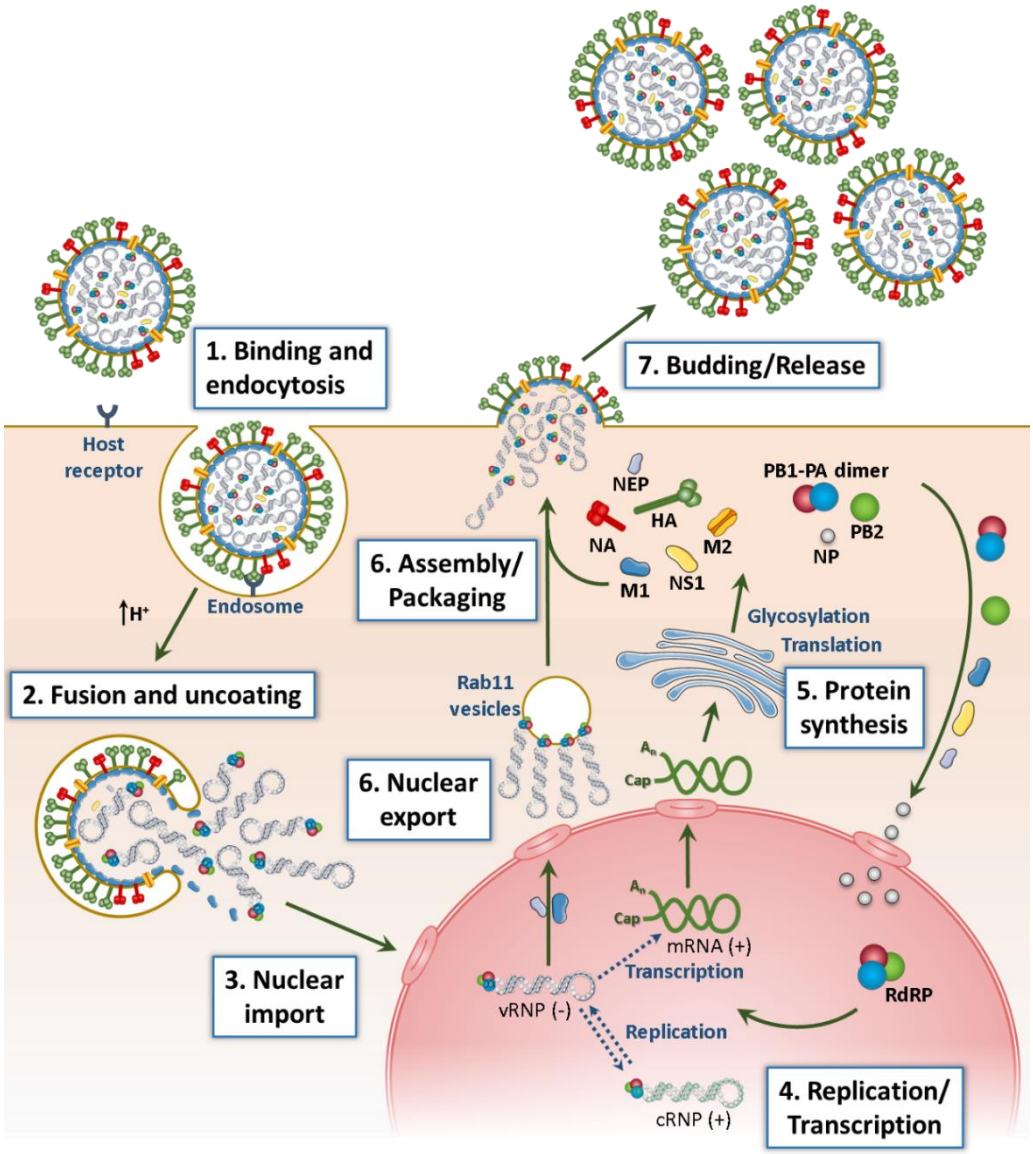

Figure 1.3 Schematic representation of the virus life cycle. (1) IAV attaches to the host cell via sialic acids on the cell surface and enters the cell by endocytosis. (2) The virus then follows the endocytic pathway inside the endosome, where acidification of the endosome triggers viral and endosome membrane fusion mediated by HA and release of the vRNPs into the cytoplasm of the host cell. (3) The vRNPs are then translocated to the nuclear pore complex (NPC) and enter the nucleus via the classical importin-α-importin-β1 pathway. (4) In the nucleus the vRNA is replicated into positive-sense cRNA that is amplified back to negative-sense vRNA for progeny virions. The RdRp also carries out vRNA transcription to produce viral mRNAs. During this process, it adds a cap at the 5' end from cellular mRNAs by cap-snatching and poly(A) tails at the 3' end. (5) Viral proteins are translated from their mRNAs and the internal proteins are translocated back into the nucleus while the viral transmembrane proteins migrate to the apical plasma membrane. (6) The newly formed vRNPs are exported out of the nucleus via the Crm1 nuclear export machinery and are trafficked to the apical cell membrane in a microtubule-dependent manner following the endocytic recycling pathway. (7) The viral proteins assemble at lipid raft domains and the progeny virions are released from the host cell. Cartoon drawn and kindly provided by Rute Pinto.

HA1 which contains the receptor-binding domain and HA2 which contains the transmembrane domain and the fusion peptide (Palese & Shaw, 2007). Regarding receptor binding, it was reported that HA of human and swine strains of IAV preferentially bind SA receptors with an α2,6 linkage, while avian and equine strains recognise with high specificity receptors with α2,3-linked sialic acid (Connor et al., 1994).

Following recognition of the receptor, the entry process begins with cleavage of the HA0 precursor by proteases outside the host cell, exposing the receptor binding domain in the HA1 subunit, which is held together with the HA2 via disulphide bonds (Skehel & Wiley, 2000). Spherical virions enter the cell mainly via clathrin-mediated endocytosis; however, IAV entry has also been reported in the absence of clathrin-coated pits (Matlin et al., 1981; Sieczkarski & Whittaker, 2002). In contrast, Rossman et al. recently showed that filamentous virions enter the host cell primarily via macropinocytosis when the cell engulfs large amounts of fluid, but this feature is not exclusive of filamentous virions and is rather induced by IAV infection (de Vries et al., 2011; Rossman et al., 2012). Once the virus enters the cell, it traffics along the endosomal trafficking pathway, thus being subject to more acidic pH in the maturing endosomes (Edinger et al., 2014). This low pH triggers a conformational change in HA, exposing the hydrophobic fusion peptide present in the N-terminus of the HA2 subunit, which inserts into the endosome membrane and brings into close proximity the viral and endosomal membranes, thus driving fusion of both membranes. Alongside the fusion event, the M2 ion channel protein allows for the entrance of protons into the virion, which results in acidification of the virus interior and dissociation of the M1 protein from the vRNPs, thus allowing the release of the vRNPs into the host cell cytoplasm via the pore formed by HA-mediated fusion (Bui et al., 1996; Pinto et al., 1992).

1.4.2. Import of vRNPs to the nucleus

Once the vRNPs reach the cytoplasm of the host, these need to be translocated to the nucleus where the vRNA is transcribed and replicated. The nucleus is surrounded by a double membrane, termed the nuclear envelope, and inserted into this are protein complexes that form the nuclear pore complex (NPC). The nuclear envelope is a relatively permeable membrane that

allows the diffusion of molecules smaller than ~ 40 kDa through the NPC, though bigger molecules, such as proteins, mRNA and others, can only enter (or leave) the nucleus via the NPC in an energy-dependent process (Kabachinski & Schwartz, 2015). To cross the NPC and enter the nucleus via the classical importin-α/importin-β1 (IMPα-IMPβ1)-dependent pathway, the cargo must contain a nuclear localisation signal (NLS) (Stewart, 2007). In fact, NLSs have been identified in all four proteins of the vRNP complex and it has been demonstrated that PB2 and NP enter the nucleus alone, while PB1 and PA enter the nucleus as a complex (Fodor & Smith, 2004; Mukaigawa & Nayak, 1991; Nath & Nayak, 1990; Nieto et al., 1992; O'Neill et al., 1995). Therefore, the newly M1-dissociated vRNPs are recognised by the IMPα adaptor proteins, which in turn recognise the IMPβ transport receptor on the NPC and start the translocation of the IMPα-IMPβ-vRNP complex into the nucleus. The dissociation of IMPβ from the IMPα-vRNP complex is an energy-dependent process induced by binding of RanGTP to IMPβ, therefore releasing the cargo-carrier complex in the nucleus (Stewart, 2007). Lastly, dissociation of IMPα from the vRNP occurs by binding of the export carrier of IMPα, which sends IMPα back to the cytoplasm. Both IMPα and IMPβ are then individually recycled to undergo another cycle of nuclear translocation.

1.4.3. Transcription and replication of the viral genome

Once in the nucleus, the negative sense RNA genome of IAV is transcribed to mRNA to produce the viral proteins, and replicated via a full length cRNA intermediate which serves as a template for the synthesis of the full length negative sense RNA genome that will be incorporated into progeny virions (Eisfeld et al., 2015). The first step in transcription consists of the recognition of the viral promoter at the 5' and 3' ends of the vRNA by PB1, which activates the primer binding and endonuclease activities of the viral polymerase (Lee et al., 2003; Luytjes et al., 1989). Following this, the PB2 subunit binds to 5' 7-methylguanosine (m7GpppXm) capped pre-mRNAs from the host cell and the endonuclease activity of the PA subunit cleave off the 5' cap from the host pre-mRNA in a process called cap-snatching (Blaas et al., 1982; Dias et al., 2009; Plotch et al., 1981). This process leaves a hydroxyl group at the 3' end of the mRNA fragment that is used by PB1, which has polymerase activity, as a primer to initiate transcription of the negative

sense vRNA into positive sense mRNA in the 3' to 5' direction using the 3' end of the vRNA as a template (Braam et al., 1983). The elongation of the mRNA transcript continues until the active site of the polymerase finds a relatively long stretch of uracil nucleotides, positioned between 17 and 22 nucleotides upstream of the 5' end of the vRNA segments which acts as a polyadenylation signal (Robertson et al., 1981). The polymerase is forced to begin non-processive transcription on this homopolymer due to spatial constraints, as the 5' end of the vRNA remains associated with the viral polymerase during transcription, causing the viral polymerase to stutter on the poly(U) stretch resulting in the addition of a poly(A) tail to the newly synthesised viral mRNA (Zheng et al., 1999). The mRNAs are then exported to the cell cytoplasm, which are then translated in the host ribosome and spliced as required by the cell splicing machinery (see section 1.1.2: genome organisation). Equally important, the expression of the 8 viral genes does not occur simultaneously. Immediately following infection, PB2, PB1, PA, NP and NS1 proteins are detected, while the expression of HA, NA, M1 and M2 proteins is more strongly detected in a later stage of infection, even though the mRNA of early proteins is also detected at this stage of infection (Yamanaka et al., 1991). Following translation in the cytoplasm of the cell, the four vRNP protein components are transported back to the nucleus to carry out replication of the viral genome as well as amplified transcription.

Regarding the first step of genome replication, synthesis of cRNA, a functional switch in the viral polymerase's mode of transcription initiation and termination needs to occur. Unlike transcription, genome replication produces a cRNA that is a full-length positive sense reverse-complement copy of the vRNA, which includes the UTR at the 5' and 3' ends, the segment-specific packaging signals and the ORF (Palese & Shaw, 2007). Genome replication is initiated *de novo* in a primer-independent manner as both cRNA and vRNA contain a 5' triphosphate (Hay et al., 1982). The second stage of genome replication, synthesis of progeny vRNA from the cRNA replicative intermediates, occurs subsequently. To date it is still not clear if this is carried out by *cis-* or *trans-acting* viral polymerases and what the exact mechanism for this functional switch of the polymerase is (Fodor, 2013; Hay et al., 1977; Moeller et al., 2012).

1.4.4. Nuclear export of the vRNPs

Following replication of the viral genome and formation of new vRNPs, these need to be exported out of the nucleus into the cytoplasm to be incorporated into progeny virions. This is performed in a CRM1-dependent manner via the NPC, as inhibition of this nuclear export receptor led to retention of vRNPs in the nucleus of infected cells (Elton et al., 2001; Watanabe et al., 2001). CRM1 recognises and binds cargo with a leucine-rich nuclear export signal (NES) and shuttles through the NPC in conjunction with RanGTP through interactions with nucleoporins at the NPC. After crossing the pore, RanGTP provides the energy necessary to dissociate CRM1 from its cargo in the cytoplasm of the cell (Hutten & Kehlenbach, 2007). The viral proteins shown to aid nuclear export of vRNPs are M1 and NEP (Martin & Helenius, 1991; O'Neill et al., 1998). In the nucleus, M1 binds to newly synthesised vRNPs through interactions with NP, while NEP binds to M1 and directs the vRNPs to the nuclear export machinery, by forming a bridge between vRNPs and CRM1 via its nuclear export signal (Huang et al., 2001; Neumann et al., 2000; O'Neill et al., 1998; Yasuda et al., 1993). Before nuclear export, vRNPs accumulate at the nuclear periphery by tethering to chromatin, enabling the access to CRM1, therefore hijacking the nuclear export machinery of the cell (Chase et al., 2011; O'Neill et al., 1998). At the NPC, it is suggested that M1 bound to vRNPs forms a bridge to associate the vRNPs to NEP, which in turn interacts with CRM1 and facilitates shuttle of the complex through the NPC and release of the vRNPs into the cytoplasm of the cell (Akarsu et al., 2003; Yasuda et al., 1993). After nuclear export, the vRNPs need to traffic up to the apical plasma membrane to start virion assembly and budding (Misek et al., 1984; Rodriguez-Boulan et al., 1983). This starts with the accumulation of the vRNPs at the perinuclear microtubule organisation centre (MTOC) which are directed by the Y-box-binding protein 1 to the cellular microtubule network and trafficked to the apical plasma membrane (Amorim et al., 2011; Kawaguchi et al., 2012; Momose et al., 2011). This was shown to occur via the endocytic recycling pathway in Rab11-positive vesicles through interactions with the PB2 subunit (Bruce et al., 2010). Even though trafficking via the MTOC is the currently accepted model, it was recently reported that the vRNPs and Rab11(GTPase) can reach the apical cell membrane by IAV-induced extension of the ER

independently from the endosomal recycling pathway (de Castro Martin et al., 2017; Nturibi et al., 2017).

1.4.5. Assembly and budding

Once the vRNPs are exported out of the nucleus, the 8 vRNPs that comprise the IAV genome need to be packaged before budding to produce infectious particles. Both spherical and filamentous forms of influenza utilise cholesterol- and sphingolipid-rich raft domains in the apical cell membrane as the site of assembly and budding (Leser & Lamb, 2005; Scheiffele et al., 1999; Simpson-Holley et al., 2002; Takeda et al., 2003). This is initiated after the synthesis of the viral transmembrane (HA, NA and M2) proteins in the rough ER and their transport to the apical cell membrane via the Golgi network (Doms et al., 1993; Misek et al., 1984). HA and NA possess apical sorting signals in their transmembrane domains that facilitate their accumulation in lipid raft domains and insertion into the apical cell membrane, forming the assembly and budding site for IAV (Barman & Nayak, 2000; Lin et al., 1998; Takeda et al., 2003). In contrast, M2 is not raft-associated and rather accumulates in areas of the membrane surrounding the lipid raft domains, probably due to its cholesterol binding domain (Leser & Lamb, 2005; Rossman et al., 2010). The accumulation of the internal viral proteins (including the vRNPs) at the sites of assembly and budding is also required. This has been variously described to occur in an MTOC- and/or actin cytoskeleton-dependent manner, yet more recent studies suggest that the ER can mediate viral protein trafficking all the way up to the cell membrane (Amorim et al., 2011; Avalos et al., 1997; Bruce et al., 2010; de Castro Martin et al., 2017; Digard et al., 1999; Nturibi et al., 2017).

To assemble the vRNPs at the site of budding, it is currently accepted that the M1 protein forms a bridge between the vRNPs (bound to M1) and the viral transmembrane proteins. This interaction was suggested to occur between M1 and the cytoplasmic tails of HA and NA, as deletion of these latter domains resulted in viruses with altered morphology and a significant reduction in lipid-raft association and M1 and RNP incorporation, thus inhibiting viral assembly (Ali et al., 2000; Jin et al., 1997; Takeda et al., 2003; Zhang et al., 2000). Furthermore, M1 was shown to be recruited by either HA or NA, as viruses with tail-minus HA or tail-minus NA were both rescued, although replicating to much lower levels than the corresponding WT virus,

suggesting that only one envelope glycoprotein is necessary to ensure viral assembly and budding (Ali et al., 2000; Zhang et al., 2000). Although a direct interaction between M1 and HA has yet to be detected, co-evolution bioinformatics analysis suggested that there are residues in the boundary of the HA cytoplasmic tail domain that are likely to interact with residues within the C-terminus of M1 (Mintaev et al., 2014). Regarding M2, mutational analysis revealed that the cytoplasmic tail of M2 also interacts with M1 and promotes efficient virus assembly (Chen et al., 2008; Rossman et al., 2010). Therefore, M1 is thought to bridge the interaction between the vRNPs-HA/NA and M2-HA. However, recent studies showed that even though M2 possess a cholesterol-binding domain, it only accumulates adjacent to lipid rafts when raft-associated HA is present, even in the absence of M1 (Rossman et al., 2010; Thaa et al., 2010). Thus, the exact mechanism by which the viral bud zone is formed remains unclear, but it is predicted to be via a complex network of interactions between HA, NA, M1, M2 and NP (Leser & Lamb, 2017). Lastly but not least, another requirement for the formation of the viral assembly site is an intact actin cytoskeleton, as disruption of this was reported to affect filamentous virion assembly, but not assembly and budding of spherical particles (Simpson-Holley et al., 2002). In fact, Goswami et al. reported that the actin cytoskeleton is responsible for the formation of protein nanoclusters and/or maintenance of raft domains, which could explain the importance of actin in viral assembly and its presence in purified virions (Goswami et al., 2008; Shaw et al., 2008).

The mechanism by which budding initiation occurs remains largely unknown. It is known that insertion of HA and NA into the plasma membrane induces membrane curvature, possibly initiating the budding event and once M1 is recruited via interactions with the cytoplasmic tails of the glycoproteins, it may suffer a conformational change that promotes M1 polymerization at the lipid raft domains (Gomez-Puertas et al.,, 2000; Rossman & Lamb, 2011). This polymerization of M1 underneath the plasma membrane was proposed to be the major driving force for VLP budding and may be involved in the formation of filamentous virions (Gomez-Puertas et al., 2000). However individual expression of HA, NA or M2 in VLPs also suggested that these are capable of initiating virus budding, while only the presence of HA, NA, M1 and M2 promoted efficient budding and release (Chen et al., 2007; Chlanda et al., 2015; Rossman et al., 2010). Once the bud is formed with M1 providing structural support underneath, the eight

vRNPs (bound to M1) are incorporated into the nascent virion. Electron microscopy and fluorescent *in situ* hybridization studies showed that majority of IAV particles contain all eight segments and these are present in one copy per virion (Chou et al., 2012; Noda, 2012; Noda et al., 2006). These and other studies have shown that genome packaging is segment-specific rather than random, as the probability of random packaging producing infectious particles is lower than that observed in laboratory infections (Hutchinson et al., 2010). Each segment of IAV contains a conserved stretch of nucleotides within the terminal coding and UTR regions, which were shown to act as packaging signals by deletion and mutational analysis or cloning of the UTRs onto a foreign gene, resulting in its incorporation in the virion (Gog et al., 2007; Liang et al., 2005; Luytjes et al., 1989; Marsh et al., 2007; Watanabe et al., 2003). The mechanism by which IAV is able to select only one copy of each segment is still unclear, however there is evidence showing that mutation of a packaging signal in one segment affects the packaging efficiency of the other segments, suggesting that RNA-RNA interactions can be important (Muramoto et al., 2006). Once the vRNPs are recruited via interactions with M1, these are packaged in a "seven around one" (7+1) conformation perpendicular to the budding site and, in the case of bacilliform and filamentous virions, the vRNPs are packaged at the distal end of the particle (Figure 1.2) (Calder et al., 2010; Vijayakrishnan et al., 2013).

Following assembly and bud formation of the new virion with the eight vRNPs packaged, M2 catalyses membrane scission in an endosomal sorting complex required for transport (ESCRT)-independent manner (Rossman et al., 2010). The ion channel protein is recruited to lipid raft domains most likely by M1, where it inserts its amphipathic helix (present in the cytoplasmic tail) into the cell membrane, inducing membrane curvature, followed by constriction, destabilization (forming a budding neck) and scission of the membrane (Martyna et al., 2017; Roberts et al., 2013). Figure 1.4 illustrates a proposed mechanism for budding of progeny virus highlighting the role of HA, NA, M1 and M2. Once the virion is formed and in order to be released, the sialidase activity of NA is required to cleave off cell-surface sialic acid moieties to prevent aggregation of the newly formed virions (Palese & Ueda, 1974). This might explain the clustering of NA at one end of the progeny virions, predominantly seen with bacilliform and filamentous forms of influenza A virus (Calder et al., 2010). Furthermore, it was hypothesised that the

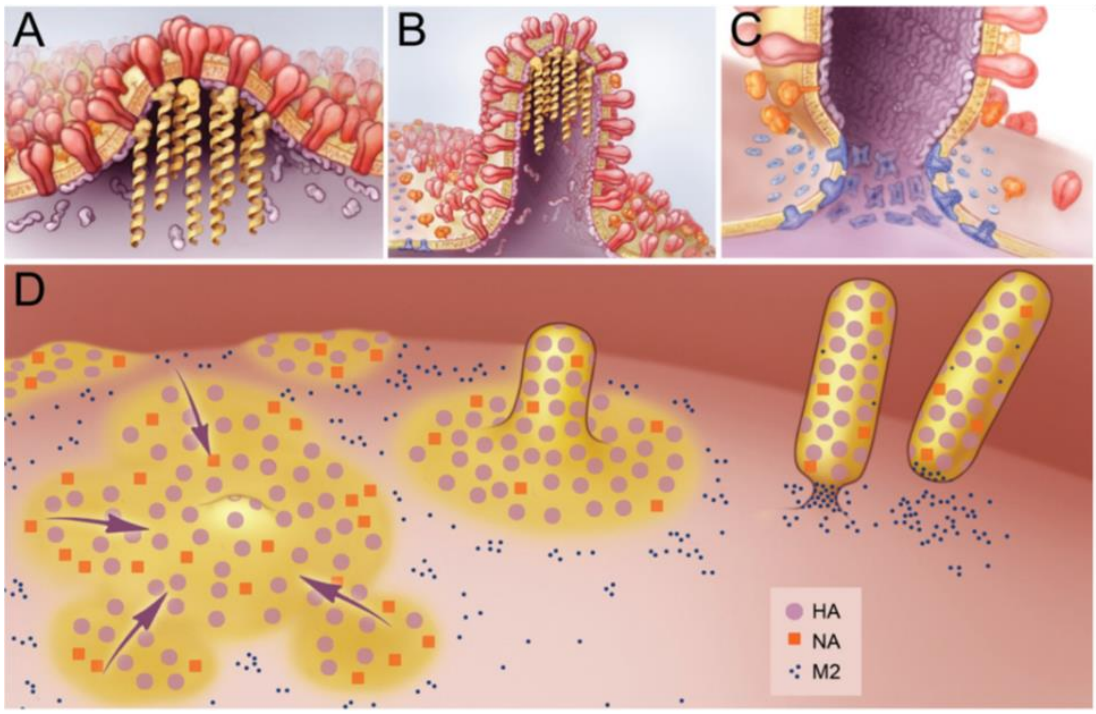

Figure 1.4 Schematic representation of the proposed mechanism for assembly and budding of IAV. (A) HA and NA initiate budding by clustering in lipid raft domains and the vRNPs are assembled in this region via association with M1, which is in turn recruited via interactions with the cytoplasmic tails of HA and/or NA. (B) This interaction triggers a conformational change in M1 which initiates oligomerization underneath the plasma membrane and, consequently, promotes elongation of the virion with the vRNPs at the opposite end of budding. (C) Once the membrane has elongated enough, M2, which accumulates in regions adjacent to the lipid rafts domains, is recruited by M1 and inserts its C-terminal amphipathic helix into the plasma membrane, causing membrane constriction and scission of the newly formed virion at the budding site. An overview of the viral transmembrane protein distribution during virus budding is illustrated in (D). Figure taken from Rossman & Lamb, 2011 (with permission from Elsevier).

clustering of NA at one end might result in the formation of filamentous virions with high amounts of sialic acid moieties which in turn can be recognised and bound by HA of filaments in the vicinity, thus promoting the formation of cord-like bundles of filamentous virions, as often seen by confocal or other forms of microscopy on the surface of infected cells (Dadonaite et al., 2016). However, it remains unclear whether filaments exit the cell as an individual particle or as a bundle of filamentous virions.

1.5. Host range

Wild aquatic birds, such as waterfowl and shorebirds, are the natural reservoir of IAV, which explains (or is suggested by) the high number of HA and NA subtypes isolated from these hosts (Webster et al., 1992). However, a subset of IAV subtypes have been isolated in chickens, turkeys, pigs, horses, dogs, seals and human hosts, thus showing that avian IAV is a epizootic and zoonotic pathogen with a wide host range, as illustrated in figure 1.5. Although avian IAV can infect a broad range of hosts, these are usually sporadic infections that result from direct (with the infected animal) or indirect (aerosols, infected material) contact and typically are poorly transmitted by the new host (Cauldwell et al., 2014). On the other hand, the mammalian strains of IAV largely infect only one single species, with the exception of a few subtypes, such as H3N8 equine IAV that can infect both dogs and horses or various H3N2 and H1N1 strains, which have been reported to infect pigs and humans (Crawford et al., 2005; Olsen et al., 2006).

1.5.1. Avian influenza

Influenza virus in wild aquatic birds predominantly replicates in the intestinal mucosa and is therefore transmitted faecal-orally through water (Webster et al., 1992). By contrast, avian IAVs isolated from domestic poultry have acquired the ability to preferentially replicate in the respiratory tract, which can facilitate transmission in densely-populated poultry houses(Vandegrift et al., 2010). Bird populations are affected by two types of avian IAV: LPAI and HPAI. The difference in virulence between these two types is largely associated with disease severity, namely in the order *Galliformes* (domestic poultry) (Yoon et al., 2014). As explained before, HA is cleaved by host cellular proteases, which in the case of LPAI

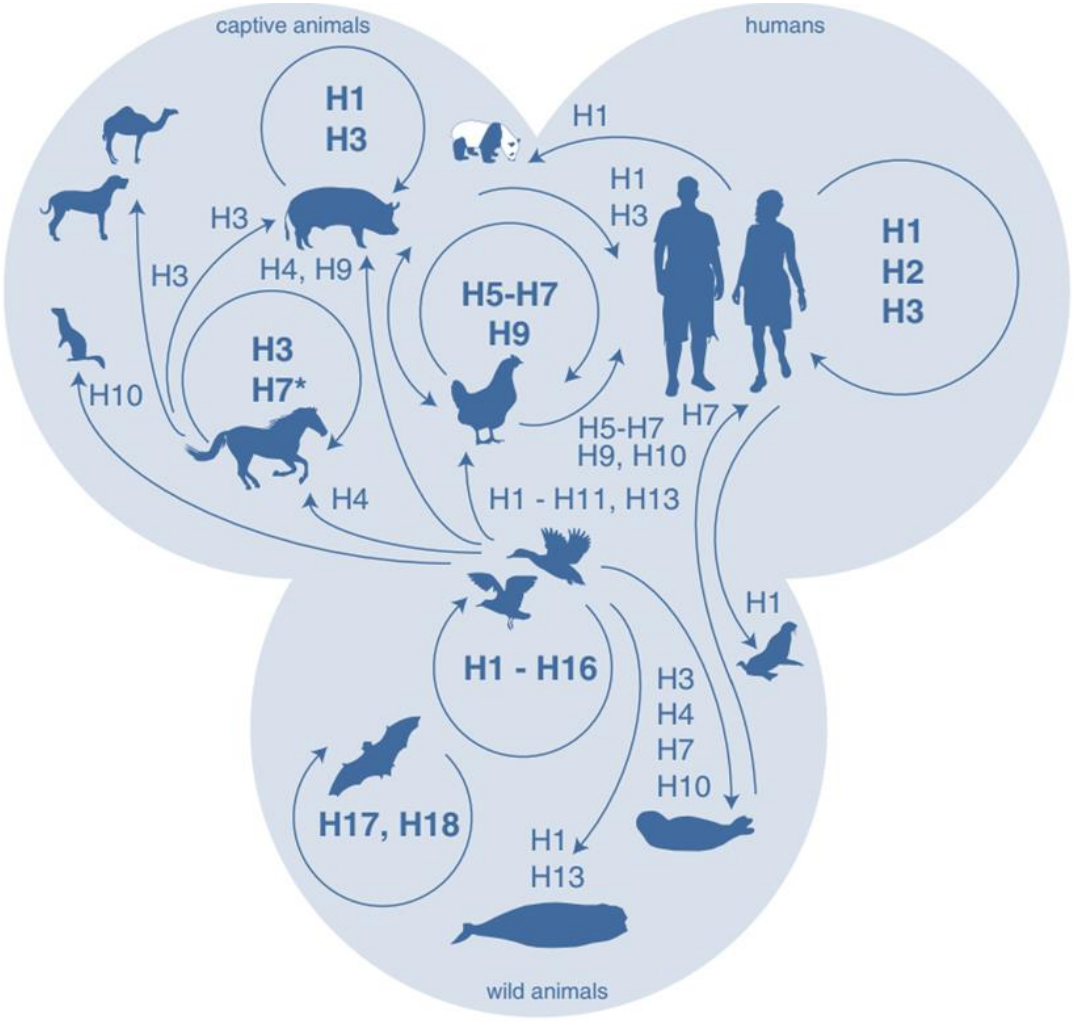

Figure 1.5 IAV host range. All HA and NA subtypes of IAV (excepting two bat-specific HA and NA subtypes), in almost all possible combinations have been isolated from their natural reservoir (wild aquatic birds). A large amount of these subtypes can be transmitted to other avian species, such as poultry, or mammalian species. Crossing of the species barrier occurs predominantly from wild birds to other mammalian species, but the fact that only a minority of HA subtypes are found in mammalian species suggest that these transmission events are usually dead-ends for the virus, as it is not adapted to the new host. For instance, the main subtypes maintained in humans are H1, H2 and H3. Currently, the origin of H17 and H18 isolated in bats is of unknown ancestry. Figure adapted from Short et al., 2015.

HA subtypes, is mainly by extracellular trypsin-like enzymes, which limits the spread of the virus within the host to the respiratory or intestinal epithelia (Boycott et al., 1994). However, some strains evolve into HPAI HA subtypes by insertional mutations, resulting in a polybasic cleavage site that is recognised by ubiquitous intracellular proteases found within the host, therefore leading to a systemic infection and increased pathogenicity (Horimoto & Kawaoka, 2005; Wright et al., 2007). Thus, while LPAI infection of poultry causes mild infections that result in trouble breathing, reductions in egg production and depression, HPAI infection causes severe morbidity (respiratory distress, diarrhoea, thrombosis) and/or sudden death (Horimoto & Kawaoka, 2005). H5, H6, H7 and H9 IAV subtypes currently circulate in domestic poultry and are predominantly LPAI, with the exception of H5 and H7 that have evolved to HPAI phenotypes and can now cause high morbidity and mortality in the order *Galliforme*. However, in more recent years, the HPAI strains have also been detected in wild birds of the orders *Anseriformes* (waterfowl) and *Charadriiformes* (shorebirds) (Yoon et al., 2014).

1.5.2. Host adaptation

It was noted that when avian IAV spreads and adapts to other hosts, the virus goes through rapid evolution with the emergence of new strains that evolve into individual clades (Worobey et al., 2014). Regarding avian IAV transmission to mammalian hosts, the first barrier encountered by the virus is the different binding affinity of the HA receptor. As described previously, the cellular receptor recognised by HA is the sialic acid moiety present on glycoproteins or glycolipids on the cell surface. However, avian strains of IAV have a preference for sialic acids with α2,3 linkages, which are abundant in the intestine of avian species but mainly found in the lower respiratory tract of humans. In contrast, mammalian-adapted HAs have a preference for α2,6-linked sialic acids, which are commonly found in the upper respiratory tract of humans, including trachea, nasal mucosa, pharynx and bronchi (Connor et al., 1994; Matrosovich et al., 2004). This barrier, however, can be lifted by amino acid substitutions in the receptor binding domain of HA, as reported for H1, H2 and H3 avian IAVs following transmission to mammalian hosts (Matrosovich et al., 2000). Another barrier associated with HA is its stability in an acidic environment, as it is important that pH-mediated exposure of the fusion peptide

occurs inside the endosome so the virus can fuse with the endosomal membrane. It has been reported that avian HAs fuse at higher pH values, while mammalian strains of IAV fuse at more acidic pH (fusion reported to occur below pH 5.3); therefore avian strains of IAV are limited in their transmissibility to and between mammalian hosts until the rise of adaptive mutations that stabilise HA in the human nasal mucosa, which show pHs as low as 5.3 (England et al., 1999; Galloway et al., 2013).

Further evidence suggests that the balance between the activities of HA and NA is another determinant of host range, as changes in either of the viral glycoproteins that affect HA affinity for sialic acid or NA sialidase activity can affect viral replication (Mitnaul et al., 2000). However, NA alone can also modulate host range, as de Wit et al. reported that mutations in NA of an avian H7N7 virus, following infection in humans, increased NA activity even when this particular NA was inserted in the backbone of another avian H7N7 isolate (de Wit et al., 2010). Other studies have also shown that the length of the NA stalk affects viral replication and transmission. For instance, Sorrell et al. reported that adaptation of an H2N2 avian virus from wild aquatic birds to domestic poultry resulted in a 27 amino acid deletion in the NA stalk, which changed virus tropism in the respiratory tract, promoting transmission to naïve birds via indirect respiratory contact (Sorrell et al., 2010). On the other hand, Blumenkrantz et al. reported that the short stalk of HPAI H5N1 subtypes in the 2009 pandemic H1N1 backbone limits virus transmission via respiratory contact between ferrets, showing by insertional mutation that a longer NA stalk is needed for efficient transmission in a mammalian host (Blumenkrantz et al., 2013).

Other viral proteins that have been associated with host adaptation are the components of the viral polymerase and the 'non-structural' proteins. Regarding the virus polymerase, it is known that an avian IAV polymerase is not always as efficient in a mammalian host. Compensatory mutations are therefore required to ensure viral fitness in these hosts, which can be achieved by co-evolution of the components of the RNP complex (Naffakh et al., 2008). For instance, a single amino acid substitution at position 627 of the PB2 subunit of avian influenza strains can result in a polymerase with enhanced activity in mammalian hosts (Subbarao et al., 1993). Equally important, a study carried out a screen of the chicken genome and identified the

host protein ANP32A as a host factor that the PB2 627 E/K variant depends on to increase avian polymerase activity in chickens and mammalian hosts, thus adding another layer to the understanding of host barriers (Long et al., 2016). More recently, Bussey et al. reported that the avian-origin human PA from a 2009 pandemic H1N1 strain showed three amino acid substitutions at residues 85, 186 and 338 when compared with the PA of an avian H3N2 strain. Following replacement of the avian PA with the human PA in the backbone of the avian viral polymerase, the authors reported that the chimeric avian polymerase was actively transcribing the reporter gene at 37°C (upper respiratory tract of humans) and at 39°C (avian gut), suggesting that adaptive mutations in PA also contribute to host adaptation of avian strains of IAV (Bussey et al., 2011). As a last example of specific changes in viral polypeptides that mediate host adaptation, several studies have reported that amino acid substitutions in the NS1 protein increased avian H5N1 pathogenicity in mammalian hosts, while mutations in NEP of human H5N1 isolates were shown to increase virus replication (Mänz et al., 2012; Seo et al., 2002).

Another possible and less well addressed determinant of host adaptation is virion morphology. As described in section 1.1.1, influenza viruses are able to produce spherical or filamentous virions and the latter can reach several μm in length. There are many studies addressing the viral and cellular determinants that govern production of the two morphologies (discussed in more detail in section 1.6), however, to date, their biological significance remains unclear. Nonetheless, the generally accepted assumption is that these morphologies can also be a modulator of host adaptation. This possibility rises from the fact that following adaptation into domestic poultry or mammalian hosts, avian IAVs that usually replicate in the bird gut gain the ability to replicate in the respiratory tract. Consequently a potential route of transmission to other hosts will be airborne in addition to faecal-oral (Tellier, 2009; Webster et al., 1992).

1.5.3. Influenza epidemics and pandemics

As discussed in the previous section, it is clear that for avian IAV to cross the species barrier and establish itself in mammalian hosts, the virus requires a number of adaptive mutations to ensure fitness in the new species. In majority of the cases, avian IAVs are unable to establish a sustained infection chain in mammalian species, explaining the relatively low

number of HA subtypes isolated from these hosts. However, when avian strains of IAV are able to infect and successfully adapt to transmit within (for instance), humans, seasonal epidemics or pandemics are likely to occur.

In humans, influenza pandemics are sometimes the direct result of IAV genome reassortment or antigenic shift. This gives rise to a new virus with novel HA and NA combinations that render the host population generally susceptible, as there is little or no cross-protection between different IAV subtypes (Krammer et al., 2018). To date, there are definitive records of five pandemics in the human population that span the last 100 years. The most famous IAV pandemic for which the virus strain is known was in 1918 (Spanish flu), which is estimated to have caused a death toll in the order of 50 million and temporarily reduced overall life expectancy figures by approximately 10 years (Taubenberger & Morens, 2006). This pandemic was caused by an H1N1 influenza virus of unknown source, but phylogenetic studies point to it having originated from direct transmission and adaptation of avian influenza to a human host, as there are many avian virus-like sequence features of the viral polymerase and other internal genes (Taubenberger et al., 2005; Worobey et al., 2014). This pandemic was of particular importance because it was the ancestor of subsequent seasonal lineages that persisted for the remainder of the 20th century (Taubenberger & Morens, 2006). The other three pandemics of the 20th century were in 1957 (Asian flu), 1968 (Hong Kong flu) and 1977 (Russian flu), which were caused by H2N2, H3N2 and H1N1 viruses, respectively (Kilbourne, 2006). The 1957 pandemic originated in China after reassortment of an avian H2N2 virus with the existing H1N1 strain, however this novel virus caused much lower mortality than seen in the previous human pandemic (Scholtissek et al., 1978). Approximately 10 years later, an avian H3 virus entered the human population, as a result of genome reassortment between the avian virus and the circulating human H2N2 virus, giving rise to an H3N2 pandemic human virus that still circulates in humans as seasonal H3N2 influenza (Kilbourne, 2006; Scholtissek et al., 1978). These first three pandemics of the 20th century each drove the previous virus into extinction in the human population. The last pandemic of the 20th century, in 1977, has a controversial origin, as it showed high RNA sequence similarity with the 1950s descendants of the 1918 H1N1 viruses, suggesting that the reported outbreak was a re-emergence of this strain (Nakajima et al., 1978).

Therefore the seasonal H1N1 viruses had somehow gone latent rather than extinct between 1957 and 1977. True latency within the host is not a known feature of IAV so the most likely hypothesis is that the 1977 pandemic viruses reappeared due to failed laboratory containment during live virus vaccine trials with the H1N1 pandemic strain (Kilbourne, 2006). Unlike previous pandemics, the re-emergence of H1N1 IAV did not replace the previous H3N2 virus in the human population, resulting in two seasonal strains of IAV that persist until the present day.

The first pandemic of the 21st century was reported in 2009 in Mexico, caused by a swine-derived H1N1 virus that entered the human population and spread worldwide in a short period of time, making it the most highly transmissible influenza virus of the 21st century (Fraser et al., 2009). Even though the WHO only reported around 18,000 laboratory-confirmed deaths, it is estimated that the 2009 pandemic caused between 123,000 to 203,000 fatalities in 2009 alone. However this pandemic was not considered deadlier than the previous seasonal strains of IAV (Simonsen et al., 2013). Sequence and phylogenetic analyses revealed that the 2009 pandemic H1N1 virus had a mixed origin that included viruses from avian, swine and human hosts, representing the result of reassortment events between swine viruses of mixed origins. Firstly, the viral polymerase components (PB2, PB1 and PA) were derived from a swine IAV lineage that is a triple reassortment of avian, swine and human origin viruses (Garten et al., 2009). The HA, NS and NP genes came from a swine H1N1 strain circulating in North America, while the remaining genes (NA and M) were originally derived from an avian virus that adapted to and established an endemic infection in pigs in Europe and Asia (Campitelli et al., 1997; Taubenberger & Morens, 2006). This H1N1 subtype has now replaced the previous seasonal H1N1 IAV and now circulates alongside H3N2 and strains of IBV in the human population.

The most notable avian IAV outbreak occurred in 1996, when a HPAI H5N1 virus spread within the poultry population in Hong Kong (Lewis, 2006). This outbreak got special attention due to the zoonotic risk of the HPAI H5N1 virus, which caused 6 fatal cases out of 18 recorded in poultry workers (Lewis, 2006). Furthermore, this resulted in the culling of over 1.5 million chickens by the end of 1997 to contain the outbreak, which contributed to the extinction of this HPAI H5N1 virus (Chan, 2002). However, reassortment of the parental H5N1 viruses with LPAI strains circulating in domestic poultry and wild birds resulted in the re-emergence of HPAI H5N1

viruses in 2003/2004, which were reported to cause the death of 52 people in south east Asia (Lewis, 2006). Since then, infections with avian HPAI H5 subtypes have been reported worldwide in humans, with mortality ratios of up to 80% (WHO, 2018a). Thankfully, transmission of HPAI H5 subtypes in humans is unlikely at best, but there is evidence for limited person to person spread, thus raising the concern of H5 subtypes as the source of a human pandemic (Ungchusak et al., 2005).

More recently, from 2013 onwards, the exposure of domestic birds to wild birds and the reassortment between wild and domestic strains of IAV resulted in the emergence of H7N9 and H7N7 viruses (Liu et al., 2013). These viruses possess a LPAI phenotype and have caused several waves of infection in live bird markets, causing only mild symptoms in domestic poultry (Su et al., 2017). However, these subtypes of avian IAV have drawn attention due to their zoonotic risk, as up until now these have caused over 600 deaths in humans (FAO, 2018). Although these viruses possess an increased binding affinity to human receptors and airborne transmission in ferrets, human-to-human transmission remained limited and most cases of infection resulted from direct exposure to infected poultry (Herfst et al., 2012; Imai et al., 2012). Even though these subtypes were mild to the poultry population, in September 2017 the Chinese government set up a mass vaccination campaign using an inactivated bivalent vaccine containing H5 and H7 viruses (Zeng et al., 2018). Surveillance up until June 2018 revealed that only a few birds were positive for H7N9 and only three human cases were reported, suggesting that the vaccination campaign was successful although continued surveillance is under way (Zeng et al., 2018).

1.6. Virion morphology of IAV

Spherical and filamentous forms of influenza virus have been detected in influenza A, B and C genera (Morgan et al., 1956; (Nishimura et al., 1990) however the majority of the studies performed to date have focused on strains of IAV and these will be summarised in this section. The first report that described the presence of spherical and filamentous particles was by Mosley and Wickoff, who showed by electron microscopy that purified preparations of A/Puerto Rico/8/1934 (PR8) and A/WSN/1933 (WSN) strains of influenza A viruses were composed of

both filaments and spheres (Mosley & Wickoff, 1946). Later, in 1949, Chu et al. compared the morphology of freshly isolated human viruses with low egg passage and PR8 strain (which by then had undergone extensive egg passage). The authors reported that the human viruses showed a greater number of long filamentous particles than PR8, thus suggesting that filamentous virions are lost upon egg passage (Chu et al., 1949). This hypothesis was later corroborated by several laboratories, as the authors showed that serial passage (over 12 times) of a filamentous virus in the allantoic cavity of chicken eggs resulted in the loss of the filamentous morphology, which was associated with suboptimal growth in this system (Burnet & Lind, 1957; Choppin & Tamm, 1960; Kilbourne & Murphy, 1960). More recently, Seladi-Schulman et al. also showed that a human filamentous strain loss its filamentous morphology upon serial passage in embryonated eggs, while the spherical strain PR8 (re-)acquired the ability to produce filamentous particles upon passage in guinea pigs, thus providing evidence of the benefit of the filamentous morphology *in vivo* (Seladi-Schulman et al., 2013). Equally importantly, Burnet and Lind showed that filaments were a genetically-encoded trait of IAV, as filtration of the virus population to remove filaments still resulted in a virus able to produce the characteristic elongated forms upon infection (Burnet & Lind, 1957). This was corroborated by Kilbourne and Murphy, as they showed that genetic reassortment of a filamentous human IAV strain with PR8 resulted in a predominantly spherical reassortant with the replication phenotype of PR8 (Kilbourne & Murphy, 1960). Even though both morphologies of virion were detected in virus preparations, the initial hypothesis was that spherical particles were a result of the fragmentation of the longer filamentous particles. However, this was proved not to be the case when Morgan et al. showed by electron microscopy that spherical and filamentous particles extruded from the surface of infected cells concomitantly at 6-8 hours p.i., therefore demonstrating that both morphologies were produced independently (Morgan et al., 1956).

1.6.1. Viral determinants of virion morphology

1.6.1.1. M1 and M2

Filamentous morphology was shown to be a genetic trait of influenza virus in the late 1950s, but it was not until the late 1990s that the first report appeared demonstrating the clear

importance of the segment 7-encoded M1 and M2 proteins for the phenotype. M1 is a 252-amino acid protein that forms a helix underneath the viral envelope, providing support and structure to the virion. Biochemical and structural studies with M1 showed that this protein has three largely α-helical domains; N-terminal and middle domains that have been crystallised, attached by a flexible linker sequence to a C-terminal domain that remains unknown structure-wise due to its inability to crystallise, but it is suggested to be more disordered than the N-terminus. The domains of M1 and their respective functions are illustrated in figure 1.6 A. Conversely, M2 is a 97-amino acid protein that plays roles in viral uncoating inside the endosome and viral budding. This protein is composed of an ectodomain, tetramers of single-pass transmembrane helices and an amphipathic helix within the cytoplasmic tail as illustrated in figure 1.6 B. In a study led by Roberts et al, the authors used a now well-known filamentous strain, A/Udorn/1972 (Udorn), to show that treatment of infected cells with an antibody against M2 (14C2) prevented the formation of filamentous particles (Roberts et al., 1998). Furthermore, they found that antibody-resistant variants of Udorn presented mutations in M2 (at residues 71 and 78) but retained their filamentous morphology, while another variant that presented a single mutation in M1 (at position 41) showed a predominantly spherical morphology, thus demonstrating the importance of M1 as a major determinant of budding morphology. Later, Bourmakina & Garcia-Sastre built a reassortant virus with the M segment of Udorn in the backbone of WSN and showed that this genetic reassortment conferred a filamentous budding that was determined solely by M1, as

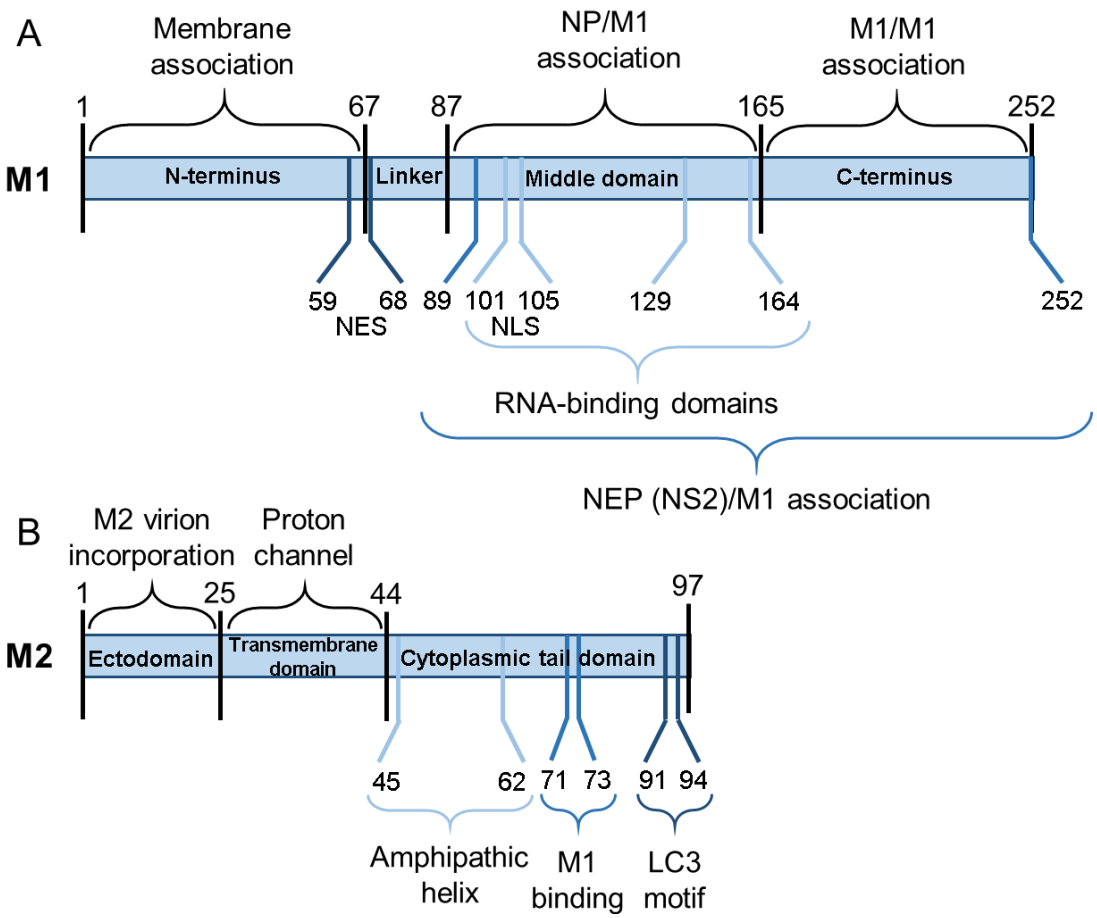

Figure 1.6 Schematic representation of domains within IAV M1 and M2 proteins. (A) The N-terminal and middle domains of M1 have been associated with virion incorporation of M1 and the vRNPs via interactions with NP and non-sequence specific interactions with the vRNA, respectively (Noton et al., 2007; Sha & Luo, 1997; Ye et al., 1989). Once translated, M1 enters the nucleus via its NLS to aid in the nuclear export of vRNPs, which requires a bridge between M1 and CRM1 at the NPC that has been reported to occur via NEP (Ye et al., 1995). M1 associates with NEP via its middle and C-terminal domains and in turn NEP associates with CRM1 via its NES (Ward et al., 1995). However, a NES in M1 was recently reported and shown to impair M1 and NEP export, suggesting that M1 might interact directly with CRM1 (Cao et al., 2012). The C-terminus domain of M1 was recently reported to regulate the ability of M1 to associate or dissociate at different pH, suggesting a role in M1 dimerization (Shtykova et al., 2017). (B) The ectodomain (or extracellular domain) of M2 is a highly conserved sequence that has been used as part of a "universal" vaccine for IAV, but this domain is also thought to be involved in incorporation of M2 into the virion (Park et al., 1998; Pica & Palese, 2013). The transmembrane domain of M2 is embedded in the virion lipid bilayer and it forms a proton channel that promotes virion acidification and release of the vRNPs into the cytoplasm (Pinto et al., 1992). The cytoplasmic tail of M2 was shown to be composed of: (i) an amphipathic helix that promotes membrane scission between newly formed virions and the host cell; (ii) a M1 binding motif that most likely helps recruit M2 to the lipid raft domains to initiate membrane scission; and (iii) a LC3-binding motif that allows M2 to recruit this protein to hijack the autophagy cell machinery to source budding virions with cellular membrane (Beale et al., 2014; Chen et al., 2008; Roberts et al., 2013; Rossman et al., 2010).

shown by individual expression of Udorn M1 in the WSN backbone (Bourmakina & Garcia-Sastre, 2003). Moreover, the authors also showed by mutational analysis that the amino acid identity at positions 95 and 204 of M1 were important genetic signatures for virion morphology determination. A similar study by Elleman and Barclay also showed that virion morphology was a transferable trait encoded on segment 7 regardless of subtype and, by constructing the Udorn strain expressing its own M1 but M2 from the spherical WSN strain the authors showed that M1 was the sole determinant of virion morphology in the M segment (Elleman & Barclay, 2004). Similarly to the previous study, the authors also showed that amino acid identity at positions41, 95 and 218 were sufficient determinants to transfer the filamentous morphology of Udorn to the WSN strain. More recently, by comparing M1 amino acid sequences between classical swine H1N1 strains and human H1N1 strains from the 2009 pandemic, Bialas et al. showed that substituting amino acid position 207 of the human M1 gene to swine virus-like conferred a filamentous morphology to the human pandemic strain (Bialas et al., 2012). Campbell et al. identified a natural occurring polymorphism at the highly conserved position 41 of M1 between human and swine influenza. The authors showed that amino acid substitution at this position of human M1 to swine-like M1 resulted in a human virus with a filamentous morphology (Campbell et al., 2014; Furuse et al., 2009). Although the majority of these studies were performed in human strains of IAV, Elton et al. also showed that segment 7 was the main morphology determinant of H3N8 equine strains of IAV and by mutational analysis identified positions 85 and 231 within M1 as capable of transferring budding morphology between strains (Elton et al., 2013).

Other studies that were not directly focussed on identifying the genetic determinants of IAV budding morphology have inadvertently found other M1 residues that affect particle shape. For instance, Burleigh et al. reported a study that set out to identify functional properties of the helix 6 domain of M1, which included acting as an NLS, binding to vRNPs, viral assembly and others. However, the authors found by alanine substitution mutation that amino acid substitutions at positions 95, 98, 101 and 102 resulted in WSN virions with a range of morphologies. Mutant 102 was the most notable for the production of filamentous virions in the WSN background (Burleigh et al., 2005). Another study looking at the mechanism of M1

oligomerization also showed that residues in the C-terminus are important determinants of virion morphology. Also using scanning alanine mutagenesis, the authors reported that substitutions at residues 183 and 185 altered the oligomerization pattern of M1 and conferred a filamentous morphology to WSN strain (Zhang et al., 2015). Although the residues identified in these studies do not constitute a natural “filamentous signature”, they nonetheless provide information on filament formation itself, which appears to be highly dependent on the folding of M1 into an ordered helix capable of forming a rigid filamentous structure as reported by Calder et al. following cryo-electron microscopy of purified Udorn virus (Calder et al., 2010).

In addition to M1, M2 is also known to affect virion morphology. For instance, Roberts et al. showed that mutations in the highly conserved residues of the amphipathic helix of M2, namely residues 47, 48, 51, 52 and 55 (within the cytoplasmic tail), largely abrogated the formation of filaments by Udorn, suggesting that this domain, thought to be involved in membrane scission during budding, also plays a role in virion morphology (Roberts et al., 2013). More recently, Beale et al. reported that PR8-MUd viruses (segment 7 of Udorn in a PR8 backbone) with amino acid substitutions at positions 91 and 94 of M2 produced fewer filamentous bundles on the surface of infected cells (Beale et al., 2014). The authors identified these positions as lying within an LC3-interacting motif with which M2 interacts to hijack the autophagy cell machinery, suggesting that M2 contributes to filament formation by using the autophagy machinery as a source of cell membrane.

1.6.1.2. Other viral proteins

Several studies have focused on the importance of other proteins on viral morphogenesis. For instance, Jin et al. reported that WSN virions lacking the cytoplasmic tail of HA (known to interact with M1) retained their spherical morphology, however, when the cytoplasmic tails of both glycoproteins were absent the spherical shape was largely replaced by long irregularly shaped virions, suggesting that the interaction between the cytoplasmic tail of NA and M1 mediates budding morphology of spherical particles (Jin et al., 1997). This was corroborated by Gomez-Puertas et al., who showed by electron microscopy that expression of M1 by itself or in combination with the viral glycoproteins in a VLP system induced the formation

of elongated structures compatible with IAV virions; however, when NA was not present, the VLPs were predominantly spherical and formed aggregates (Gomez-Puertas et al., 2000). More recent studies have suggested that NA itself can also induce filamentous particle formation. For example, Campbell et al. showed that inserting the NA gene of a filamentous human strain into an otherwise spherical PR8 virus resulted in a few filamentous virions on the surface of infected cells. However, only the combination of the M segment and the viral glycoprotein NA of the filamentous human strain increased filament formation by the spherical PR8 virus (Campbell et al., 2014). Similarly, Chlanda et al. showed that expression of NA alone in transfected cells resulted in the formation of irregularly shaped long filamentous structures on the surface of the cells, yet only when the M protein was expressed alongside the glycoprotein did the authors observed regularly shaped filamentous influenza particles characteristic of a filamentous virus (Chlanda et al., 2015).

Another viral protein that has not received as much emphasis as the viral membrane-associated polypeptides but has also been reported to influence virion morphology is NP. For example, Liu et al. reported that the association of PR8 M1 and NP (spherical) was stronger than the association of M1 and NP of a human filamentous strain, suggesting that the strength of the interactions between the M1 and vRNP is associated with viral morphology but it remains unclear which drives which (Liu et al., 2002). A more recent study showed that the M segment of a 2009 H1N1 pandemic human strain containing a typical "filamentous signature" at the M1 amino acid level did not induce filament formation in its natural background, but it did when the M segment was placed in a PR8 backbone (Bialas et al., 2014). By genetic reassortment, the authors showed that this inhibition was caused by NP and identified residues 214 and 217 in NP as the main determinants of filament abrogation in the WT human strain.

1.6.2. Cellular determinants of morphology

It is well established that serial passage of influenza strains in embryonated eggs results in the loss of the filamentous phenotype, therefore it has been suggested that host factors could play a role in viral morphogenesis. For example, Roberts and Compans showed that polarised epithelial cells from different host species infected with Udorn strain displayed the characteristic

filamentous structures on their surface, while cells of fibroblast origin did not, suggesting that polarisation is an important factor in filament formation even though both morphologies of virion bud at the apical plasma membrane (Roberts & Compans, 1998). However, other studies using fibroblasts or other non-polarised cell types found that filaments were still detected on the surface of these cells, thus cell polarisation could be a more complex trait in determining filament formation than first thought (Al-Mubarak et al., 2015; Bruce et al., 2009). A potentially significant observation made by Al-Mubarak et al. revealed that fibroblast cells of chicken origin prevented filament formation upon infection with a duck filamentous strain, while duck-origin fibroblast cells displayed filamentous structures on their surface. However, filamentous structures were detected on both cell types upon infection with a filamentous equine strain of IAV, indicating that filament formation could also be host species-dependent (Al-Mubarak et al., 2015). Furthermore, filament formation is dependent on an intact actin cytoskeleton, whose disruption was shown to severely inhibit the formation of long filamentous structures on the cell surface upon infection with a filamentous strain (human or avian), yet it had little to no effect on the assembly and budding of spherical particles (Al-Mubarak et al., 2015; Roberts & Compans, 1998). Other cellular factors identified as capable of modulating virion morphology were Rab11 and Rab11-family interacting protein 3 (FIP3) (Bruce et al., 2010). As described previously, Rab11 is a component of the endosomal recycling pathway involved in the apical transport of the viral vRNPs, while FIP3 mediates the transport of the viral components-Rab11 complex up the microtubules via interactions with a kinesin motor complex (Bouchet et al., 2018). As reported by Bruce et al, depletion of Rab11 affected budding of both spherical and filamentous particles, while depletion of FIP3 particularly inhibited filament formation, thus suggesting that FIP3 plays a role in filament formation that remains to be elucidated (Bruce et al., 2010).

1.7. Functions associated with virion morphology of IAV

1.7.1. Escaping host barriers

It is well established that human and avian IAVs adapted to domestic poultry preferentially replicate in the epithelial cells of the respiratory mucosa. In fact, budding of

spherical and filamentous influenza particles has been documented *in vitro* from the microvilli of differentiated human airway epithelial cells, providing further evidence of the importance of epithelial cells within the respiratory mucosa (Kolesnikova et al., 2013). Therefore, one of the first functions suggested for filament formation was the more efficient clearance of the mucous layer that coats the respiratory epithelium, facilitating virus entry to the epithelial cells underneath (Roberts & Compans, 1998). The respiratory mucosa is composed of a rigid gel-like mucous layer that sits on top of a more fluid periciliary layer, which is composed of basement membrane with connective tissue underneath (lamina propria) where the mucous secretory gland is embedded, as represented in figure 1.7 (Fahy & Dickey, 2010). Both ciliated epithelial cells with microvilli on their surface and goblet cells sit underneath the mucous layer that is composed of mucins, which are heavy glycosylated sialic acid-rich proteins that provide the viscoelastic properties associated with mucous membranes. Influenza A virus is known to interact with these mucins and block of neuraminidase activity by NAI drugs showed that NA is important in the clearance of the mucous layer to allow virus penetration of the barrier (Cohen et al., 2013). Studies using NAI inhibitors and/or exogenous NA support a role of viral NA in the diffusion and penetration of the mucous layer by the virus (Yang et al., 2014). Consequently, it is possible that the sialidase function of NA is involved in two processes: facilitating viral penetration of the mucous barrier downwards to allow virus entry into the mucosal epithelial cells or clearance of the surrounding viscoelastic barrier to enable viral release into the upper mucous layer, promoting viral transmission from host-to-host. Therefore, since filamentous virions have an increased neuraminidase activity compared with their spherical counterparts and can reach up to 30 μm in length, it has been suggested that these viral particles can cross through the periciliary fluid layer (7 μm in depth), invade the upper mucous layer and likely transmit more efficiently than spherical particles (Cox et al., 1980; Dadonaite et al., 2016; Seladi-Schulman et al., 2014) . Furthermore, it was recently reported that HA and NA viral glycoproteins act as motile machinery in IAV and influenza C virus (ICV) that allow the virus to travel along a sugar-coated surface until several HA attach and start viral entry (Sakai et al., 2017; Sakai et al., 2018). Spherical PR8 IAV particles were shown to move randomly in any direction except backwards, as the NA cleaves off the sialic acid. However, a filamentous strain of ICV displayed a more regulated movement in one direction on the surface, thus suggesting that filamentous influenza

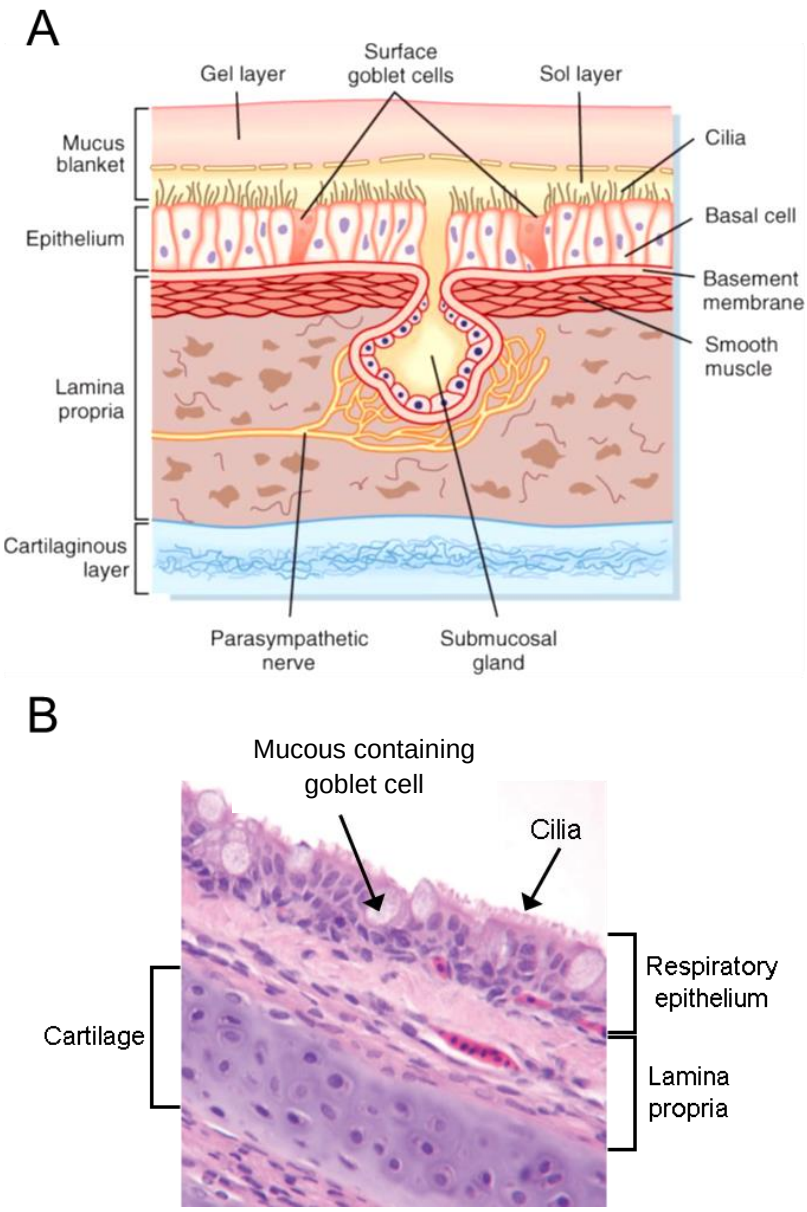

Figure 1.7 Respiratory mucosal membrane. (A) Schematic representation of the respiratory mucosal surface of the lumen-side of the trachea. The mucous blanket is composed of a gel layer that contains mucous (produced by the goblet cells) and mucins which contribute to the high viscoelasticity of the gel layer. This layer also contains immune cells, chemicals and antibodies, providing the first barrier against respiratory pathogens. The sol layer underneath (also termed the periciliary layer) is a more fluid layer that involves the cilia on the surface of the epithelial cells. This layer also contains mucins, though to a lesser extent. The cilia move in a rhythmic beating motion, facilitating movement of the secretions upwards to the central airways (throat) where these are disposed of. These layers make up the respiratory epithelium, which is anchored by a basal membrane on top of the lamina propria that contains the mucus gland. Figure provided by Dr Xiaoyun Yang. (B) Cross section and Haematoxylin and Eosin staining of the tracheal tissue indicating the main areas of the respiratory mucosal membrane. Adapted from Grgic et al., 2008.

virus have an advantage when travelling along the respiratory mucosa when compared with spherical particles.

Another barrier IAV needs to evade when entering a new host is the innate and adaptive immune responses. Upon entry, the virus first encounters physical barriers, such as the mucus barrier. Additionally, an innate immune response is elicited upon recognition of pathogen-associated molecular patterns (PAMPs) by host pathogen recognition receptors, leading to the activation of transcription factors that will turn on interferon (IFN)-stimulated genes (ISGs) (Iwasaki & Pillai, 2014). This response produces IFN and cytokines that compose the first line of the immune response in combination with neutralising antibodies (e.g. IgA or IgM), making this a rapid but unspecific response. The adaptive immune response then starts when antigen presenting cells (APCs) such as dendritic cells present viral antigens to naïve $CD8^+$ T cells and activates these to cytotoxic T lymphocytes (CTLs), which in turn are capable of kill virus-infected cells. Regarding this, two main functions have been hypothesised for filaments: (i) lure the host immune response away from infectious spherical particles or (ii) evade the innate immune response by cell-to-cell transmission (Roberts & Compans, 1998). The first hypothesis was proposed following observations that filamentous particles often lack a complete set of vRNPs, suggesting that these non-infectious particles could act as a "decoy" for neutralising antibodies, allowing the establishment of infection by infectious particles, yet this remains to be confirmed (Vijayakrishnan et al., 2013). On the other hand, filamentous particles were hypothesised to evade the innate immune response (e.g. neutralising antibodies) by cell-to-cell transmission without the need to be released due to their elongated form (Roberts & Compans, 1998). This has yet to be observed; however Roberts et al. showed that filamentous IAV vRNPs can travel to neighbouring naïve cells via intercellular junctions without by manipulating the actin cytoskeleton of the host cell (Roberts et al., 2015).

1.7.2. Viral transmission

In the 1940s, Andrewes and Glover reported that airborne transmission of IAV was possible, as transmission was detected between ferrets in close proximity, at great distances or even in animals placed several centimetres upwards (Andrewes & Glover, 1941). Thereafter,

several studies have reported the ability of mammalian and avian strains of IAV to transmit via respiratory droplets from the respiratory tract of infected animals (Campbell et al., 2014; Herfst et al., 2012; Imai et al., 2012; Lakdawala et al., 2011). However, it still remains unclear the role of the filamentous morphology in this transmission. Of note, clinical isolates of human and veterinary (equine and porcine) origin have revealed the predominant presence of filamentous forms mixed with a smaller amount of spherical particles (Choppin & Tamm, 1960; Chu et al., 1949; Elton et al., 2013; Kilbourne & Murphy, 1960; Nakajima et al., 2010; Seladi-Schulman et al., 2013). Even though true evidence from *in vivo* IAV budding morphology is difficult to obtain, a couple of studies have shown filamentous forms budding out from lung slices *ex vivo*, thus is reasonable to suggest that filamentous forms are produced *in vivo* (Nakajima et al., 2010; Weinheimer et al., 2012). Regarding the morphology of avian influenza isolates, there is only a few reports showing that avian isolates of IAV are composed of filamentous virions, however it remains unclear if that is the predominant phenotype as in the case of mammalian isolates (Al-Mubarak et al., 2015; Pu et al., 2017; Smirnov et al., 1991).

Lakdawala et al. reported that viruses with the NA and M segments of the pandemic H1N1 2009 human strain showed higher neuraminidase activity and a filamentous morphology (Lakdawala et al., 2011). Later, another study showed that insertion of the HA, NA and M segments of a pandemic H1N1 2009 human strain enhanced contact transmissibility of the poorly transmissible PR8 strain in guinea pigs (Campbell et al., 2014). The resultant reassortant virus also showed a filamentous morphology and, in fact, the authors suggested that the M segment and changes in virion morphology are able to modulate NA activity and, therefore, enhance transmissibility. Overall, the studies described here suggest that virion morphology is a complex trait of influenza viruses that deserves more attention.

1.8. Aims of the study

To date, majority of the studies that address virion morphology have focused on mammalian (human, swine or equine) strains of IAV, which we now know display a range of morphologies as described above. However, up to my knowledge, only three reports exist that explicitly address the virion morphology of avian strains of IAV (Al-Mubarak et al., 2015; Pu et

al., 2017; Smirnov et al., 1991). Singly and collectively, these studies fail to elucidate the biological significance of particle shape in avian IAV. For mammalian strains of IAV, it is well established that the M segment is a major determinant of budding morphology and specific amino acid residues within M1 have been proposed to compose a "filamentous signature" that, as the name suggests, can modulate virion morphology and be used as a tool to predict virus behaviour from nucleotide sequence. However, regarding avian strains, it remains unclear whether the M segment is also a determinant of morphology and, if so, whether avian strains also present this or another "filamentous signature" in their M1 gene. Finally, reverse genetics coupled with microscopy studies with the pandemic 2009 strains revealed that the M segment conferred a filamentous morphology to these viruses. This is particularly important because the M segment is derived from an avian strain of IAV that adapted to and circulates in pigs in Europe and Asia (Campitelli et al., 1997). Knowing this and that M1 is the most conserved protein in both avian and human strains of IAV, it is plausible to ask whether avian IAVs could also be filamentous (Furuse et al., 2009).

Therefore, the main aim of this study was to assess the budding morphology of avian strains of IAV and, if filaments are present, determine their biological significance *in vivo*. Chapter 2 addresses the budding phenotype seen with avian IAVs and tests the importance of the M segment in determining virion morphology. The definition of a novel "filamentous signature" is described in chapter 3 and the behaviour of mutant and WT viruses with opposing budding morphologies are characterised *in vitro* and *in ovo* in chapter 4. Lastly, in chapter 5, the biological significance of filaments produced by an avian IAV *in vivo* is addressed. Concluding remarks and future work are presented in chapter 6 and materials and methods in chapter 7.

Chapter 2: Characterisation of avian IAV budding morphology *in vitro*

2.1. Introduction and aims

As discussed in chapter 1, influenza A viruses are able to produce spherical particles of ~ 100 nm in diameter (Chu et al., 1949) and long filamentous virions, with an average diameter of 80 nm that can be up to 30 μm in length (Choppin & Tamm, 1960; Chu et al., 1949; Cox et al., 1980; Morgan & Murphy, 1956; Roberts et al., 1998; Valentine & Isaacs, 1957; Vijayakrishnan et al., 2013). Spherical particles are commonly seen with laboratory-adapted strains that have been serially passaged in cells and/or eggs, such as A/Puerto Rico/8/1934 (PR8) and A/WSN/33 (WSN) (Burnet & Lind, 1957; Kilbourne & Murphy, 1960). Conversely, filamentous virions are predominantly selected *in vivo* and can be found in clinical isolates and/or early egg or cell passage viruses (Choppin & Tamm, 1960; Chu et al., 1949; Nakajima et al., 2010; Seladi-Schulman et al., 2013). These strain-dependent variations in IAV budding morphology are mainly due to sequence polymorphisms in the viral matrix protein M1, encoded by segment 7 (Bialas et al., 2012; Bourmakina & Garcia-Sastre, 2003; Elleman & Barclay, 2004; Elton et al., 2013; Roberts et al., 1998). The M1 protein forms a lattice that underlies the viral envelope and determines particle shape (Noda, 2012). The majority of the IAV virion morphology studies have focused on mammalian strains of the virus, which have identified single amino acid mutations in M1 that can alter particle shape. Within the M1s of human H1N1 and H3N2 strains, the amino acid identity at positions 41, 95, 204, 207 and 218 (Bialas et al., 2012; Bourmakina & Garcia-Sastre, 2003; Elleman & Barclay, 2004; Roberts et al., 1998) have been termed as the "signature" that define filamentous morphology (Elton et al., 2013), with a later addition of position 85 identified in equine H3N8 strains (Elton et al., 2013). However, it remains unclear to what extent this M1-determined filamentous versus spherical pleomorphism applies to avian IAVs.

Therefore, the aim of this part of the study was to characterise the budding morphology of avian isolates of IAV with (if variability was found), the next step correlating M1 sequence polymorphisms with morphology, in order to identify single amino acid substitutions that determined virus particle shape.

2.2. Results

2.2.1. Validation of plant lectin staining as a substitute for antibody stain in fully avian viruses

The most commonly used approach to test whether a given IAV produces filamentous particles is to infect cells and then examine the cell surface by microscopy after the onset of budding (> 6-8 h p.i) for the characteristic filamentous structures (Cox et al., 1980). Typically this is done by confocal microscopy after staining for the viral HA (Roberts & Compans, 1998; Simpson-Holley et al., 2002). The first aim of this part of the study was to test the budding morphology of avian strains of IAV in MDCK cells and characterise their budding phenotype by immunofluorescence assays (IF). However, specific antibodies against the surface proteins for each strain where not available. In order to overcome this, plant lectins were tested as alternatives for staining the surface of infected cells. Plant lectins are carbohydrate-binding proteins that bind both mono- and oligo-saccharides present on glycolipids and glycoproteins (Lagarda-Diaz et al., 2017). These can be found inside or outside the cells, either as soluble or membrane-associated proteins. Although the function of plant lectins remains uncertain, it has been shown that these confer protection against pathogens (Lagarda-Diaz et al., 2017). Lectins are able to bind glycans in proteins. Glycosylation of N-linked proteins starts in the endoplasmic reticulum, continuing in the Golgi complex (Schwarz & Aebi, 2011). The addition of the glycan to newly formed proteins is initiated in the endoplasmic reticulum, where the glycan is transferred to an asparagine residue, designated N-linked or asparagine-linked glycosylation. Further processing of the N-glycan occurs in the Golgi complex, where the glycan is trimmed to its core structure (figure 2.1 A) for posterior addition of carbohydrates. The most common glycan structures found within N-linked glycans are represented in figure 2.1 A (Stanley et al., 2009). The final structure of the glycan determines if the protein will be membrane-bound (i.e. glycoprotein) or secreted (Schwarz & Aebi, 2011; Xu & Ng, 2015).

Upon budding, IAV incorporates the cell membrane and associated proteins into newly produced particles (Berri et al., 2014). Given that cell membranes are rich in carbohydrates (typically as N-linked glycans); plant lectins present a good alternative to replace antibody

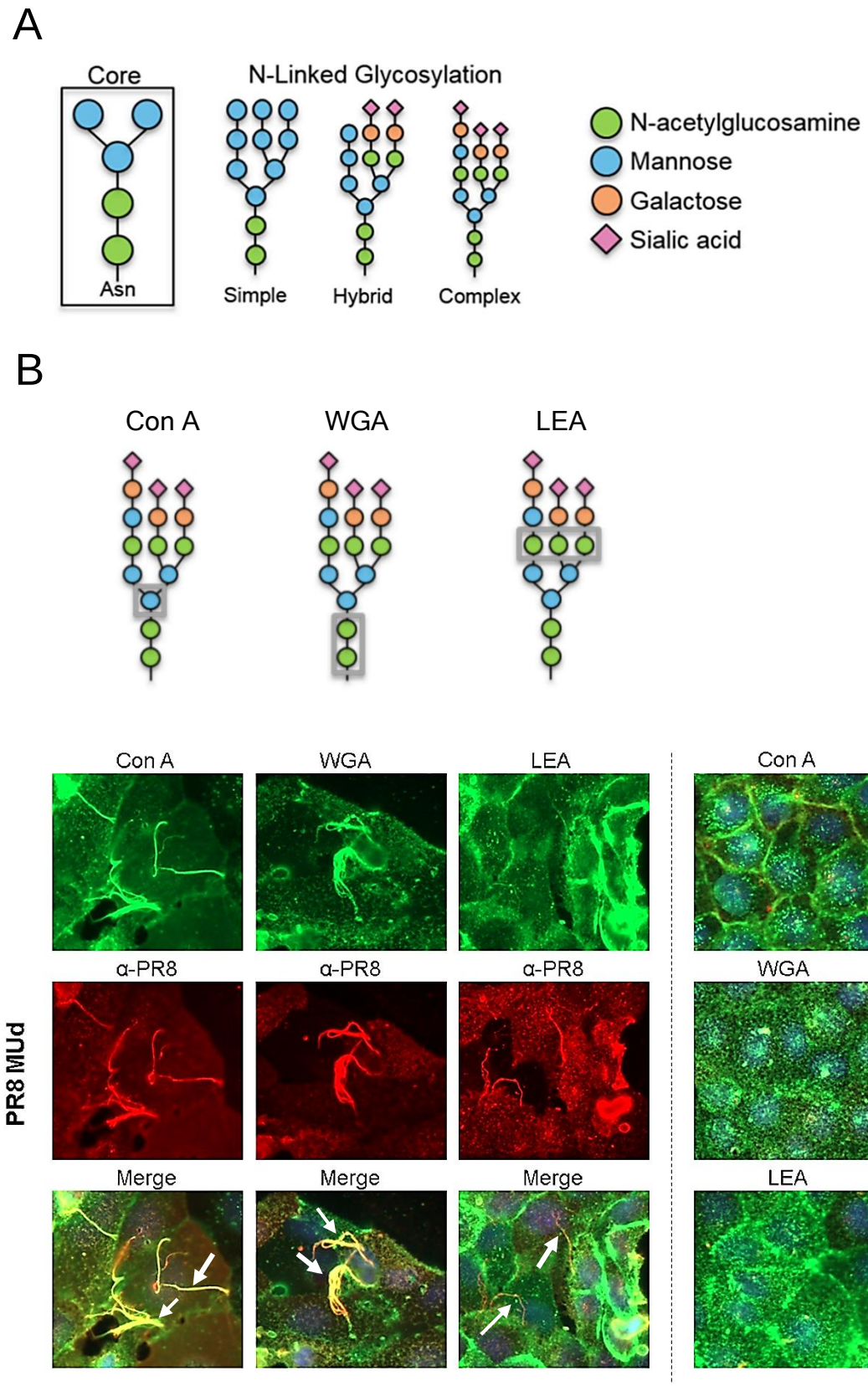
A
Core
N-Linked Glycosylation
Asn
Simple
Hybrid
Complex
N-acetylglucosamine
Mannose
Galactose
Sialic acid
B
Con A
WGA
LEA
Con A
WGA
LEA
Con A
α-PR8
α-PR8
α-PR8
WGA
Merge
Merge
Merge
LEA
PR8 MUd
Mock

Figure 2.1 Validation of plant lectin staining as an alternative to antibody staining. (A) Schematic representation of N-linked glycans. (B) Candidate plant lectins with the recognition sites identified (grey boxes): concanavalin A (Con A), wheat germ agglutinin (WGA) and *L. esculentum* agglutinin (LEA). MDCK cells were infected (or mock-infected) with PR8 MUd virus at a MOI of 3 and fixed 16 h p.i. Cell surface was stained with plant lectins Con A (Alexa 488-conjugated), WGA or LEA (both biotin-conjugated) in green, rabbit anti-PR8-Alexa 594 antibody for viral surface proteins (red staining) and DAPI (blue staining). Biotin-conjugated lectins were detected with a secondary streptavidin-FITC conjugate. Images were collected using the widefield LEICA DLMB microscope with the 40x objective and are representative of two independent experiments. White arrows indicate filamentous bundles.

staining. The main consideration for a successful choice of lectin was based on the fact that its recognition site could not contain sialic acids, as these are cleaved off by the viral NA protein during budding (Els et al., 1989). Therefore, based on this criterion three plant lectins were selected to determine their ability to detect virions on the surface of infected cells. These were from: *Canavalia ensiformis* (Concanavalin A, abbreviation Con A), *Triticum vulgaris* (Wheat germ agglutinin: WGA) and *Lycopersicon esculentum* (*Lycopersicon esculentum* agglutinin: LEA). Their recognition sites within N-linked glycans are represented in figure 2.1 B (Dorscheid et al., 1999; Yi et al., 2001). Con A and WGA lectins are able to recognise the core structure of the glycan, whereas LEA is only able to recognise carbohydrate structures on more complex N-linked glycans.

In order to test the selected lectins, MDCK cells were infected (or mock-infected) with a well-characterised (Beale et al., 2014; Bruce et al., 2010; Bruce et al., 2009; Elton et al., 2013; Noton et al., 2007) filamentous strain previously generated by the Digard laboratory containing segment 7 from A/Udorn/301/72 in the background of A/PR/8/34 (PR8 MUd) at a MOI of 3 and fixed 16 h post infection (p.i.). Prior to imaging, the cells were stained with Con A (Alexa 488-conjugated), WGA (biotin conjugated-streptavidin complex) or LEA (biotin conjugated-streptavidin complex) lectins all in green, rabbit-anti PR8 antibody for PR8 surface proteins (mainly HA) in red and DAPI to delineate the nuclei. As expected, mock-infected cells showed no red staining, while the green lectin staining was dotted and showed a diffused pattern (figure 2.1 B, bottom half), also as expected (Yi et al., 2001). On infected cells, it was possible to observe the characteristic long bundles of filamentous particles produced by the virus, prominently stained with the anti-PR8 antibody in red (figure 2.1 B, white arrows). Obvious colocalization of antibody and lectin (green) happened with Con A and WGA lectins, but not with LEA. This lack of recognition of virions with LEA lectin was unexpected as in theory removal of sialic acid should not have affected the carbohydrate structure it recognises. Nevertheless, these data identified two lectins that could substitute for HA antibody staining as a means of staining viral filaments. Therefore, Con A lectin (488-conjugated) was used throughout the study whenever the viral glycoproteins present on the virus were not of PR8 origin.

Next, the budding phenotype of 7 avian IAV isolates available in the laboratory (Table 2.1, bold strains) was examined. First, MDCK cells were infected with these strains to determine if the cells were permissive to infection with avian IAV isolates. MDCK cells were infected with these isolates at a MOI of 3 for 16 h. Cells were fixed, permeabilised and stained with antibody against viral NP and DAPI to delineate nuclei prior to imaging by confocal microscopy. Z-stacks were taken maximum intensity projections were collected. Expression of viral NP was detected in almost 100% of infected cells, indicating that these avian isolates were able to infect MDCK cells upon high MOI infection (figure 2.2). To determine the budding phenotype of the avian isolates, MDCK cells were infected and the surface stained using Con A staining. In addition, WT PR8 and PR8 MUd were used as controls for viruses with well-defined spherical and filamentous budding morphologies, respectively. MDCK cells were infected with these strains at a MOI of 3 and fixed 16 h p.i.. Cells were stained with Con A lectin and DAPI to indicate nuclei prior to imaging by confocal microscopy. As seen above, mock-infected cells presented punctate foci of Con A staining across the plasma membrane along with apparently more continuous staining of the lateral membranes (Figure 2.3). PR8-infected cells showed a more diffuse pattern of lectin staining with fewer bright puncta but still with staining of the lateral membranes, while PR8 MUd infected cells showed a dramatic reorganisation of Con A staining into long filamentous structures on their surface (Figure 2.3, white arrows). When cells infected with the panel of avian strains of IAV were examined, cells inoculated with the Dk/Singapore, Ck/Israel, Ck/Saudi Arabia and Ck/Italy strains of virus showed a reorganised pattern of surface Con A staining comparable to that seen with WT PR8, suggesting the cells had been successfully infected but were not producing filamentous structures visible by light microscopy. Conversely, infection with Dk/England, Dk/Netherlands and Tk/Canada promoted the formation of long filamentous bundles on the surface of infected cells, similar to what was isolates, both filamentous and non-filamentous budding could be observed. Overall, these data allowed the detection and classification of viral morphology for a number of avian isolates and suggested that these can be as pleomorphic as mammalian IAVs.

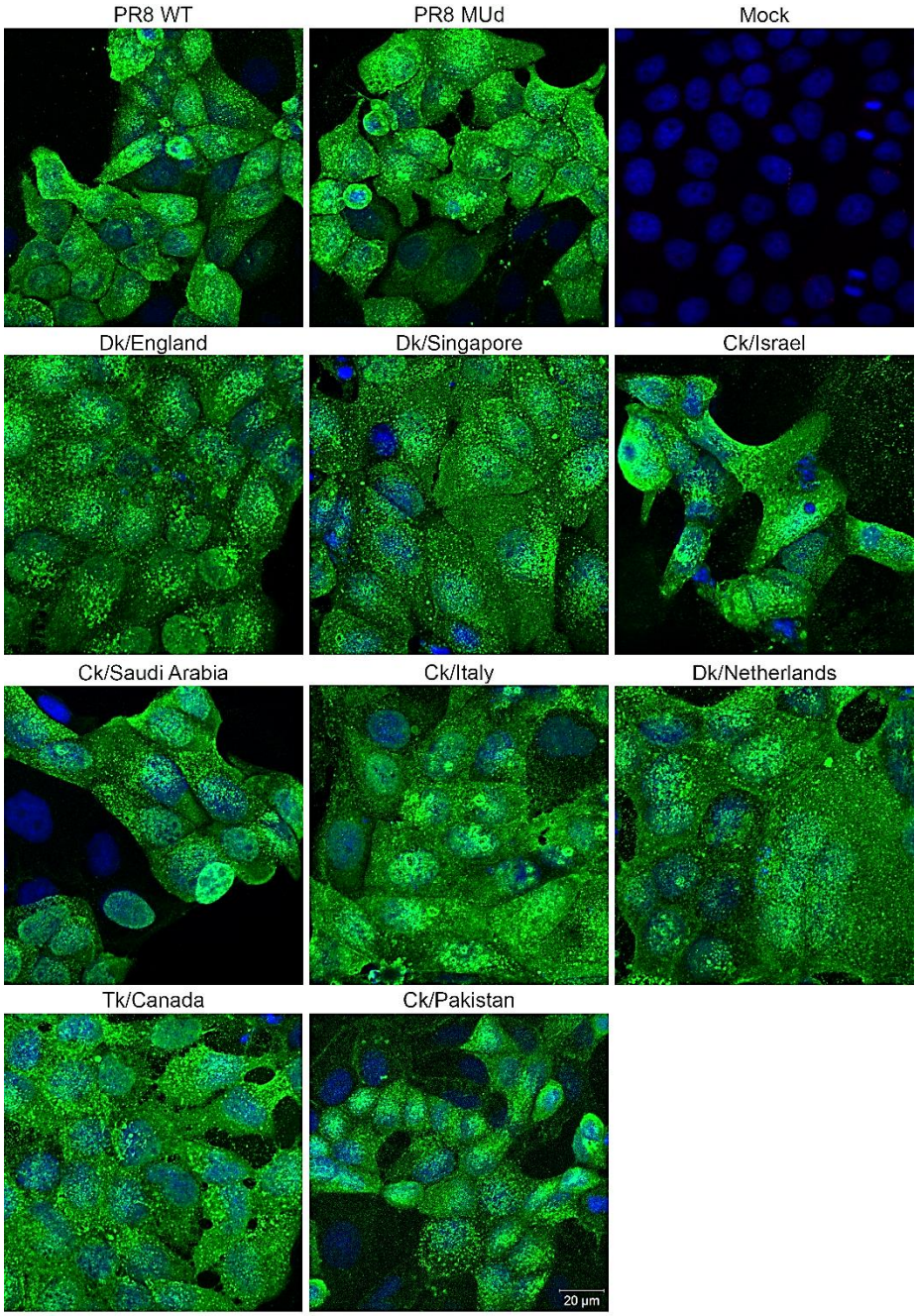

Figure 2.2 Detection of infectivity of avian strains in MDCK cells. Cells were infected with the viral strains indicated at a MOI of 3, fixed 16 h p.i and permeabilised. Cells were stained with mouse anti-NP antibody (green staining) and DAPI (blue staining) prior to imaging. Images were collected using the Zeiss 710 confocal with a 63x objective and are representative of three independent experiments. Images represent maximum intensity projections from Z-stacks.

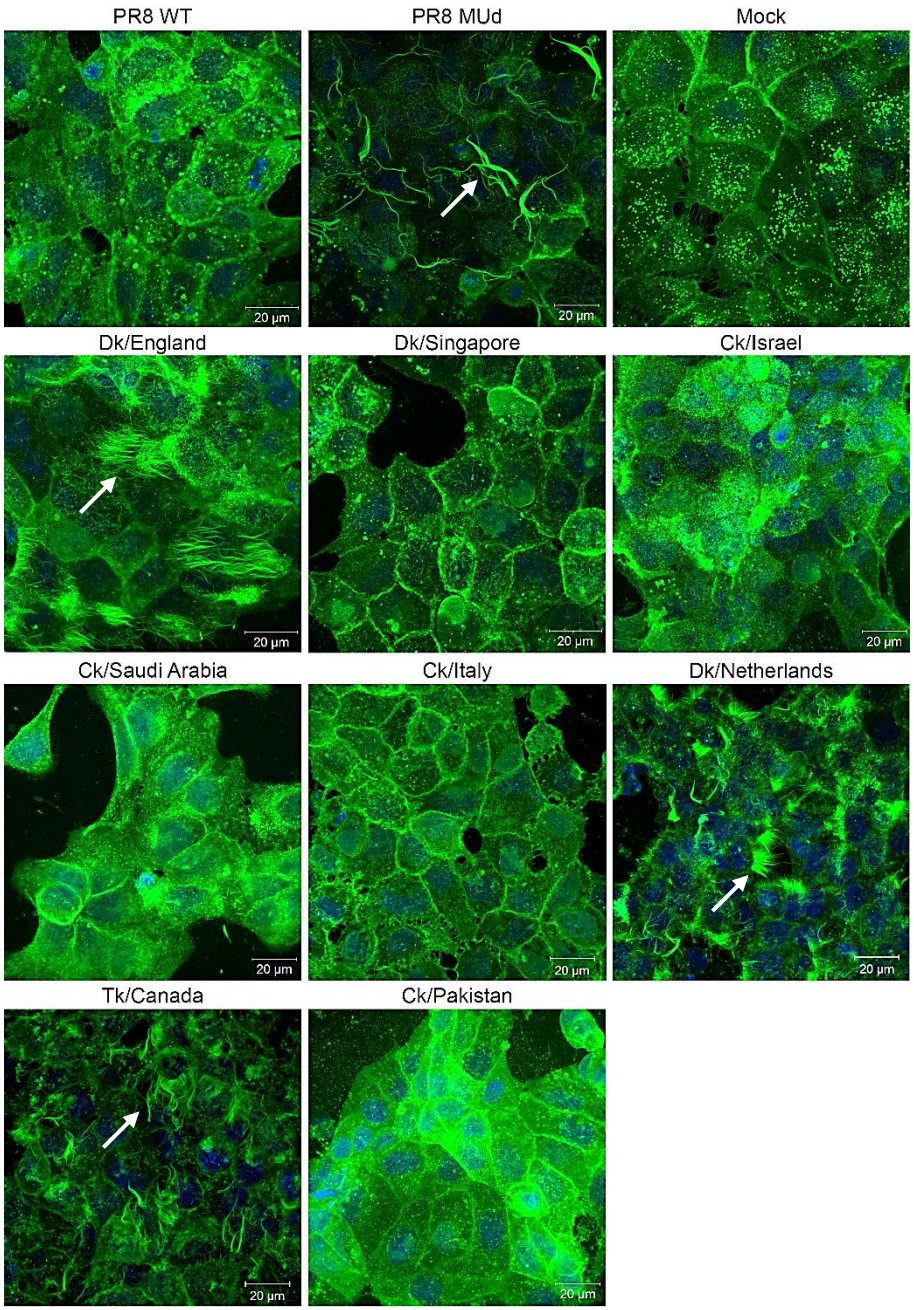

Figure 2.3 Determination of the budding phenotype of avian IAV strains by IF. MDCK cells were infected (or mock-infected) with the indicated viruses at a MOI of 3 for 16 h before fixation. Plant lectin Con A was used to stain surface carbohydrates (green) and DAPI used to stain nuclei (blue). PR8 WT and PR8 MUd viruses were used as positive controls for spherical and filamentous budding, respectively. Images were collected on the Zeiss 710 confocal microscope with a 63x objective and are representative of three independent experiments. Images represent maximum intensity projections from Z-stacks. Filamentous bundles present on the surface of infected cells are indicated by white arrows. Scale bar (20 µm) indicated.

2.2.2. Segment 7 is the major determinant of budding morphology

A small panel of avian IAVs showed a mix of budding phenotypes that did not obviously correlate with passage history (Table 2.1, bold strains), suggesting that filamentous budding might be a less common trait for avian viruses. However, it was desirable to test a larger and wider range of viruses before making further conclusions. The variety of HA and NA subtypes and the biosafety rules required to work with highly pathogenic avian IAVs, as well as strain availability presented as limiting steps to characterisation of a panel that would be representative of avian strains. To overcome this, using 7:1 reassortant viruses with segment 7 of avian strains in a PR8 backbone was considered. As discussed in more detail in chapter 1, budding morphology studies on mammalian IAVs have often focused on 7:1 reassortant viruses, typically with segment 7 of a filamentous strain in a spherical strain backbone (Bourmakina & Garcia-Sastre, 2003; Elleman & Barclay, 2004; Elton et al., 2013). From these studies, it became clear that the viral matrix protein M1 encoded by segment 7 is a strong determinant of budding phenotype. However, in addition to segment 7, other studies have identified segments 4 (HA), 5 (NP) and 6 (NA) as capable of modulating morphology of IAVs (Bialas et al., 2014; Chlanda et al., 2015; Jin et al., 1997; Liu et al., 2002). Segment 5 was shown to inhibit filament formation in the context of an avian isolate (Bialas et al., 2014). In contrast, segments 4 and 6 were shown to modulate filament size and formation (Chlanda et al., 2015; Gomez-Puertas et al., 2000). Chlanda et al suggested that NA in particular plays an important role in filamentous particle assembly and release, shown by electron microscopy of membranes of transfected 293T cells (Chlanda et al., 2015). Thus, to test this in our system, we took advantage of the fact that the filamentous Dk/Netherlands virus tested above was made by reverse genetics from a complete set of cloned segments (kindly provided by Dr Laurence Tiley), which were also available in the laboratory. Accordingly, reassortant viruses with segments 4, 5, 6 and 7 individually or in combination in a PR8 backbone were built to determine the importance of these segments on the morphology of avian IAVs.

Firstly, 293T cells were transfected with reverse genetics plasmids (pDUAL) of segments 4, 5, 6 and 7 of Dk/Netherlands strain (Bourret et al., 2013) individually or in combination in the backbone of PR8 to generate P0 stocks (section 7.2.3.1). The fully avian

Dk/Netherlands virus was also similarly rescued. A positive control rescue with PR8 WT and a negative control lacking a PB1 plasmid and thus unable to generate infectious particles, were also included. Generation of P1 stocks consisted of infecting MDCK cells with the P0 stocks for 48 h. Throughout the courses of infection, CPE was monitored using microscopy and compared to cells inoculated with the supernatant from the negative control (lacking PB1) cells to determine if the rescues were successful or not. The P1 viruses were titrated by plaque assay. All viruses were rescued twice independently, with titres ranging 10^5-10^8 PFU/ml (figure 2.4 A). Reassortant viruses with (HA NP M), (HA M NP), (HA NA) and (M HA NA) were associated with more difficult rescues and lower titres. Thus, as a further measure of viral fitness, plaque phenotype was done in monolayers of MDCK cells under avicel. Cells were fixed, permeabilised and plaques visualised by immunostaining for viral NP (Figure 2.4 B). The viruses that showed the smallest plaques were the ones described before as difficult to rescue, which suggest that these viruses do not spread well on a monolayer of cells.

To determine the importance of segments 4, 5, 6 and 7 in the budding morphology of avian IAVs, the reassortants and parental WT viruses rescued were used to infect MDCK cells at a MOI of 3 for 16 h. Cells were fixed and stained for surface carbohydrates as described previously (Figure 2.5). Since all reassortants were made with the non-filamentous PR8 strain backbone, PR8 WT-infected cells were used as a morphology control. As before, mock-infected cells showed a dotted and diffused pattern of Con A staining, while cells infected with PR8 WT showed the more irregular distribution of lectin staining associated with infection by a virus with a spherical phenotype. Next, the budding morphologies of the 7:1 reassortant virus with segment 7 of Dk/Netherlands in a PR8 backbone (PR8:Dk/Netherlands M) and Dk/Netherlands WT were determined. Both viruses showed a filamentous phenotype with many elongated bundles of particles present on the surface of the cells (Figure 2.5, white arrows). However, although obviously filamentous, PR8:Dk/Netherlands M reassortant virus produced fewer bundles of filamentous virions when compared with Dk/Netherlands WT. Thus, it appeared that other viral proteins along with M1/M2 promoted a stronger filamentous budding phenotype. Individual PR8 7:1 reassortant viruses with Dk/Netherlands segments 4, 5 or 6 showed a Con A staining pattern comparable to WT PR8, as well as 6:2 reassortant with both HA and NA from the avian virus,

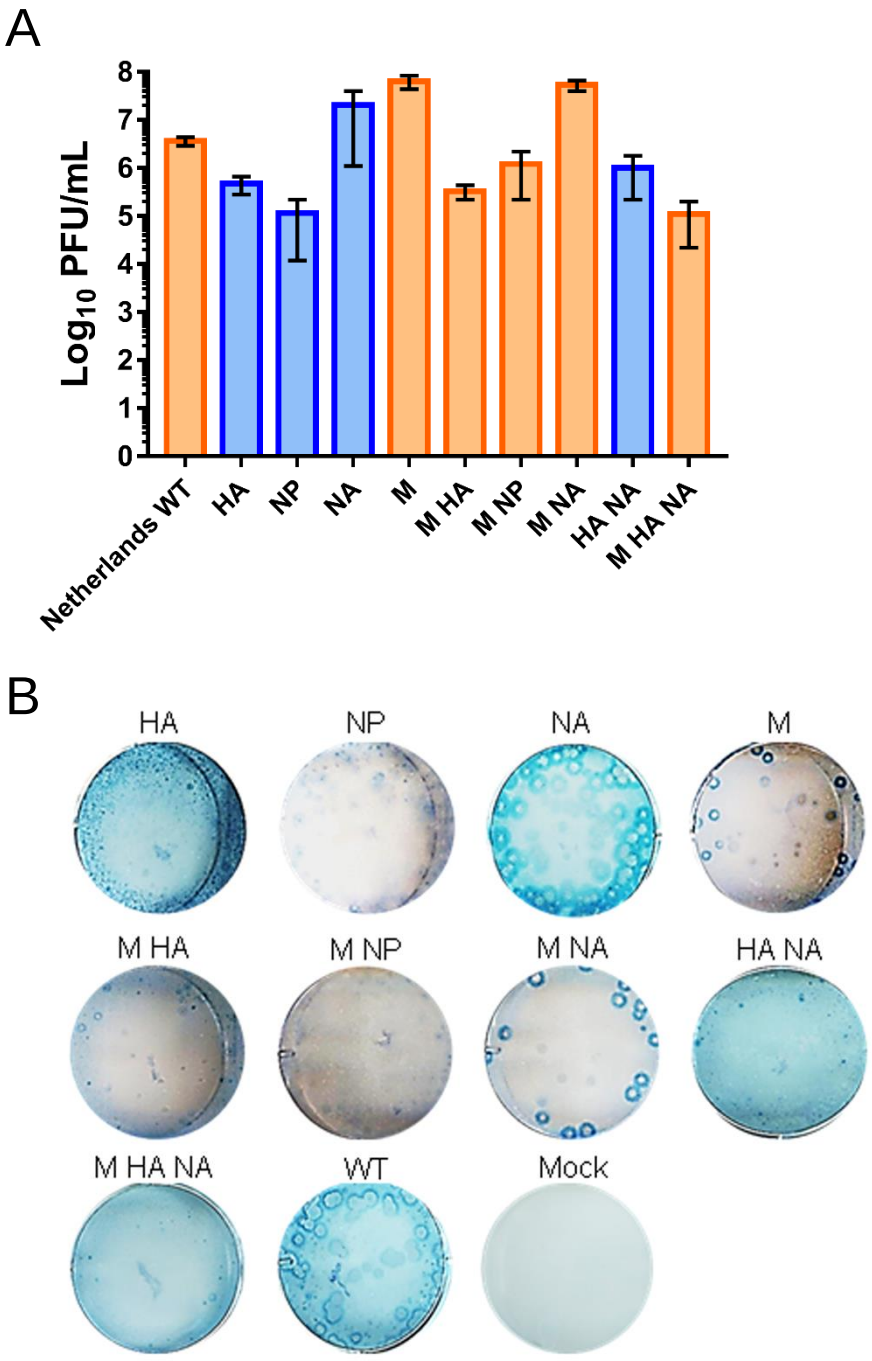

Figure 2.4 Replication phenotypes of reassortant viruses between Dk/Netherlands and PR8. (A) MDCK cells were infected with 1:10 dilutions of P0 stocks and left for 48 h before supernatants were collected and plaque titred on MDCK cells. Data represent mean +/- SEM (n = 2) from two independently rescued stocks of viruses. Blue bars indicate viruses with a spherical budding phenotype while orange bars represent filamentous viruses (see later). (B) Plaque phenotypes were assessed in monolayers of MDCK cells under Avicel. Cells were permeablised, stained with antibody against NP and plaques detected with horseradish peroxidase

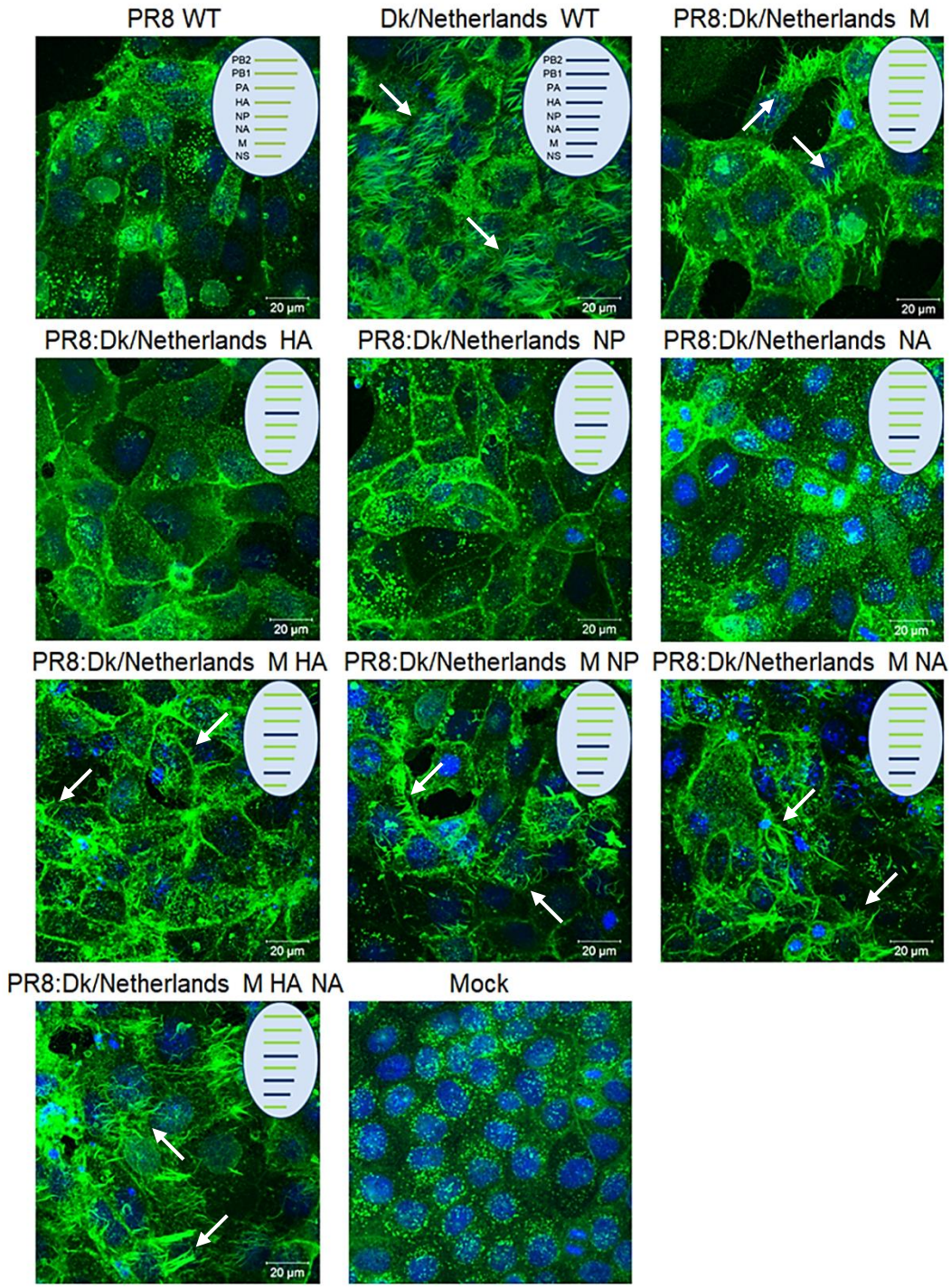

Figure 2.5 Budding phenotypes of reassortant viruses between Dk/Netherlands and PR8. WT or reassortant viruses with the indicated segments of Dk/Netherlands (blue lines) in a PR8 backbone (green lines) were used to infect MDCK cells at a MOI of 3 and fixed 16 h p.i.. Cells were stained with Con A (green) for surface carbohydrates and DAPI (blue) prior to imaging on a Zeiss LSM710 confocal microscope with a 63x objective. Images were collected as maximum intensity projections and are representative of three independent experiments. Arrows indicate bundles of filaments. Scale bar (20 µm) indicated.

suggesting a spherical budding phenotype had been maintained. On the other hand, when the Dk/Netherlands segment 7 was added to these reassortants to produce 6:2 viruses or a 5:3 with HA, NA and M, filamentous bundles were observed on the surface of the cells, but the reassortant with Dk/Netherlands M HA and NA was the virus that showed the phenotype closest to Dk/Netherlands WT.

In order to provide a more quantitative measure of the IAV filamentous budding phenotype, the confocal images were used to determine the percentage of filament- producing cells and the filament bundle size. For the first metric, a minimum of 80 infected cells were scored per virus over three independent experiments with 2 separate rescues for the presence or not of at least one bundle of filaments and the % of filament- producing cells determined. For the filament length, 20 filament bundles (when visible) produced by the cells were measured from each of three independent experiments (see chapter 7, section 7.2.7, figure 7.3). WT Dk/Netherlands showed approximately 100% of infected cells producing filaments (Figure 2.6), whereas all the reassortant viruses without Dk/Netherlands segment 7 (M) showed predominantly a spherical phenotype, with only a few cells displaying filamentous structures (blue bars). The addition of the avian virus segment 7 to the PR8 backbone resulted in about 50% of infected cells producing filaments. This percentage was significantly increased by the addition of NP (segment 5) and the glycoproteins HA and NA (segments 4 and 6, respectively); however, only the 5:3 reassortant PR8:Dk/Netherlands M HA NA virus induced a filamentous budding in a comparable percentage of infected cells to Dk/Netherlands WT. When the sizes of the viral filaments were considered, it was observed that all reassortants with M segment of Dk/Netherlands strain induced the formation of filamentous bundles that ranged between 7-10 μm (Figure 2.6 B). WT Dk/Netherlands and PR8 reassortant viruses with Dk/Netherlands M and NA and M, HA and NA showed equivalent lengths, while reassortant viruses with M, M and HA and M and NP all formed significantly smaller filamentous bundles on the surface of the cells, suggesting that NA played a role in determining filament length.

Taken together, these data suggested that segment 7 could be a major morphology determinant for avian strains of IAV, as the 7:1 reassortant with segment 7 of Dk/Netherlands in a PR8 backbone showed a prominent filamentous phenotype. Furthermore, the addition of

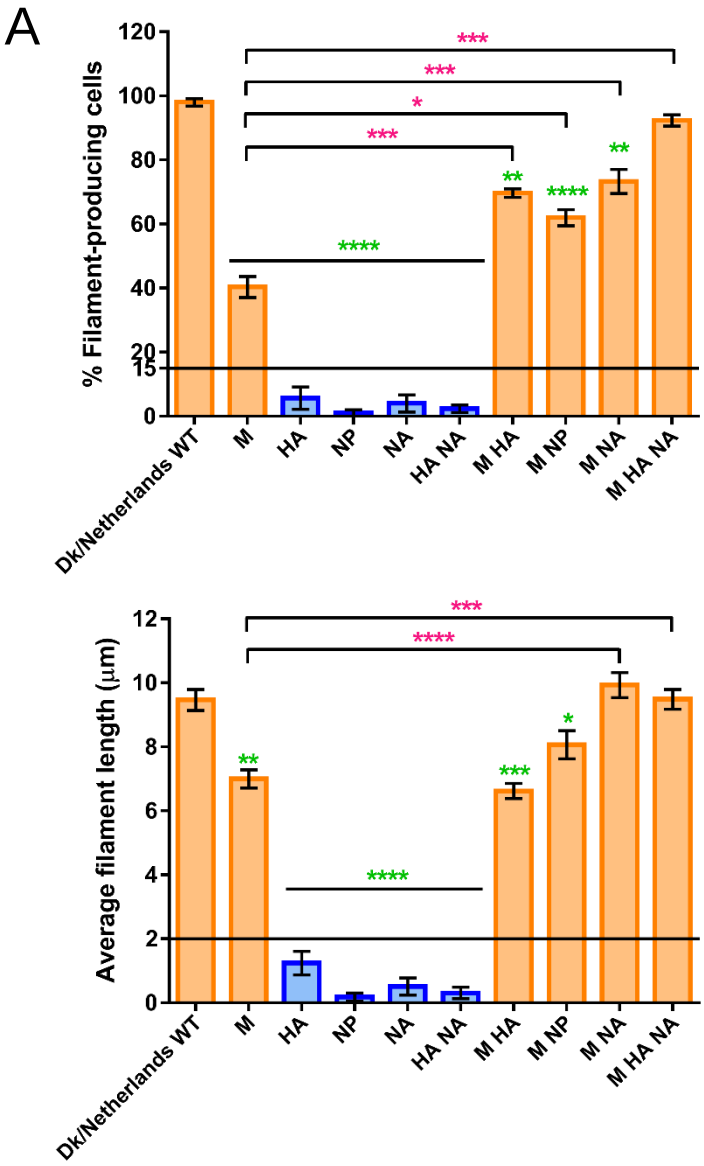

Figure 2.6 Quantification of the budding phenotypes of reassortant viruses between Dk/Netherlands and PR8. WT or reassortant viruses with the indicated segments of Dk/Netherlands in a PR8 backbone were used to infect MDCK cells at a MOI of 3 for 16 h. (A) A minimum of 80 infected cells were counted per virus and the percentage of filament-producing cells was determined. (B) 60 filaments were measured per virus (when visible). Data are the mean +/- SEM (n = 3). ANOVA statistical analysis was used to compare all viruses against Dk/Netherlands WT (green asterisks) and compare all reassortants with M (pink asterisks) individually or in combination with HA, NP and/or NA. * $p<0.05$; ** $p<0.01$; *** $p<0.001$; **** $p<0.0001$. Limits for viruses to be classified as possessing a filamentous budding morphology are indicated (> 15% of infected cells producing at least one bundle of filaments of 2 µm or longer). Bars are colour coded for spherical (blue) and filamentous (orange) morphology.

segments 4 (HA), 5 (NP) and 6 (NA) resulted in modulation of the filamentous phenotype, by increasing the number of cells producing visible filamentous bundles on their surface. Additionally, the presence of segments 4 (HA) and 6 (NA) promoted the formation of longer filamentous particles, as previously reported by Chlanda et al. with human strains of IAV (Chlanda et al., 2015). However, although the addition of other avian virus segments to the PR8 reassortant with the foreign segment 7 modulated the budding phenotype closer to Dk/Netherlands WT, segment 7 by itself determined filament production, confirming the value of 7:1 reassortant viruses to virion morphology studies. This allowed characterisation of avian IAV morphology to proceed based on testing 7:1 reassortant viruses, therefore eliminating constrains on the selection of avian IAVs.

2.2.3. Determination of the budding phenotype of IAVs through characterisation of PR8-based 7:1 reassortant viruses with segment 7s from avian strains

To further characterise the budding morphology of avian IAVs, several segment 7s were selected and used to rescue 7:1 reassortant viruses in a PR8 backbone. Several avian virus segment 7s were already available within the laboratory from other projects. However, to more systematically choose candidate viruses to donate their M genes, complete nucleotide sequences of segment 7 were collected from the online Influenza Research Database in May of 2016. From a sample of 8,000+ sequences, a subsample of 2000+ was selected based on HA sequence diversity, the nucleotide sequences aligned using MEGA6 and grouped into a phylogenetic tree using the neighbour-joining algorithm with 100 bootstraps (Hillis & Bull, 1993). The scripts necessary to this analysis were built using R by Dr Samantha Lycett. Grouping M1 sequences by phylogeny resulted in a tree that showed two main branches: one composed mainly of samples from Eurasia and the other branch formed of samples collected in the American continent (Figure 2.7). For clear visualisation, countries that represented Europe (blue), Asia (blue) and American (red) continents were colour coded. The next step

was to divide this tree further into clades, where Eurasia contained clades 1 to 6 and America contained clades 7 to 11. The avian strains already tested (Figure 2.2) and the segment 7s already available were fitted into these clades. Then, for the clades with no representation at least one segment 7 was randomly selected for gene synthesis. Exclusively, A/Zhejiang/DTID-ZJU01/2013 (H7N9) was of human-origin isolated during the 2013 epidemic in China (Chen et al., 2013), but the sequence of the M gene in this virus is identical to that of a contemporary virus isolated from a live bird market in the same area, A/chicken/Zhejiang/DTID-ZJU01/2013 (Li et al., 2014), so for the purpose of this study the segment was considered as Ck/Zhejiang. The final sample of segment 7s included a variety of HA and NA subtypes from across the world collected over the last 50 years (Table 2.1).

Following selection, the segment 7s were commercially synthesised or kindly provided by colleagues in the laboratory. For brevity, segments/viruses were named after the host species and the country/city where the avian strain was collected (Table 2.1). The synthesised segments were then subcloned into the pDUAL vector plasmid to proceed with reverse genetics. As described before, generation of P0 stocks of 7:1 reassortant viruses with segment 7 of avian strains in a PR8 backbone was performed in 293T viruses with segment 7 of avian strains in a PR8 backbone was performed in 293T cells. These P0 stocks were then propagated once on MDCK cells (P1) and titrated by plaque assay to use thereafter. WT PR8 and PR8 MUd were also rescued in parallel because these viruses were important morphology controls for this study. All viruses rescued readily twice, with the exception of the PR8:Ck/Penn/1. This reassortant rescued once and it was not possible to rescue it again. More than 10 rescues were attempted in either mammalian (293T) or avian cells (QT-35 and DF-1). Ck/Penn/1 HA with an altered polybasic cleavage site (due to the high pathogenic nature of Ck/Penn/1) along with NA were used to rescue 6:2 and 5:3 reassortants but with no success. Moreover, from clade 3, the first avian strain selected – A/duck/Zhejiang/925169/2014 (H5N8) – was not possible to rescue the PR8-based 7:1 reassortant virus with the segment 7 of the avian virus. Further attempts were performed as 6:2 reassortants with Dk/Netherlands HA or NA and 5:3 with Dk/Netherlands HA and NA and the internal genes of PR8, but with no success. Accordingly, further viruses were chosen from clade 3, synthesised, cloned and

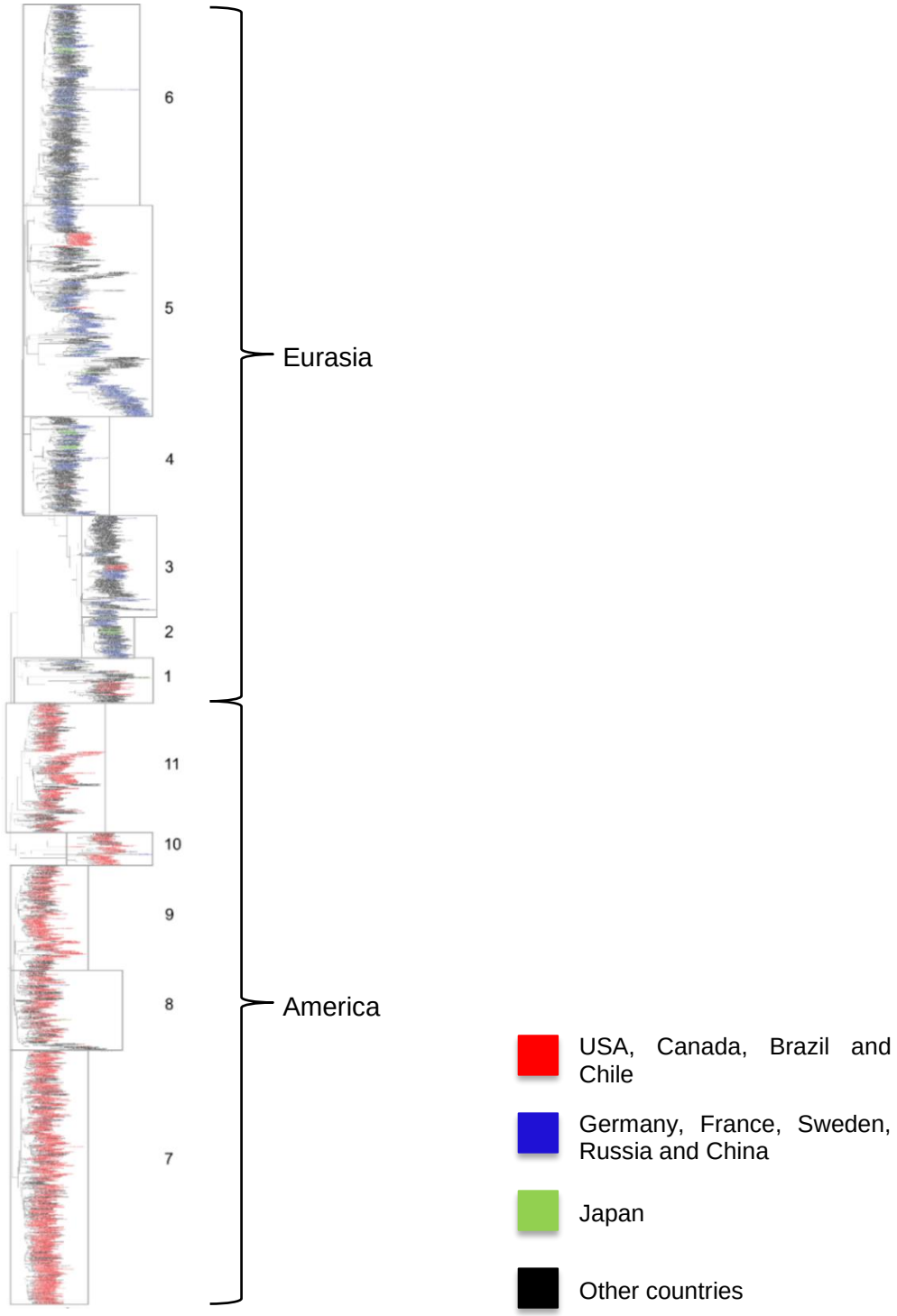

Figure 2.7 Phylogeny of viral matrix protein M1 from avian strains. More than 8,000 segment 7 sequences were retrieved from Influenza Research Database and a subsample of approximately 2000 sequences were aligned and organised into a phylogenetic tree based on the nucleotide sequence of M1. The tree showed two main branches: Eurasia and America continents with the countries that represent each branch colour coded as red for countries of the American continent and blue and green for countries of Eurasia, while black represent other countries. The phylogenetic tree was done with the help of Dr Sam Lycett.

Table 2.1 IAV strains used in this study. One or more segment 7s were selected from each of the clades of the phylogenetic tree from the avian viruses indicated. Fully avian viruses are represented in bold and are referred as isolate. Origin of the virus and passage history is indicated. RG indicate viruses from reverse genetics. Top two mammalian strains were used as controls throughout this study. Avian strains at the bottom of this table (below the second bold line) were added to strengthen the bioinformatics analysis performed in section 3.2.

Full name	Abbreviation	Subtype[1]	Clade	Distribution	Origin	Passage history	Reference or accession number
A/Puerto Rico/8/1934 (mammalian)	PR8	H1N1	-	-	RG	High (various)	Francis, 1934
A/Udorn/1972 (mammalian)	PR8 MUd	H3N2	-	-	7:1 RG	-	Noton et al., 2007
A/duck/England/1962	Dk/England	H4N6	1	Eurasia	Isolate	Low	GQ404577
A/duck/Korea/GJ54/2004	Dk/Korea	H5N2	1	Eurasia	7:1 RG	Isolate	GU351861
A/duck/India/02CA10/2011	Dk/India	H5N1 (HP)	2	Eurasia	7:1 RG	Isolate	Kumar et al., 2017
A/duck/Tripura/103597/2008	Dk/Tripura	H5N1 (HP)	2	Eurasia	7:1 RG	Isolate	Kumar et al., 2017
A/duck/Shandong/Q1/2013	Dk/Shandong	H5N6	3	Eurasia	7:1 RG	Isolate	KM504104
A/duck/Dongguan/2685/2013	Dk/Dongguan	H5N8	3	Eurasia	7:1 RG	Low	KP285008
A/Duck/Shantou/1588/2000	Dk/Shantou	H9N1	4	Eurasia	7:1 RG	Isolate	AF523499
A/chicken/Pakistan/UDL-01/2008	Ck/Pakistan	H9N2	5	Eurasia	WT/7:1 RG	Isolate	Iqbal et al., 2013
A/duck/Singapore/5/1997	Dk/Singapore	H5N3	5	Eurasia	Isolate	Low	GU052803
A/chicken/Israel/215/2007	Ck/Israel	H9N2	5	Eurasia	Isolate	Low	Wang et al., 2016
A/Zhejiang/DTID-ZJU01/2013	Ck/Zhejiang	H7N9	5	Eurasia	7:1 RG	Human isolate[2]	KC885959
A/chicken/Saudi Arabia/SP02525/3AAV/2000	Ck/Saudi Arabia	H9N2	5	Eurasia	Isolate	Low	de Geus et al., 2011

A/chicken/Italy/1067/1999	Ck/Italy	H7N1 (HP)	6	Eurasia	Isolate/7:1 RG	Low	Molesti et al., 2013
A/duck/Mongolia/200/2015	Dk/Mongolia	H3N8	6	Eurasia	7:1 RG	Low	LC339876
A/mallard/Netherlands/10-Cam/1999	Dk/Netherlands	H1N1	6	Eurasia	WT/7:1 RG	Moderate (various)	Bourret et al., 2013
A/mallard/Wisconsin/1719/1983	Dk/Wisconsin	H4N2	7	America	7:1 RG	Isolate	CY179300
A/mallard/New York/170/1982	Dk/New York	H1N2	8	America	7:1 RG	Isolate	CY014902
A/chicken/Pennsylvania/1/1983	Ck/Penn/1	H5N2	9	America	7:1 RG	Isolate	Kawaoka & Webster, 1985
A/chicken/Pennsylvania/1370/1983	Ck/Penn/1370	H5N2 (HP)	9	America	7:1 RG	Low	Swayne, 2006
A/turkey/Canada/1965	Tk/Canada	H3N2	9	America	Isolate	Low	GU052877
A/gull/Maryland/1824/1978	Gull/Maryland	H13N9	10	America	7:1 RG	Low	JX982948
A/turkey/South Dakota/7034/1986	Tk/South Dakota	H1N1	11	America	7:1 RG	Low	EU743168
A/chicken/Shandong/lx1023/2007	Ck/Shandong	H9N2	5	Eurasia	Isolate	Low	Pu et al., 2017
A/chicken/Jiangsu/TS/2010	Ck/Jiangsu	H9N2	5	Eurasia	Isolate	Low	Pu et al., 2017
A/mallard duck/England/7277/2006 [3]	Dk/England/06	H2N3	1	Eurasia	Isolate	Low	Al-Mubarak et al., 2015

[1]HP indicates the parental virus has a HPAI phenotype.

[2]Human isolate collected during the 2013 epidemic in China (Chen et al., 2013).

[3]Kindly provided by Dr Janet Daly (University of Nottingham).

rescued as before. Of the viruses which would rescue, average titres were approximately 10^8 PFU/ml, with no significant differences between the reassortants (Figure 2.8 A). However, clear differences in plaque size were noticeable between some of the strains (Figure 2.8 B); PR8 produced large plaques, as did some of the reassortants (*e.g.* Ck/Zhejiang and Ck/Pakistan), while others produced smaller ones (e.g. PR8 MUd and Gull/Maryland), indicating subtle differences in replication fitness *in vitro*.

To determine the budding morphology of these 7:1 reassortant viruses, MDCK cells were infected at a MOI of 3 and fixed 16 h p.i. Cells were stained with antibody against whole PR8 virions (green), which mainly detects HA, and DAPI for nuclei (blue). As expected, mock-infected cells showed no signs of infection, only giving background staining associated with the *in-house* made nature of the polyclonal anti-PR8 antibody. WT PR8 and PR8 MUd reassortant viruses were used as spherical and filamentous positive controls. PR8 WT-infected cells showed an evenly distributed green staining, while cells infected with PR8 MUd showed the characteristic filamentous bundles on the surface of the cells (Figure 2.9). The PR8-based 7:1 reassortants with segment 7 of Dk/Korea, Dk/Tripura, Dk/Dongguan, Dk/Shantou Dk/Netherlands, Dk/Mongolia, Dk/Wisconsin, Dk/New York, Ck/Penn/1370, Gull/Maryland and Tk/South Dakota induced the formation of long filamentous bundles on the surface of the cells, comparable to PR8 MUd but rather shorter filaments. Cells infected with the 7:1 reassortants with the segment 7s from Dk/India, Dk/Shandong, Ck/Pakistan, Ck/Zhejiang, Ck/Italy and Ck/Penn/1 did not alter the evenly distributed staining characteristic of spherical budding phenotype as seen with the PR8 WT.

In order to better define the budding phenotype of the virus strains tested, cell counts and filament measures were performed. MDCK cells were infected three times with two independent rescues, stained as described before (Figure 2.9) and two maximum intensity projections were collected per experiment for subsequent counting. The threshold previously defined (Figure 2.6) where a virus was considered filamentous if more than 15% of infected cells produced filaments of at least 2 μm in length was applied. As observed previously, PR8 WT fell below the threshold to be considered a filamentous strain, whereas PR8 Mud virus was

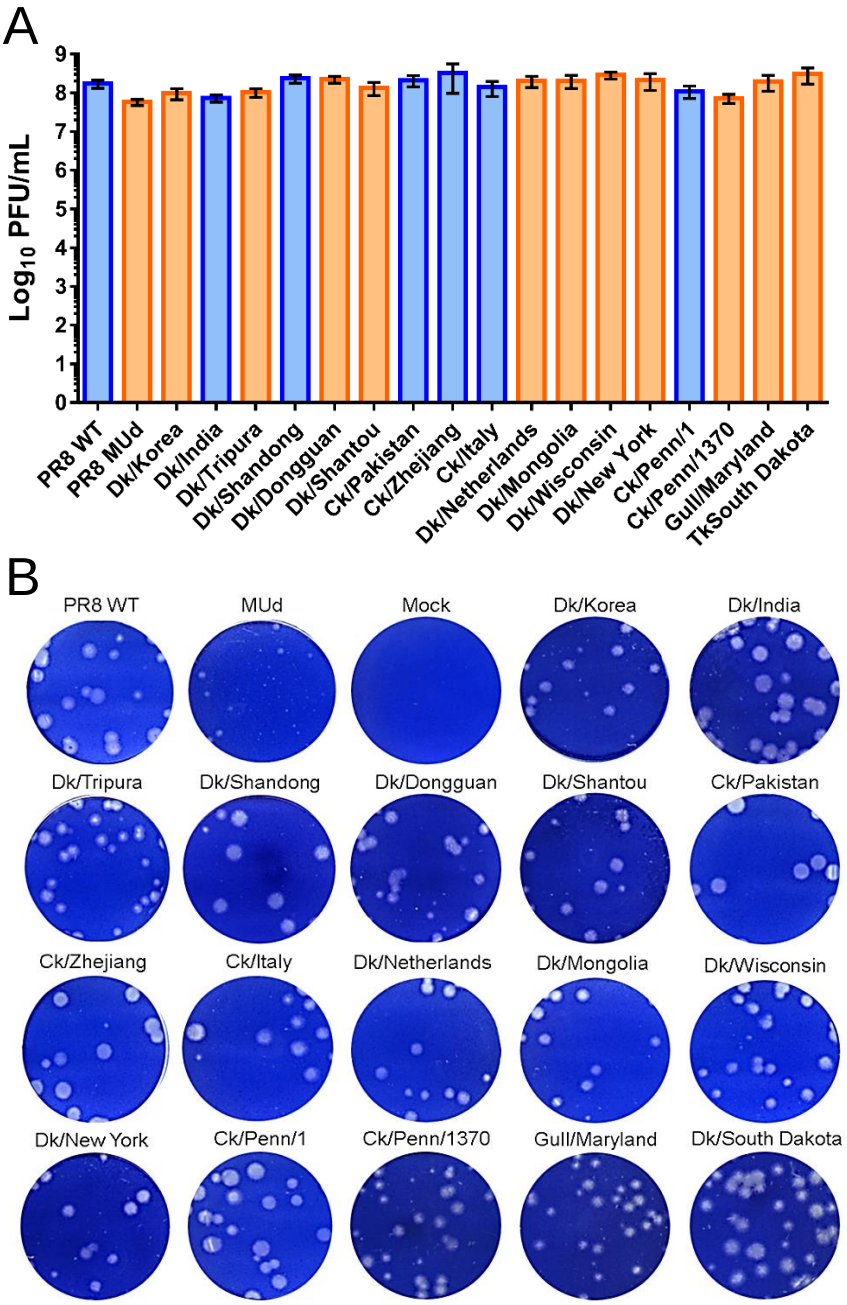

Figure 2.8 Replication phenotypes of PR8 7:1 reassortants with the selected avian M segments. (A) MDCK cells were infected with 1:10 dilutions of P0 stocks and left for 48 h before supernatants were collected and plaque titred on MDCK cells. Data represent mean +/- SEM (n= 2) from two independent rescues, with the exception of Ck/Penn/1 which was only possible to rescue once. Numerous attempts were performed in avian and mammalian cells and/or with HA and NA of Ck/Penn/1 but with no success. Colour coding divides the viruses in spherical (blue) and filamentous (orange) budding phenotypes (see later). (B) Plaque phenotypes were visualised in infected monolayers of MDCK cells under Avicel which were fixed and stained with toluidine blue.

MDCK

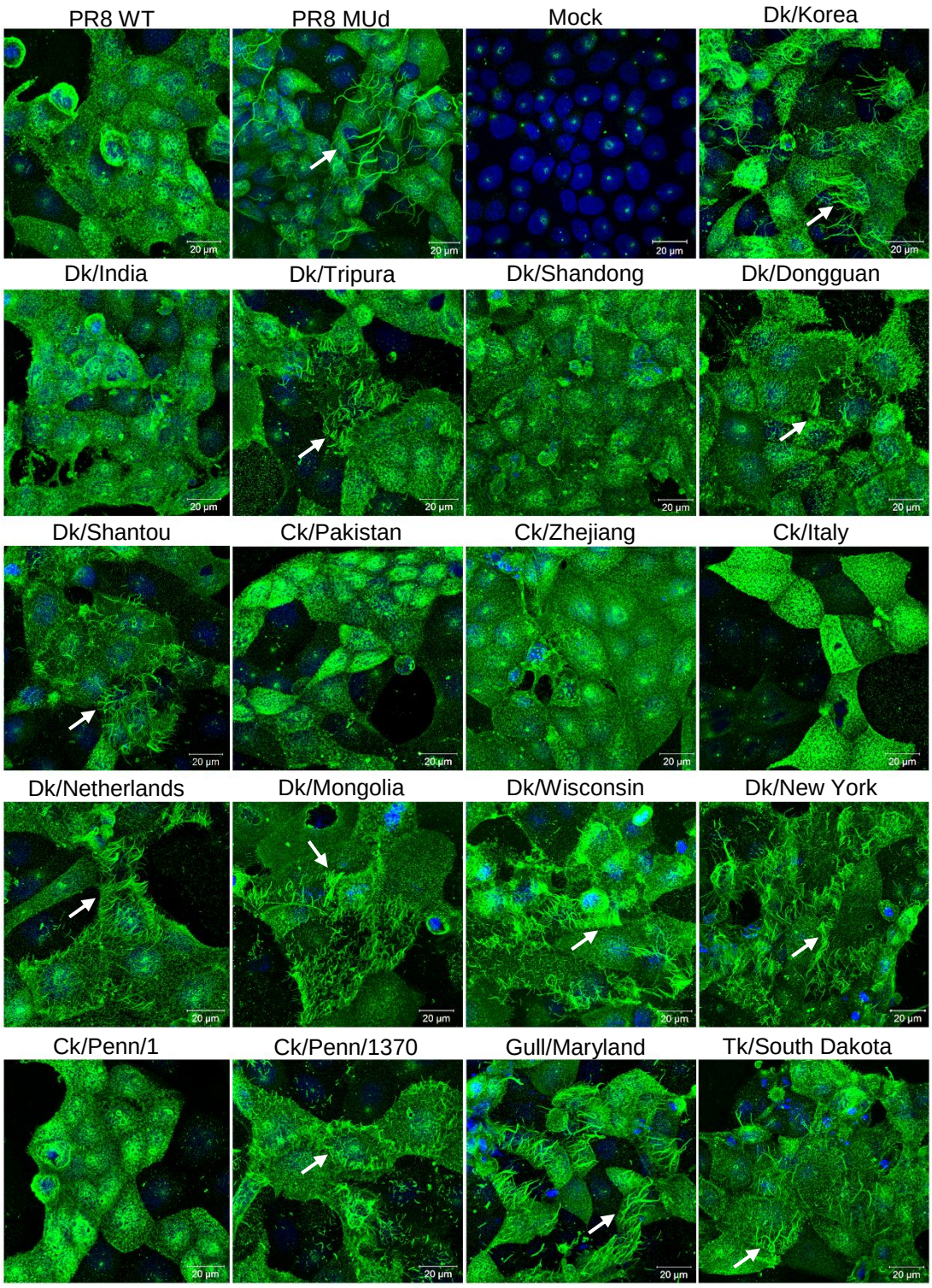
PR8 WT
PR8 MUd
Mock
Dk/Korea
Dk/India
Dk/Tripura
Dk/Shandong
Dk/Dongguan
Dk/Shantou
Ck/Pakistan
Ck/Zhejiang
Ck/Italy
Dk/Netherlands
Dk/Mongolia
Dk/Wisconsin
Dk/New York
Ck/Penn/1
Ck/Penn/1370
Gull/Maryland
Tk/South Dakota
20 µm

Figure 2.9 Budding phenotype of PR8 7:1 reassortant viruses in MDCK cells. Reassortant viruses were constructed with the segment 7s from table 2.1 in a PR8 backbone and used to infect MDCK cells at a MOI of 3 for 16 h. Cells were fixed and the surface stained with anti PR8 antibody for viral proteins (green) and DAPI for DNA (blue). Images were collected as maximum intensity projections on the Zeiss 710 confocal microscope with a 63x objective and are representative of three independent experiments. PR8 WT and PR8 MUd viruses were used as spherical and filamentous positive controls, respectively. Mock-infected cells were used as an experimental control. Arrows indicate bundles of filaments. Scale bar (20 μm) indicated.

well above it, inducing filaments in approximately 60% infected cells (Figure 2.10 A). By this threshold, 11 out of the 17 avian reassortant strains showed a prominent filamentous phenotype, which differed significantly from PR8 WT. The filamentous 7:1 reassortant viruses all presented more than 30% of infected cells with filamentous bundles on their surface (orange bars), whereas the spherical strains (blue bars) were all well below the defined threshold (15%). Regarding filament length, all strains considered filamentous according to the percentage of cells they induced filaments in, promoted formation of filamentous bundles ranging from 6 - 10 µm, whereas strains that failed to produce obvious filament bundles in a substantial proportion of infected cells showed lengths below the threshold (2 µm) in the rare instances seen, comparable with the WT PR8 virus control (Figure 2.10 B). Thus similarly to the results obtained with a panel of authentic avian IAV isolates, a broader set of avian virus segment 7s that represented all major clades of the M1 gene conferred a mixture of filamentous and non-filamentous budding phenotypes. The classification of the 7:1 reassortants according to their budding phenotypes allowed correlations to be drawn with virus replication in tissue culture. Looking back at Figure 2.8, there was no obvious link between end-point titres of virus replication in MDCK cells and budding morphology. However, plaque size can be a more sensitive measure of virus spread in tissue culture (Medvedeva et al., 1968). Therefore, to test this, the 7:1 reassortant viruses were used to infect monolayers of MDCK cells under Avicel and the plaque size examined after staining with toluidine blue (figure 2.8 B). To provide quantitative data, a minimum of 72 plaques were measured per virus. These data showed that filamentous reassortant viruses presented significantly smaller plaques when compared with PR8 WT, while spherical strains showed plaques equivalent to PR8 WT (Figure 2.11 A). Furthermore, the filamentous budding phenotype as assessed by the % of cells displaying filaments was plotted against plaque size (Figure 2.11 B). The data was fitted by linear regression and showed an inverse linear relationship between plaque measure and percentage of filamentous phenotype. Additionally, the *t-test* showed that the spherical and filamentous virus populations significantly differed in terms of plaque size, with spherical viruses having larger plaques while filamentous viruses formed smaller plaques (Figure 2.11 C). Given the good fit of the data ($R^2 = 0.659$), this will be used as a linearized model throughout the study.

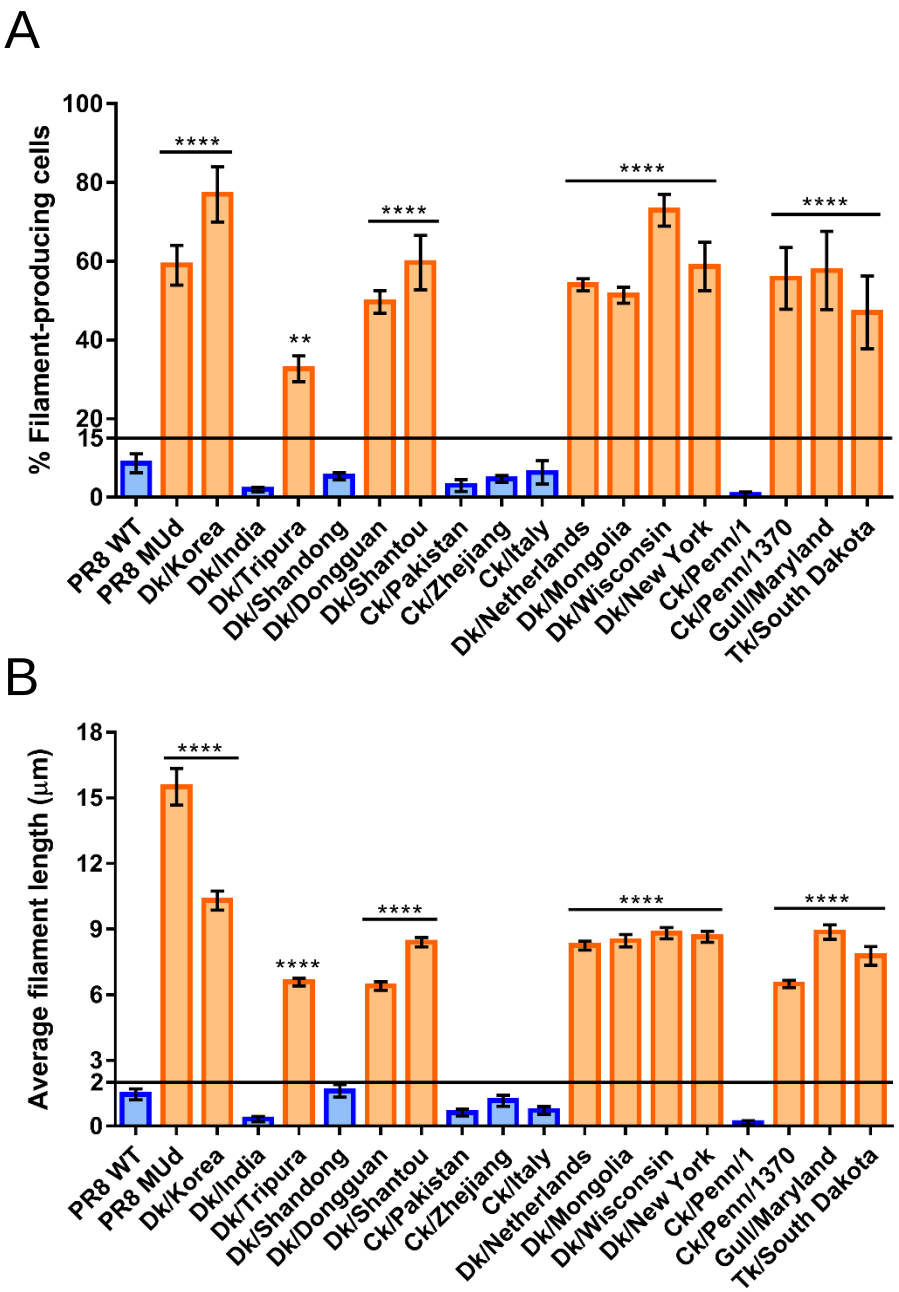

Figure 2.10 Quantification of the budding phenotypes of PR8 7:1 reassortant viruses. MDCK cells were infected at an MOI of 3 for 16 h before fixing. (A) A minimum of 100 infected cells were counted per virus and the percentage of filament-producing cells was determined. (B) 90 filaments were measured per virus (when visible). Data are the mean +/- SEM (n = 3). ANOVA statistical analysis was performed to compare all 7:1 reassortant viruses to PR8 WT. ** $p<0.01$; **** $p<0.0001$. Limits for viruses to be classified as possessing a filamentous budding morphology are indicated (> 15% of infected cells producing at least one bundle of filaments of 2 μm or longer). Bars are accordingly colour coded for spherical (blue) and filamentous (orange) budding morphology.

A

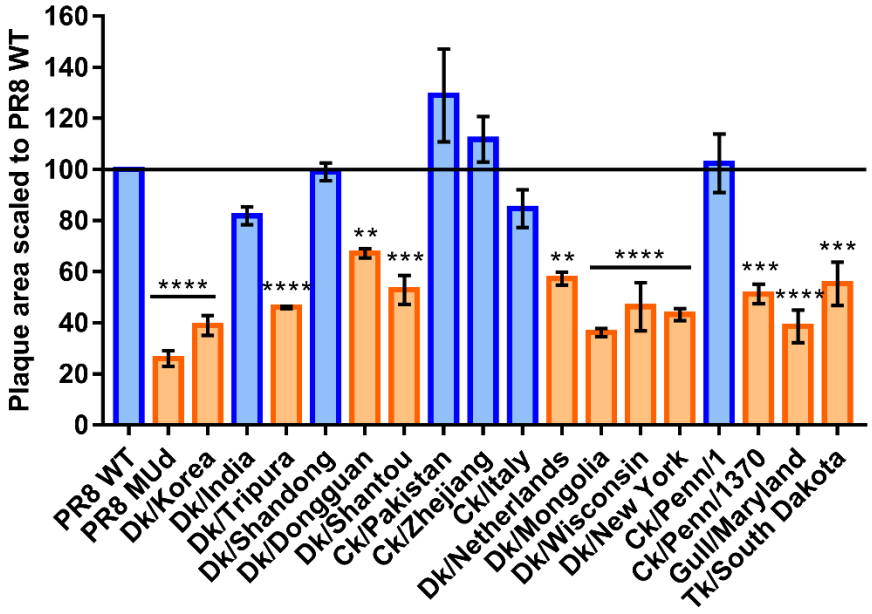
Plaque area scaled to PR8 WT
160
140
120
100
80
60
40
20
0
****
****
**
***
**
****
***
****
***
PR8 WT
PR8 MUd
Dk/Korea
Dk/India
Dk/Tripura
Dk/Shandong
Dk/Dongguan
Dk/Shantou
Ck/Pakistan
Ck/Zhejiang
Ck/Italy
Dk/Netherlands
Dk/Mongolia
Dk/Wisconsin
Dk/New York
Ck/Penn/1
Ck/Penn/1370
Gull/Maryland
Tk/South Dakota

B

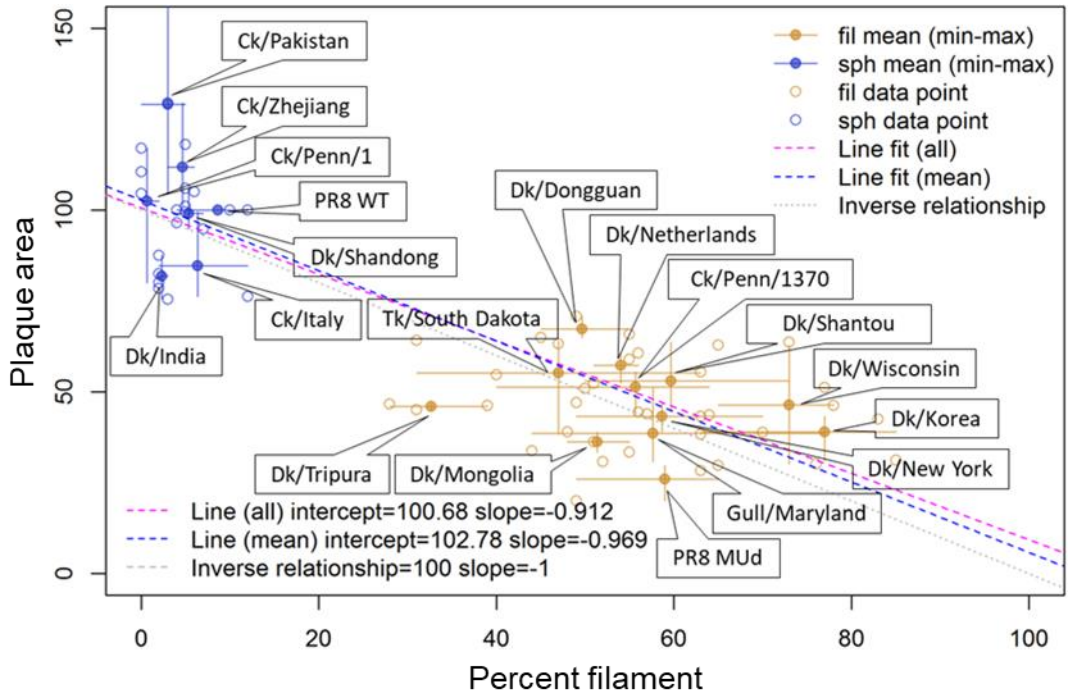
Plaque area
Percent filament
0
50
100
150
0
20
40
60
80
100
fil mean (min-max)
sph mean (min-max)
fil data point
sph data point
Line fit (all)
Line fit (mean)
Inverse relationship
Ck/Pakistan
Ck/Zhejiang
Ck/Penn/1
PR8 WT
Dk/Shandong
Ck/Italy
Tk/South Dakota
Dk/India
Dk/Dongguan
Dk/Netherlands
Ck/Penn/1370
Dk/Shantou
Dk/Wisconsin
Dk/Korea
Dk/New York
Gull/Maryland
PR8 MUd
Dk/Tripura
Dk/Mongolia
Line (all) intercept=100.68 slope=-0.912
Line (mean) intercept=102.78 slope=-0.969
Inverse relationship=100 slope=-1

C

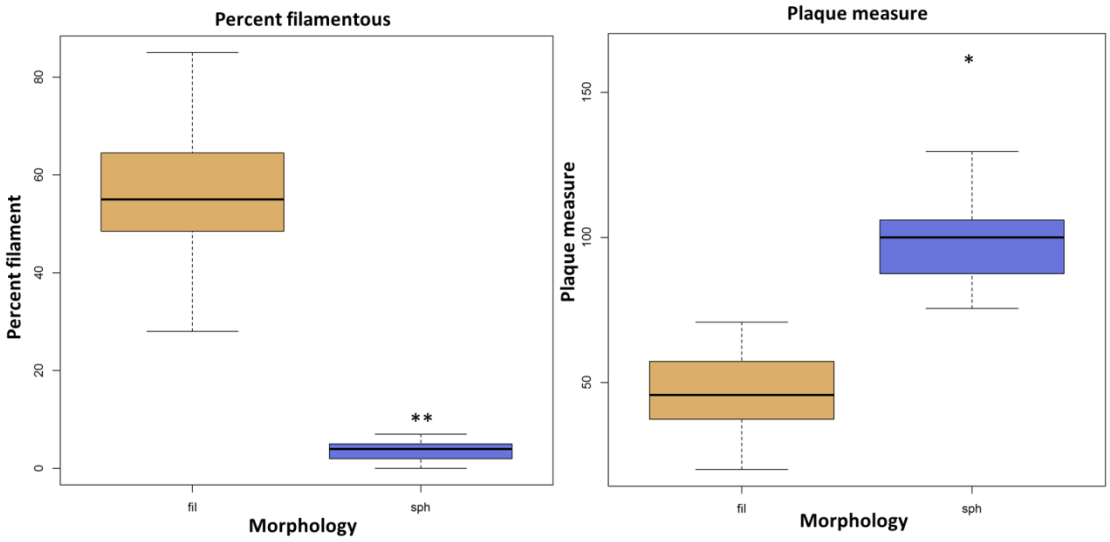

Figure 2.11 Plaque phenotype of PR8 7:1 reassortant viruses and its association with budding morphology. (A) Plaques represented in figure 2.8 B were measured and the dimensions were scaled to PR8 WT (considered 100%). A minimum of 72 plaques were measured. Data represent mean +/- SEM (n = 3). One-way ANOVA was performed to compare all 7:1 reassortant viruses to PR8 WT. ** p<0.01 *** p<0.001 **** p<0.0001. Spherical viruses are represented in blue while filamentous in orange. PR8 WT and PR8 MUd were used as spherical and filamentous positive controls, respectively. (B) Data points represent individual (circle outline) or average (circle coloured in) of plaque measure plotted against % filament-producing cells. The data was fitted to a linear regression and the trendlines for the individual and average data points are represented. Spherical viruses are represented in blue while filamentous in orange. Graph drawn by Dr Sam Lycet (C) *t-test* was performed to compare spherical and filamentous virus populations regarding percentage of filamentous phenotype and plaque size. ** p<0.01 * p<0.05. Spherical viruses are represented in blue while filamentous in orange. Graphs drawn by Dr Sam Lycett.

Thus as previously noted, filamentous budding is not advantageous for virus spread in tissue culture monolayers (Bourmakina & Garcia-Sastre, 2003; Roberts et al., 1998)

Given that the viruses tested were of avian-origin but only tested in mammalian cells, the next step was to test these PR8-based 7:1 reassortants in avian cells: chicken embryo fibroblasts (CEF) and duck embryo fibroblasts (DEF). CEF cells infected with PR8 WT presented a uniformly distributed staining characteristic of a spherical phenotype. PR8 MUd-infected cells showed long filamentous bundles characteristic of this virus, arising mainly from the centre of the cells (Figure 2.12 A). The 7:1 reassortant viruses that maintained the spherical phenotype of PR8 WT in MDCK, also kept that budding phenotype in CEF cells (Dk/India, Dk/Shandong, Ck/Pakistan, Ck/Zhejiang, Ck/Italy and Ck/Penn/1). The 7:1 reassortant viruses with Dk/Korea, Dk/Tripura, Dk/Dongguan, Dk/Shantou Dk/Netherlands, Dk/Mongolia, Dk/Wisconsin, Dk/New York, Ck/Penn/1370, Gull/Maryland and Tk/South Dakota promoted the formation of filamentous bundles in infected CEF cells, comparable to PR8 MUd but consistent with a spherical phenotype. PR8 MUd-infected DEF cells showed the characteristic filamentous bundles as previously observed in MDCK and CEF cells. DEF cells showed a pattern similar to CEF cells, but with a less accentuated filamentous phenotype when compared to MDCK cells. With DEF cells, it was observed that some 7:1 reassortant viruses lost their ability to promote filament formation (e.g. Ck/Penn/1370 and Tk/South Dakota), but generally the budding phenotypes observed with DEF cells were similar to those observed with MDCK and CEF cells. Thus, these data suggest that avian strains maintain their spherical or filamentous budding phenotypes regardless of cell origin.

The finding that avian IAV strains exhibited a mixture of filamentous and non-filamentous budding phenotypes allowed the correlation of M1 sequence polymorphism with virion morphology. The M1 amino acid sequences from all the virus strains tested, grouped into non-filamentous and filamentous categories, were aligned using MEGA6, as shown in

A

CEF

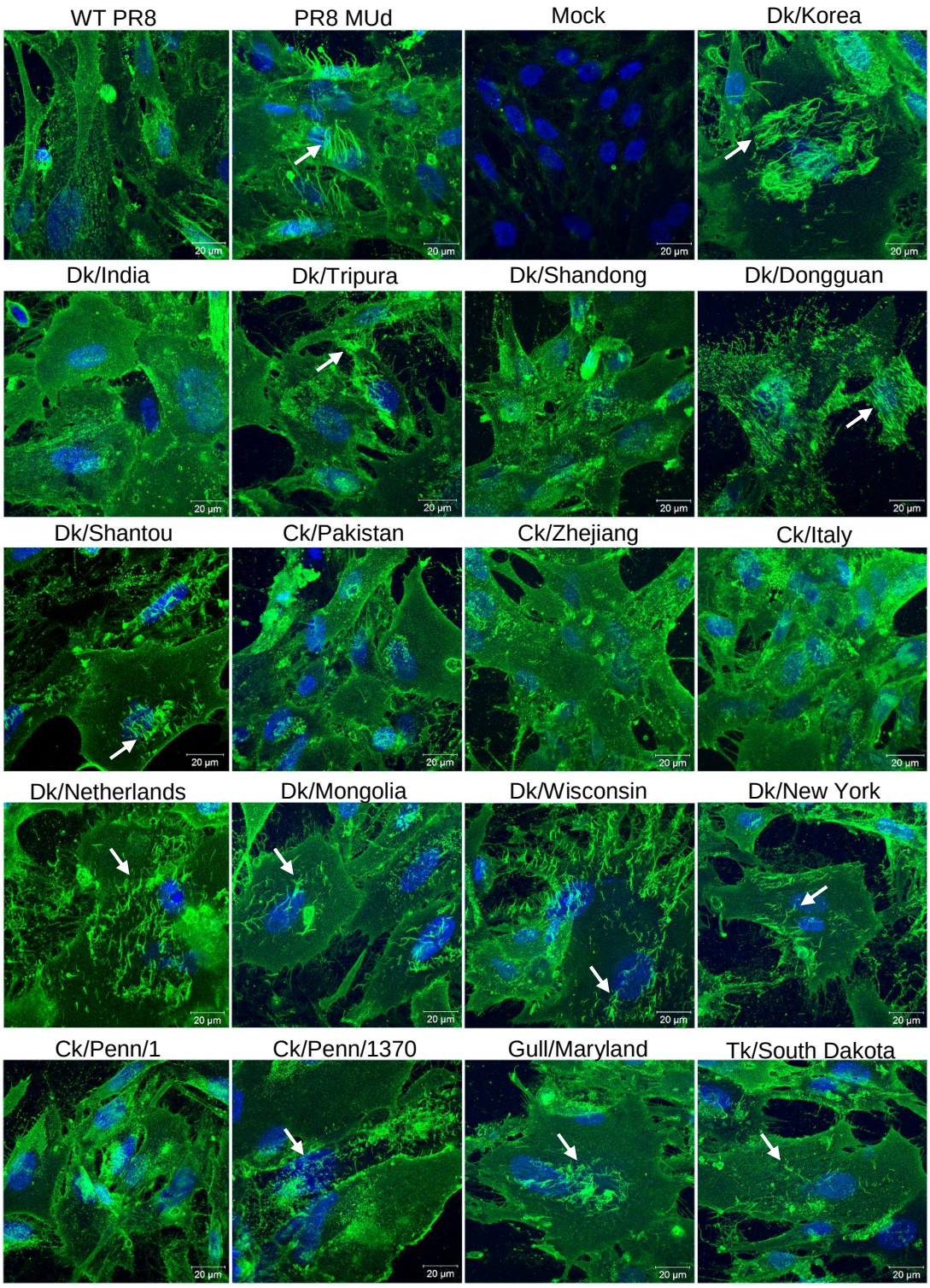
WT PR8
PR8 MUd
Mock
Dk/Korea
Dk/India
Dk/Tripura
Dk/Shandong
Dk/Dongguan
Dk/Shantou
Ck/Pakistan
Ck/Zhejiang
Ck/Italy
Dk/Netherlands
Dk/Mongolia
Dk/Wisconsin
Dk/New York
Ck/Penn/1
Ck/Penn/1370
Gull/Maryland
Tk/South Dakota
20 µm

B

DEF

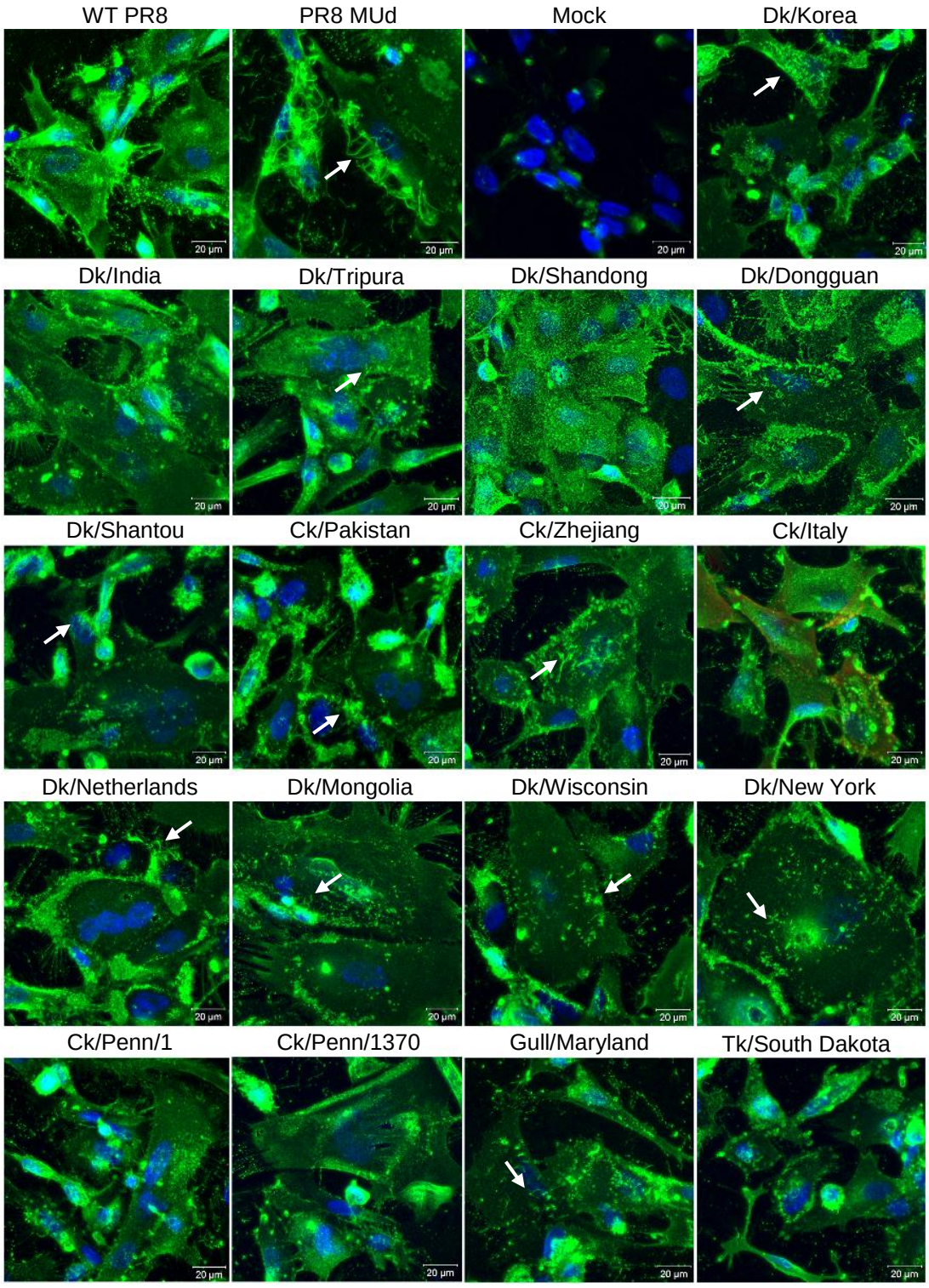
WT PR8
PR8 MUd
Mock
Dk/Korea
Dk/India
Dk/Tripura
Dk/Shandong
Dk/Dongguan
Dk/Shantou
Ck/Pakistan
Ck/Zhejiang
Ck/Italy
Dk/Netherlands
Dk/Mongolia
Dk/Wisconsin
Dk/New York
Ck/Penn/1
Ck/Penn/1370
Gull/Maryland
Tk/South Dakota
20 µm

Figure 2.12 Budding phenotype of PR8 7:1 reassortant viruses in chicken embryo fibroblast (CEF) and duck embryo fibroblast (DEF) cells. Reassortant viruses were constructed with the segment 7s from table 2.1 in a PR8 backbone and used to infect CEF (A) and DEF (B) cells at a MOI of 3 for 16 h. Cells were fixed and the surface stained with anti-PR8 antibody for viral proteins (green) and DAPI for DNA (blue). Images were collected as maximum intensity projections on the Zeiss 710 confocal microscope with a 63x objective and are representative of three independent experiments. PR8 WT and PR8 MUd viruses were used as spherical and filamentous positive controls, respectively. Mock-infected cells were used as an experimental control. Arrows indicate bundles of filaments. Scale bar (20 μm) indicated.

figure 2.13.

As described in chapter 1, it has been shown in human and equine strains of IAV M1 that the amino acid identity of residues 41, 85, 95, 204, 207 and 218 are major morphology determinants (figure 2.13, grey rectangles). However, a closer look at these positions in the aligned avian M1 sequences revealed no consistent differences between spherical and filamentous avian strains (above and below the line of figure 2.13, respectively). In fact, at the aforementioned positions, the amino acid composition was very similar within all avian M1 sequences. Residues 85, 204 and 218 did not vary in all avian M1 sequences, while residues 41, 95 and 207 varied but this variation did not correlate with the different budding morphologies seen with avian IAVs. This suggested that residues identified in M1s of human and equine strains of IAV as determining filamentous budding are not the same in avian IAV M1s. Therefore, if there are "rules" for determining avian IAV budding morphology, these will be different from those previously identified for mammalian strains.

2.3. Discussion

Characterisation of the budding morphology of mammalian strains of IAV (equine and human) revealed that these strains are able to produce both spherical and filamentous particles (Bourmakina & Garcia-Sastre, 2003; Chu et al., 1949; Elleman & Barclay, 2004; Elton et al., 2013; Roberts et al., 1998). In fact, filamentous viruses are commonly found in clinical isolates and selected *in vivo* (Chu et al., 1949; Nakajima et al., 2010; Seladi-Schulman et al., 2013) while spherical strains are selected *in vitro*, normally following serial passage in cells and/or eggs (Burnet & Lind, 1957; Kilbourne & Murphy, 1960; Seladi-Schulman et al., 2013). Several studies have reported the viral matrix protein M1 as the main determinant of budding morphology (Bourmakina & Garcia-Sastre, 2003; Chlanda et al., 2015; Elleman & Barclay, 2004; Gomez-Puertas et al., 2000; Roberts et al., 1998), where the amino acid identity at positions 41, 85, 95, 204, 207 and 218 play a role in determining the resulting budding phenotype (Bialas et al., 2012; Bourmakina & Garcia-Sastre, 2003; Elleman & Barclay, 2004; Elton et al., 2013; Roberts et al., 1998).

Figure 2.13 Sequence alignment of the avian M1 proteins from viruses and/or segment 7s tested for budding morphology in this study. All avian M1 sequences tested in this study were aligned using MEGA6. Strains are organized from the top from spherical to filamentous budding phenotypes (the black line divides between the two morphologies). Positions highlighted with grey rectangles correspond to amino acids previously identified in mammalian strains of IAV as morphology determinants (41, 85, 95, 204, 207 and 218).

These residues are known as the filamentous 'signature' of mammalian strains of IAV (Elton et al., 2013). However, regarding avian strains of IAV it still remains largely unknown what is their predominant budding phenotype. Therefore, the aim of this section of the study was to characterise the budding morphology of avian IAVs and, if these produce filaments, then determine if there are specific residues within M1 that can regulate budding morphology and compare these with the ones previously identified in mammalian IAVs.

The avian isolates tested for budding morphology in this study indicated that avian strains of IAV are as pleomorphic as mammalian strains, with 3 of the 5 isolates showing the characteristic filamentous structures on the surface of infected cells (Figure 3.3). However, a sample of 5 avian isolates could not be used as a representative sample of avian strains of IAV. The only way to test more strains would be to get more isolates, but there were a few limiting steps, such as isolate availability, biosafety measures to handle HPAI strains and antibodies for all the different HA and NA subtypes of avian viruses. Therefore, in order to overcome this, PR8-based 7:1 reassortant viruses were considered as alternatives. To test the viability of using 7:1 reassortant viruses with an avian segment 7 in a PR8 backbone. Therefore, reassortant viruses with segments 4, 5, 6 and/or 7 of Dk/Netherlands strain were built, since all these segments were previously shown to affect budding morphology of mammalian and avian strains (Bialas et al., 2014; Chlanda et al., 2015; Gomez-Puertas et al., 2000; Jin et al., 1997; Liu et al., 2002; Roberts et al, 1998). PR8- based 7:1 reassortant viruses with segments 4, 5 and 6 of Dk/Netherlands individually did not altered the spherical phenotype characteristic of PR8 WT (Figure 2.5). This is in agreement with reports by Gomez-Puertas et al. and Chlanda et al., which showed that segments 4, 5 and 6 of human strains did not alter the budding morphology of the virus (Chlanda et al., 2015; Gomez-Puertas et al., 2000). Combination of segments 4 and 6 of Dk/Netherlands in a PR8 backbone also resulted in a spherical budding phenotype, as previously shown for human strains (Chlanda et al., 2015). When segment 7 of Dk/Netherlands was added to PR8, it induced filament formation on the surface of budding morphology of the virus like mammalian segment 7s (Bourmakina & Garcia-Sastre, 2003; Elleman & Barclay, 2004; Roberts et al., 1998). M and NP of Dk/Netherlands in PR8 promoted the formation of filaments, unlike previously published for another avian strain

(Bialas et al., 2014). In fact, the authors showed that the avian segment 5 prevented filaments even with an avian segment 7 that was able to induce filament formation in the backbone of a human spherical strain. Lastly, addition of segments 4, 6 and 7 of Dk/Netherlands to PR8 resulted in a virus with a budding phenotype that mimicked Dk/Netherlands WT budding morphology (Figure 2.6 A and Figure 2.6 B), in agreement to previous reports in human strains (Chlanda et al., 2015). This comes as no surprise, since HA (4) and NA (6) proteins were shown to modulate filamentous budding morphology (Jin et al., 1997) due to their interaction (via the cytoplasmic tails) with the M1 protein (Ali et al., 2000; Jin et al., 1997). Nonetheless, these data showed the importance of 7:1 reassortant viruses and their viability in budding morphology studies instead of the avian isolates.

The segment 7s selected for characterisation of the budding phenotype of avian IAVs was based on availability in the Digard laboratory and random selection based on M1 phylogeny. M1 sequences grouped into a phylogenetic tree showed two main branches (America and Eurasia), which were divided into clades from where at least one segment 7 was collected in order to have avian strains representative of each clade (Figure 2.7). This allowed for a great range of HA and NA subtypes to be tested, as well as HPAI strains, resulting in a reasonable representation of avian strains of IAV (Table 2.1). The PR8-based 7:1 reassortant viruses with avian segment 7 were built and the budding morphology characterised qualitatively (Figure 2.9) and quantitatively (Figure 2.10) in MDCK cells. This characterisation revealed that majority of the avian strains tested showed a filamentous budding phenotype with 30% - 80% of infected cells producing filaments ranging 6 – 10 µm in length. Significantly, as previously reported for human H3N2 strains (Roberts et al., 1998), avian strains with a filamentous phenotype showed a strong negative correlation with plaque size, i.e., these produced smaller plaques in monolayers of infected MDCK cells.

Characterisation of the PR8-based 7:1 reassortant viruses with segment 7 of avian strains was mainly done in mammalian cells, therefore, to test whether the budding phenotypes observed were transferable to their original host, CEF and DEF cells were infected with the reassortant viruses. Overall, CEF and DEF cells infected with these viruses showed that the 7:1 reassortants kept their original budding phenotype as seen in MDCK cells

(compare figure 2.9 with figure 2.12 A and figure 2.12 B). However, in these cells, the filamentous phenotype was much less accentuated, more remarkably so in DEF cells as 7:1 reassortants that were producing long filamentous structures in MDCK cells hardly produced visible filaments in DEF cells (e.g. Dk/Netherlands, Dk/Mongolia). However, to determine if these data was cell-type dependent, CK cells were also infected with the PR8-based 7:1 reassortant viruses, showing that the filamentous phenotype was as prominent in these cells as in MDCK cells, indicating that the budding phenotype is maintained regardless of cell origin. This contradicts the study performed by Al-Mubarak et al, which showed that the budding morphology on an avian isolate differed between CEF and DEF cells (Al-Mubarak et al., 2015).

Lastly, since it is now known that avian strains can be as pleomorphic as mammalian strains, the next step was to identify sequence polymorphisms in avian M1s based on the previously characterised filamentous "signature" of mammalian strains. As mentioned before, amino acid identity at positions 41, 85, 95, 204, 207 and 218 is an important regulator of budding morphology (Elton et al., 2013). To determine if these positions would be morphology determinants for avian strains, all the avian M1s used in this study (for which budding morphology was known) were aligned and separated by budding phenotypes (Figure 2.13). At residues 85, 204 and 218, all the avian M1s possessed asparagine, glutamic acid and threonine, respectively, thus these positions were disregarded. By contrast, at position 41 there were strains with alanine or valine, at position 95 amino acids lysine or arginine were represented and at position 207 there were strains with asparagine, serine or glycine. In human H1N1 and H3N2 strains, it is known that V41A, K95R and N207S substitutions successfully promote the formation of filaments (Bialas et al., 2012; Elleman & Barclay, 2004; Roberts et al., 1998). However, these substitutions on avian M1s did not form a consistent pattern that would explain the different budding morphologies observed. For instance, at position 41 majority of the avian strains possessed an A, while two strains with opposite budding morphologies possessed a V. At position 95, only three spherical strains presented a K, while the remaining spherical and the entirety of the filamentous strains possessed a R. At residue 207 a similar trend was observed, where majority of strains possessed an S and a combination

of spherical and filamentous strains presented a N. The mixed budding phenotypes observed with avian strains that contain the filamentous "signature" on their M1 amino acid sequence has also been reported by Louisirirotchanakul et al, however this study fails to indicate which residues can then modulate avian IAV budding morphology (Lourisirirotchanakul et al., 2013). Therefore, one can conclude that avian strains clearly do not follow the mammalian filamentous "signature".

Overall, this section of the study revealed that avian strains are as pleomorphic as mammalian strains of IAV and, considering that almost all avian strains were isolates or with a low passage number in the laboratory (see table 2.1), it is tempting to suggest that, like mammalian strains, avian IAVs could be predominantly filamentous on their original host. Just like in the case of mammalian strains, avian segment 7s are able to govern the budding morphology of avian IAVs and avian HA and NA proteins can also modulate the filamentous budding phenotype. Equally important, the budding phenotype observed with the PR8-based 7:1 reassortant viruses in MDCK cells was maintained in CEF, DEF and CK cells, indicating that this is truly a genetic aspect of the virus not dependent on cell origin. Significantly, this section of the study also pointed out that the previous identified "signature" for M1 sequence polymorphisms that determine the filamentous phenotype in human and equine strains of virus were not confirmed for avian IAVs, suggesting that avian strains may possess a different "signature". This brings on the challenge of finding a filamentous "signature" for avian strains of IAV, which will be addressed in chapter 3.

Chapter 3: Identification of sequence polymorphisms in avian IAV M1 polypeptides correlating with different budding morphologies

3.1. Introduction and aims

As previously discussed in chapter 1, various human and equine IAV strains have been shown to produce either spherical or mixtures of filamentous and spherical virus particles, defined by sequence polymorphisms within M1. In particular, the identities of amino acids at positions 41, 85, 95, 204, 207 and 218 were reported to be important filamentous "signatures" for human and equine strains of IAV. Within human H1N1 and H3N2 strains, it was reported that substitutions A41V (Roberts et al., 1998), R95K (Bourmakina & Garcia-Sastre, 2003), E204D (Bourmakina & Garcia-Sastre, 2003) abrogated the production of filaments, whereas substitutions V41A, K95R, N207S (Bialas et al., 2012) and T218A (Elleman & Barclay, 2004) successfully promoted the formation of filaments by a previously spherical strain. The importance of position 85 was demonstrated with equine H3N8 strains, where Elton et al switched serine (predominantly represented in filamentous H3N8 equine strains) to asparagine in the M1 sequence, abolishing the filamentous budding phenotype (Elton et al., 2013).

In the previous chapter, avian isolates of IAV as well as 7:1 reassortant viruses with segment 7 from avian strains in a PR8 backbone were characterised for budding phenotype. Confocal microscopy and quantification of budding phenotype showed that avian IAVs differed in budding phenotype, with some but not all strains producing filamentous particles of 6 - 10 µm in length. However, sequence alignment of the avian M1 polypeptides showed no consistent differences at positions 41, 85, 95, 204, 208, 214 and 218 that could explain the different budding morphologies seen. Therefore, it was concluded that avian IAVs deviate from the M1 filamentous "signatures" identified in human and equine strains.

Thus, the aim of this part of the work was to (1) investigate the sequence polymorphisms seen within the avian M1s and to correlate these with virus particle shape; and (2) if sequence polymorphisms were identified as morphology determinants, test whether

these were virus strain-specific or could form the basis for a new filamentous “signature” for avian IAVs.

3.2. Results

3.2.1. Identification of sequence polymorphisms in avian M1s

Simply aligning all M1 amino acid sequences of the avian strains tested had not revealed a consistent pattern between spherical and filamentous avian strains (Figure 2.13, strains above and below the line). However, a closer look at the sequences showed pairs of closely related avian strains with opposite budding phenotypes that nevertheless shared very similar M1 sequences. These were: (1) Dk/India and Dk/Tripura; (2) Ck/Penn/1 and Ck/Penn/1370; and (3) Ck/Italy and Dk/Netherlands. Pairwise alignment of these strains showed three amino acid substitutions between Dk/India and Dk/Tripura strains and only one single amino acid substitution between the other two pairs (Ck/Penn/1 and Ck/Penn/1370; Ck/Italy and Dk/Netherlands) (Figure 3.1, grey boxes). Since these were the only differences on M1 amino acid sequence between the pairs identified, these positions represented good candidates to justify the different budding morphologies observed. Amino acid sequence similarity between the M2 of these pairs was also assessed to determine whether there were differences in regions of this protein known to affect budding morphology. These are: (1) a region of interaction with M1 (residues 70 to 77) (McCown & Pekosz, 2006) and (2) the amphipathic helix domain of M2 (residues 50 to 61), which was reported to modulate budding morphology (Roberts et al., 2013). The M2 polypeptides of Dk/India and Dk/Tripura pair showed two amino acid differences at positions 10 and 82, while those of Ck/Penn/1 and Ck/Penn/1370 varied at positions 43 and 44. By contrast, Ck/Italy and Dk/Netherlands shared a 100% identical M2 amino acid sequence (data not shown). Given that the variable positions identified were outside of regions known to affect budding morphology, these were disregarded.

3.2.2. Correlating sequence polymorphisms in M1 with budding morphology of Dk/India and Dk/Tripura avian strains

The M1 proteins of Dk/India and Dk/Tripura varied at three positions: T37A, I59M and I205V, where the first amino acid listed was present in Dk/India M1 and the second in M1 Dk/Tripura (figure 3.1, top pair). Therefore, the first step was to build Dk/India and Dk/Tripura 7:1 reassortant viruses with these residues reciprocally mutated. WT segment 7 of both Dk/India and Dk/Tripura strains was mutated individually or in combination at positions 37, 59 and 205 by site-directed mutagenesis. Monolayers of 293T cells were then transfected with the reverse genetics plasmids of the PR8 backbone and the segment 7s (WT or mutated M1) of Dk/India and Dk/Tripura strains to generate P0 stocks. These P0 stocks were propagated in MDCK cells for 48 h and titred by plaque assay. All viruses rescued readily twice, and replicated to average titres of approximately 10^8 PFU/ml with no significant differences between them (Figure 3.2 A). Plaque phenotype was assessed in monolayers of infected MDCK cells stained with toluidine blue. Mock-infected cells showed no detectable levels of infectious particles. As seen in the previous chapter (figure 2.8 B) the plaque phenotype of Dk/India and Dk/Tripura 7:1 reassortant viruses was distinguishable, with the former producing noticeably larger plaques than the latter. Mutation of position 37 and/or 205 had little obvious effect on plaque size in either virus background. However, mutation of position 59, either singly or in combination with the other sites decreased the plaque size of Dk/India or conversely, increased the plaque size of Dk/Tripura, suggesting subtle differences in replication fitness *in vitro* (Figure 3.2 B).

The next step was to determine the budding phenotype of the WT and M1-mutant 7:1 reassortant viruses of Dk/India and Dk/Tripura with single, double and triple mutations at positions 37, 59 and 205. MDCK cells were infected at a MOI of 3 for 16 h. Cells were fixed and the surface stained with anti-PR8 antibody for viral surface proteins (green) and DAPI to indicate nuclei (blue) prior to imaging. Mock-infected cells showed no signs of infection and the spherical (PR8 WT) and filamentous (PR8 MUd) positive controls showed their expected phenotypes (data not shown). As expected, WT Dk/India showed the evenly distributed pattern of punctate plasma membrane staining associated with a spherical budding

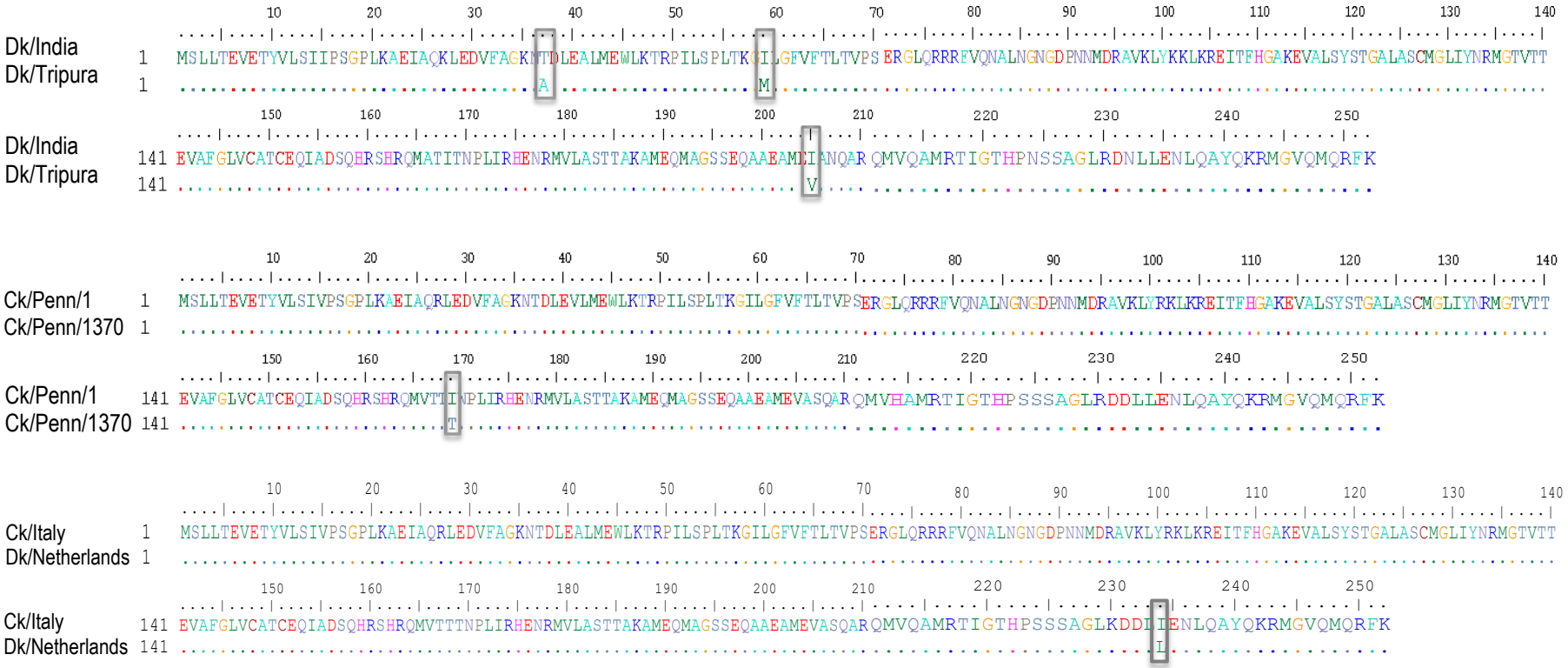

Figure 3.1 M1 sequence alignments of closely related avian strains with opposite budding morphologies. Pairwise alignments of the indicated avian M1 amino acid sequences were performed using BioEdit 7.0.0 ed. Spherical viruses are represented on the top of all 3 alignments. The residues highlighted display the positions that differed between these closely related avian strains (positions 37, 59, 205, 169 and 234).

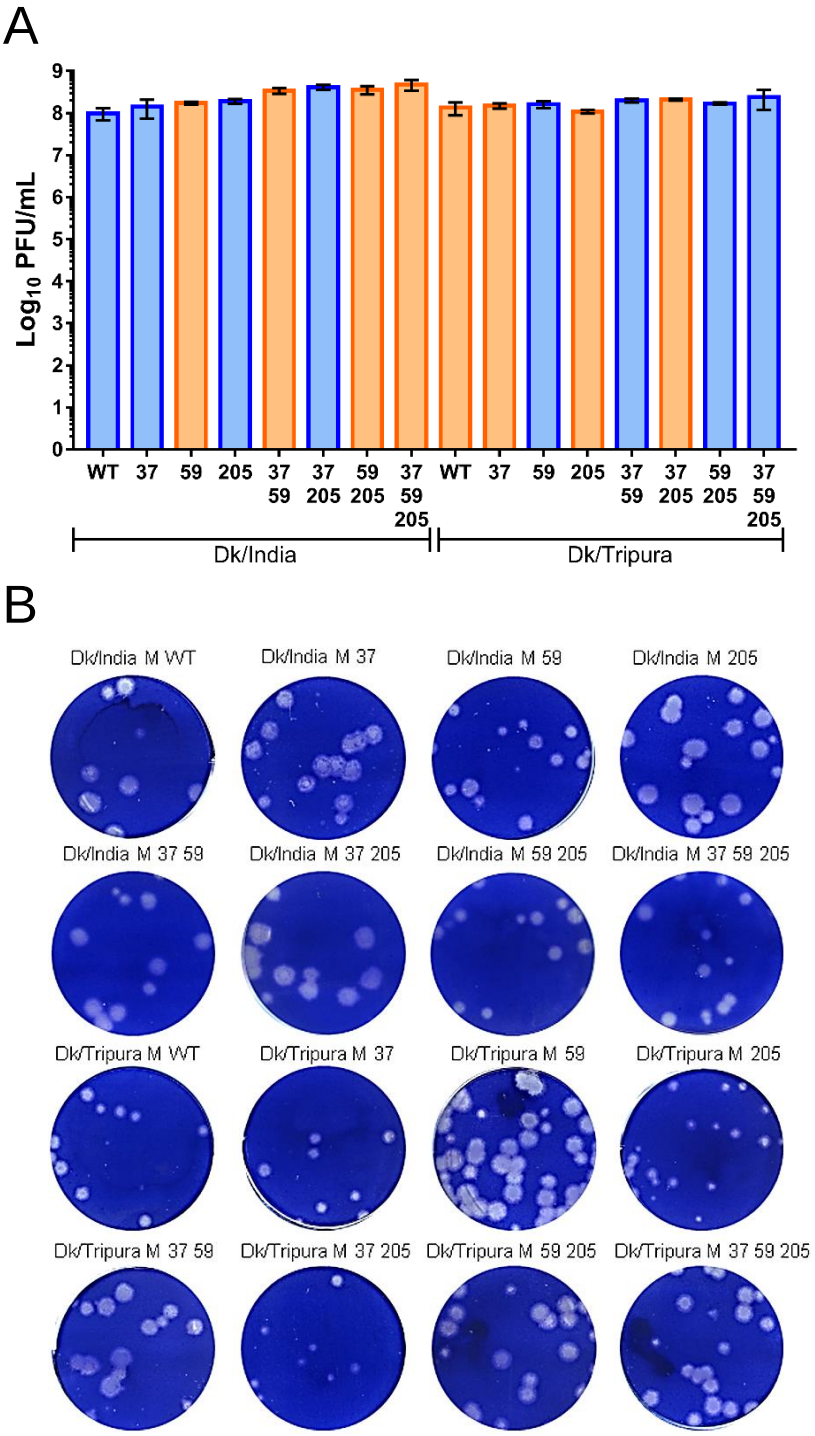

Figure 3.2 Replication fitness of WT and M1-mutant Dk/India and Dk/Tripura 7:1 reassortant viruses. (A) MDCK cells were infected with 1:10 dilutions of P0 stocks of the indicated viruses and left for 48 h, supernatants collected and titred by plaque assay in MDCK cells. Data represent mean +/- SEM (n = 3) from two independent rescues. Bars are coloured to indicate spherical (blue) or filamentous (orange) budding phenotypes. (B) Plaque phenotype in monolayers of MDCK cells was visualised by staining with toluidine blue.

phenotype, whereas Dk/Tripura showed on obviously filamentous budding phenotype, producing (Figure 3.3, top panel; filamentous bundles indicated with white arrows). Reciprocal changes of amino acids at positions 37 or 205 did not alter the budding morphologies of Dk/India and Dk/Tripura strains. In contrast, alteration of amino acid 59 reciprocally altered Dk/India and Dk/Tripura budding morphologies; Dk/India became filamentous while a spherical budding phenotype was transferred to Dk/Tripura. For mutant viruses that already had position 59 altered, the further change of amino acids at positions 37 and/or 205 did not substantially affect the outcome; i.e., the budding morphologies remained reciprocally altered (Figure 3.3, lower panels). Additionally, mutant viruses with double reciprocal changes at positions 37 and 205 showed no major alteration compared to the corresponding WT budding morphologies of Dk/India and Dk/Tripura. Thus, M1 position 59 was the major virion morphology determinant between Dk/India and Dk/Tripura strains.

In order to quantify the budding phenotype of these mutants, cell counts and filament measures were performed as described before. MDCK cells were infected at a MOI of 3 for 16 h with two independently rescued virus stocks and cell surface HA stained and imaged. Two maximum intensity projection confocal images were collected per repeat for scoring (Chapter 2, section 2.2.2). As before, a threshold was defined whereby a virus was considered filamentous if more than 15% of infected cells produced filaments and these were longer than 2 μm. By these criteria, WT Dk/India and Dk/Tripura viruses showed a spherical and filamentous budding phenotype, respectively (Figure 3.4 A, B). However, reciprocal change of amino acids at position 59 caused an alteration in the budding morphologies of both viruses, where Dk/India showed a great increase (over 50%) in the number of cells producing filamentous particles (Figure 3.4 A). Conversely, the Dk/Tripura budding phenotype was converted to a spherical phenotype, although the magnitude of the decrease in the percentage of cells displaying filaments was somewhat lower (only circa 25%). Changes in the length of filamentous particles (when present) for both strains were also not perfectly reciprocal when amino acids at position 59 were altered, as while mutation of Dk/India produced bundles of filaments around 5 μm long, the remaining filaments produced by Dk/Tripura were still reasonably (over 2 μm) long (figure 3.4 B).

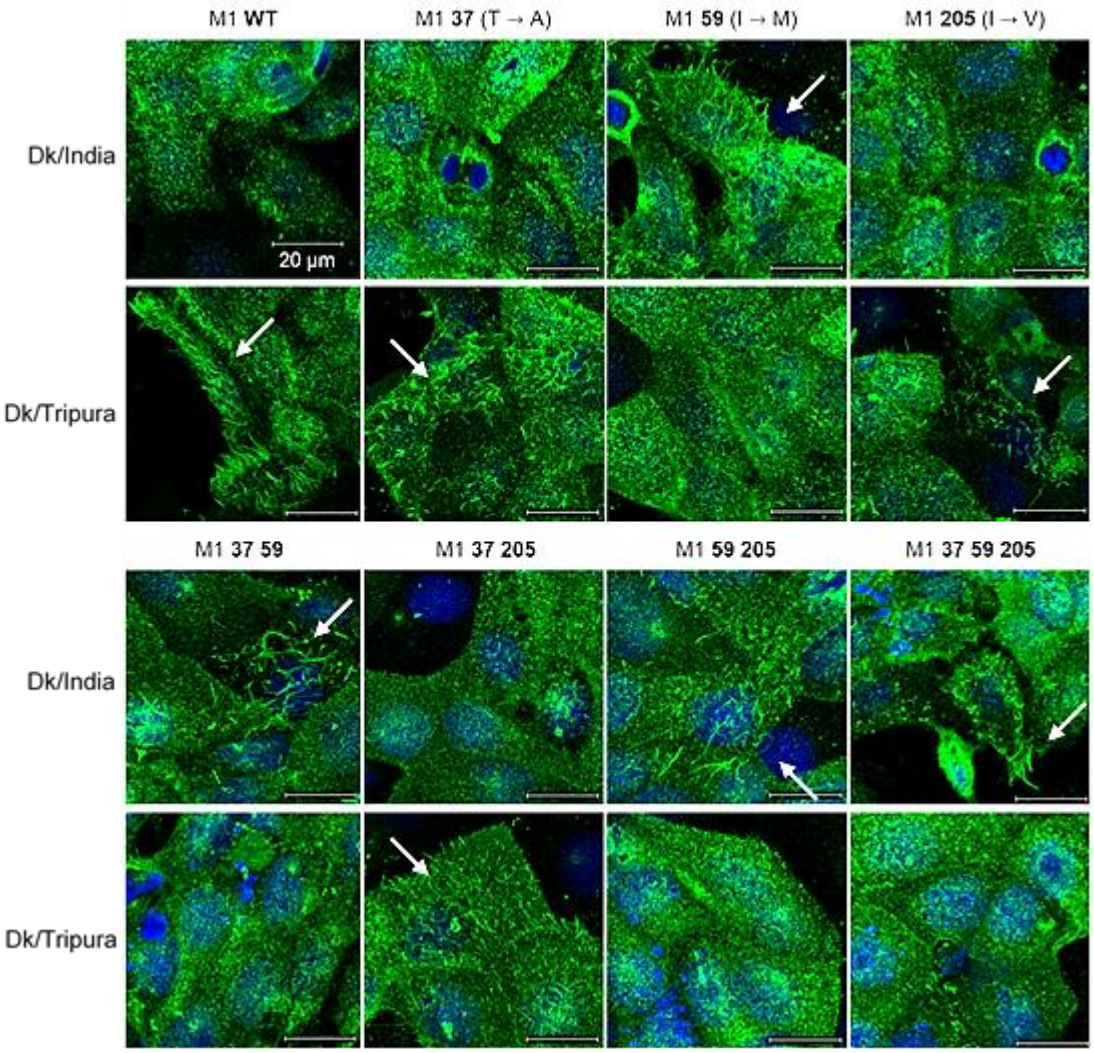

Figure 3.3 Budding phenotype of Dk/India and Dk/Tripura strains with WT or mutated M1 proteins. M1 genes of Dk/India and Dk/Tripura were mutated either individually or in combination at the positions indicated and the viruses were rescued as 7:1 reassortants in a PR8 backbone. WT and mutant viruses were used to infect MDCK cells at a MOI of 3 for 16 h. Cells were fixed and the surface stained with anti PR8 antibody (green) and DAPI (blue) prior to imaging. Images were collected as maximum intensity projections from Z-stacks on the Zeiss 710 confocal microscope with a 63x objective and are representative of three independent experiments. Filamentous bundles on the surface of the cells are indicated (white arrows). Scale bar (20 µm) indicated.

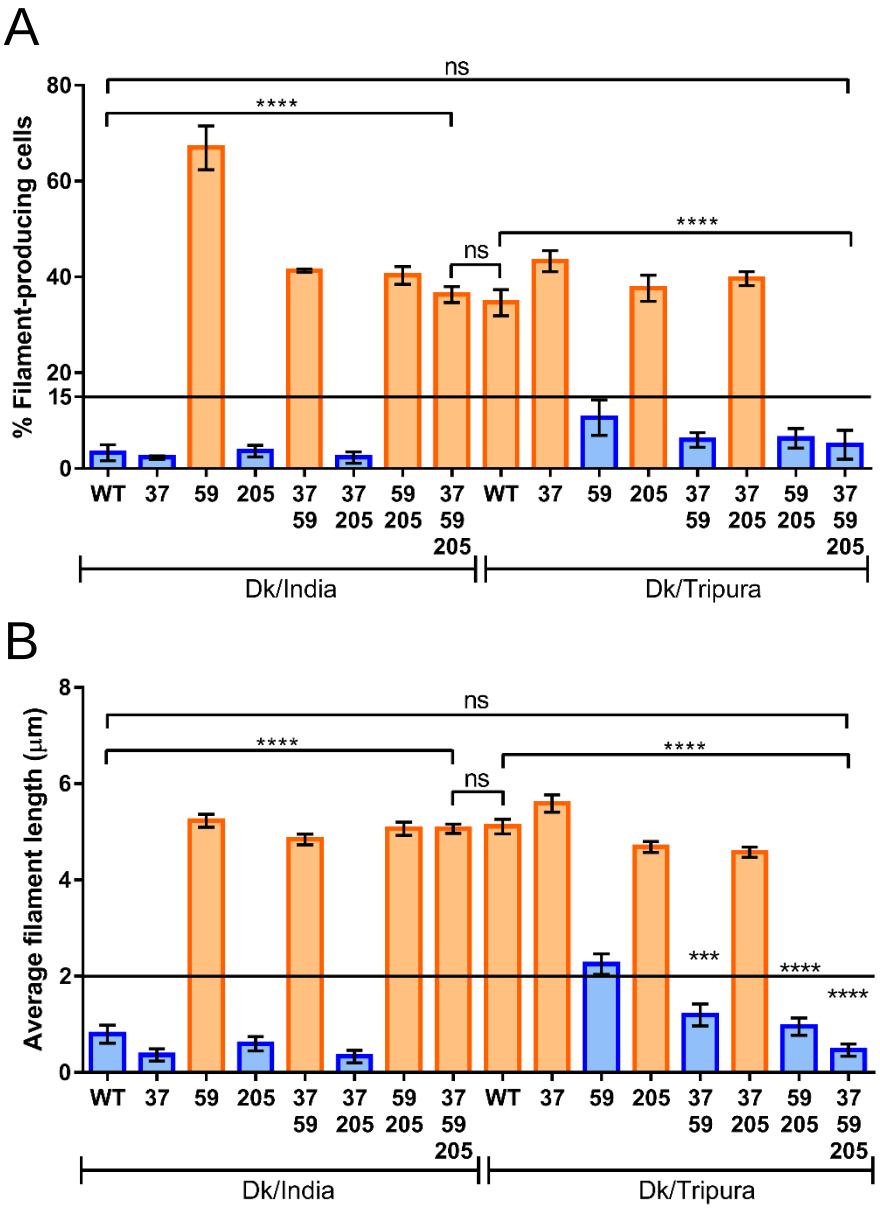

Figure 3.4 Quantification of the budding phenotype of the PR8-based Dk/India and Dk/Tripura WT and M1-mutant viruses. MDCK cells were infected at a MOI of 3 for 16 h and stained as in figure 3.3. (A) A minimum of 100 infected cells were counted and the percentage of filament-producing cells was determined from 3 independent experiments. (B) A total of 90 filaments were measured per virus (when visible). One-way ANOVA was performed to compare WT and M1-mutant viruses of Dk/India and Dk/Tripura avian strains. *** $p<0.001$; **** $p<0.0001$; ns not significant. Limits for viruses to be classified as possessing a filamentous budding morphology are indicated (> 15% of infected cells producing at least one bundle of filaments of 2 µm or longer). Spherical strains are represented in blue and filamentous in orange.

On the other hand, reciprocal change at positions 37 and/or 205 did not significantly alter the budding phenotype of the mutant viruses in comparison with the WT counterpart of Dk/India or Dk/Tripura. However, the cumulative effect when all differing positions were swapped resulted in a triple mutant Dk/India virus that was considerably different from its WT counterpart in both % of filament-producing cells and average filament length (Figure 3.4). For Dk/Tripura, reciprocal changes at positions 37, 59 and 205 considerably reduced the % of filament-producing cells. The average filament length of Dk/Tripura was significantly reduced with the alteration of position 59, however, only the addition of positions 37 and/or 205 reduced the average filament length of Dk/Tripura to below the defined threshold. In fact, the triple mutant of Dk/Tripura was significantly different from its WT counterpart regarding filamentous phenotype, yet similar to Dk/India WT and conversely was observed for Dk/India. Therefore, this indicated that although position 59 was the strongest determinant of virion morphology for Dk/India and Dk/Tripura strains, positions 37 and 205 also played a role.

Having established the budding phenotype of the mutated Dk/India and Dk/Tripura viruses, the previous observation that switching the amino acids at position 59 individually or in combination with positions 37 and 205 affected their plaque phenotype was revisited. To obtain quantitative data, a minimum of 70 plaques (as seen in figure 3.2 B) were measured per virus. Dk/India WT and mutants mutated at positions 37 and/or 205 showed significantly larger plaques than Dk/India M1 59 mutant virus, either individually or in combination with positions 37 and 205 (Figure 3.5 A). Conversely, Dk/Tripura mutant viruses with position 59 mutated individually or in combination with positions 37 and 205 showed generally larger plaques than their WT counterpart or the mutants at positions 37 and/or 205 (Figure 3.5 B). In both virus backgrounds, plaque size correlated well with budding phenotype. As a further test of this correlation, the % of filament-producing cells was plotted against plaque size; this grouped Dk/India and Dk/Tripura WT and M1-mutant viruses into two clusters: one composed of viruses where position 59 was altered, thus budding morphology was affected, and the other formed of viruses without alteration at position 59, maintaining their WT budding phenotype (Figure 3.5 C and D).

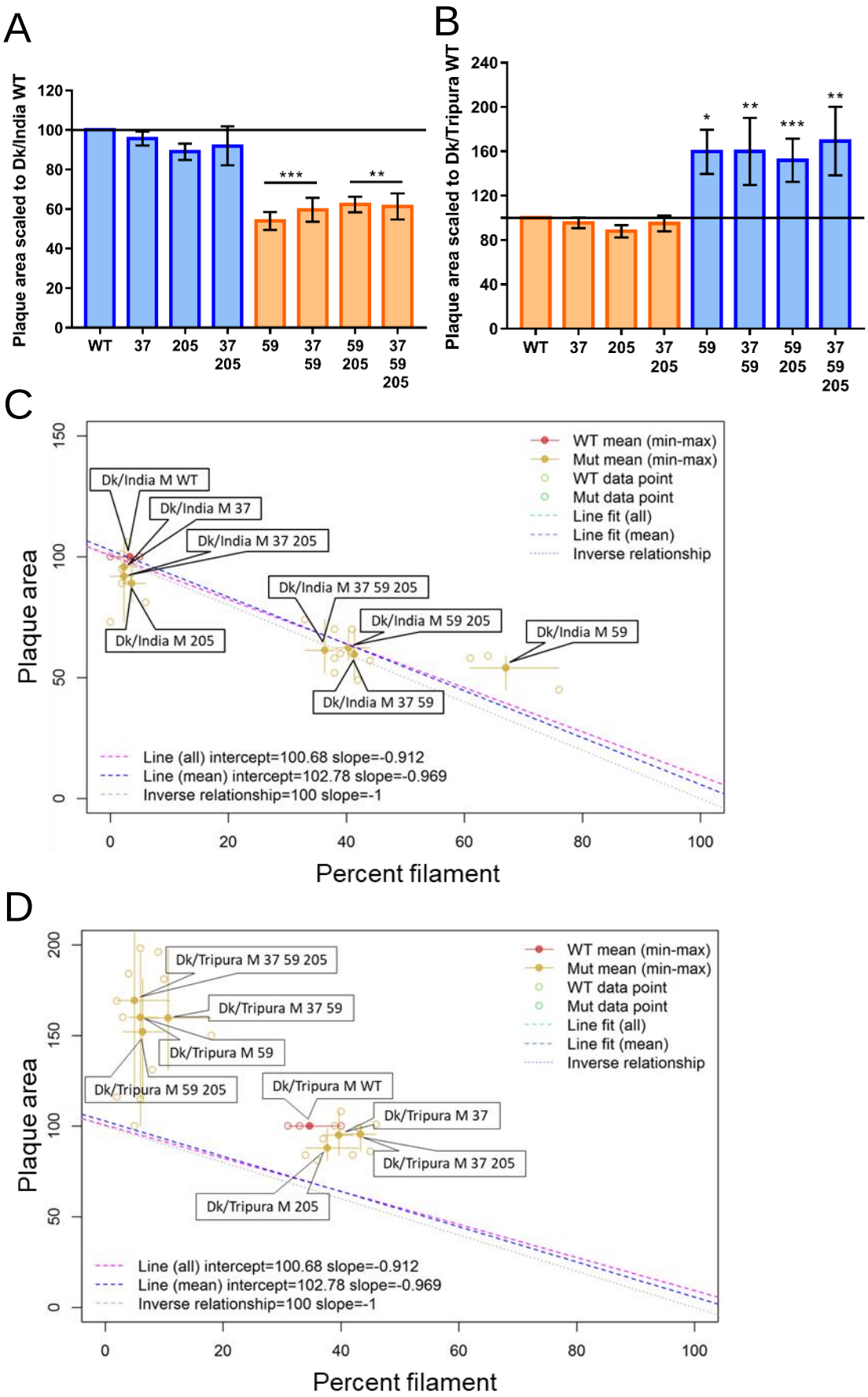
A
Plaque area scaled to Dk/India WT
120
100
80
60
40
20
0
***
**
WT
37
205
37 205
59
37 59
59 205
37 59 205
B
Plaque area scaled to Dk/Tripura WT
240
200
160
120
80
40
0
*
**
***
**
WT
37
205
37 205
59
37 59
59 205
37 59 205
C
Plaque area
150
100
50
0
WT mean (min-max)
Mut mean (min-max)
WT data point
Mut data point
Line fit (all)
Line fit (mean)
Inverse relationship
Dk/India M WT
Dk/India M 37
Dk/India M 37 205
Dk/India M 37 59 205
Dk/India M 59 205
Dk/India M 59
Dk/India M 205
Dk/India M 37 59
Line (all) intercept=100.68 slope=-0.912
Line (mean) intercept=102.78 slope=-0.969
Inverse relationship=100 slope=-1
0
20
40
60
80
100
Percent filament
D
Plaque area
200
150
100
50
0
WT mean (min-max)
Mut mean (min-max)
WT data point
Mut data point
Line fit (all)
Line fit (mean)
Inverse relationship
Dk/Tripura M 37 59 205
Dk/Tripura M 37 59
Dk/Tripura M 59
Dk/Tripura M 59 205
Dk/Tripura M WT
Dk/Tripura M 37
Dk/Tripura M 37 205
Dk/Tripura M 205
Line (all) intercept=100.68 slope=-0.912
Line (mean) intercept=102.78 slope=-0.969
Inverse relationship=100 slope=-1
0
20
40
60
80
100
Percent filament

Figure 3.5 Plaque size of Dk/India and Dk/Tripura WT and M1-mutant 7:1 reassortant viruses and its association with the % of filament-producing cells. (A, B) Plaques represented on figure 3.2 B were measured and the dimensions were scaled to Dk/India WT (A) or Dk/Tripura WT (B). A minimum of 70 plaques were measured per virus over 3 independent experiments. Spherical viruses are represented in blue while filamentous ones are depicted in orange. Data represent mean +/- SEM (n = 3). One-way ANOVA was performed to compare the M1-mutant viruses to the corresponding WT (considered as the 100% value), within Dk/India or Dk/Tripura groups. * $p<0.05$; ** $p<0.01$; *** $p<0.001$. (C, D) Data points represent individual (circle outline) and average (circle coloured in) plaque measure plotted against % filament-producing cells for (C) Dk/India and (D) Dk/Tripura viruses. The data was linearized and fitted against the model data from figure 2.11 B. WT viruses are represented in red and mutant viruses in orange. Graphs drawn by Dr Sam Lycett.

These analyses showed an inverse linear relationship between filamentous phenotype and plaque size. The data was linearized and plotted against the linearly fitted data from figure 2.11 B (linearized model). The good fit of Dk/India and Dk/Tripura viruses to the model data indicated that there was a trend for spherical viruses to produce bigger plaques whereas filamentous viruses formed smaller plaques. This further supported the generalisation discussed in Chapter 2 that viruses with filamentous phenotype tend to have smaller plaques than spherical strains, suggesting differences in viral replication *in vitro* (Roberts et al., 1998).

Overall, reciprocal changes of amino acids at M1 positions 37, 59 and 205 of the spherical Dk/India and filamentous Dk/Tripura viruses revealed the importance of the I59M polymorphism as a major morphology determinant between these two strains. However, further reciprocal changes of amino acids at positions 37 and 205 were required to completely swap the budding morphologies of the two strains of IAV.

3.2.3. Importance of position 169 in M1 of Ck/Pennsylvania strains

Ck/Penn/1 and Ck/Penn/1730 showed one sequence polymorphism in M1: I169T, as well as two amino acid polymorphisms in M2 at positions 43 and 44, which were disregarded as previously mentioned in section 3.2.1. Thus, the aim was to test whether the change at position 169 in M1 was the sole determinant that explained the opposite budding morphologies observed with the Ck/Pennsylvania strains.

Firstly, codon 169 of the M1 genes of Ck/Penn/1 (isoleucine) and Ck/Penn/1370 (threonine) were reciprocally changed by site-directed mutagenesis. PR8 7:1 reassortant viruses with WT or mutated avian virus segment 7s were rescued and titred by plaque assay as before. All viruses were rescued twice, with the exception of Ck/Penn/1 WT (which could only be rescued once as explained in chapter 2.2.3) and the M1-mutant (M 169) virus, for which all (> 10) rescue attempts were unsuccessful (more details in figure 7.1). The viruses that were rescued gave an average titre of 10^8 PFU/ml, with no significant differences between them (Figure 3.6 A). Examination of the plaque phenotype in monolayers of MDCK cells

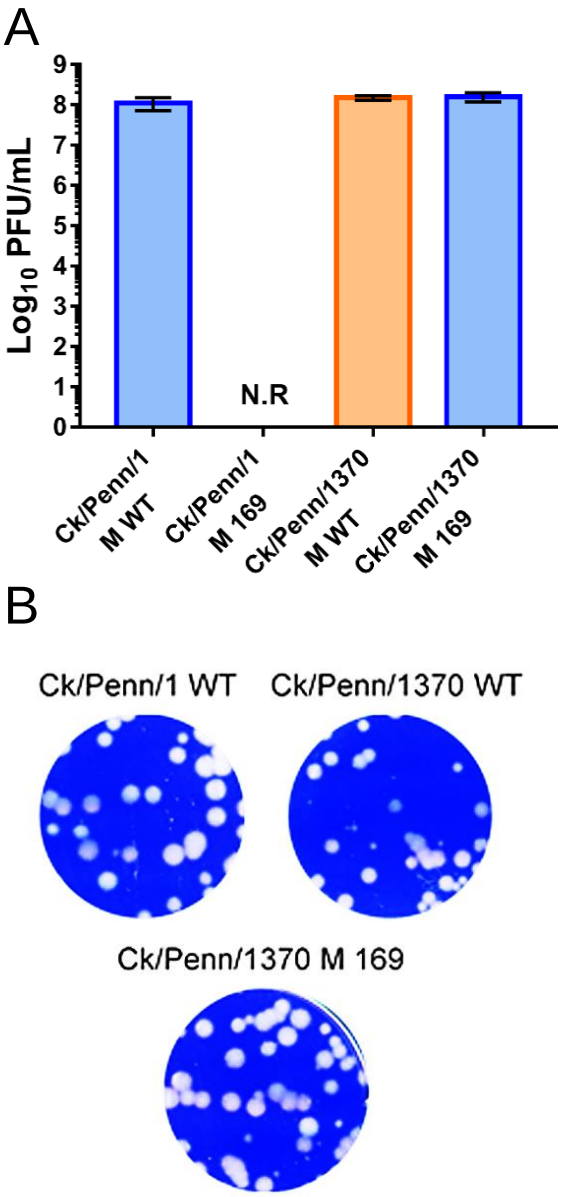

Figure 3.6 Replication fitness of Ck/Penn/1 and Ck/Penn/1370 strains with WT or mutated M1 at position 169. (A) P0 stocks were used to infect MDCK cells at a 1:10 dilution for 48 h. Supernatants were collected and titred by plaque assay in MDCK cells. Data represent mean +/- SEM (n = 3) of two independent rescues, with the exception of Ck/Penn/1 (one stock) and Ck/Penn/1 M 169 (N.R – not rescued). Coloured bars indicate spherical (blue) or filamentous (orange) budding phenotypes. (B) Plaque assays were performed in a monolayer of MDCK cells under Avicel overlay and plaque phenotype was visualised by staining with toluidine blue.

showed that plaques for Ck/Penn/1370 M WT were smaller than those generated by Ck/Penn/1370 M 169; the latter showed larger plaques more comparable to the ones produced by Ck/Penn/1 (Figure 3.6 B). Thus the T169I change in Ck/Penn/1370 likely had a subtle effect on virus fitness *in vitro*. The M1 T169I change resulted in different plaque sizes between WT and M1-mutant Ck/Penn/1370 viruses, which also drastically reduced filament production by Ck/Penn/1370 strain. Therefore, as previously seen, a filamentous phenotype was disadvantageous for plaque formation *in vitro*.

To test the importance of position 169 for the budding phenotype of Ck/Penn/1 and Ck/Penn/1370, MDCK cells were infected with the rescued viruses at a MOI of 3 for 16 h. Cells were fixed and stained for surface viral glycoproteins as before prior to imaging. The standard controls of mock-infected, PR8 WT and PR8 MUd infected cells gave the expected outcomes of no substantial staining; spherical and filamentous patterns of plasma membrane HA (data not shown). Ck/Penn/1 showed a predominantly spherical budding phenotype with an evenly distributed pattern of viral antigen staining, whereas Ck/Penn/1370 presented prominent filaments on the surface of infected cells (Figure 3.7). The single change of a threonine to an isoleucine at position 169 in the M1 of Ck/Penn/1370 abolished the formation of filaments by this virus. Although the reciprocal effect on Ck/Penn/1 could not be tested as the virus did not rescue, this suggested that the amino acid side chains at position 169 had a significant role in determining the budding phenotype of the Ck/Penn/1370 strain.

To strengthen these observations, MDCK cells were infected with the viruses over three independent occasions using (where possible) two separately rescued stocks. Per repeat, two maximum intensity projection images were collected for scoring of the budding phenotype. As described before, for a virus to be considered filamentous, it had to promote filament assembly in over 15% of infected cells and these filaments had to be longer than 2 µm. By these measures, it was clear that Ck/Penn/1 showed a predominantly spherical budding phenotype in contrast to Ck/Penn/1370, which was strongly filamentous (Figures 3.8 A, B). Significantly, when position 169 in M1 of Ck/Penn/1370 was mutated to an isoleucine, the filamentous budding phenotype was drastically reduced. In fact, comparison of Ck/Penn/1370 M 169 with Ck/Penn/1 M WT revealed no significant differences in both the %

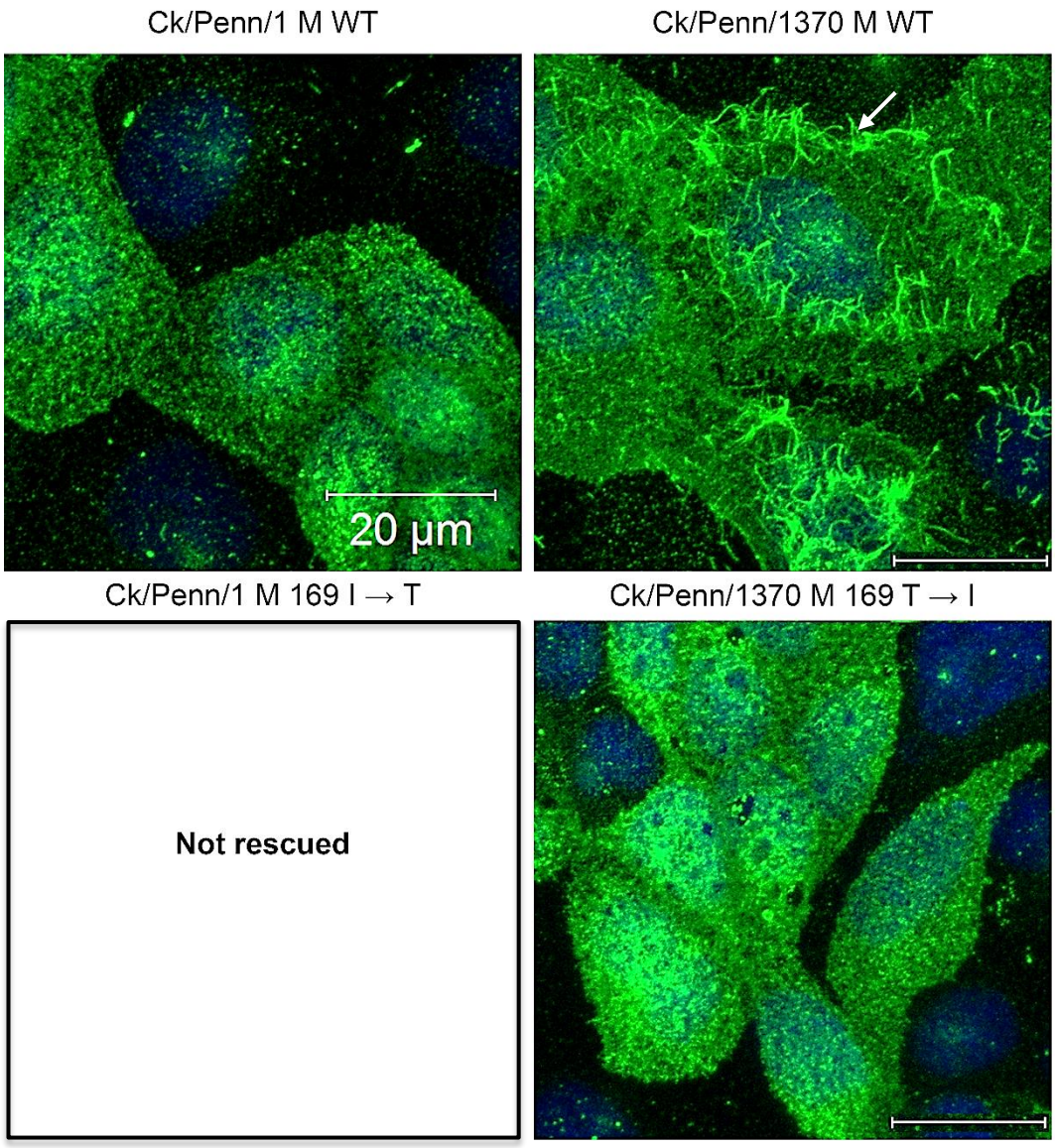

Figure 3.7 Budding phenotype of 7:1 Ck/Pennsylvania reassortant strains with WT or mutated M1 at position 169. WT and M1-mutant viruses were used to infect MDCK cells at a MOI of 3 for 16 h. Cells were fixed and the surface stained with anti-PR8 antibody (green) and DAPI (blue) prior to imaging. Images were collected as maximum intensity projections from Z-stacks on the Zeiss 710 confocal microscope with a 63x objective and are representative of three independent experiments. Arrow indicates filamentous bundles. Scale bars (20 µm) indicated.

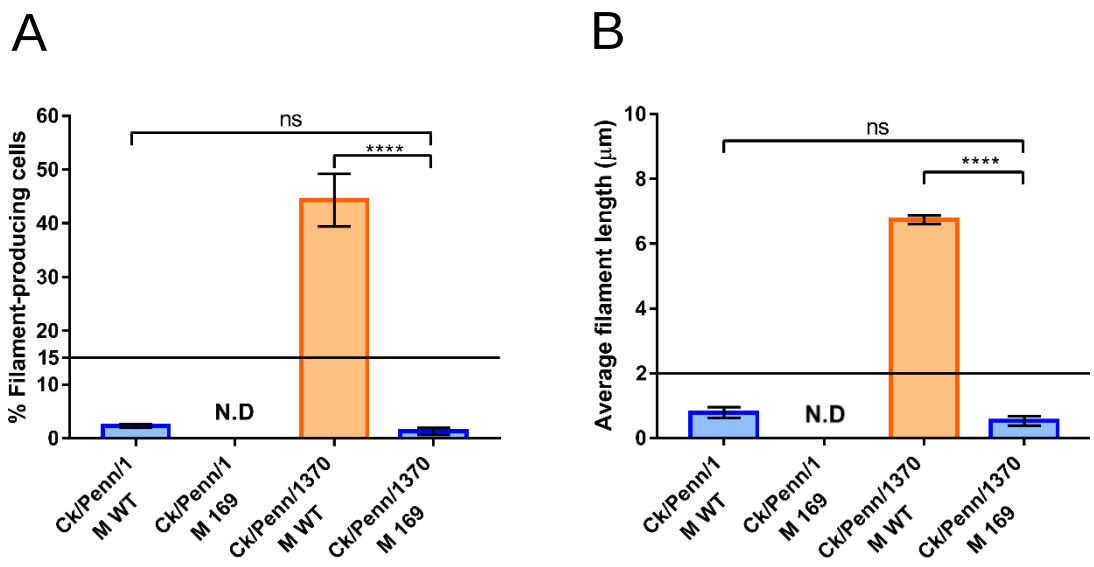

Figure 3.8 Quantification of the budding phenotype of the Ck/Pennsylvania reassortant strains. MDCK cells were infected with the viruses indicated at a MOI of 3 for 16 h and stained as in figure 3.7. (A) A minimum of 100 infected cells were scored per virus to determine the percentage of filament-producing cells. (B) A total of 90 filaments were measured per virus (when visible). Data represent mean +/- SEM (n = 3). One-way ANOVA was performed to compare all the viruses within the group. **** $p < 0.0001$; ns not significant. Limits for viruses to be classified as possessing a filamentous budding morphology are indicated (> 15% of infected cells producing at least one bundle of filaments of 2 μm or longer).

of filament-producing cells and filament length, while Ck/Penn/1370 M 169 was significantly different from its WT counterpart in both factors quantified.

3.2.4. Assessing the importance of M1 position 234 in Ck/Italy and Dk/Netherlands strains

Pairwise alignment of M1s of Ck/Italy and Dk/Netherlands showed one sequence polymorphism between these at position 234, where isoleucine was present in Ck/Italy and leucine in Dk/Netherlands strain. These strains shared a 100% identical M2 amino acid sequence; therefore M2 was not assessed further.

The first step was to reciprocally change the M1 codons at position 234 of Ck/Italy and Dk/Netherlands by site-directed mutagenesis, followed by rescue of the viruses using a PR8 backbone. In addition, given that a full set of reverse genetics plasmids for the Dk/Netherlands strain was available, the entirely avian virus was also rescued with WT or mutant M1 alongside the 7:1 reassortant viruses. All viruses rescued readily twice, with an average titre of 10^8 PFU/ml for the 7:1 reassortant viruses and 10^6 PFU/ml for the avian Dk/Netherlands (Figure 3.9 A). Once again, the titres of the WT and mutated 7:1 reassortant or avian viruses were not significantly different. Plaque phenotypes were visualised in MDCK cells as described before. As seen in figure 2.8 B, Ck/Italy 7:1 reassortant virus produced considerably larger plaques than Dk/Netherlands 7:1 reassortant virus. Mutation of position 234 reduced the plaque size of Ck/Italy or conversely, increased the plaque size of Dk/Netherlands, suggesting subtle differences in replication fitness *in vitro* (Figure 3.9 B).

To determine the importance of M1 position 234 on the budding morphology of Ck/Italy and Dk/Netherlands strains, MDCK cells were infected with the viruses and imaged as before; PR8 reassortant-infected cells with anti-PR8 antiserum, while cells infected with the avian viruses were stained with Con A lectin. Cells infected with Ck/Italy WT M1 virus showed evenly distributed punctate staining of the cell surface, characteristic of viruses with spherical budding phenotypes. By contrast, Dk/Netherlands M1 WT promoted the formation of long filamentous

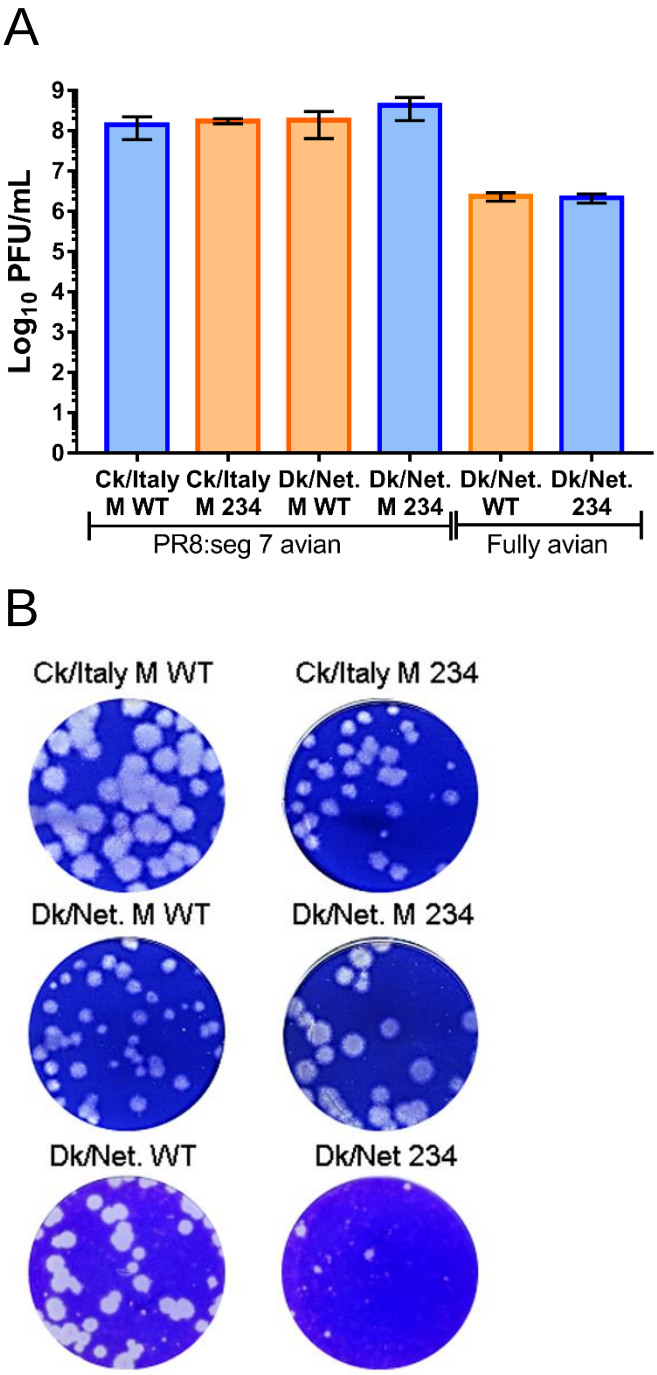

Figure 3.9 Replication fitness of Ck/Italy and Dk/Netherlands strains with WT and mutated M1 genes. (A) MDCK cells were infected with 1:10 dilutions of P0 stocks and left for 48 h before the supernatants were collected and titred by plaque assay. Data represent mean +/- SEM (n = 3) from two independently rescued stocks of viruses. Blue bars correspond to spherical viruses and orange bars to filamentous ones. (B) Monolayers of MDCK cells were infected under Avicel, fixed and stained with toluidine blue to visualise the plaque phenotype of the viruses indicated.

structures on the surface of the cells, similar to the ones produced by the non- reassortant avian WT Dk/Netherlands, albeit in smaller quantities (Figure 3.10, top half). However, when the amino acids at position 234 of M1 were reciprocally changed between Ck/Italy and Dk/Netherlands, Ck/Italy-infected cells presented long filamentous bundles on their surface, while the Dk/Netherlands filamentous phenotype was abrogated (Figure 3.10, bottom half). Like the 7:1 reassortant virus of Dk/Netherlands, the WT avian virus with an isoleucine instead of a leucine at position 234 of M1 also lost its filamentous phenotype.

To quantify the budding morphology of the Ck/Italy and Dk/Netherlands strains, MDCK cells were infected as before with two independently generated virus stocks and two maximum intensity projections were collected per repeat for scoring of the budding phenotypes. Ck/Italy showed a predominant spherical budding phenotype, as number of filament-producing cells and length of the few filaments visible fell well below the previously defined thresholds (Figure 3.11 A). By contrast, the 7:1 reassortant Dk/Netherlands induced filament formation on approximately 60% of infected cells. The fully avian virus Dk/Netherlands also showed a prominent filamentous budding morphology, with almost all the infected cells producing filaments. Regarding filament length, the Dk/Netherlands segment 7, both as a 7:1 reassortant and in its parental avian virus promoted the formation of filamentous bundles that ranged between 8 – 9 μm, whereas Ck/Italy showed much shorter filamentous bundles that fell well below the defined threshold (Figure 3.11 B). The change of an isoleucine to a leucine at position 234 of M1 in Ck/Italy resulted in a virus that promoted filament formation on approximately 60% of infected cells, while the reciprocal change of amino acids at position 234 in M1 of Dk/Netherlands caused the virus to lose its filamentous phenotype. The percentage of cells producing filaments after infection with the mutant Dk/Netherlands 7:1 reassortant virus or the fully avian virus dropped by around ten-fold. With respect to filament length, Ck/Italy M1 produced filaments approximately 8 μm long when position 234 of M1 was altered, while the reassortant Dk/Netherlands decreased from approximately the same value to around 1 μm. The WT Dk/Netherlands virus also showed a pronounced decrease, and although the remaining filaments were just above the defined threshold of 2 μm it was still regarded as a virus with a spherical phenotype because these were rare, appearing on less than 10% of

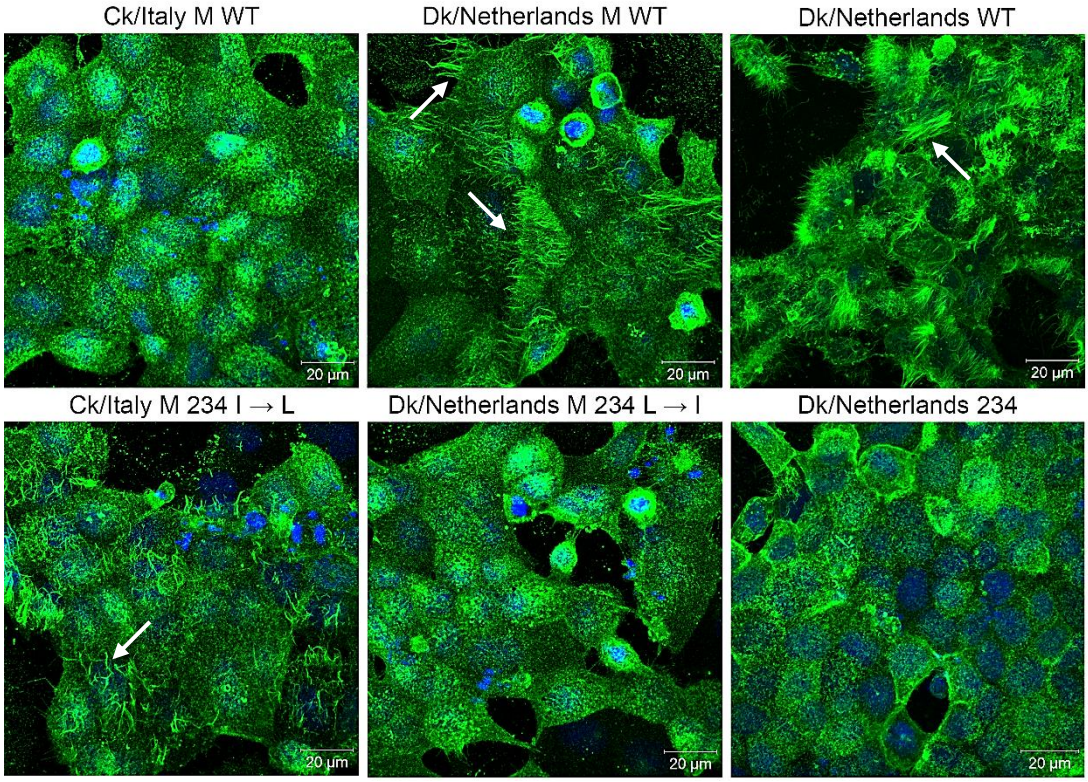

Figure 3.10 Budding phenotypes of Ck/Italy and Dk/Netherlands strains with WT or M1 I234L mutations. M1s of Ck/Italy and Dk/Netherlands strains were mutated at position 234 and the viruses were rescued as 7:1 reassortants in a PR8 backbone or as fully avian viruses (Dk/Netherlands strain). WT and M1-mutant viruses were used to infect MDCK cells at an MOI of 3 for 16 h. Cells were fixed and the surface stained with anti-PR8 antibody for the 7:1 reassortants or Con A lectin for the full Dk/Netherlands viruses (both in green) and DAPI (blue). Images were collected as maximum intensity projections of Z-stacks taken on a Zeiss 710 confocal microscope with a 63x objective and are representative of three independent experiments. Arrows indicate filamentous bundles. Scale bars: 20µm.

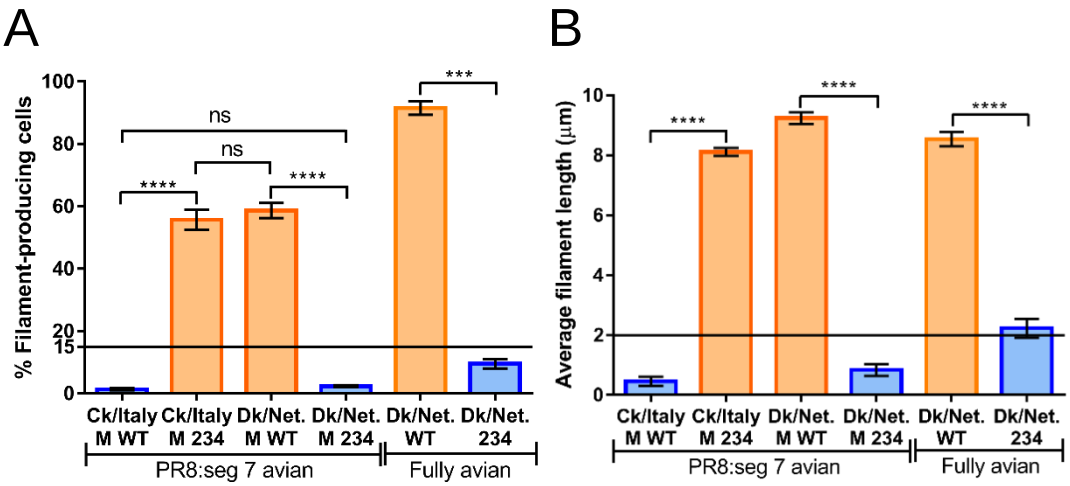
A
% Filament-producing cells
100
80
60
40
20
15
0
ns
ns
****
****
***
Ck/Italy M WT
Ck/Italy M 234
Dk/Net. M WT
Dk/Net. M 234
Dk/Net. WT
Dk/Net. 234
PR8:seg 7 avian
Fully avian
B
Average filament length (μm)
10
8
6
4
2
0
****
****
****
Ck/Italy M WT
Ck/Italy M 234
Dk/Net. M WT
Dk/Net. M 234
Dk/Net. WT
Dk/Net. 234
PR8:seg 7 avian
Fully avian

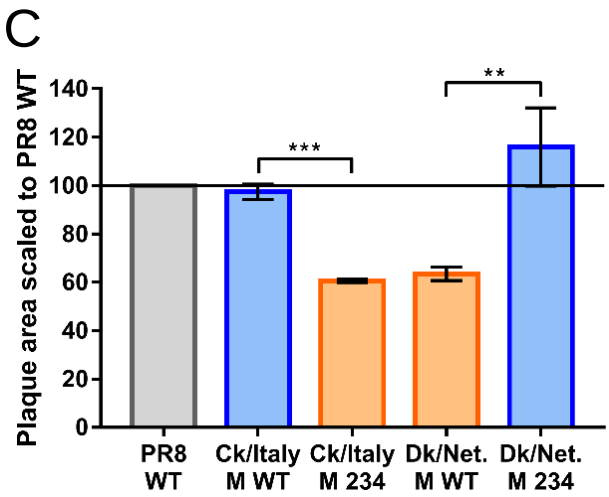
C
Plaque area scaled to PR8 WT
140
120
100
80
60
40
20
0
***
**
PR8 WT
Ck/Italy M WT
Ck/Italy M 234
Dk/Net. M WT
Dk/Net. M 234

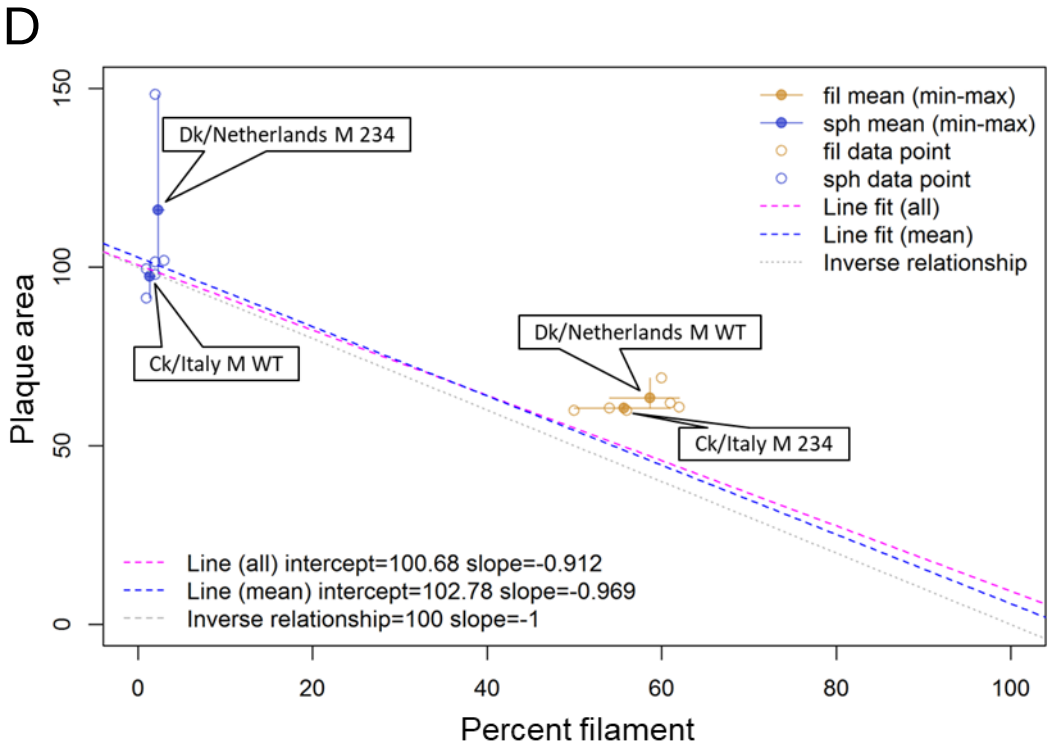
D
Plaque area
150
100
50
0
Dk/Netherlands M 234
Ck/Italy M WT
Dk/Netherlands M WT
Ck/Italy M 234
fil mean (min-max)
sph mean (min-max)
fil data point
sph data point
Line fit (all)
Line fit (mean)
Inverse relationship
Line (all) intercept=100.68 slope=-0.912
Line (mean) intercept=102.78 slope=-0.969
Inverse relationship=100 slope=-1
0
20
40
60
80
100
Percent filament

Figure 3.11 Quantification of the budding phenotype of Ck/Italy and Dk/Netherlands strains and its association with plaque size. (A, B) MDCK cells were infected with the viruses indicated at a MOI of 3 for 16 h and imaged as in figure 3.10. (A) A minimum of 100 infected cells were counted per virus to determine the percentage of infected cells producing filaments. (B) A total of 90 filament bundles were measured per virus (when visible). Data represent mean +/- SEM (n = 3). One-way ANOVA was performed within the group of 7:1 reassortant viruses and a *t-test* was performed within the group of fully avian viruses. *** p<0.001; **** p<0.0001. (C) A minimum of 72 plaques (as seen in figure 3.9 B) were measured per virus. All measurements were scaled to PR8 WT plaque size (set as 100%). Data represent mean +/- SEM (n = 3). One-way ANOVA was performed to compare all viruses against PR8 WT. ** p<0.01; *** p<0.001. (D) Data points represent individual (circle outline) or average (circle coloured in) plaque size plotted against % filament-producing cells. The data was linearized and fitted against the model data from figure 2.11 B. Spherical viruses are represented in blued while filamentous in orange. Graph drawn by Dr Sam Lycett.

infected cells. Overall, these analyses showed that the budding phenotypes of Ck/Italy and Dk/Netherlands were determined by the I234L polymorphism in M1.

To test if the phenomenon of changes to budding morphologies reciprocally affecting plaque phenotype was consistent for Ck/Italy and Dk/Netherlands, a minimum of 70 plaques (as seen in figure 3.9 B) were measured per virus and these were scaled to PR8 WT plaque size measured from the same experiments. Ck/Italy (spherical) exhibited plaques similar in size to PR8, while Dk/Netherlands (filamentous) showed plaques approximately 40% smaller than PR8 (Figure 3.11 C). Conversely, reciprocal alteration of position 234 in M1 of Ck/Italy and Dk/Netherlands resulted in a reduction of the plaque size of Ck/Italy by approximately 40% and an increase of approximately 60% of the plaque size of Dk/Netherlands. The plaque size difference between WT and M1-mutant of the full avian Dk/Netherlands virus was not assessed since the M1-mutant virus produced extremely small plaques that in a majority of experiments were too small to get accurate measurements from. To further confirm the correlation between budding phenotype (i.e. % filament-producing cells) and plaque size, the data was linearly fitted to the model data from figure 2.11 B and showed a linear inverse relationship between plaque size and budding phenotype. This inverse relationship confirmed the association of a small plaque phenotype in MDCK cells with filamentous budding (Figure 3.11 D).

Overall, reciprocal changes of amino acids at position 234 in M1 of Ck/Italy and Dk/Netherlands viruses showed that a single sequence polymorphism in M1 determined the resultant budding morphology. More importantly, in this case, the viruses shared a 100% identical M2 amino acid sequence, which further supported the strength of M1 as the major budding morphology determinant. Furthermore, as observed previously, alteration of budding morphology to a filamentous phenotype also affected plaque phenotype, as demonstrated by the negative correlation calculated between % filament-producing cells and plaque size.

3.2.5. Statistical studies of the association of M1 sequence polymorphisms with budding morphology, genetic background and/or host species

Systematic characterisation of the budding morphology of the avian strains under study (both as 7:1 reassortant viruses and avian virus isolates), suggested that there was no correlation between budding morphology and segment 7 clade from which the M1 genes were sampled. For instance, clades 2, 3, 6 and 9 contained a mixture of viruses that showed either spherical or filamentous budding phenotypes. However, a closer look at the avian hosts of the viruses tested showed a tendency for duck IAVs to be filamentous while chicken strains of IAVs were predominantly spherical (Table 3.1). For instance, the two duck strains on clades 2 and 3 showed opposite budding morphologies, while two of the three stains in clades 6 and 9 were filamentous. A limitation of this tentative conclusion is that it was based on testing only 22 avian M segments out of around 22,000 unique sequences. However, the work described above showed that avian IAV budding morphologies could (at least for the specific strains tested) be determined by positions M1 amino acids 59, 169 and 234; findings that could be used for a more detailed statistical approach to testing the hypothesis that host strain might affect the morphology of avian IAV budding.

To test whether the M1 sequence polymorphisms identified above could be used to predict the budding morphology of a wider sample of chicken and duck IAVs, Fisher's exact tests were performed to determine significant associations between M1 positions and specific hypotheses (Table 3.2). The Fisher's test was performed in R by Dr Sam Lycett with further processing of the results in Microsoft Excel with the help of Dr Sam Lycett. These tests measured the probability of a "condition A" being correlated with another "condition B", giving back a p-value for it. In this study, M1 codons 1 to 252 were condition A, while the hypotheses to be tested were condition B. All 22 M1 amino acid sequences from chicken and duck IAVs with known budding morphology were used for this analysis, including the ones published by other authors (see table 2.1). M1 sequences were aligned and individual positions were selected for analysis when these showed amino acid variability above 15%. This resulted in 14 positions being chosen, across the length of the protein (Table 3.2). Following this selection, the M1 positions were tested for the presence of significant associations with: budding

Table 3.1 Summary of the budding morphology and segment 7 clade distribution of the virus strains used and corresponding clade distribution within the phylogenetic tree. Avian strains were grouped by host and clade (see figure 2.7). Host species are identified in bold and the avian strains of IAV that were tested as original isolated instead of as PR8-based reassortants are underlined. Asterisks denote strains tested by both routes.

Strains	Clade	Spherical	Filamentous
A/**duck**/England/1962	1		✓
A/**duck**/Korea/GJ54/2004	1		✓
A/**duck**/Tripura/103597/2008	2		✓
A/**duck**/India/02CA10/2011	2	✓	
A/**duck**/Shandong/Q1/2013	3	✓	
A/**duck**/Dongguan/2685/2013	3		✓
A/**Duck**/Shantou/1588/2000	4		✓
A/**duck**/Singapore/5/1997	5	✓	
A/**mallard**/Netherlands/10-Cam/1999 *	6		✓
A/**duck**/Mongolia/80/2012	6		✓
A/**mallard**/Wisconsin/1719/1983	7		✓
A/**mallard**/New York/170/1982	8		✓
A/Zhejiang/DTID-ZJU01/2013 (**Chicken**)	5	✓	
A/**chicken**/SaudiArabia/3AAV/2000	5	✓	
A/**chicken**/Israel/215/2007	5	✓	
A/**chicken**/Pakistan/UDL-01/2008 *	5	✓	
A/**chicken**/Italy/1067/1999	6	✓	
A/**chicken**/Pennsylvania/1/1983	9	✓	
A/**chicken**/Pennsylvania/1370/1983	9		✓
A/**turkey**/Canada/1965	9		✓
A/**gull**/Maryland/1824/1978	10		✓
A/**turkey**/South Dakota/7034/1986	11		✓

Table 3.2 Associations between M1 positions and budding morphology, genetic background and avian host. The hypotheses tested by Fisher's exact tests and the condition by which these were defined are represented. A total of 22 duck and chicken M1 sequences were aligned (see table 2.1) and positions tested selected based on amino acid variability (i.e. one amino acid had to appear in more than 4 sequences). The M1 positions identified in bold were the only residues that showed a significant association with at least one of the hypotheses used in the test. The reported p-values were corrected using Bonferroni correction.

Hypotheses	**Condition**	**Total number**	**Positions of M1 tested**	**107**	**144**	**234**
				p-value	p-value	p-value
Morphology	Spherical or filamentous	22 avian strains of IAV	15, 27, 37, 95, 101, 107, 144, 157, 166, 207, 224, 230, 232, 234	ns	ns	ns
Fully avian	Avian virus rescued by RG versus avian isolate available in the lab			ns	ns	ns
7:1 viruses	PR8 reassortants			ns	ns	ns
Host	Chicken or duck			**0.016**	**0.016**	**0.003**

morphology, avian backbone, PR8-based 7:1 reassortants and duck or chicken host species, as seen in table 3.2. Fisher's exacts revealed three M1 positions that showed a significant association with at least one of the hypotheses tested. However, to prevent the occurrence of false positives, these data were subjected to Bonferroni correction. This consisted of multiplying the p-value by the number of M1 positions tested (14 positions). Following this, the remaining significant associations were between positions 107, 144 and 234 of M1 with host species (chicken or duck). Positions 107 and 144 had not been identified via multiple alignments, but position 234 had been previously identified as a budding morphology determinant by examining a pair of closely related avian strains (see section 3.2.4).

Given that M1 is an important factor in determining viral budding morphology, the amino acid variability was determined for the positions in M1 identified by site-directed mutagenesis (59, 169 and 234) and Fisher's exact test (107, 144 and 234) within chicken and duck isolates. Firstly, all the 10,635 available sequences of segment 7 with the complete coding region from avian IAVs were collected from Influenza Research Database (May 2017) and organised into the most common avian hosts (Figure 3.12 A). From this, approximately two quarters of the samples were of chicken or duck-origin. Next, in order to chart the overall M1 sequence variation from avian viruses at the positions of interest, the prevalence of all amino acids seen at positions 59, 169, 107, 144 and 234 were recorded (Figure 3.12 B). This revealed a high prevalence of isoleucine at positions 59 and 107, whereas leucine was predominantly present at position 234. Phenylalanine was overrepresented at position 144, while threonine was predominant at position 169. Overall, this analysis (unsurprisingly) showed that there was a preference for specific amino acids at the indicated positions within avian M1s. However, since the main focus of this study was viruses isolated from chicken and duck host species, the same prevalence analysis was performed based on sequences derived from these hosts. Positions 59 and 169 that were not significant by Fisher's exact test showed a very similar amino acid distribution between the two hosts. Chicken and duck viruses had almost equal percentages of isoleucine or methionine at position 59 and threonine at position 169. Isoleucine at position 169 was only found in chicken IAV isolates but as this represented only 8 out of 2270 sequences it was too rare to be of much biological significance. On the other

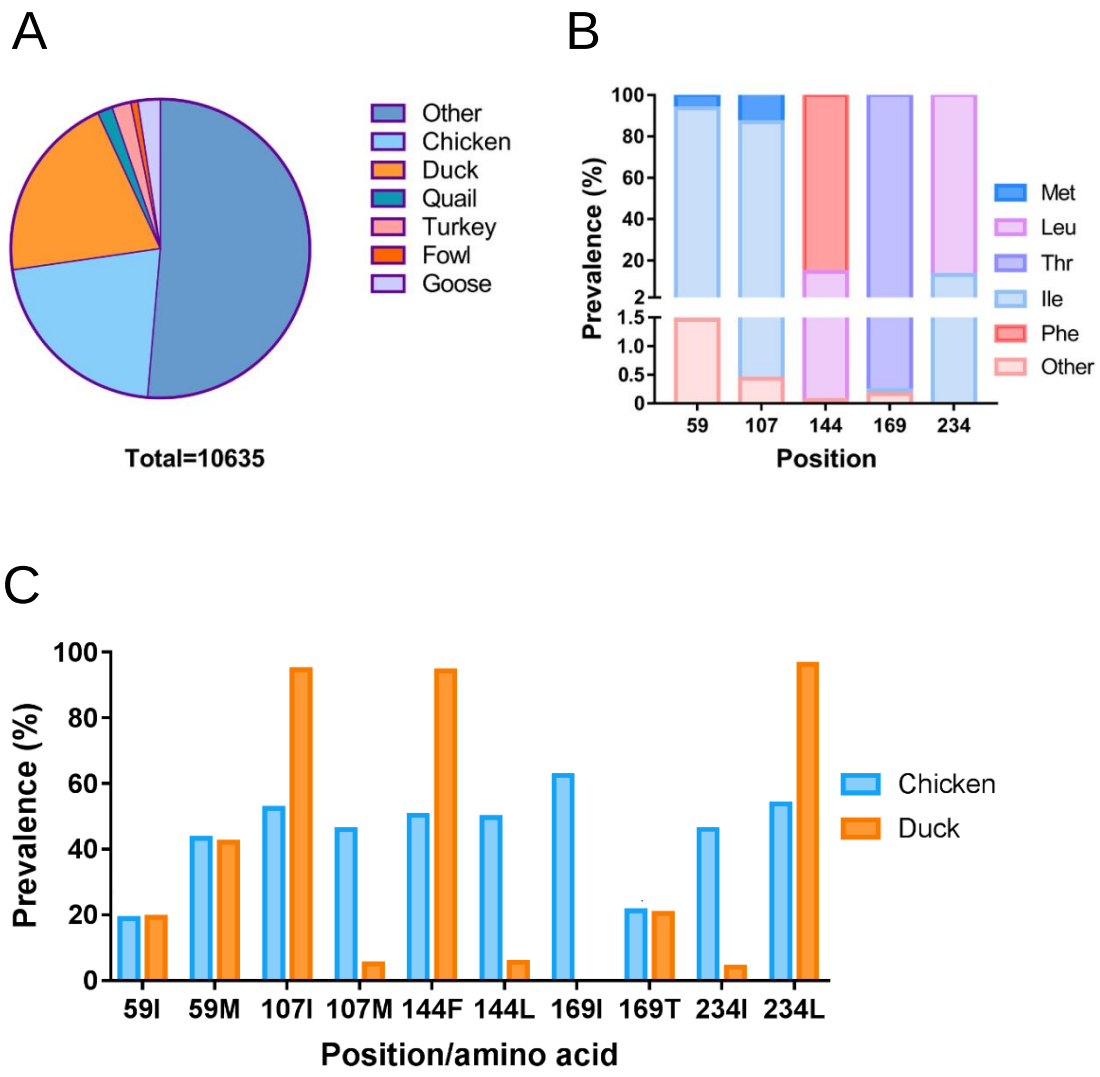

Figure 3.12 Diversity of amino acids at M1 positions 59, 107, 144, 169 and 234 within IAV isolates from avian host species. (A) 10,635 complete avian IAV segment 7 sequences were retrieved from Influenza Research Database on 16/05/2017 and organized into the main hosts present on the overall sample. (B) M1 sequences from A were used to determine the prevalence of specific amino acids at positions 59, 107, 144, 169 and 234 (Figure 3.1 and Table 3.2). (C) From the overall sample, chicken (2024) and duck (1899) M1 sequences were isolated and the prevalence of the specific amino acids determined for each of the positions under study. Numbers above the bars correspond to the total number of sequences. Percentages were derived as explained in chapter 7, section 7.2.7.

hand, the positions that showed an association with chicken or duck host species by Fisher's exact test (107, 144 and 234), showed a skewed pattern of amino acid distribution, particularly within M1s of duck IAVs. Over 90% of duck IAVs had isoleucine at position 107, phenylalanine at position 144 and leucine at position 234 while very few had 107M, 144L and 234I (Figure 3.12 C). In contrast, chicken viruses were much more evenly split, with each of the I107M, F144L and I234L polymorphisms making up around 50% of the available sequences. These observations helped explain the significant association determined by Fisher's exact test between positions 107, 144 and 234 and avian host species. M1 position 234 was chosen for further experimental work because it was identified independently by two different methods. Given that previous observations suggested that chicken IAVs were predominantly spherical and duck IAVs mainly filamentous, it was hypothesised that position 234 of M1 could be a host species-specific virion morphology determinant.

3.2.6. Testing the importance of position 234 in another chicken virus

The statistical and bioinformatics analyses presented above showed that most duck IAVs had a leucine at M1 position 234, while chicken viruses had either leucine or isoleucine in roughly equal proportions. Experimental data so far indicated that chicken IAVs predominantly showed a spherical budding phenotype whereas duck IAVs were mostly filamentous and that in the case of two viruses with closely related M segments, Ck/Italy and Dk/Netherlands, budding morphology could be swapped by I234L mutations. Therefore, in order to test the hypothesis that M1 position 234 could be an avian host species-specific virion morphology determinant, a spherical chicken virus was chosen for site-directed mutagenesis at position 234 of M1. A/chicken/Pakistan/UDL-01/2008 (H9N2) (Ck/Pakistan) was chosen because it showed a high number of sequence polymorphisms when compared with other avian strains under study, both those with spherical and filamentous budding phenotypes (see chapter 2, section 2.2.3, figure 2.13). Before the statistical and bioinformatics analyses reported above, this diversity had made it difficult to predict which residue would be responsible for the spherical budding phenotype of Ck/Pakistan. Accordingly, Ck/Pakistan segment 7 was mutated at M1 codon 234, where isoleucine was changed to leucine and the

WT and M1-mutant viruses were rescued, either as 7:1 reassortants or as full Ck/Pakistan viruses. The 7:1 reassortant viruses were readily rescued twice in mammalian cells as described previously. For reasons that defied trouble shooting and remain unknown, the Ck/Pakistan viruses could not be rescued in the Roslin Institute. These were therefore rescued once at the Pirbright Institute by another member of the group, Anabel Clements, and sent to the Edinburgh laboratory. The 7:1 reassortant viruses reached titres of approximately 10^8 PFU/ml, for both WT and M1-mutant virus. The avian viruses replicated to a lower titre of approximately 10^7 PFU/ml (Figure 3.13 A). Plaque phenotype was assessed in monolayers of MDCK cells by toluidine blue staining. Ck/Pakistan 7:1 reassortant virus showed considerably large plaques, which were reduced to approximately half the size when position 234 of M1 was altered from an isoleucine to a leucine (Figure 3.13 B). The fully avian Ck/Pakistan produced rather small plaques in the Edinburgh laboratory even though at the Pirbright Institute the plaques observed by Anabel Clements were much larger (similar to PR8 WT, see figure 2.8). This made it difficult to determine whether the plaque sizes of Ck/Pakistan WT or 234 were truly different. Therefore, the alteration of amino acid residues at position 234 seemed to have little effect on the plaques produced by the fully avian virus; however this did not exclude subtle differences in replication *in vitro*, which happened to be more noticeable in the PR8-based 7:1 reassortant viruses.

To determine the effect on the budding phenotype of swapping amino acids at position 234 in M1 of Ck/Pakistan, MDCK cells were infected with the viruses, fixed and stained as before prior to imaging. Mock-infected cells showed no detectable levels of infection (data not shown). PR8 WT and PR8 MUd infected cells were also imaged as controls for spherical and filamentous budding morphologies, respectively and showed their expected patterns of cell surface HA staining (Figure 3.14). Ck/Pakistan showed cell surface staining indicative of a spherical budding phenotype, either as an M gene in a PR8 backbone or on its own avian virus background. In contrast, when isoleucine was changed to a leucine at position 234 in M1 of Ck/Pakistan, the budding phenotype of both 7:1 reassortant and avian viruses changed considerably to show a prominent filamentous budding phenotype; similar to PR8 MUd but generally shorter.

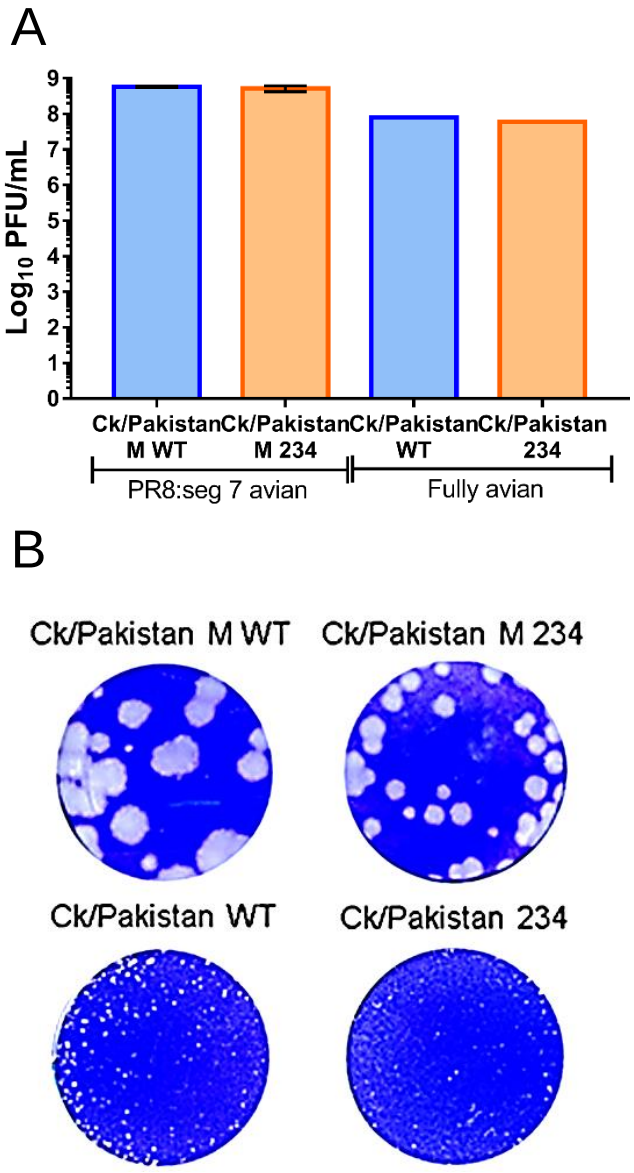

Figure 3.13 Fitness of PR8-based and fully avian viruses with WT and mutant Ck/Pakistan segment 7. (A) P0 stocks of the viruses indicated were (Ck/Pakistan M viruses, at a 1:10 dilution) used to infect MDCK cells or 10-day old embryonated chicken eggs (full avian Ck/Pakistan viruses, with 100 µl of the P0 stock) for 48 h before collection of the supernatant/allantoic fluid, which was titred by plaque assay on MDCK cells. Blue bars correspond to spherical viruses and orange bars to filamentous ones. Data represent mean +/- SEM (n = 3) from two independent stocks for the Ck/Pakistan M reassortant viruses or a single rescue for the CK/Pakistan viruses. (B) Plaque assays were performed on monolayers of MDCK cells under Avicel overlay and visualised following toluidine blue staining.

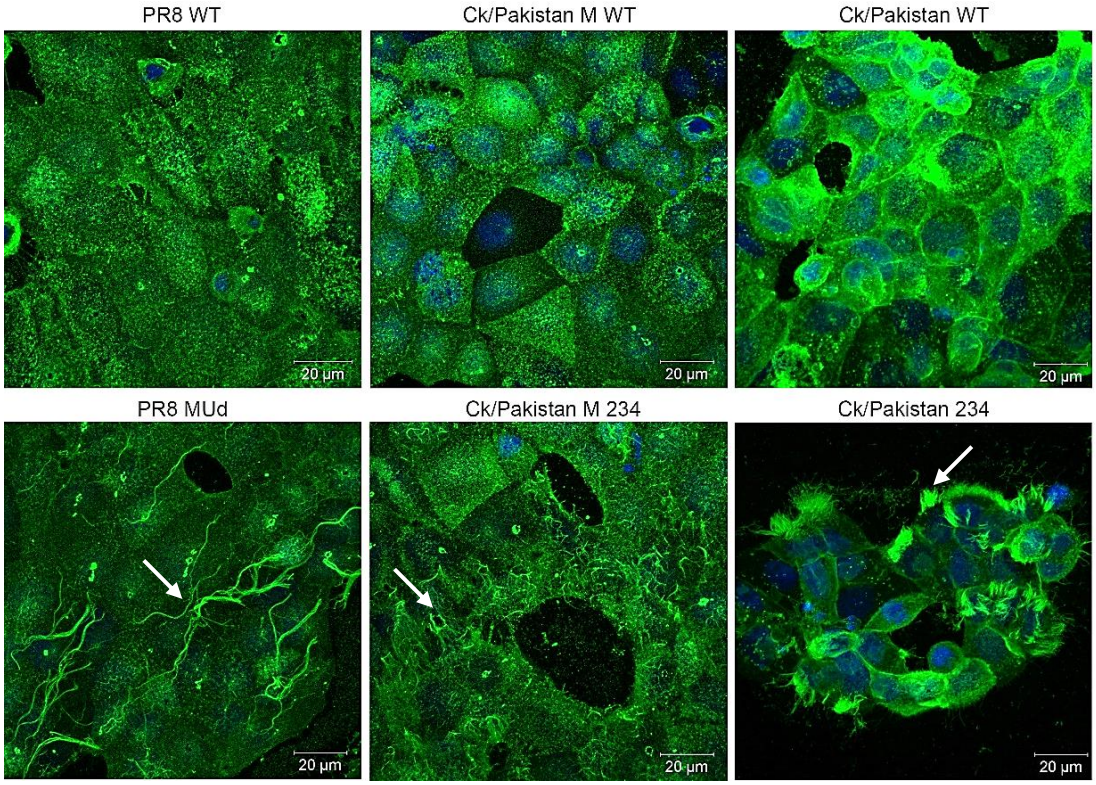

Figure 3.14 Budding phenotype of Ck/Pakistan WT and M1-I234L. The Ck/Pakistan M1 gene was mutated from an isoleucine to a leucine at position 234 and rescued either as 7:1 reassortants with PR8 or in the full Ck/Pakistan background were used to infect MDCK cells at a MOI of 3 for 16 h. Cells were fixed and the surface stained with anti-PR8 antibody (green) for 7:1 reassortants or Con A lectin for Ck/Pakistan (green) viruses and DAPI to indicate nuclei (blue). Images were collected as maximum intensity projections from Z-stacks on the Zeiss 710 confocal microscope with a 63x objective and are representative of three independent experiments. Arrows indicate filamentous bundles. Scale bars (20 µm) indicated.

In order to extend the information given by the microscopy data, budding of the WT and mutant Ck/Pakistan viruses was quantified. MDCK cells were infected, once each with the two independently rescued 7:1 reassortant viruses and twice more with the avian viruses. Two maximum intensity confocal projections of the cell surfaces were collected per repeat for scoring of budding phenotype. As described previously, a virus was classified as filamentous if more than 15% of infected cells were producing filaments and these were longer than 2 µm. By these criteria, Ck/Pakistan WT showed a predominantly spherical budding phenotype, while Ck/Pakistan M1-I234L virus induced filament formation on approximately 50% of infected cells, both as a 7:1 reassortant or avian virus (figure 3.15 A). In both genetic backgrounds, Ck/Pakistan M1-I234L promoted the formation of filamentous bundles on the surface of the cells that ranged 7 to 8 µm (figure 3.15 B). Thus the budding phenotypes of Ck/Pakistan WT and M1-I234L mutant viruses proved to be drastically different. Furthermore, these experiments further confirmed the importance of the M1 I234L polymorphism as a determinant of avian IAV virion shape.

To determine the effect of changing an isoleucine to a leucine at position 234 on the folding of Ck/Pakistan M1, these mutations were mapped on the structure of this protein. Firstly, since the crystal structure of M1 from another orthomyxovirus (infectious anaemia salmon virus – IASV) had been recently solved, this was considered to map the mutations of interest (Zhang et al., 2017). The ISAV M1 is a 196-amino acid protein with an N-terminus formed of eight helices and a C-terminal domain composed of four helices with both domains connected by a short loop linker. The authors showed that helices one to five of ISAV M1 were present in the same location as helices one to five of IAV, but helix 6 of IAV was absent from ISAV M1. ISAV M1 helices six to eight were mapped to the same location as helices seven to nine of IAV. Therefore, the reasoning was that the C-terminus of ISAV M1 could be used to get a more accurate prediction of the C-terminus of IAV M1, as the latter was also predicted to encode for four helices in its C-terminus (Sha & Luo, 1997). However, structural alignment of ISAV M1 with IAV M1 showed that the C-terminus was more distant structure-wise than the N-terminus. For instance, the C-terminus of IAV M1 was reported to be a flexible relatively

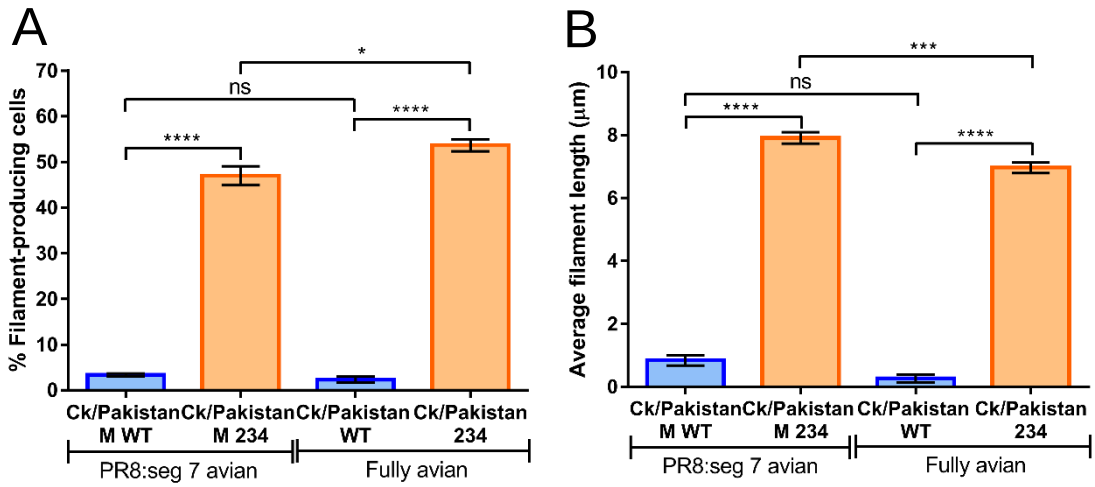

Figure 3.15 Quantification of the budding phenotype of viruses with the Ck/Pakistan M gene. MDCK cells were infected with the viruses indicated at a MOI of 3 for 16 h and imaged as in figure 3.14. (A) A minimum of 100 infected cells were counted per virus to determine the percentage of infected cells producing filaments. (B) A total of 90 filaments were measured per virus (when visible). Data represent mean +/- SEM (n = 3). *t-tests* were performed to compare within the 7:1 reassortants and fully avian virus groups. **** $p<0.0001$. Viruses are colour-coded by budding morphology: spherical in blue and filamentous in orange.

disordered domain, while the C-terminal domain of ISAV M1 showed a more compact and organised conformation with four helices that could not be mapped on the C-terminus of IAV M1 (data not shown) (Zhang et al., 2017). These structural differences between IAV M1 and ISAV M1 were considered too great to determine the effects of changing specific residues on the folding of IAV M1. Therefore, the online prediction tool (I-TASSER (I-TASSER, 2017)) was used to predict the three domain structure of M1 and also provided information on the conformational changes of the protein upon amino acid substitution. This program used all the known available protein structures and their amino acid sequences to predict the structure of another protein based on its amino acid sequence and likely secondary structures. Therefore, I-TASSER was used to obtain a predicted structure for M1 of Ck/Pakistan where the structure of the N and M domains were based on the PR8 M1 structure (Sha & Luo, 1997) and the missing C-terminal domain was organised by structure comparison. The predicted M1 structure of Ck/Pakistan with isoleucine at position 234 showed a C-terminal domain comprised mainly of random coil with three α-helices arranged into a roughly triangular shape with the C-terminus of the protein pointing away from the plane defined by the packed array of α-helices present in the N and M domains (Figure 3.16 A). The side chain of isoleucine 234 was located on helix 2 pointing out into the solvent. Conversely, the predicted structure of the C-terminal domain of M1 with leucine at position 234 was substantially different, both in conformation and how it was arranged with respect to the N and M domains. As well as being flattened to a more horizontal direction, it also showed a more compact folding with three α-helices (Figure 3.16 B). Furthermore, in M1 with isoleucine at position 234 the long helix of the M domain showed a prominent kink to the left of the helix axis, whereas the change to leucine at this position caused the long helix to tilt slightly to the right. Thus, even though alteration of isoleucine to leucine is a common occurrence in nature (Henikoff & Henikoff, 1992), the predicted structure of M1 with either amino acid at position 234 showed major differences in folding. Although only a prediction, this difference was consistent with the major phenotypic difference seen in budding morphologies. Collectively, these results support the hypothesis that position 234 could be a strong budding morphology predictor in an avian host species-specific dependent manner.

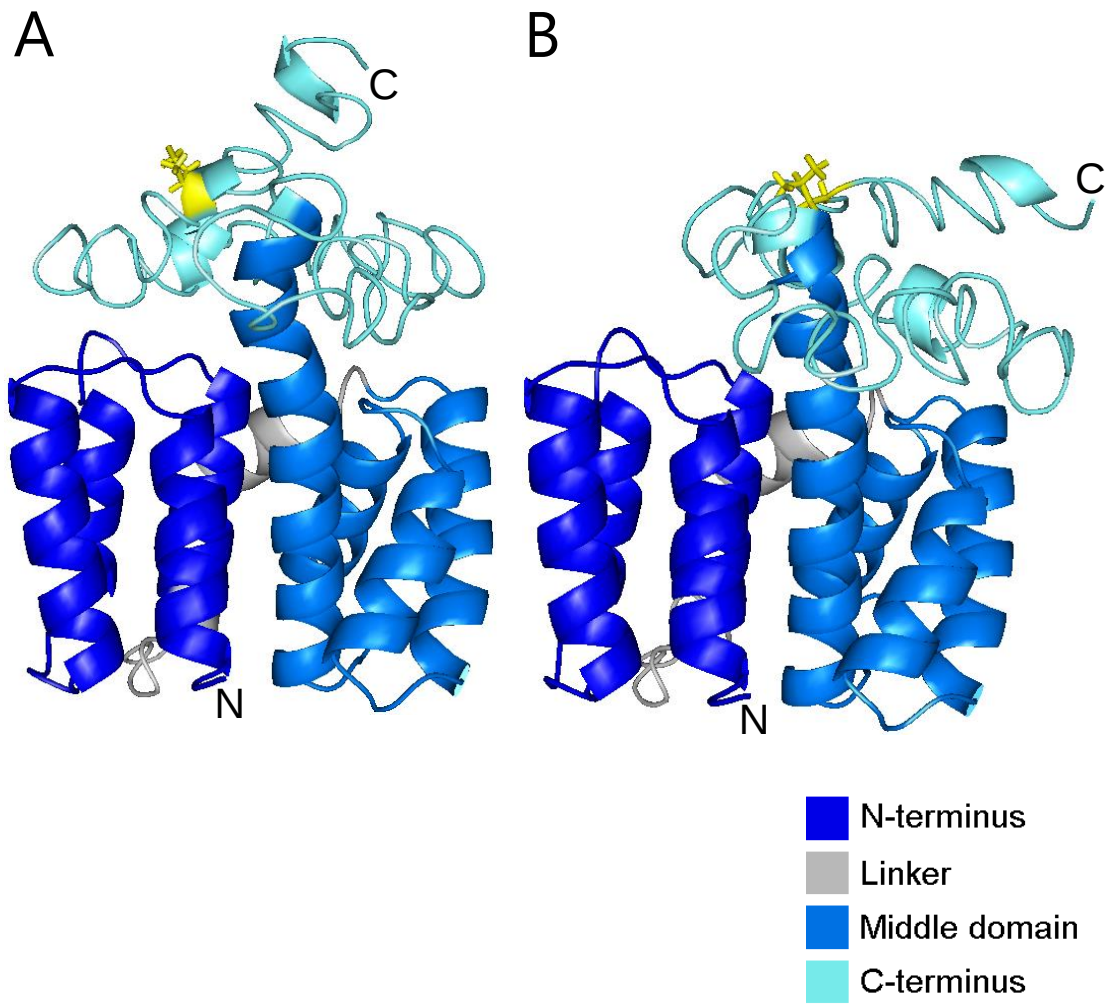

Figure 3.16 Predicted structures of Ck/Pakistan strain M1 with either isoleucine or leucine at position 234. The structure of Ck/Pakistan M1 was predicted using the I-TASSER online tool, based on the crystal structure of PR8 M1 (1AA7). Ck/Pakistan M1 amino acid sequence was submitted to I-TASSER with an isoleucine (A) or a leucine (B) at position 234. Protein structures were further processed in Pymol software. The side chain of amino acid 234 is displayed in yellow. Established structural domains of M1 (N-terminus, linker, middle domain and C-terminus) are colour-coded as indicated.

3.3. Discussion

The importance of the viral matrix protein M1 in determining the budding morphology of IAVs has been well characterised (Smirnov et al., 1991; Roberts et al., 1998; Gomez-Puertas et al., 2000; Bourmakina & Garcia-Sastre, 2003; Elleman & Barclay, 2004; Chou et al., 2011; Campbell et al., 2014), in the process, defining the importance of amino acid identity at positions A41V, S85N, K95R, E204D, S207N and T218A in human and equine strains of IAV (Roberts et al., 1998; Bourmakina & Garcia-Sastre, 2003; Elleman & Barclay, 2004; Bialas et al., 2012; Elton et al., 2013). These residues have been described as the filamentous "signature" of mammalian IAVs (Elton et al., 2013). However, characterisation of avian strains of IAV revealed that these do not obey the same "rules"; therefore the aim of this part of the study was to identify the potential signatures that govern avian IAV budding morphology.

As described in chapter 2, general alignment of the avian M1 sequences tested here did not show a consistent pattern of mutations that would explain the different budding morphologies observed. However, examination of closely related avian strains, defined as having a very similar M1 amino acid sequence, revealed some that nevertheless showed opposite budding phenotypes. In this section, three pairs of strains that met these conditions were characterised. Dk/India and Dk/Tripura presented three sequence polymorphisms (residues 37, 59 and 205), while Ck/Penn/1 and Ck/Penn/1370 pair and Ck/Italy and Dk/Netherlands pair both showed a single amino acid polymorphism at positions 169 and 234, respectively (Figure 3.1). Characterisation of Dk/India (spherical) and Dk/Tripura WT (filamentous) and M1-mutant viruses showed that reciprocal change of amino acids at position 59 was capable of swapping the phenotype of the two strains, suggesting that position 59 was the main morphology determinant (Figure 3.3). However, only the addition of the other two positions (37 and 205) accurately exchanged the budding phenotype of the two strains (Figure 3.4). On the other hand, Ck/Pennsylvania strains and Ck/Italy and Dk/Netherlands only showed a single sequence polymorphism in M1 and characterisation of WT and M1-mutant viruses confirmed the importance of residues 169 and 234 as morphology determinants in these pairs of viruses.

A consistent observation throughout this section was related to the relative replication fitness of spherical and filamentous budding phenotypes. For all the viruses characterised, the spherical viruses replicated to titres similar to the filamentous viruses (Figure 3.2 A, figure 3.6 A, figure 3.9 A and figure 3.13 A), but spherical viruses showed a clear advantage *in vitro* as these produced larger plaques (Figure 2.11 B), in agreement with previously published reports on the advantage of the spherical phenotype over the filamentous phenotype *in vitro* (Seladi-Schulman *et al.*, 2013; Roberts et al., 1998).

Following identification of residues 59, 169 and 234 in M1 as modulators of budding morphology between closely related avian strains that showed opposite budding phenotypes, the next step was to access whether these residues had the potential to form a filamentous "signature" for avian strains of IAV. Therefore, Fisher's exact tests were performed using all the M1 sequences deriving from strains of known morphology, including strains not characterised here but previously published (Al-Mubarak et al., 2015; Pu et al., 2017) (Table 2.1). These tests calculated the presence of a significant association between avian virus M1 codons (1 to 252) and specific hypotheses (Table 3.2). The positions identified by site-directed mutagenesis – 37, 59, 169 and 205 – did not show a significant association with any of the hypotheses tested. By contrast, two new positions identified in this study (residues 107 and 144) along with an already identified residue (codon 234, see section 3.2.4) revealed a significant association with avian host species (Table 3.2). Therefore, this suggested that there was a consistent pattern of amino acid distribution at positions 107, 144 and 234 between chicken and duck strains of IAV. This was corroborated by bioinformatics analysis of the amino acid prevalence of the positions identified within a bigger sample of avian segment 7s, where amino acid identity at positions 107, 144 and 234 showed a clear pattern of distribution between chicken and duck IAVs. However, considering that position 234 was identified independently by two different methods, the main focus of this section of the study was on that position. Therefore, bioinformatics and statistical analysis coupled with the observation that chicken IAVs tended to be spherical with isoleucine at position 234 while duck IAVs were predominantly filamentous with leucine at position 234, gave rise to the hypothesis that position 234 could be a determinant of budding morphology in an avian host species-specific

dependent manner. To test the aforementioned hypothesis, a spherical chicken virus with isoleucine at 234 was selected (Ck/Pakistan) and mutated to encode a leucine at this position of M1. The M1-mutant virus of Ck/Pakistan induced the formation of the characteristic filamentous structures on the surface of infected cells (Figure 3.14) in both PR8-based 7:1 reassortant viruses and in the avian virus background. Although interchange of isoleucine to leucine is a current occurrence in nature (Henikoff & Henikoff, 1992), the striking differences in the budding morphology indicate that at position 234 this naturally occurring amino acid alteration has a significant impact on the virus.

In this study, mapping of residues T37A and I205V, singly or in combination, onto the predicted three domain structure of M1 from Dk/India or Dk/Tripura showed no striking differences on the folding of M1 (data not shown). Mapping of isoleucine at position 59 of Dk/India showed a C-terminus composed of some random coil and four helices that were perpendicular and dispersedly organised around the M domain (Figure 3.17 A). However, alteration to a methionine induced a conformational change on the C-terminus, resulting in a domain mainly composed of random coil that was more tightly compacted around the M domain with only three helices (Figure 3.17 B). Similar observations were made with Dk/Tripura M1, therefore these are not shown. Although methionine at position 59 of Dk/India M1 only slightly affected the folding of the protein therefore explaining the different morphologies, another hypothesis would be that this start codon is encoding for another gene product. The M segment has several start codons and is known to produce at least four mRNA transcripts (Wise et al., 2012). As explained before, mRNA 1 translates into M1 while mRNA 2 gives M2. More recently, it was identified M42 from mRNA 4, which can functionally replace M2 (Wise et al., 2012). However, unlike in the case of M1, M2 or M42, the Kozak sequence surrounding the start codon at position 59 is relatively weak; therefore this hypothesis was discarded and the difference in budding morphology was solely allocated to conformational changes within M1. By contrast, alteration of threonine to an isoleucine at position 169 of Ck/Penn/1370 M1 did not reveal any striking differences that would explain the different budding morphologies (data not shown). However, considering that position 169 was mapped to a predicted domain of M1 (C-terminus), it could just mean the differences were subtle and

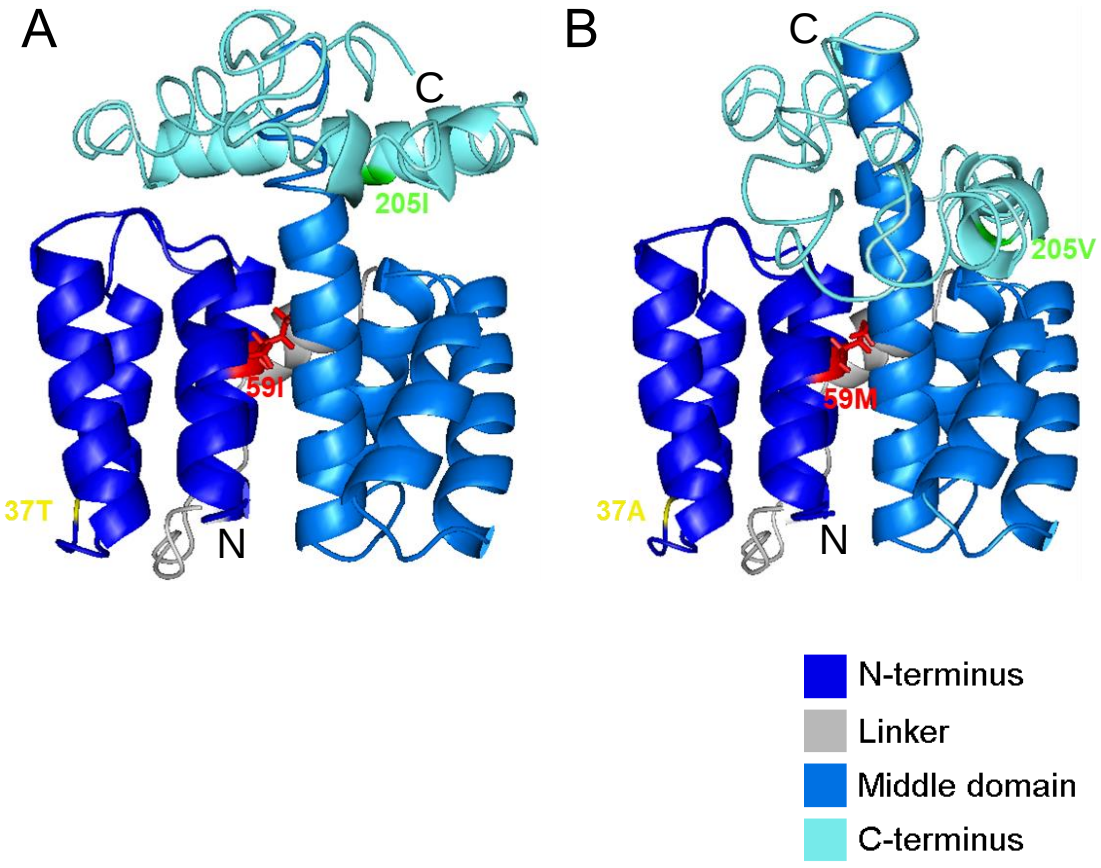

Figure 3.17 Predicted structures of Dk/India M1 with either isoleucine or methionine at position 59. The three domain structure of Dk/India M1 was predicted using the I-TASSER online tool, based on the two domain crystal structure of PR8 M1 (1AA7). Dk/India M1 amino acid sequence was submitted to I-TASSER with 37T, 59I and 205I (A) or 37A, 59M and 205V (B). Protein structures were further processed in Pymol software. The side chain of amino acid 59 is displayed in red, while the location of amino acids 37 (yellow) and 205 (green) is indicated. Established structural domains of M1 (N-terminus, linker, middle domain and C-terminus) are colour-coded as indicated.

therefore not detected by the I-TASSER program. Overall, the most striking differences observed were with reside I234L (Figure 3.16).

The work described so far had led to the identification of a suite of M1 sequence polymorphisms that affected virus budding morphology and/or potentially acted as host-dependent "signatures", namely residues at positions T37A, I59M, I107M, F144L, 169T, I205V and I234L. However, it did not inform on how the changes affected virion shape. Indeed, inspection of the list of key residues showed a preponderance of conservative changes to hydrophobic side chains; something that would perhaps not normally immediately suggest changes to protein function. As a first step to addressing this question, the amino acid positions of interest were mapped onto the crystallographic structure of the two domain M1, including for comparison, residues known to be important for determining particle shape in mammalian strains of IAV (Figure 3.18 A and B). On the other hand, the residues of interest in the C-terminus of M1 were mapped based on the structural prediction given by I-TASSER as mentioned before (Figure 3.18 C and D). Residues T37A, A41V and I59M all mapped to the N domain of M1, with S85N in the linker region and K95R, I107M and F144L all present in the M domain (Figure 3.18 A). Of these, majority were clearly exposed on the surface of the two-domain structure of M1 (T37A, A41V, S85N, K95R and I107M) (Figure 3.18 B). The residues I169T, E204D, S207N and T218A in the C-terminus were mapped to disordered regions of this domain while residue I234L was mapped to a helix (Figure 3.18 C). Similar to what was observed with the residues mapped in the N and M domains, majority of the residues in C-terminus were clearly visible on the surface of M1 (I169T, E204D, T218A and I234L) (Figure 3.18 D).

As mentioned before, the N domain of M1 is known to be involved in association of the protein to the lipid membrane that composes the virion (Figure 1.6). While residue 37 was surface exposed, residue 59 (avian) was buried within the N domain of M1. Residue T37A did not cause any changes to the virion shape or folding of M1, unlike the other surface exposed residue - mammalian A41V – that was reported to alter virion morphology and promote overexpression of M42, which unpublished data from the Digard laboratory suggest that it decreases filamentous bundles formation (Wise et al., 2012). On the other hand, residue 59

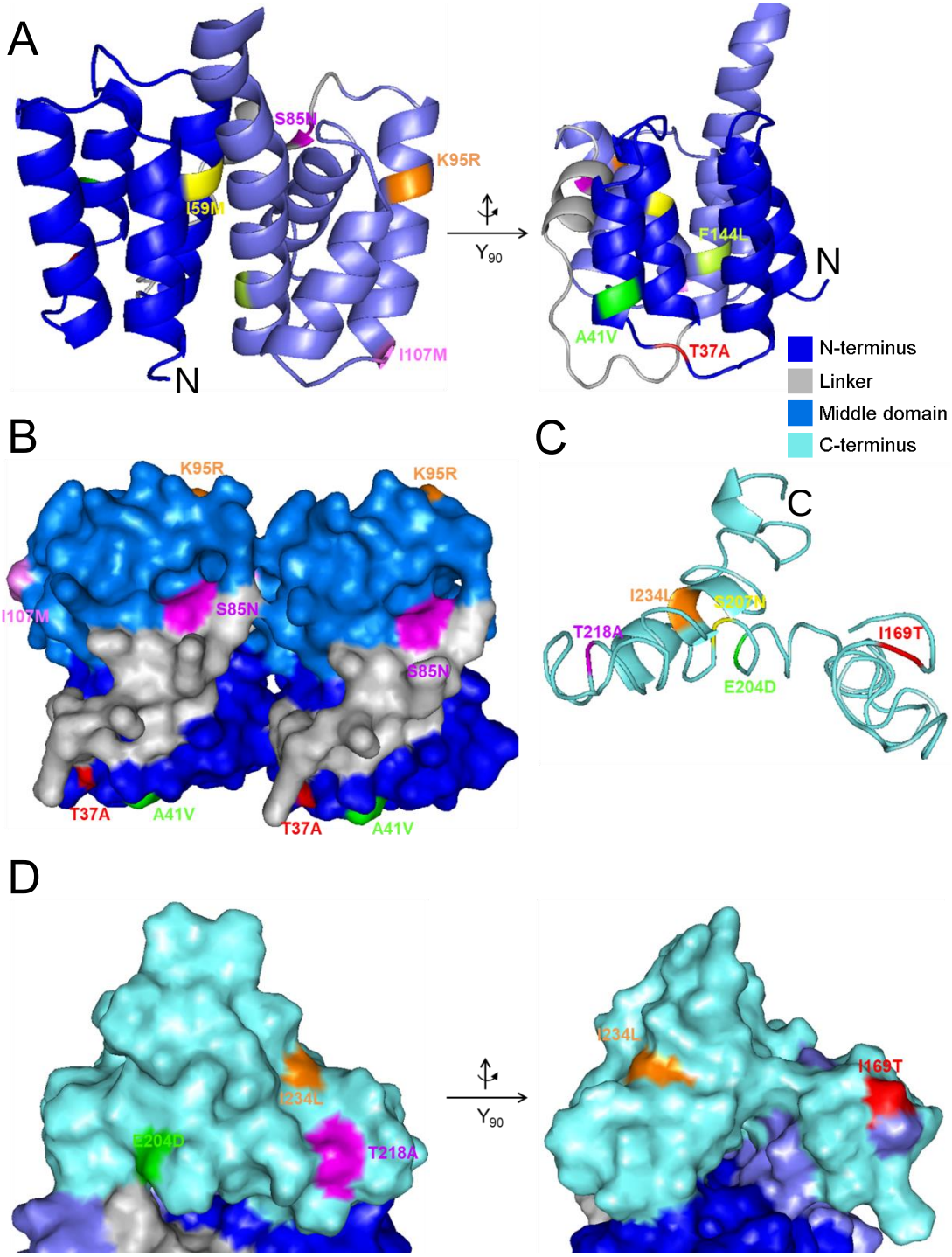
A
S85N
K95R
L59M
I107M
N
Y90
F144L
N
A41V
T37A
N-terminus
Linker
Middle domain
C-terminus
B
K95R
K95R
I107M
S85N
S85N
T37A
A41V
T37A
A41V
C
C
I234L
S207N
T218A
I169T
E204D
D
I234L
E204D
T218A
Y90
I234L
I169T

Figure 3.18 Predicted structure of Ck/Pakistan M1 with previously identified mammalian residues and the newly identified avian residues. (A) The two domain crystal structure of Ck/Pakistan was predicted based on the PR8 M1 crystallographic structure of M1 (1AA7). The mammalian (41, 85, 95, 204, 207 and 218) and the avian (37, 59, 169, 205 and 234) with the corresponding amino acid substitutions were mapped onto this structure and are colour-coded as indicated. A rotation of 90ºC in the y axis is shown to clearly show all positions mapped. (B) Surface of a M1 dimer with the residues mapped to the N and M domains showing and colour-coded as indicated. Only the residues indicated on the picture were visible on the surface of the M1 dimer. (C) The C-terminus of Ck/Pakistan M1 represented was derived by structure comparison using I-TASSER. The residues mapped to this domain are colour-coded as indicated and majority were clearly visible on the surface of the C-terminus of M1 (D). A rotation of 90ºC in the y axis is shown to clearly show all positions mapped. Established structural domains of M1 (N-terminus, linker, middle domain and C-terminus) are colour-coded as indicated.

could be involved in intramolecular interactions important for M1 stability, since amino acid substitution considerably affected folding of the C-terminus of M1. Interestingly, this residue is also at the beginning of a recently identified NES within M1 (see figure 1.6), therefore changes at the amino acid level could also have an impact on export of M1 from the nucleus but this was not further addressed on this study. Given that the M domain of M1 was reported to be involved in M1 and NP association, the avian residues identified in that domain (I107M and F144L) could play a role in M1-NP interactions. For instance, Liu et al reported that spherical viruses presented a stronger association of M1-NP than filamentous viruses (Liu et al., 2002). Moreover, Bialas et al reported that a human M segment with a typical "filamentous signature" only produced filaments in a PR8 backbone, as in the human virus NP was preventing filament formation (Bialas et al., 2014). Furthermore, it was reported that NP also binds actin microfilaments to retain the newly formed vRNPs in the cytoplasm that are then incorporated into progeny virions (Digard et al., 1999). Therefore, it is possible that residues 107 and 144 modulate the strength of M1-NP association which in turn can affect the interaction of NP with the actin cytoskeleton that was reported to be a detrimental factor in filament formation (Roberts & Compans, 1998).

Residues I169T and I234L were exposed in the C-terminus of M1 while I205V was buried within M1. The C-terminal domain is a relatively flexible and disordered domain, which limits its ability to crystalize. This domain is known to be involved in M1-M1 oligomerisation and it was recently reported to promote M1 polymerisation at physiological pH, but as the pH drops (below 6) the C-terminus prevents M1-M1 association, explaining the release of vRNPs into the cytoplasm in late endosomes during viral entry (Calder et al., 2010; Shtykova et al., 2017). Furthermore, while the N and M domains of M1 seem to share a considerably conserved structure, the conformation of the C-terminal domain changes between M1s, even though M1 is the most conserved protein in IAV (compare C-terminus of figures 3.16 and 3.17). Residue I169T mapped to the edge between the M and C-terminal domains, but within the avian strains where it was identified caused no striking difference on the folding of M1, which was also the case of I205V even though an alteration in the nearby region (E204D) was identified in mammalian IAVs as a morphology modulator (Bourmakina & Garcia-Sastre, 2003). By

contrast, the amino acid alteration I234L was shown to more tightly pack the C-terminus around the M domain, similar to what was observed with I59M alteration. Although it is not documented how the C-terminus is packed in the matrix layer of a filamentous virus, it was reported by Calder et al that filamentous strains typically display an ordered helical matrix which forms a relatively rigid structure that supports the virion (Calder et al., 2010). Therefore, the more compact conformation of the C-terminus could lead to a more tightly packed M1 with closer M1-M1 interactions, leading to the formation of a more rigid structure that provides support to filamentous virions.

Even though the genetic determinants within M1 identified in this section of the study were shown to be the main determinants of budding morphology, there are other viral and cellular determinants of virion morphology. As previously discussed (sections 1.6.1 and 1.6.2), HA and NA were also shown to affect budding morphology, more specifically a filamentous NA was reported to promote the formation of a few filamentous virions by the spherical strain PR8 (Campbell et al., 2014). Therefore, it is possible that a cumulative effect exists between M1 and NA that promotes filament formation. Cellular components such as Rab11 or Rab11-FIP3 were shown to considerably affect virus budding, with Rab11-FIP3 causing abrogation of the filamentous phenotype of PR8 MUd (Bruce et al., 2010). Furthermore, components of the ESCRT pathway were also identified interacting with IAV M1, namely VPS28; however it is known that IAV buds out of the cell in an ESCRT-independent manner (Bruce et al., 2009; Rossman et al., 2010). Yet, like in the case of FIP3, the role of VPS28 in budding morphology remains unknown. Nonetheless, considering that the endosomal recycling and ESCRT pathways are both associated with membrane scission during cell division, it is possible that their components play a role in promoting membrane fission or stabilising the site of budding alongside the viral protein M2 (Roberts et al., 2013; Rossman et al., 2010).

Overall, this section of the study showed that avian strains of IAV have their own filamentous “signature”, involving positions I59M, I169T and I234L which were identified by comparison of closely related avian strains that showed opposite budding phenotypes. This section also showed that budding morphology was not clade-dependent, but potentially host-dependent as spherical budding phenotypes were common in chicken but rare in duck IAVs.

Therefore, to test whether positions 59, 169 and 234 could make a filamentous “signature” for a wider sample of chicken and duck IAVs, Fisher’s exact test was performed leading to the identification of positions 107, 144 and 234. Positions 107 and 144 were not further studied, but this study does not exclude their potential to be morphology determinants, but perhaps a bigger sample of chicken and duck IAVs with known morphology would be needed. By contrast, the strength of position 234 was so great that even in a small sample (22 sequences) it was possible to identify it. Thus, it was hypothesised that this position could be a morphology determinant in an avian host dependent manner. This hypothesis was corroborated by alteration of the amino acid identity at position 234 of M1 from a spherical chicken virus (Ck/Pakistan). Not only position 234 altered the budding phenotype of Ck/Pakistan, it also potentially altered the folding of the M1 protein, which could explain the differences observed. Therefore, this section strongly supports the importance of position 234 of M1 in determining budding morphology in an avian host dependent manner and adds this position towards the formation of an avian filamentous “signature”.

Chapter 4: Functional characterisation of spherical and filamentous budding phenotypes *in vitro* and *in ovo*

4.1. Introduction and aims

As discussed in chapter 3, pairwise alignment of closely related avian strains that showed opposite budding phenotypes revealed sequence polymorphisms in M1 correlating with the different budding morphologies. Site-directed mutagenesis confirmed the importance of M1 amino-acids 59, 169 and 234 in determining budding morphology. Characterisation of these WT and M1-mutant viruses gave a clear idea of how different the budding morphology of these viruses can be, but it did not address the question of how the viruses would behave in an avian host. Recently, Al-Mubarak et al showed that a duck strain of IAV replicated to higher titre in CEF when compared with DEF cells (Al-Mubarak et al., 2015). The authors showed that this duck isolate of IAV had a spherical budding phenotype in CEF cells but a prominent filamentous budding phenotype in DEF cells. Therefore, the authors suggested that the different growth kinetics observed could be due to the different budding morphologies present in these cells. Furthermore, several studies have also reported that spherical viruses showed a growth advantage *in ovo* and filamentous viruses were selected against (Kilbourne & Murphy, 1960; Seladi-Schulman et al., 2013).

Hence, the aim of this part of the study was to (1) assess the growth kinetics of the viruses in different avian cell types and (2) investigate *in ovo* fitness and pathogenesis of the M1-mutant viruses versus their WT counterparts.

4.2. Results

4.2.1. *In vitro* and *in ovo* characterisation of Dk/India and Dk/Tripura WT and M1-mutant viruses

Identification of sequence polymorphisms in M1 of closely related avian strains with opposite budding phenotypes allowed the construction of mutant viruses where spherical and

filamentous budding morphologies were promoted or abrogated. Given that these M1-mutant viruses were built in the same genetic backgrounds as their WT counterparts, they provided tools to functionally characterise spherical and filamentous budding phenotypes *in vitro* and *in ovo*. First, the PR8 background Dk/India and Dk/Tripura reassortants were tested. WT versions of these viruses showed either spherical or filamentous budding phenotypes, where amino acid identity at position 59 of M1 was the main determinant of their different budding morphologies. However, the other sequence polymorphisms identified at positions 37 and 205 were also important to achieve a complete exchange of budding morphologies between the two avian strains. Therefore, *in vitro* and *in ovo* characterisation was performed with Dk/India and Dk/Tripura 7:1 reassortants containing WT segment 7, segment 7 with M1 reciprocally changed at position 59 or with M1 reciprocally changed at positions 37, 59 and 205.

The first step to better characterise the WT and M1-mutant viruses was to evaluate their growth kinetics in mammalian and avian cells and embryonated chicken eggs. The viruses were used to infect MDCK, CEF or DEF cells at a MOI of 0.01 for a period of 48 h. Time points were collected over the 48 h, clarified by centrifugation and titred by plaque assay. The PR8-based 7:1 reassortants with WT and mutated M1 from Dk/India and Dk/Tripura replicated well with no significant differences throughout the 48 h in MDCK cells, reaching maximum titres of approximately 10^8 PFU/ml by 24 h (Figure 4.1 A). In both CEF and DEF cells, similar outcomes were observed, where WT and M1-mutant viruses reached maximum titres by 24h of approximately 10^6 PFU/ml in CEF (Figure 4.1 B) and 10^7 PFU/ml in DEF (Figure 4.1 C) cells. In all cell types, Dk/India and Dk/Tripura WT or M1-mutant viruses replicated similarly over the 48 h period, thus suggesting that viral fitness was not affected by budding morphology in these settings.

The reassortant Dk/India and Dk/Tripura viruses were also used to infect 10-day old embryonated chicken eggs with 100 PFU via the allantoic cavity (Burnet, 1941) for 48 h. Following infection, the allantoic fluid was harvested, clarified by centrifugation and titred by plaque assay. Mock-infected eggs showed no signs of infection by plaque assay.

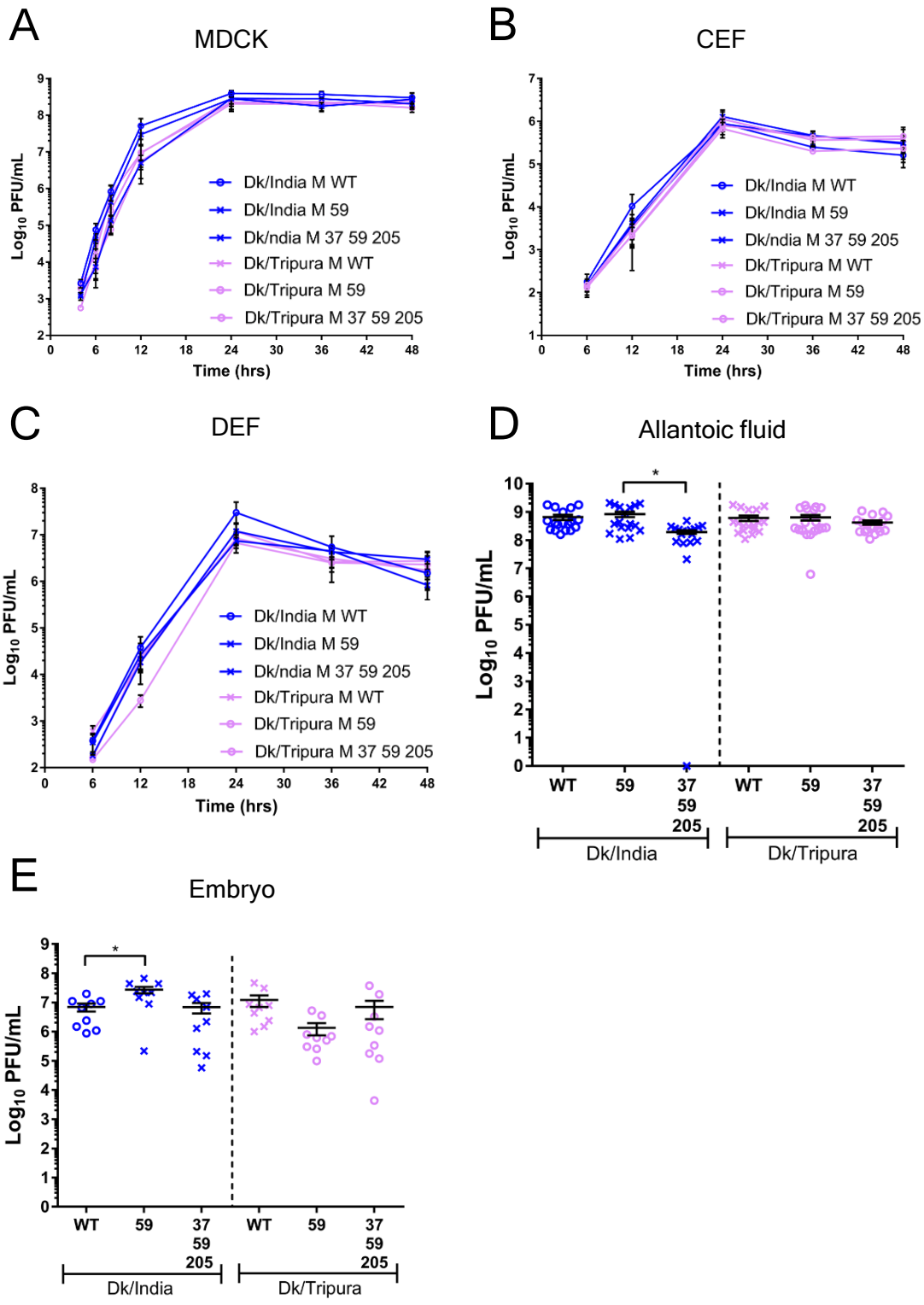
A
MDCK
Log10 PFU/mL
Time (hrs)
Dk/India M WT
Dk/India M 59
Dk/ndia M 37 59 205
Dk/Tripura M WT
Dk/Tripura M 59
Dk/Tripura M 37 59 205
B
CEF
Log10 PFU/mL
Time (hrs)
Dk/India M WT
Dk/India M 59
Dk/ndia M 37 59 205
Dk/Tripura M WT
Dk/Tripura M 59
Dk/Tripura M 37 59 205
C
DEF
Log10 PFU/mL
Time (hrs)
Dk/India M WT
Dk/India M 59
Dk/ndia M 37 59 205
Dk/Tripura M WT
Dk/Tripura M 59
Dk/Tripura M 37 59 205
D
Allantoic fluid
Log10 PFU/mL
*
WT
59
37 59 205
WT
59
37 59 205
Dk/India
Dk/Tripura
E
Embryo
Log10 PFU/mL
*
WT
59
37 59 205
WT
59
37 59 205
Dk/India
Dk/Tripura

Figure 4.1 Growth characteristics of Dk/India and Dk/Tripura WT and M1-mutant viruses *in vitro* and *in ovo*. (A-C) MDCK, CEF and DEF cells were infected at an MOI of 0.01 for 48 h with the indicated viruses. Supernatants were collected at the indicated time points, cleared by centrifugation and the viral titre assessed by plaque assay. Data represent mean +/- SEM (n = 3). (D, E) Embryonated 10-day old chicken eggs were infected with 100 PFU of the indicated viruses for 48 h. Allantoic fluid and embryos were harvested for viral titre determination by plaque assay. Viral titre determination of the embryos was preceded by maceration of the embryo and centrifugation. A total of 18 embryos were used, where 9 were macerated and the other 9 were used for histology studies. One-way ANOVA was performed to compare the viruses within Dk/India and Dk/Tripura groups. * $p < 0.05$ Data points represent individual samples and bars mean +/- SEM (D: n = 18 E: n = 9). Spherical viruses are represented by circles and filamentous viruses by crosses.

The PR8-based Dk/India 7:1 reassortant viruses with WT M1, M1 59 and M1 37, 59 205 mutations replicated to titres ranging between 10^8 and 10^9 PFU/ml (Figure 4.1 D). Even though Dk/India M 59 and Dk/India M 37 59 205 both possessed a filamentous budding morphology, the latter replicated to a significantly lower average titre at 48 h p.i (approx. 10^8 PFU/ml), suggesting that mutating positions 37 and 205 caused subtle changes which in turn affected viral replication in the allantoic fluid. The Dk/Tripura reassortants with WT or mutated M1 all replicated to indistinguishable average titres of approximately 10^9 PFU/ml. To determine viral replication in the embryo, 9 embryos were sampled from a total of 18. These were harvested, washed twice in PBS, macerated, debris pelleted by centrifugation and the supernatants collected for titre by plaque assay. Mock-infected embryos showed no detectable levels of infection by plaque assay (data not shown). Dk/India reassortants with WT M1 or M1 37 59 205 gave virus titres of approximately 10^7 PFU/ml (Figure 4.1 E). By contrast, Dk/India 59 replicated to a greater titre than its WT counterpart. Conversely, Dk/Tripura 59 showed a (non-statistically significant) tendency to replicate to a lower titre than Dk/Tripura WT and Dk/Tripura 37 59 205, for which the average titres were approximately 10^7 PFU/m. Dk/India M1 59 showed an advantage in viral replication in the allantoic fluid compared with the triple mutant, reaching a similar titre to the WT virus. In the embryo, Dk/India M1 59 replicated to a higher titre when compared with the WT and Dk/India M1 37 59 207 viruses. However, the reciprocal effect was not definitively observed with any of the Dk/Tripura M1-mutant viruses, thus suggesting this result could be strain-specific.

Following assessment of the growth kinetics of Dk/India and Dk/Tripura reassortants in embryonated chicken eggs, the next step was to examine the gross and tissue pathology of chicken embryos infected with these viruses. For gross pathology, pictures of the embryos were taken on the day of harvest and representative pictures of the embryos were chosen. Mock-infected embryos showed no obvious signs of haemorrhage, as characterised by the pale colour these displayed (Figure 4.2). Embryos inoculated with Dk/India M WT (a spherical virus) showed considerable haemorrhage in both head and body. In contrast, Dk/Tripura M WT (a filamentous virus) infected embryos showed only subtle signs of bleeding when compared to Dk/India M WT. The filament-inducing amino acid change at position 59 in M1 of

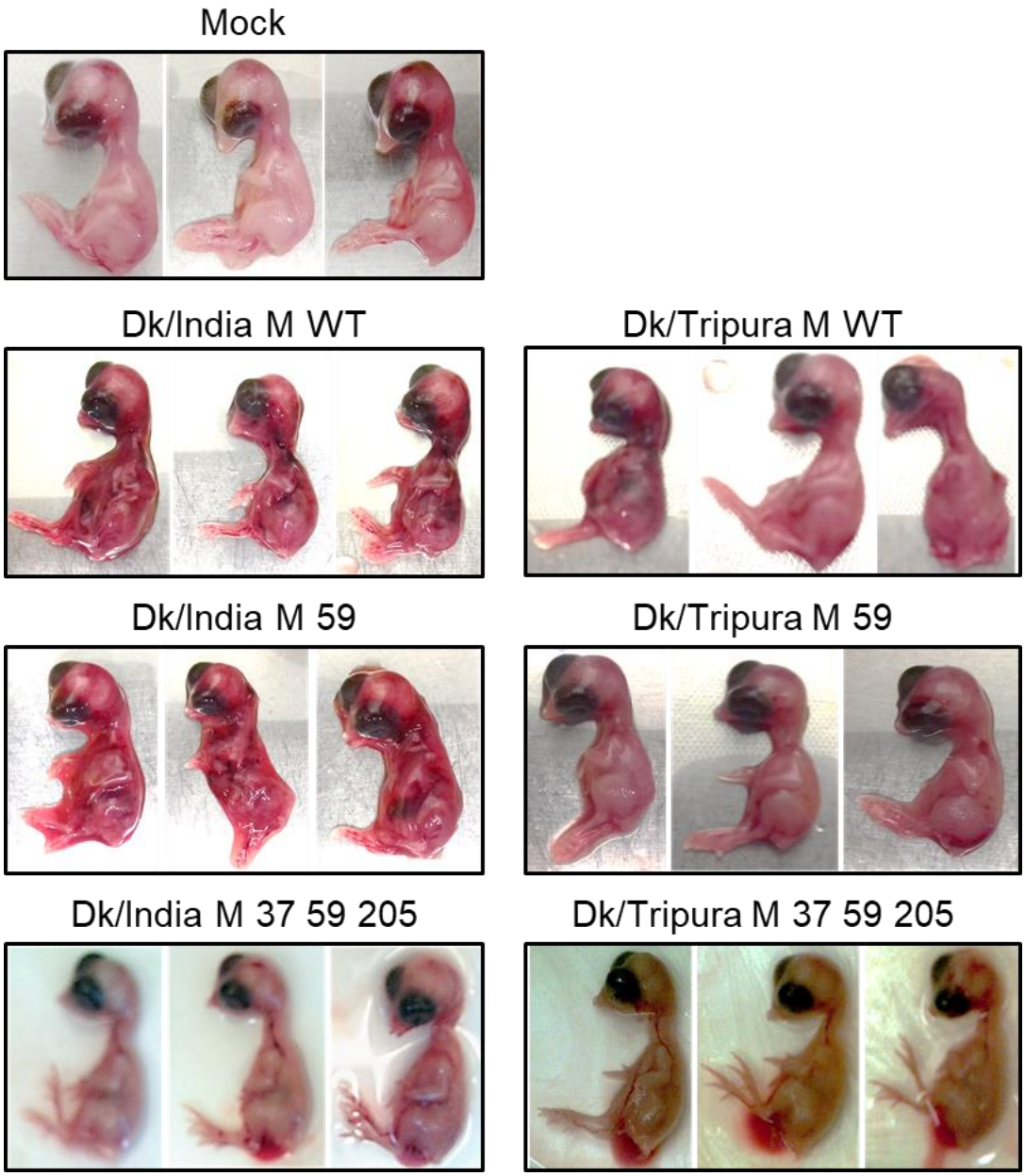

Figure 4.2 Gross pathology of chicken embryos infected with Dk/India or Dk/Tripura WT and M1-mutant viruses at 48 h p.i.. Chicken embryos from eggs inoculated (or mock infected) with 100 PFU of the viruses indicated were harvested at 48h and washed twice in PBS. Embryos were placed on a light coloured background before photographing. These are representative embryos from three independent experiments.

Dk/India caused more severe pathogenesis which affected embryo integrity, something which was not observed with its WT counterpart. However, the converse change in Dk/Tripura did not obviously change the overall pathology compared to the matching WT virus. Furthermore, embryos infected with the triple mutants of Dk/India or Dk/Tripura showed similarly mild gross pathology with only subtle haemorrhages observed in the neck area, even though these M1-mutant viruses showed opposite budding morphologies. In fact, if anything, the reciprocal change of amino acids 37, 59 and 205 of Dk/India decreased viral pathogenicity compared to the WT counterpart. However, the Dk/Tripura triple mutant did not increase the pathogenesis when compared with the WT counterpart, which would be expected since this virus became Dk/India WT-like *in vitro* (see chapter 3, section 3.2.2). Thus, embryos infected with Dk/India M1 37 59 205 showed pathology similar to Dk/Tripura WT-infected embryos, but the reciprocal outcome was not observed for Dk/Tripura viruses.

To better assess the pathogenesis caused by these viruses, six representative embryos were chosen from the nine collected over the three independent repeats to be sectioned for histopathology. The embryos were fixed in 10% formalin, sectioned and stained with haematoxylin and eosin (H&E). Histopathology of mock-infected embryos showed no pathogenesis, characterised by no noticeable presence of red blood cells in tissues other than the heart. In agreement with the information provided by gross pathology, Dk/India M WT infected embryos showed severe haemorrhages throughout the embryo, with emphasis in the liver and kidney tissues (Figure 4.3). By contrast, embryos inoculated with Dk/Tripura M WT virus showed only subtle haemorrhages, mainly localised to the kidney. Dk/India M1 59 infected embryos showed haemorrhages spread throughout the body, particularly in the liver and kidney tissues, similar to the WT counterpart. In contrast, the alteration of position 59 in M1 of Dk/Tripura showed clearly decreased pathogenicity when compared with its WT counterpart; a difference which was less obvious in the gross pathology data. Embryos infected with the triple mutants of Dk/India or Dk/Tripura showed an overall reduced pathogenesis when compared with their WT counterparts. Gross pathology of embryos upon infection with Dk/India triple mutant only showed subtle pathology, but the histopathology sections revealed noticeable haemorrhages in the liver and kidney tissues, but less obviously

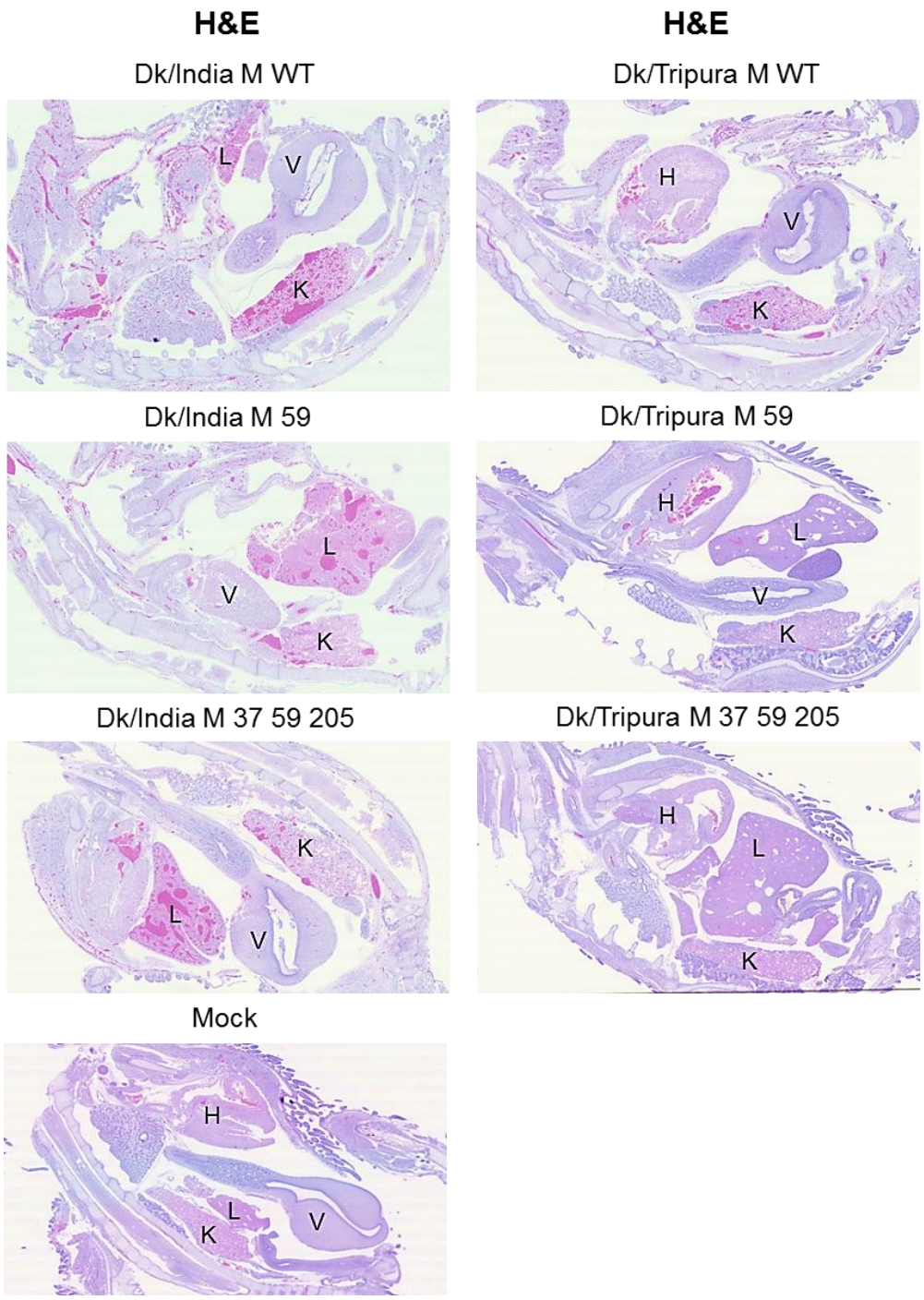

Figure 4.3 Histopathology of chicken embryos infected with Dk/India or Dk/Tripura WT and M1-mutant viruses. Embryonated 10-day old chicken eggs were infected (or mock-infected) with 100 PFU of the indicated viruses and the embryos were harvested 48 h p.i., fixed in 10% formalin before sectioning and staining with haematoxylin and eosin stain (H&E). Sectioning and staining was performed by the Pathology Unit at the Royal (Dick) Veterinary School. Embryos were randomly selected from the 3 independent experiments performed. The organs indicated are heart (H), liver (L), ventriculus (V) and kidney (K).

throughout the body. Conversely, embryos infected with Dk/Tripura triple mutant showed very little pathogenesis and were generally similar to mock-infected embryos.

To quantify the information given by the gross and tissue pathology data, the embryos were scored blindly according to the observed pathology. For the purpose of assessing whole embryos, a score of 0 was defined as no noticeable levels of pathology in the embryo while score of 1 corresponded to the observation of subtle bleeding. Scores 2 and 3 were characterised by the presence of considerable bleeding and obvious haemorrhages with loss of embryo integrity, respectively. Tissue pathology was performed blindly by Prof Lonneke Vervelde. The scoring was as follows: a score of 0 was characterised by the lack of bleeding (except in the heart) and infiltration of immune cells to the identified organs, while a score of 3 was characterised by the presence of severe haemorrhages, infiltration of immune cells and disruption of the organ's structure due to inflammation, Another metric assessed was embryo length, to test whether there would be any association with pathogenesis. For this, embryo length was measured using ImageJ software from pictures as in figure 4.2 relative to a scale bar. As previously observed, mock-infected embryos showed no noticeable haemorrhaging in any tissue with the exception of the heart, which translated in scores of 0 for both gross and tissue pathology. Embryos inoculated with Dk/India M WT and Dk/India M 59 showed the most severe gross pathology, which resulted in average scores > 2 (Figure 4.4 A). However, alteration of Dk/India M1 at positions 37, 59 and 205 significantly reduced the severity of disease, resulting in a gross pathology score of approximately 1. On the other hand, Dk/Tripura infected embryos showed a similar low score (approximately 1) regardless of the mutations inserted in the M1 amino acid sequence. Furthermore, scoring of the embryos made it obvious that while Dk/India triple mutant adopted a gross pathology similar to Dk/Tripura WT, the reciprocal change was not observed following mutation of the Dk/Tripura M1. Regarding the histopathology data, Dk/India M WT-again displayed the most severe pathological signs, which translated into an average score of 2 (Figure 4.4 B). However, neither the single or triple mutant gave significantly different scores from the WT virus. Conversely, Dk/Tripura M WT and Dk/Tripura M 59 infected embryos displayed overall histopathology scores of 1.5 while the

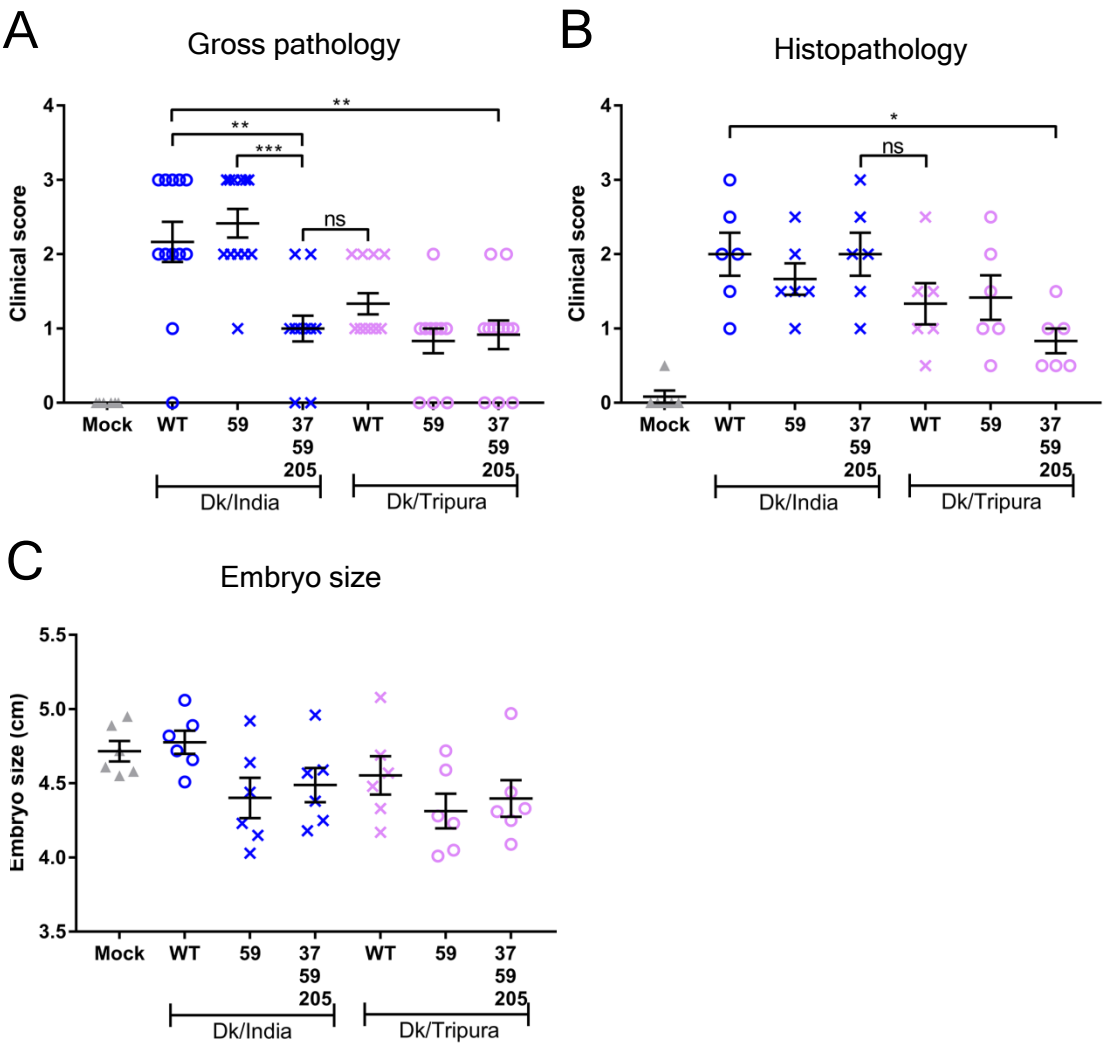

Figure 4.4 Characterisation of chicken embryo pathology following infection with Dk/India or Dk/Tripura WT and M1-mutant viruses. (A) Embryo gross pathology scoring of pictures taken on the day of harvesting (Figure 4.2) was performed blindly by two independent observers using a scale defined as follows: 0 – no bleeding seen on the embryo; 1 – subtle bleeding in the embryo; 2 – considerable bleeding in the embryo; 3 – very obvious bleeding in the embryo and/or loss of embryo integrity. (B) Tissue pathology scores were taken from the H&E staining (Figure 4.3) using a similar scoring system focussing on the degree of haemorrhage seen in the tissues. Scoring was performed by Professor Lonneke Vervelde on blinded images. One-way ANOVA was performed to compare all the viruses against each other. Data represent individual embryos and bars the mean +/- SEM (A: n = 12; B: n = 6). * $p < 0.05$ ** $p < 0.01$ *** $p < 0.001$ ns not significant (C) Embryo length was measured from a single experiment from photographs using ImageJ. Data represent individual embryos and bars the mean +/- SEM (n = 6). Data were non-significant. Circles represent spherical viruses and crosses represent filamentous ones.

triple mutant gave an average just below 1, which was significantly different from Dk/India M WT even though the viruses had identical M1 sequences and indistinguishable budding phenotypes. Regarding embryo size, no differences were observed between the mock-infected, Dk/India or Dk/Tripura infected embryos, which measured between 4.5 and 5 cm in length (Figure 4.4 C), thus excluding any association between viral pathogenesis and embryo development.

Overall, in MDCK, CEF or DEF cells no significant differences were observed in viral replication kinetics for either Dk/India or Dk/Tripura WT or M1-mutant viruses. However, *in ovo*, differences in virus replication were observed for Dk/India viruses in both the allantoic fluid and the embryo. Additionally, the most severe pathogenesis was observed for Dk/India reassortant viruses, as Dk/India M WT (spherical) and M 59 (filamentous) viruses caused obvious haemorrhaging in the embryos, whereas the Dk/India triple mutant (Dk/Tripura-like) showed a noticeable reduction in damage. A similar pattern of the lowest pathology occurring with the triple mutants was observed with Dk/Tripura reassortant viruses, but overall these presented more subtle signs of pathogenesis and none of the pathology scores were significantly different. In summary, these results showed that alteration of Dk/India budding morphology to Dk/Tripura-like caused Dk/India to be less pathogenic. On the other hand, alteration of Dk/Tripura budding morphology to Dk/India-like did not significantly change the pathogenic nature of Dk/Tripura, thus suggesting that the differences observed could be mainly strain-specific instead of budding morphology-specific.

4.2.2. *In vitro* and *in ovo* characterisation of Ck/Italy and Dk/Netherlands WT and M1-mutant viruses

To further explore the correlation between budding phenotype and IAV biology, the Ck/Italy and Dk/Netherlands sets of PR8-based reassortant viruses were studied. The M1 genes of these viruses were previously shown to possess single sequence polymorphisms at position 234 in M1, which accounted for the different budding morphologies observed (see chapter 3, section 3.2.4). Ck/Italy was predominantly spherical while Dk/Netherlands showed

a prominent filamentous budding phenotype. Reciprocal change of amino acids at position 234 in M1 of both strains swapped their budding phenotype.

To better characterise effect of altered budding phenotypes on the replication of these viruses, mammalian and avian cells and embryonated chicken eggs were infected as before (section 4.2.1). Firstly, the growth kinetics of these viruses was assessed in MDCK, CEF and DEF cells. Cells were infected at a MOI of 0.01 over a period of 48 h and the supernatant was collected at various time points for quantification of viral load by plaque assay. In all three cell types, Ck/Italy and Dk/Netherlands with WT or M1-mutant viruses replicated similarly (with no statistically significant differences) throughout the time courses. In MDCK (Figure 4.5 A), CEF (Figure 4.5 B) and DEF (Figure 4.5 C) cells, viral replication peaked at 24 h p.i reaching titres of approximately 10^8 PFU/ml for MDCK and either side of ~ 10^6 PFU/ml for the avian cells. Replication of Ck/Italy and Dk/Netherlands M WT and M1-mutant viruses was also assessed in 10-day old embryonated chicken eggs. Allantoic fluid was harvested for titration by plaque assay 48h after infection with 100 PFU. Ck/Italy M WT replicated to near 10^9 PFU/ml whereas its M1-mutant counterpart replicated significantly less in the allantoic fluid (Figure 4.5 D). Conversely, Dk/Netherlands M WT replicated to an end point titre of approximately 10^8 PFU/ml, but its M1-mutant counterpart replicated to significantly higher titres of approx. 10^9 PFU/ml. In fact, viral replication in the allantoic fluid was similar between spherical viruses (Ck/Italy M WT and Dk/Netherlands M 234), and higher than replication observed with the filamentous viruses (Ck/Italy M 234 and Dk/Netherlands M WT). To determine viral replication within the embryo, these were collected, macerated and cleared by centrifugation before titre determination by plaque assay. In the chicken embryo, there was also a trend for spherical viruses (Ck/Italy M WT and Dk/Netherlands M 234) to replicate better than the filamentous viruses (Ck/Italy M 234 and Dk/Netherlands M WT) albeit to lower titres (approx. 10^7 PFU/ml), with only the Dk/Netherlands pair reaching statistical significance (Figure 4.5 E).

Given that the viruses with spherical or filamentous budding phenotypes showed differential growth properties in embryonated chicken eggs, the next step was to examine the gross and tissue pathology caused by their infection. Gross pathology was based on pictures

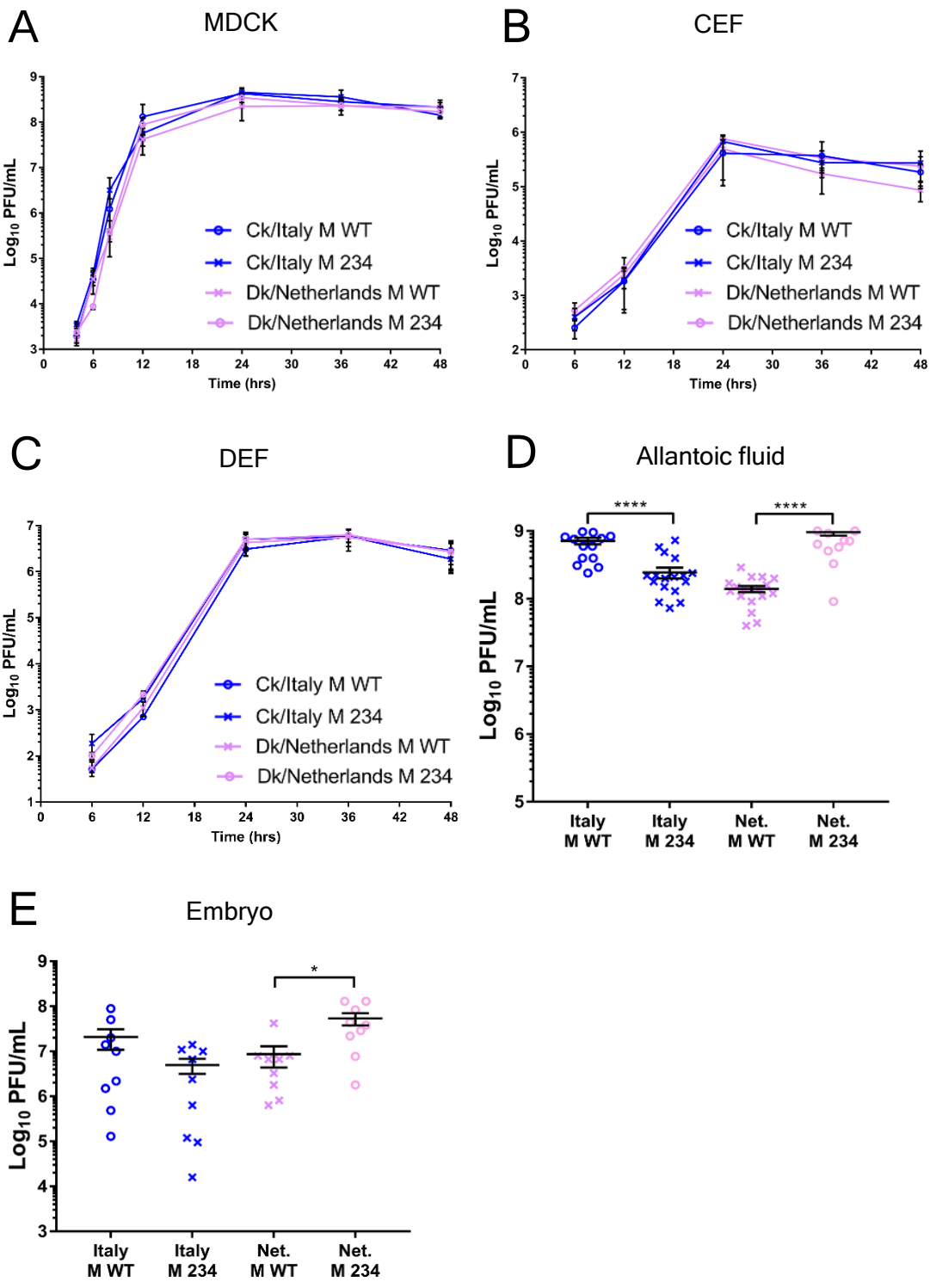
A
MDCK
Log10 PFU/mL
Time (hrs)
Ck/Italy M WT
Ck/Italy M 234
Dk/Netherlands M WT
Dk/Netherlands M 234
B
CEF
Log10 PFU/mL
Time (hrs)
Ck/Italy M WT
Ck/Italy M 234
Dk/Netherlands M WT
Dk/Netherlands M 234
C
DEF
Log10 PFU/mL
Time (hrs)
Ck/Italy M WT
Ck/Italy M 234
Dk/Netherlands M WT
Dk/Netherlands M 234
D
Allantoic fluid
Log10 PFU/mL
****
****
Italy M WT
Italy M 234
Net. M WT
Net. M 234
E
Embryo
Log10 PFU/mL
*
Italy M WT
Italy M 234
Net. M WT
Net. M 234

Figure 4.5 Replication of Ck/Italy and Dk/Netherlands strains with WT or mutated M1 genes *in vitro* and *in ovo*. (A-C) MDCK, CEF and DEF cells were infected with the viruses indicated at a MOI of 0.01 for 48 h. Viral load in the supernatant was quantified at the indicated time points by plaque assay. Data represent mean +/- SEM (n = 3). (D, E) Embryonated 10-day old chicken eggs were infected with 100 PFU of the virus indicated for 48 h. Allantoic fluid and embryos were harvested for viral titre determination by plaque assay. Embryo titres were determined after maceration and centrifugal clarification. A total of 18 embryos were used, where 9 were macerated and the other 9 were used for histology studies. One way ANOVA was performed to compare Ck/Italy and Dk/Netherlands WT and M1-mutant viruses. Data represent mean +/- SEM (C: n = 18; D: n = 9). Spherical viruses are represented by circles and filamentous viruses by crosses.

of the embryos taken on the day of harvesting as described before (section 4.2.1). Mock-infected embryos showed no obvious signs of haemorrhage. Ck/Italy M WT infected embryos showed considerable amounts of haemorrhaging throughout the body, unlike embryos inoculated with Dk/Netherlands M WT which displayed more subtle haemorrhagic signs (Figure 4.6). Ck/Italy WT-infected embryos showed considerably more bleeding than embryos infected with the filamentous mutant, which was more similar to Dk/Netherlands WT-infected embryos. In contrast, the majority of the embryos infected with the spherical budding M1 234 mutant of Dk/Netherlands presented considerable amounts of haemorrhage, more similar to the normally non-filamentous Ck/Italy M1 WT virus. Looking back at figure 4.5 D, the spherical viruses which caused obvious pathology in the embryos also replicated to higher titres in the allantoic fluid, suggesting a correlation.

To better determine the extent of the pathogenesis caused by the pairs of Ck/Italy and Dk/Netherlands M1 viruses, tissue histopathology was performed on the chicken embryos infected with these viruses as described before (section 4.2.1). As expected, mock-infected embryos showed no noticeable signs of bleeding in any of the tissues indicated. Histopathology of embryos infected with Ck/Italy and Dk/Netherlands WT or M1-mutant viruses revealed no obvious differences within the embryos (Figure 4.7), in contrast to what was observed by gross pathology. Thus, in order to get a more quantitative measure of pathology signs, the embryos were scored on three metrics: pathology (gross and tissue) and embryo length, using the system defined above (see section 4.2.1). Mock-infected embryos showed no noticeable signs of pathology, which translated in scores of 0 for both gross and tissue categories (Figure 4.8). Embryos inoculated with Ck/Italy M WT and Dk/Netherlands M 234, both spherical viruses, showed higher average signs of damage, whereas the filamentous Ck/Italy M 234 and Dk/Netherlands M WT viruses presented slightly lower average scores. However, the overall differences were subtle, translating into gross pathology scores between 1 and 2 with no significant differences between groups (Figure 4.8 A). Regarding histopathology, the average score for all the viruses was between 0.5 and 1 (Figure 4.8 B), regardless of budding morphology or viral strain. Lastly, measuring embryo length also did not reveal any association with pathogenesis, with the average body size lying between 4.5 and 5 cm (Figure 4.8 C).

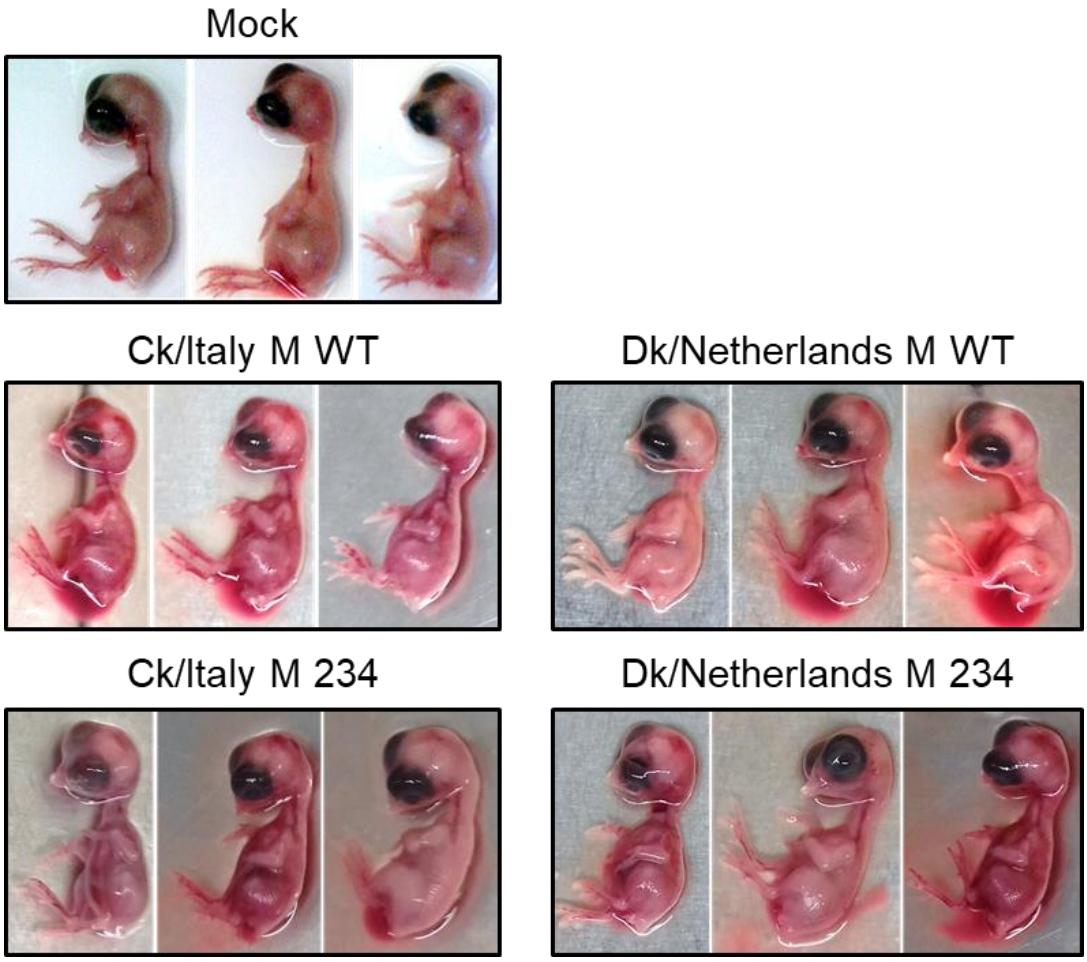

Figure 4.6. Gross pathology of chicken embryos infected with Ck/Italy or Dk/Netherlands viruses. Embryos were inoculated with 100 PFU of the viruses indicated, harvested 48 h p.i., washed twice in PBS and photographed. These are representative pictures from 3 independent experiments.

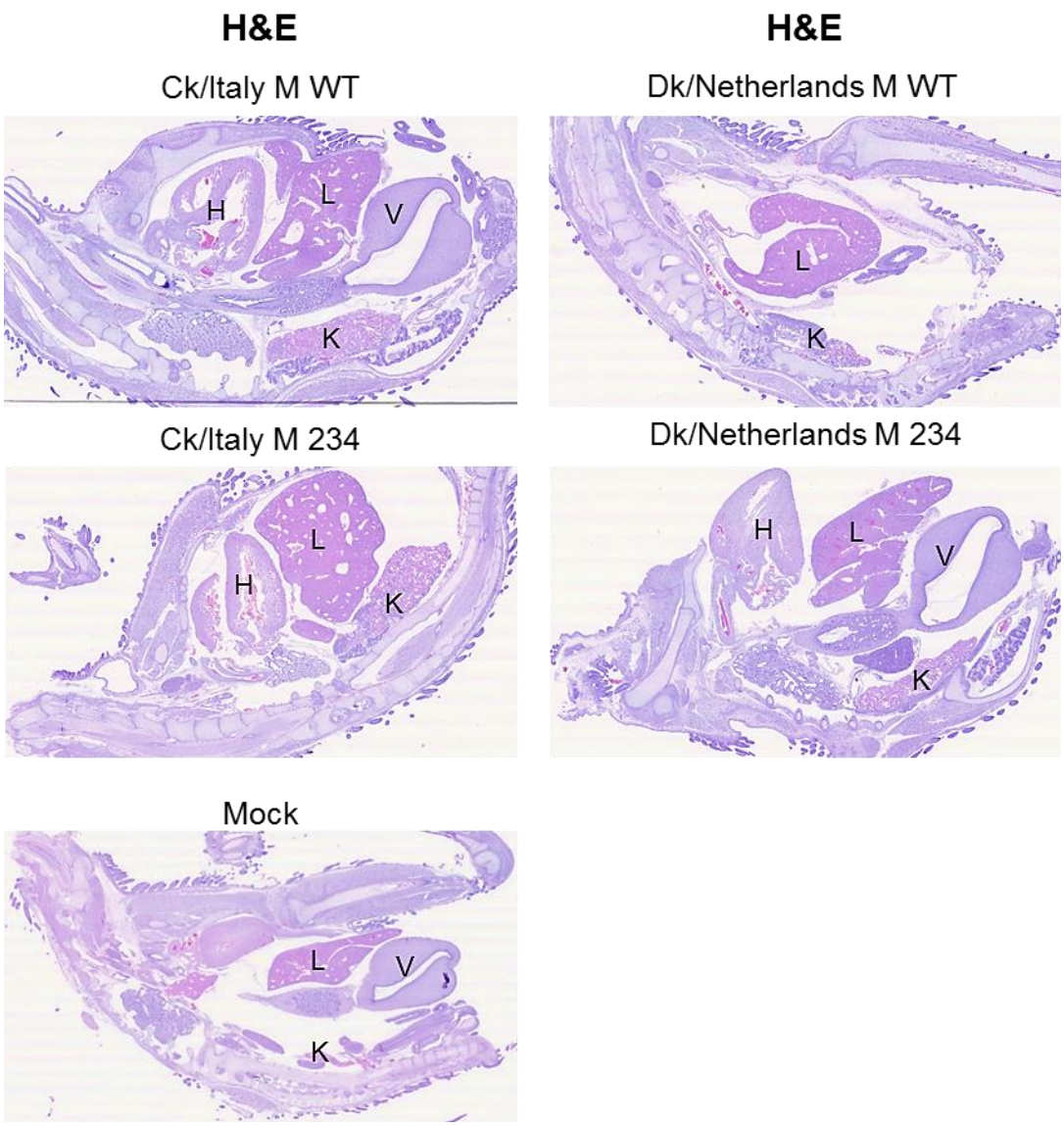

Figure 4.7 Histopathology of chicken embryos infected with Ck/Italy or Dk/Netherlands viruses. Embryonated 10-day old eggs were infected with 100 PFU of the indicated viruses and the embryos were harvested 48 h p.i. Embryos were fixed in 10% formalin for a minimum of 24 h followed by sectioning and staining with haematoxylin and eosin stain (H&E), performed by the Royal (Dick) Veterinary School pathology service. Embryos were randomly selected from the 3 independent experiments performed. The organs indicated correspond to heart (H), liver (L), ventriculus (V) and kidney (K).

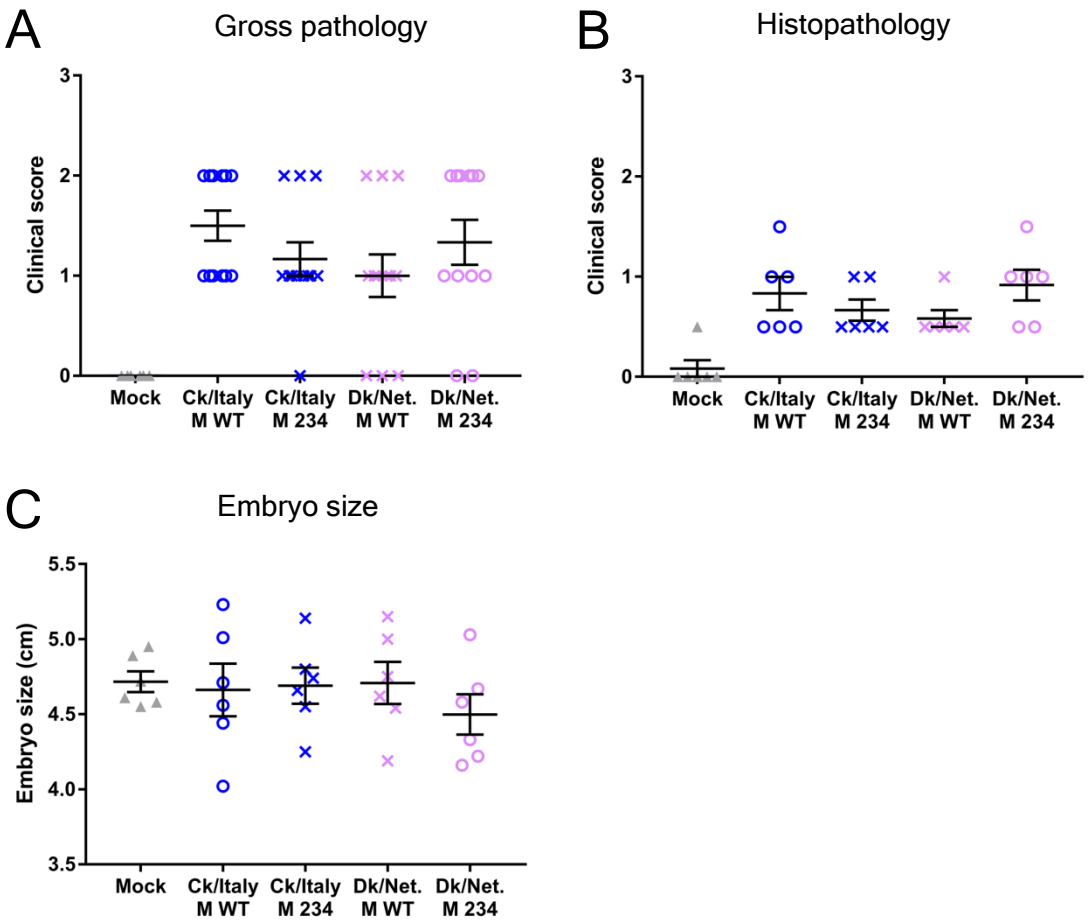

Figure 4.8 Embryo pathology and size following infection with Ck/Italy or Dk/Netherlands WT and M1-mutant viruses. (A, B) Gross pathology score was based on photographs taken on the day of harvesting (Figure 4.6), while tissue pathology score used H&E stained sections. The score was defined as follows: 0 – no bleeding detected; 1 – subtle bleeding in the embryo and tissues; 2 – considerable bleeding seen in the embryo and the tissues; 3 – very obvious bleeding in the embryo and tissues (loss of embryo integrity). Data represent mean +/- SEM (A: n = 12; B: n = 6). (C) Embryo length was measured from photographs taken for (A) using ImageJ. Embryos from one repeat were used (as seen in figure 4.6). Data represent mean +/- SEM (n = 6). Circles represent spherical viruses and crosses represent filamentous ones.

Overall, *in vitro* the WT and M1-mutant viruses had similar growth kinetics, regardless of budding morphology. However, in the allantoic fluid, spherical viruses (Ck/Italy M WT and Dk/Netherlands M 234) showed a replication advantage when compared with filamentous viruses (Ck/Italy M 234 and Dk/Netherlands M WT). Furthermore, embryos infected with spherical viruses showed subtle pathological signs not present in embryos infected with filamentous viruses, however on quantification, these differences were not significant. Nonetheless, these results showed that alteration of Ck/Italy budding morphology to Dk/Netherlands-like caused Ck/Italy to replicate less in embryonated chicken eggs. Conversely, alteration of Dk/Netherlands budding morphology to Ck/Italy-like improved Dk/Netherlands replication kinetics *in ovo*. Therefore, the differences observed suggested an association with budding morphology, where spherical viruses clearly showed an advantage in embryonated chicken eggs, even though the pathology was similar in embryos infected with either spherical or filamentous viruses.

4.2.3. Investigating the spherical and filamentous budding phenotypes of Ck/Pakistan strain *in vitro* and *in ovo*

From statistical and bioinformatic analyses of the M1 sequences of the strains tested in this study, it was hypothesised that position 234 was a strong predictor of the budding morphologies of chicken and duck strains of IAV. This was corroborated when the amino acid identity at position 234 in M1 of Ck/Pakistan was altered. Ck/Pakistan WT virus showed a spherical budding phenotype, while its M1-mutant produced prominent filamentous virions. This was confirmed in both PR8-based 7:1 reassortant viruses and in the full avian virus backbone. These two virus pairs were therefore used as tools to further assess budding morphology-dependent differences on virus growth and pathogenicity.

The first step was to characterise the effects of the different budding morphologies of Ck/Pakistan on virus replication *in vitro* and *in ovo*. MDCK and CEF cells were infected with Ck/Pakistan WT or M1-mutant viruses at a MOI of 0.01 for 48 h, after which multiple time points were collected for viral load quantification by plaque assay. The PR8-based 7:1

reassortant viruses with WT or mutated M1 from Ck/Pakistan both reached an average titre of 10^8 PFU/ml in MDCK (Figure 4.9 A) and 10^5 PFU/ml in CEF (Figure 4.9 B) cells. The authentic avian Ck/Pakistan WT and M1-mutant viruses replicated to a lesser extent in both MDCK (approximately 10^6 PFU/ml) and CEF (approximately 10^4 PFU/ml) cells. However, for neither cell type nor virus background, did the M1 I234L mutation significantly affect virus replication. To determine the effect of the M1 mutation on viral replication *in ovo*, 10-day old embryonated chicken eggs were infected with 100 PFU of the fully avian WT or M1-mutant virus of Ck/Pakistan. Allantoic fluid and embryos were collected at 48 h p.i. and processed as described before (section 4.2.1) prior to titre determination by plaque assay. Mock-infected eggs showed no detectable levels of infectious particles. Both viruses replicated to similar titres in the allantoic fluid (approx. 10^7 PFU/ml) (Figure 4.9 C) and in the embryo, albeit to a lower titre in the latter (approx. 10^6 PFU/ml) (Figure 4.9 D), indicating that in this *in vivo* system, budding morphology did not affect end point titres.

The next step was to determine the embryo pathology caused by the Ck/Pakistan strains to test whether position 234 altered the *in ovo* pathogenesis of this avian virus. Pictures for gross pathology purposes were obtained as previously described (section 4.2.1). Mock-infected embryos showed no signs of haemorrhages as characterised by their pale colour, while both Ck/Pakistan WT and M1-mutant-infected embryos showed considerable levels of bleeding throughout the embryo, with no obvious differences between the two viruses (Figure 4.10 A). However, given that gross pathology can differ from histopathology as previously noted, the embryos collected were sectioned and stained for H&E. Mock-infected embryos showed no obvious bleeding in any of the tissues indicated, while Ck/Pakistan WT-infected embryos showed noticeable bleeding throughout the body but mainly localised to the liver and kidney tissues (Figure 4.10 B). Ck/Pakistan 234-infected embryos also showed obvious bleeding in a pattern similar to Ck/Pakistan.

To better quantify the pathology caused by the Ck/Pakistan viruses, the infected embryos were scored as previously described (section 4.2.1). In agreement with the results in figure 4.10, the pathology scores of embryos infected with Ck/Pakistan or its filamentous mutant showed no significant differences in either gross (score of approx. 2) nor tissue

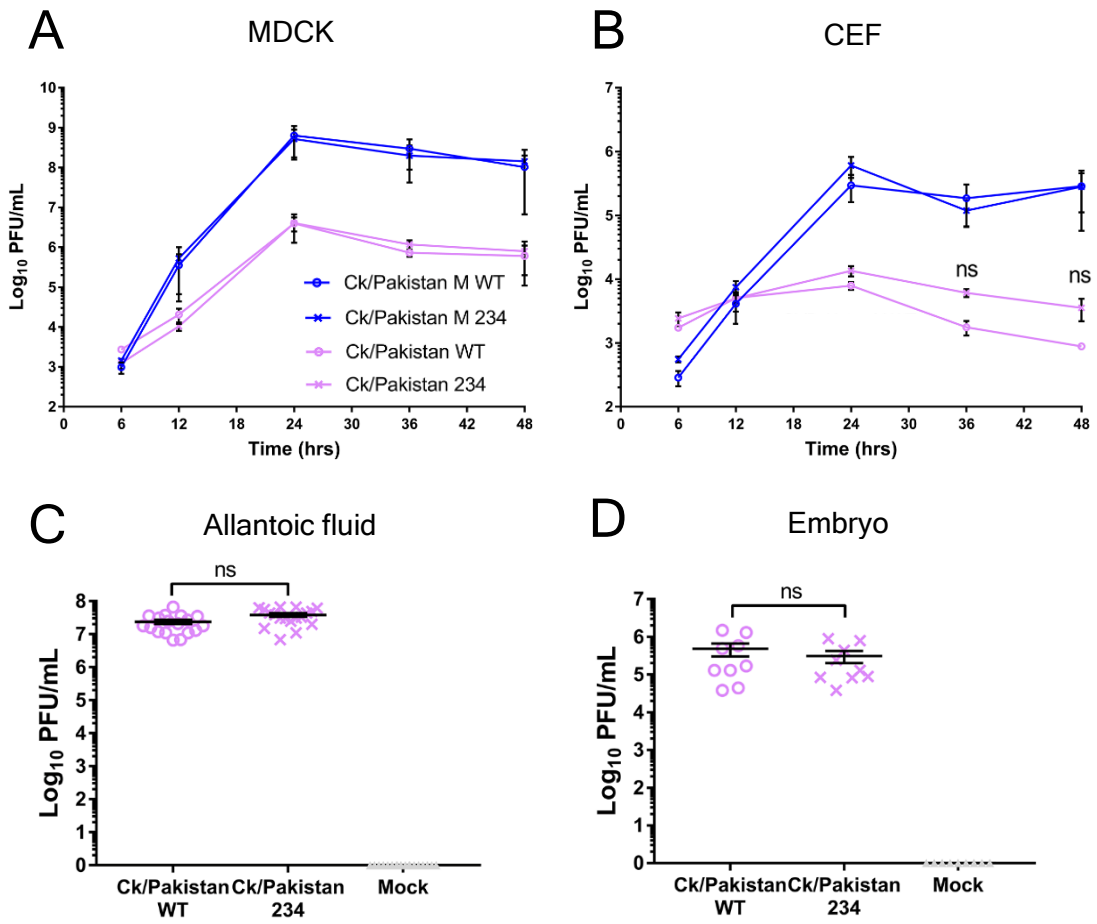

Figure 4.9 Viral fitness of Ck/Pakistan with WT or mutated M1 *in vitro* and *in ovo*. (A, B) MDCK and CEF cells were infected with the viruses indicated at an MOI of 0.01 for 48 h. Supernatants taken at the time points indicated were titrated by plaque assay. Data represent mean +/- SEM (n = 3). (C, D) Embryonated 10-day old chicken eggs were infected with 100 PFU of the viruses indicated for 48 h. Allantoic fluid and embryos were harvested for viral titre determination by plaque assay. A total of 18 embryos were used, where 9 were macerated and the other 9 were used for histology studies. *t-tests* were performed to compare Ck/Pakistan WT and M1-mutant viruses. Data represent mean +/- SEM (C: n = 18; D: n = 9). Spherical viruses are represented by circles and filamentous viruses by crosses. The 7:1 reassortant viruses are represented in blue and the fully avian viruses in pink.

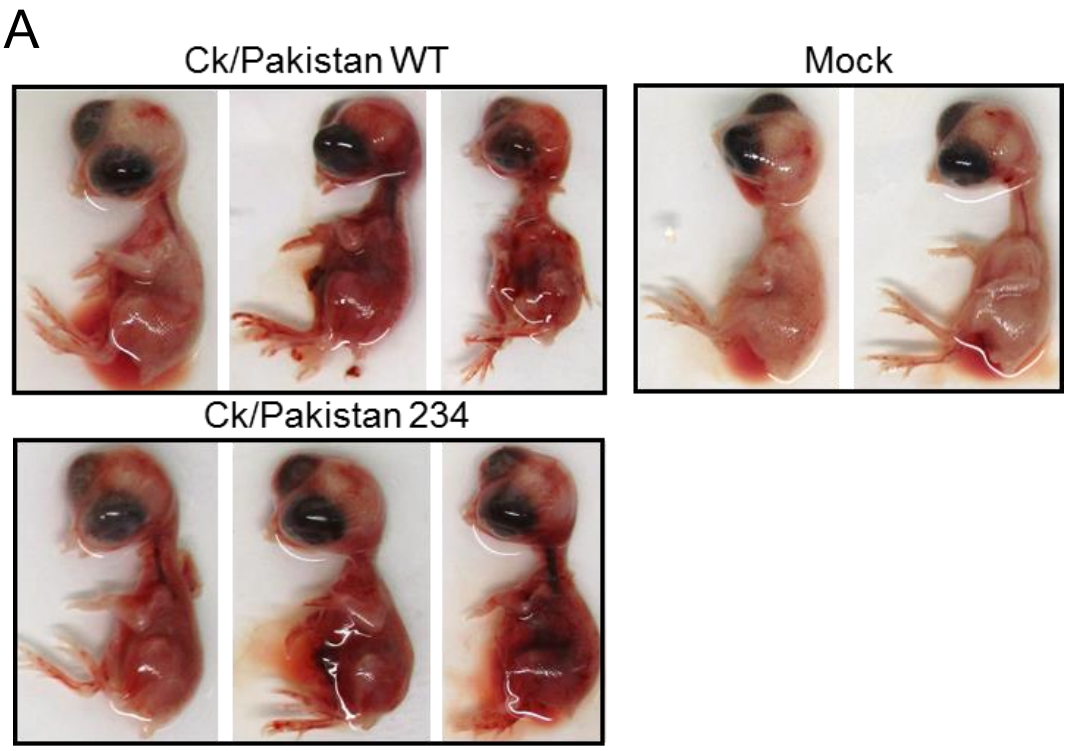
A
Ck/Pakistan WT
Mock
Ck/Pakistan 234
B
Ck/Pakistan WT
Mock
H
L
K
V
Ck/Pakistan 234

Figure 4.10 Chicken embryo pathology following infection with Ck/Pakistan WT or M1-mutant viruses. 10-old embryonated chicken eggs were inoculated with 100 PFU of the avian strain Ck/Pakistan or its M1-mutant for 48 h. (A) Embryos were collected, placed in a petri dish and washed twice in PBS. Gross pathology pictures were taken on the day of harvesting. (B) Half of the embryos were fixed in 10% formalin and sectioned for H&E staining, performed at the Royal (Dick) Veterinary School Pathology Unit. The organs indicated are: heart (H), liver (L), kidney (K) and ventriculus (V). Pictures are representative of three independent experiments.

pathology (score of approx. 1.5) (Figure 4.11 A, B). Furthermore, embryo length was also unaffected, with no significant differences detected (Figure 4.11 C). Thus, as seen previously with the other IAV strains, budding morphology did not significantly affect gross or tissue pathology or embryo development.

As a further test of the relative pathogenicity of the Ck/Pakistan virus pair, chicken embryo viability was determined upon infection with titrated doses of the spherical or filamentous strains. Embryonated 10-day old chicken eggs were infected with 10-fold dilutions from 10 PFU down to 0.001 PFU of the viruses for a period of up to 96 h. To determine embryo viability, eggs were candled every 12 h for a period of at least 60 seconds to detect embryo movement, which was recorded as 0 if present or 1 if absent. In addition, following embryo death or at the end of the experiment, allantoic fluid samples were taken and tested for virus by HA assay. By this measure, all eggs within the infected groups were productively infected with the exception of a single egg inoculated with 10 PFU of Ck/Pakistan M1 I234L (data not shown). This latter egg was discarded from the survival analysis. Of the successfully infected eggs, those infected with 10 PFU of Ck/Pakistan WT were no longer viable after 72 h, while after infection with 1 PFU or 0.1 PFU, there were embryos viable until 84 h p.i. but no later. (Figure 4.12 A). At 0.01 PFU, the majority of infected embryos remained viable and no casualties were recorded with 0.001 PFU or mock-infected embryos. From these data, the virus dose responsible for killing 50% of embryos (LD_{50}) of Ck/Pakistan WT was calculated as 0.16 PFU. With Ck/Pakistan M1 I234L, none of the embryos were viable 72 h after infection with 10 PFU, but 20-40% lasted until 96 h after inoculation with either 1 PFU or 0.1 PFU (Figure 4.12 B), similar to the WT counterpart. At 0.01 PFU, the majority of the infected embryos remained viable and no deaths were recorded with 0.001 PFU or mock-infected embryos. Overall, Ck/Pakistan 234 had a LD_{50} of 0.18 PFU.

Overall, these data showed that two almost identical avian strains of IAV, differing only at position 234 of M1 with either spherical or filamentous budding phenotypes did not behave differently *in vitro* or *in ovo*; i.e., viral replication and pathogenesis was indistinguishable for the spherical Ck/Pakistan and its M1 filamentous mutant regardless of host system tested.

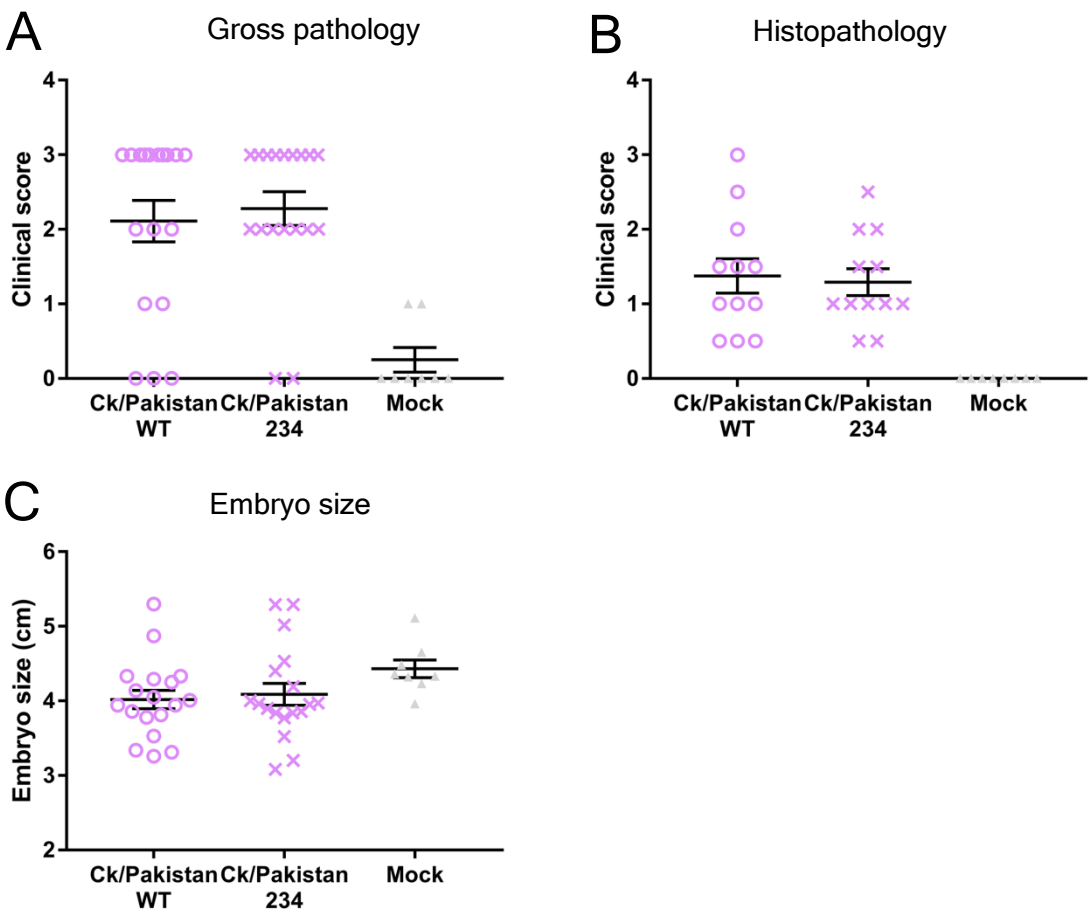

Figure 4.11 Embryo pathology following infection with Ck/Pakistan viruses. (A, B) Gross pathology score was based on photographs taken on the day of harvesting (figure 4.10), while tissue pathology scores focused on the H&E staining shown in figure 4.10. Scores were defined as follows: 0 – no bleeding detected; 1 – subtle bleeding in the embryo and tissues; 2 – considerable bleeding seen in the embryo and the tissues; 3 – very obvious bleeding in the embryo and tissues and/or loss of embryo integrity. Data represent mean +/- SEM (A: n = 18; B: n = 12). (C) Embryo length was measured from photographs (as seen in figure 4.10) using ImageJ. Data represent mean +/- SEM (n = 18). Circles represent spherical and crosses represent filamentous viruses.

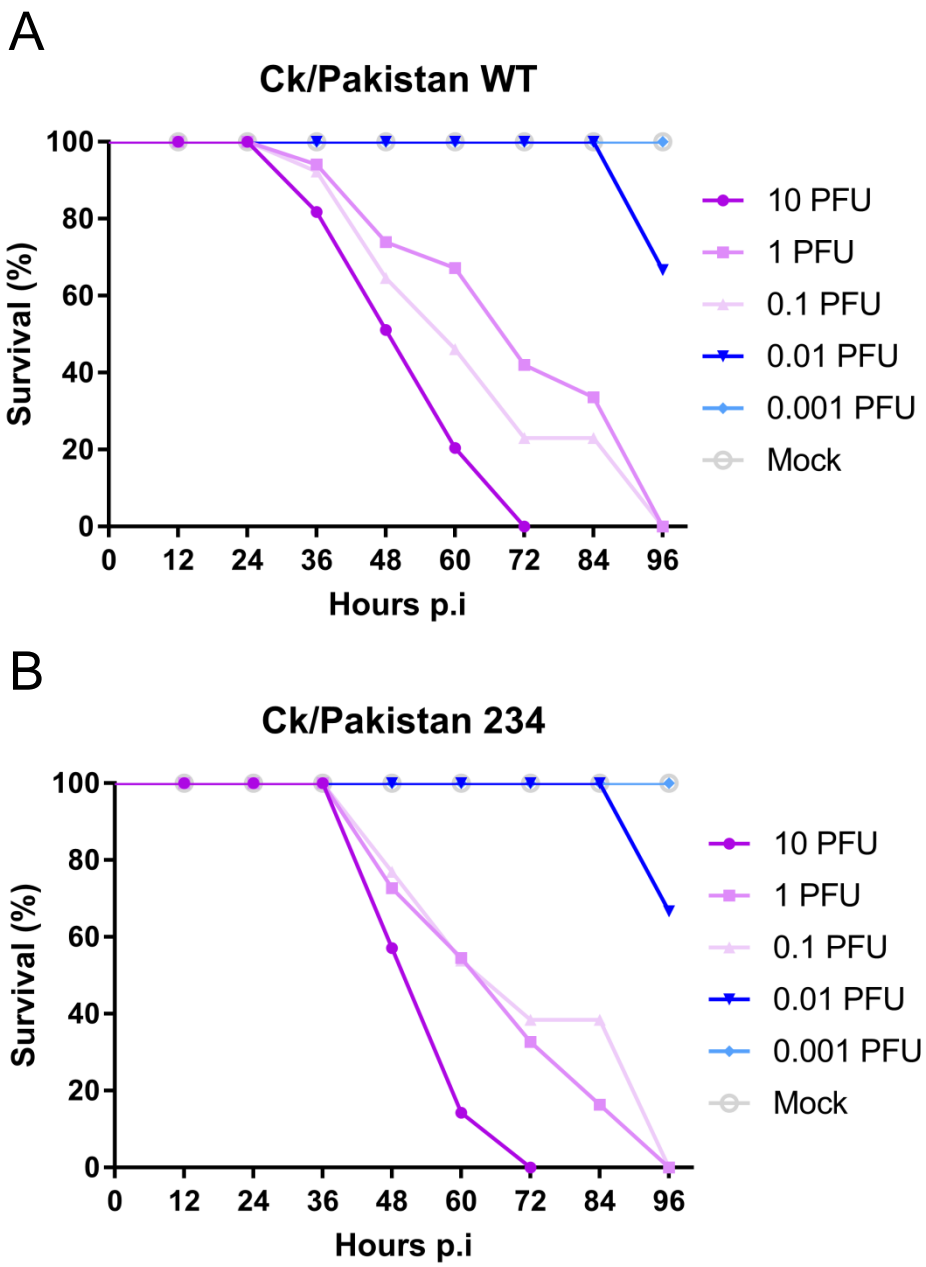

Figure 4.12 Embryo viability upon infection with Ck/Pakistan viruses. Embryonated 10-day old chicken eggs were infected with the indicated doses of Ck/Pakistan WT (A) or M1-mutant virus (B) and incubated for up to 96 h. Eggs were candled every 12 h and embryo viability (characterised by movement of the embryo over a period of 60 sec) scored to give percentage survival values.

4.3. Discussion

The main focus of this section of the study was to characterise *in vitro* and *in ovo* the WT and M1-mutant viruses built in chapter 3 that showed opposite budding morphologies. Overall, these data showed that spherical and filamentous viruses behaved similarly *in vitro*, regardless of the host system (MDCK, CEF or DEF cells). On the other hand, significant differences were detected *in ovo* between spherical and filamentous viruses but not for all the viruses tested. Regarding chicken embryo pathology, it was noted that alteration of budding morphology did not significantly affect pathogenesis of most strains, with the exception of the Dk/India reassortant virus. However, embryo viability decreased sooner for a spherical chicken virus than for the same strain with a filamentous budding morphology.

Dk/India and Dk/Tripura strains differed in M1 at position 37, 59 and 205 and while position 59 was the sole determinant of budding morphology between the two strains, the closest exchange of budding phenotype only happened when all the three positions were reciprocally replaced. Dk/India and Dk/Tripura viruses with WT M1s, M1 59 or M1 37, 59 and 205 mutations replicated similarly regardless of cell origin (Figure 4.1), despite their differences in budding morphology. Similar replication *in vitro* was also observed with Ck/Italy and Dk/Netherlands WT or M1-mutants (Figure 4.5) and the Ck/Pakistan WT or M1-mutant viruses in either the avian or PR8 backbones (Figure 4.9). These observations were in contrast with recent studies, which showed that filamentous avian strains adopt a mainly spherical budding phenotype in CEF cells, resulting in a fitness advantage in these cells when compared with DEF cells. However, this was not the case here for the PR8-based 7:1 reassortant viruses with the M genes of Dk/India, Dk/Tripura, Ck/Italy, Dk/Netherlands or Ck/Pakistan, as in both CEF and DEF cells these strains maintained their corresponding budding morphologies (Figures 2.12 A, B). One difference that could account for the different observations between the published studies and this study was the virus background, as the published studies used an avian virus genetic background while here many of the viruses were built as 7:1 reassortants in a PR8 backbone with only segment 7 of the avian strain. However, as previously shown in chapter 2, section 2.2.2 and in chapter 3, section 3.3, segment 7 was the major morphology determinant in a PR8 backbone. Furthermore, several studies on

mammalian strains have also shown that segment 7 is the predominant regulator of budding morphology (Bialas et al., 2012; Bourmakina & Garcia-Sastre, 2003; Elleman & Barclay, 2004; Elton et al., 2013 Gomez-Puertas et al., 2000; Roberts et al., 1998), therefore suggesting that the differences observed with the published studies could be more strain-specific than budding morphology- or virus backbone-specific.

Regarding *in ovo* viral replication, it was observed that the 7:1 reassortant virus of Dk/India with M1 59 replicated to a higher titre than the triple mutant (M1 37 59 205) in the allantoic cavity (Figure 4.1 D), which was unexpected as both viruses shared a filamentous budding morphology. However, in the case of Ck/Italy and Dk/Netherlands, the spherical viruses (Ck/Italy M1 WT and Dk/Netherlands M1 234) showed a clear replication advantage in the allantoic cavity when compared with the filamentous viruses (Ck/Italy M1 234 and Dk/Netherlands M1 WT) (Figure 4.5 C). The latter example is consistent with previous studies which showed that serial passage of filamentous viruses in embryonated chicken eggs resulted in the loss of the filamentous phenotype and predominance of the spherical virion morphology instead (Kilbourne & Murphy, 1960; Seladi-Schulman et al., 2013), which may explain the presence of filaments almost exclusively in clinical isolates or low-passage isolates of mammalian strains of IAV (Choppin & Tamm, 1960; Chu et al., 1949; Nakajima et al., 2010).

Following assessment of viral replication kinetics of spherical and filamentous viruses, the next step was to determine if these morphologies affected pathogenesis in the chicken embryo model. Dk/India M1 WT and M1 59 infected embryos showed severe gross pathology as the embryos were poorly developed with dilated blood-vessels throughout the body, more remarkably so for Dk/India M1 59 which drastically affected embryo integrity (Figure 4.2). Histopathology of these embryos revealed that the liver and kidney tissues were the most affected with an obvious accumulation of blood cells not seen with mock-infected embryos (Figure 4.3). This pattern was in agreement with previous reports on the pathology of chicken embryos infected with a LPAI avian IAV strain (H1N1), which showed that the most severely affected tissues were lung, liver and kidney characterised by the accumulation of blood and disruption of the organ's structure (Westwood, 1952). Furthermore, development of renal disease in chickens infected with avian influenza has also been reported in infected chickens

under laboratory conditions (Swayne & Alexander, 1994; Swayne et al., 1994) and in the field (Halvorson et al., 1979; Johnson & Maxfield, 1976). In this study, the above mentioned pathological signs of IAV infection were only observed with Dk/India WT or M1-mutant viruses and it was independent of budding morphology as Dk/India M1 WT and M1 59 viruses showed opposite budding phenotypes but similar gross and tissue pathology (Figure 4.4 A and figure 4.4 B). For Dk/Tripura, Ck/Italy, Dk/Netherlands and Ck/Pakistan chicken embryo pathology was similar regardless of budding phenotype (Figure 4.4, figure 4.8 and figure 4.11). Therefore, it is possible that Dk/India is just a naturally more virulent strain in chicken embryos when compared with the other strains. In fact, it is known that Dk/India strain is more pathogenic to ducks than Dk/Tripura strain (Kumar et al., 2017). Therefore, these data suggest that spherical or filamentous budding morphology does not alter the pathogenicity of the original parental strain, and tentatively proposes that filaments might not play a role in pathogenesis, at least *in ovo*.

So far all the viruses characterised have been in a PR8 backbone where the M1 mutations responsible for alteration of budding morphology were identified by pairwise alignment of closely related avian strains. On the other hand, the Ck/Pakistan strain was selected to test the hypothesis whether position 234 of M1 could be a morphology determinant within chicken and duck strains of IAV (see chapter 3, sections 3.2.5 and 3.2.6). Ck/Pakistan WT and M1-mutant virus were built in the avian genetic background of Ck/Pakistan, thus providing the perfect tool to test the significance of spherical and filamentous budding morphologies *in vitro* and *in ovo* without the interference of a mismatched genetic background. As previously discussed, Ck/Pakistan WT and M1-mutant virus showed no significant differences in replication kinetics in either MDCK or CEF cells or embryonated chicken eggs (Figure 4.9), thus suggesting that filamentous morphology does not deleteriously affect viral fitness of Ck/Pakistan *in vitro* (beyond an effect on plaque size) nor *in ovo*, which is not in agreement with published studies even with other H9N2 avian strains (Pu et al., 2017). Moreover, embryos infected with Ck/Pakistan WT (spherical) or its M1 filamentous mutant showed similar gross and tissue pathology (Figure 4.11), displaying the characteristic haemorrhages throughout the body and accumulation of blood cells in the liver and kidney

tissues, as seen with other avian chicken viruses (Westwood, 1952). These observations further support the idea that pathogenesis *in ovo* is not dependent on budding morphology. Furthermore, embryo viability was also tested with the WT and M1-mutant virus of Ck/Pakistan strain. Ck/Pakistan WT decreased embryo viability 12 h earlier than Ck/Pakistan 234, but at 48 h p.i both viruses reached similar embryo mortality levels (Figure 4.12). This was unexpected as all the characterisation previously done showed that both viruses behaved similarly *in vitro* and *in ovo* regardless of budding morphology. Therefore, these data perhaps suggest that spherical viruses deposited in the allantoic fluid could cross the amniotic membrane and reach the embryo faster than the filamentous counterpart, which is in agreement with spherical viruses having a fitness advantage in embryonated chicken eggs (Seladi-Schulman et al., 2013). Another explanation could be that the filaments never reach the embryo and the population of spherical particles still produced by Ck/Pakistan 234 (over 40% of infected cells do not produce filaments, figure 3.15 A) just take longer to accumulate and cause embryo mortality. However, it remains unknown whether filaments are able or not of crossing the amniotic membrane.

Overall, this section of the study mainly showed that alteration of the budding phenotype did not drastically alter the viral fitness of the parental strain *in vitro* or *in ovo*, suggesting that filaments may not play a role in pathogenesis. On the other, in an avian background, embryo viability decreased faster for a spherical chicken strain than for its filamentous derivative, hinting that there could be impairment in the transmission of the filaments within the chicken egg. However, looking back at figure 2.3 (chapter 2), some avian isolates produced filaments and characterisation of avian segment 7s showed that the majority promoted the formation of filaments; therefore there must be a positive selection for the filamentous budding phenotype *in vivo*, as seen with mammalian strains (Seladi-Schulman et al., 2013). Yet, the biological function of filaments remained unclear, which will be addressed in chapter 5 by using the avian strain Ck/Pakistan and its M1 filamentous mutant in a chicken challenge and transmission model.

Chapter 5: *In vivo* studies with spherical and filamentous forms of an avian strain of IAV

5.1. Introduction and aims

As shown in chapter 2, avian strains of IAV are as pleomorphic as mammalian strains and some can produce filamentous bundles up to 10 µm in length. Next, it was shown that the M1 "filamentous signatures" previously identified in mammalian strains of IAV do not apply to avian strains, where instead, amino acid identity at position 234 was demonstrated to be a major budding morphology determinant. However, for both mammalian and avian strains of IAV it remains unclear what is the biological function of these filamentous structures.

As previously discussed in chapter 1, spherical virions are commonly found in laboratory-adapted mammalian strains of IAV that have been serially passaged in eggs and/or cells. On the other hand, filamentous structures are often present in low-passage viruses, as seen by observation of clinical isolates of human and veterinary origin. Furthermore, Seladi-Schulman et al. showed that the filamentous phenotype was selected *in vivo* following passage of a spherical virus in guinea pigs, but it was mainly lost when passaged in chicken eggs or MDCK cells (Seladi-Schulman et al., 2013). Several studies have suggested that the advantage of the filamentous phenotype *in vivo* is associated with an increased transmissibility. For instance, Campbell et al. reported that a H1N1 2009 pandemic strain transmitted efficiently in guinea pigs and introduction of the M segment of this strain into PR8 resulted in a virus with a filamentous budding morphology and also increased transmissibility in guinea pigs, unlike PR8 WT which did not transmit (Campbell et al., 2014). Similarly, Ma et al. showed that insertion of the NA and M segments of pandemic 2009 strains in the backbone of a poorly transmissible swine influenza virus (SIV) significantly increased virus replication and transmission in pigs (Ma et al., 2012). Lakdawala et al. also showed that the M segment of the pandemic 2009 strains conferred a filamentous budding phenotype and increased the transmissibility of non-pandemic strains in the ferret model (Lakdawala et al., 2011). Therefore, these studies showed that filamentous mammalian strains of IAV have an increased

transmissibility in animal models, yet it remains unknown whether this is also the case for avian strains of IAV. However, it is known that both morphologies are present in natural influenza infections; therefore these budding morphologies could play different roles *in vivo* in order to ensure viral fitness.

As described in chapter 3, the avian strain Ck/Pakistan was built with or without a single sequence alteration at position 234 of M1, which resulted in a virus pair where it was possible to control its budding morphology. Therefore, the aim of this part of the study was to use this pair of viruses *in vivo* to interrogate the biological significance of filaments produced by an avian strain of IAV.

5.2. Results

5.2.1. Shedding profiles of chickens infected with spherical or filamentous Ck/Pakistan viruses

In vivo studies were designed to assess transmission and pathogenicity differences between the spherical WT Ck/Pakistan avian strain and its filamentous mutant (M1 I234L). A group of 10 Rhode Island Red chickens were infected nasally with 10^5 PFU of the spherical WT or the filamentous mutant of Ck/Pakistan, while a group of 9 chickens were mock-infected with PBS at day 0. To study the transmissibility of the viruses, two further groups of birds were added at days 1 and 5 p.i., designated contact group 1 and contact group 2, respectively (Figure 5.1). All birds were swabbed daily (excepting days 0 and 12) from day -1 for buccal and cloacal shedding, as it is known that IAV can be shed in both the faeces and respiratory secretions of infected birds in the field (Spickler et al., 2008). On day 12 p.i., birds were not swabbed as contact group 2 mutant-infected birds had to be culled because these displayed severe clinical symptoms. To evaluate the ability of spherical and filamentous viruses to spread within the host, several tissues representing the respiratory and gastrointestinal tracts were collected from birds culled at day 3 p.i. for the directly infected

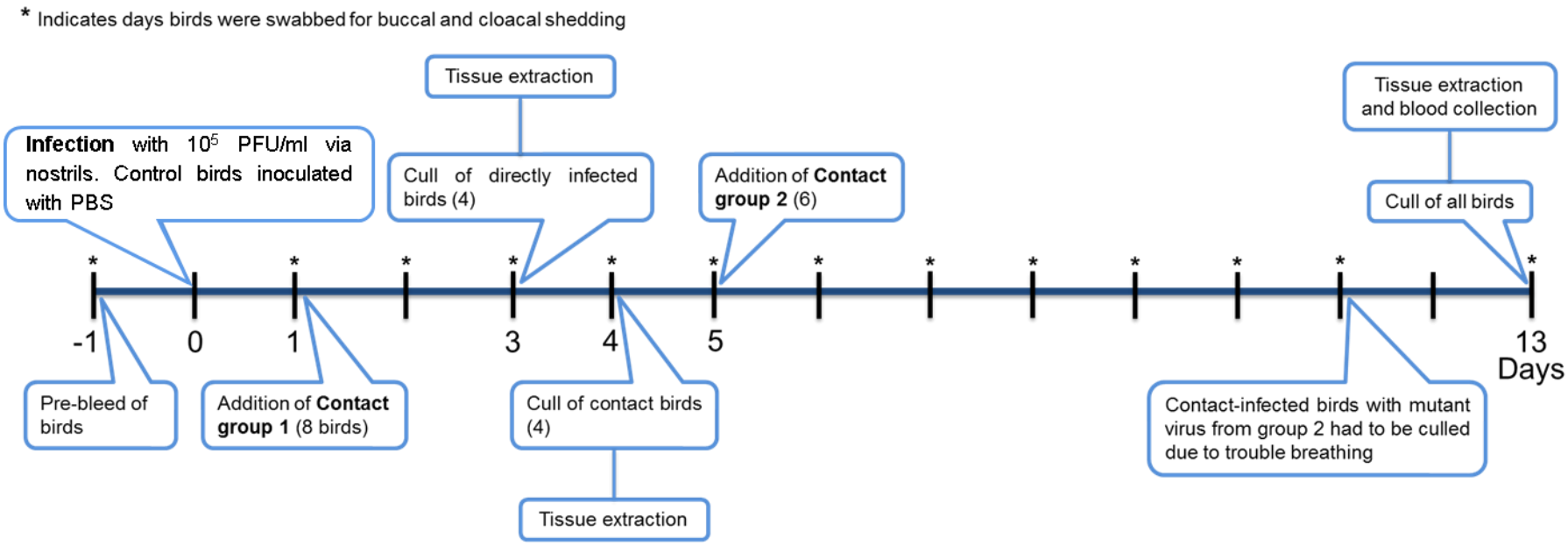

Figure 5.1 Schematic representation of the *in vivo* studies with spherical and filamentous forms of Ck/Pakistan avian strain. 3-week old Rhode Island Red chickens were mock-infected (PBS) (9 birds) or infected with the indicated amount of either virus (100 µl) via the nasal cavity (10 birds per virus group). At day 1 p.i., 8 birds were added to each group (contact group 1). At days 3 and 4 p.i. tissues were collected from directly infected birds and contact group 1 birds. At day 5 p.i. the second contact groups (6 birds) were added. All birds of contact group 2 infected with the filamentous mutant were humanely culled at day 12 p.i.. At day 13 p.i, all remaining birds were humanely culled and sera and tissues collected. Birds were swabbed daily for buccal and cloacal shedding of virus (except at days 0 and 12 p.i.).

birds, day 4 p.i. for contact group 1 and day 13 (study end) for the remaining animals. The swabs collected daily were titrated by plaque assay in monolayers of MDCK cells under agarose overlay. Mock-infected birds showed no detectable levels of infectious virus (< 4 PFU/ml). The directly infected birds (added at day 0) with either the spherical WT or the filamentous mutant of Ck/Pakistan showed no significant differences in the buccal shedding profile, reaching maximum titres of approximately 10^4 PFU/ml at day 3 p.i. and dropping below detectable levels at day 5 p.i. for the WT virus and day 6 p.i. for the filamentous mutant (Figure 5.2 A). By contrast, infectious virus in the cloaca was detected more irregularly and only up until day 3 p.i. for both WT and mutant Ck/Pakistan. The birds introduced at days 1 or 5 p.i. became infected with either WT or mutant virus. Contact group 1 birds infected with the spherical WT virus shed peak titres of approximately 10^4 PFU/ml from the buccal cavity from day 2 until day 4 p.i., then titres dropped sharply on day 5 and levels of virus were undetectable by day 6 p.i. (Figure 5.2 B). Contact-infected birds with the filamentous mutant (Ck/Pakistan M 234) reached similar peak titres in the buccal cavity to WT-infected birds over days 2-4 p.i., but the mutant-infected birds at day 5 p.i shed significantly more (> 10-fold) virus than birds infected with the WT virus. Contact-infected birds still showed sporadic cloacal shedding, although one WT-infected bird shed virus on two consecutive days. Nonetheless, for both groups of birds, cloacal shedding was detected from day 3 to day 4 p.i, corresponding with the peak viremic period detected in the buccal cavity. Lastly, contact group 2 birds (added at day 5 p.i.) infected with the spherical WT virus shed relatively high amounts of virus (10^3 – 10^4 PFU/ml) from the buccal cavity from day 6 to 9 p.i., with the peak amounts detected at day 8 p.i. (Figure 5.2 C). However, the group 2 contact birds infected with the filamentous mutant virus shed approximately 10^3 - 10^4 PFU/ml of virus from day 6 to 10, reaching a peak at day 9 p.i.. Significantly, birds infected with the filamentous mutant virus were shedding almost 100-fold more virus at day 10 p.i. than birds infected with the spherical WT virus. In addition, cloacal shedding was only detected from contact group 2 birds infected with the filamentous mutant, between days 7 to 10 p.i. with some birds shedding over 2 or 3 consecutive days. Overall, these data showed that there were no detectable differences in buccal shedding between WT- and mutant-infected birds within the direclty-infected groups. In contrast, contact-infected birds with the filamentous mutant of

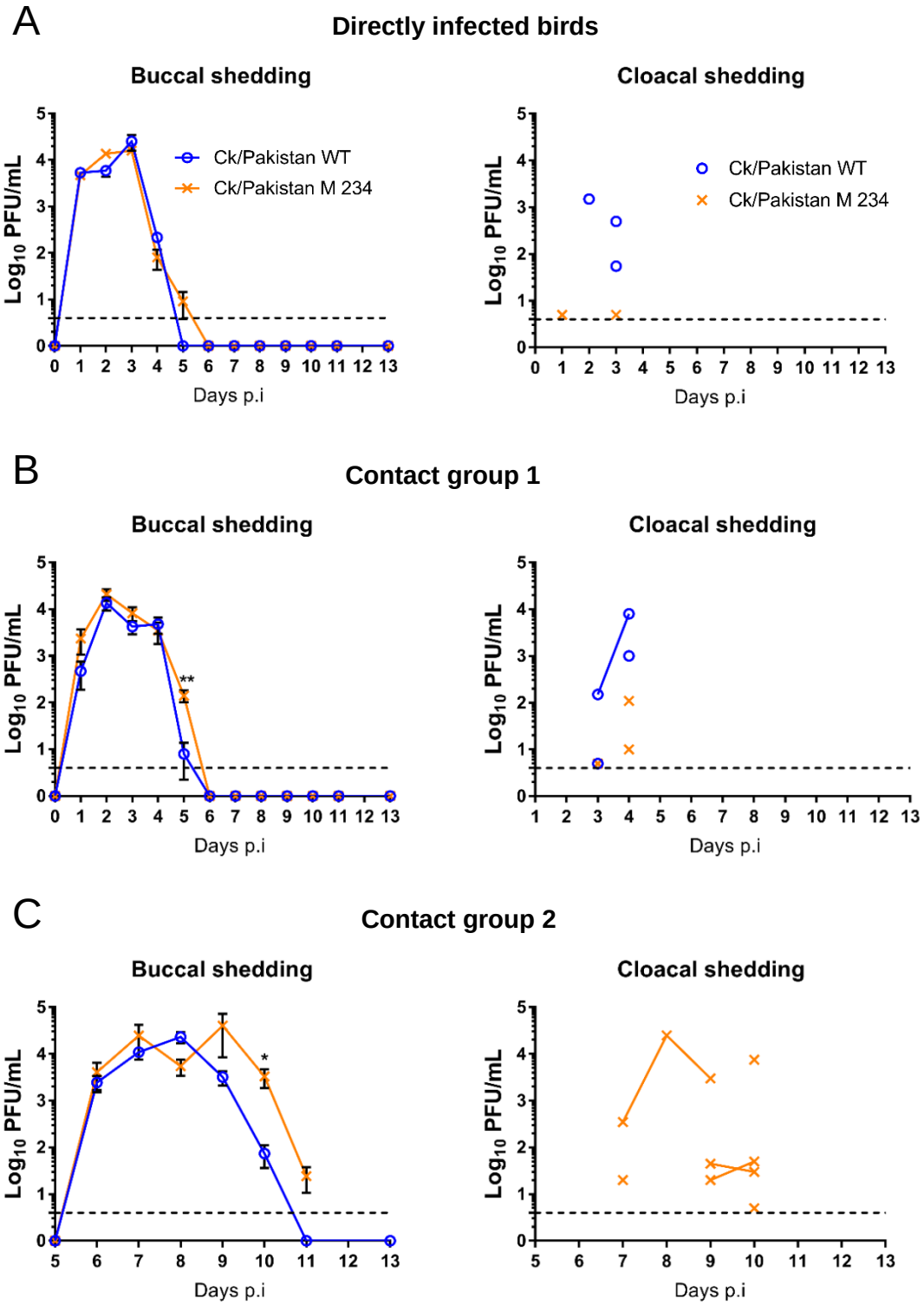
A
Directly infected birds
Buccal shedding
Cloacal shedding
Ck/Pakistan WT
Ck/Pakistan M 234
Log10 PFU/mL
Days p.i
B
Contact group 1
Buccal shedding
Cloacal shedding
**
Log10 PFU/mL
Days p.i
C
Contact group 2
Buccal shedding
Cloacal shedding
*
Log10 PFU/mL
Days p.i

Figure 5.2 Shedding profiles of Ck/Pakistan WT and M1-mutant viruses. Chickens either directly infected with WT or mutant virus of Ck/Pakistan (A), or from contact groups 1 (A) added at day 1 p.i. and contact groups 2 (C) added at day 5 p.i. were swabbed daily from buccal and cloacal cavities. Contact group 2 birds infected with mutant virus (orange) were culled at day 10 p.i.. Swabs were placed in virus transport media and titrated by plaque assay in MDCK cells. Data from birds infected with the spherical WT is represented with blue circles while that of the filamentous mutant virus is depicted with orange crosses. Data points in the buccal shedding graphs represent mean ± SEM of all the birds swabbed (n = 48) while only positive samples from cloacal swabs are shown. Data points connected in cloacal shedding graphs indicate consecutive positive samples from the same bird. One-way ANOVA and non-parametric Mann-Whitney tests were performed to compare WT- and mutant-infected birds throughout the course of the experiment (see chapter 7, section 7.2.8); ** $p < 0.01$, * $p < 0.05$. Dashed line indicates the detection limit of the plaque assay (4 PFU/ml).

Ck/Pakistan generally showed higher buccal shedding of virus than WT-infected contact birds. Therefore, these data suggest that the spherical WT and filamentous mutant virus were able to transmit to naïve birds introduced at days 1 and 5 p.i., however mutant-infected birds shed generally more virus than WT-infected birds and for longer periods of time.

Ck/Pakistan WT is a LPAI H9N2 virus endemic across Asia, Middle East and North Africa that usually affects growth rate and egg production (Spickler et al., 2008). However, it has been reported that some field strains of Ck/Pakistan-like viruses seemingly display an HPAI phenotype and can cause up to 50% mortality; something which has also been observed in the laboratory (Zhang et al., 2014). Therefore, to determine whether the spherical WT or filamentous mutant of Ck/Pakistan showed differences in lethality, the clinical signs of infected chickens during the study period were considered. Observational data throughout the experiment revealed that birds infected with the spherical WT virus presented ruffling of feathers, snicking and the birds tended to group together, but no mortality was seen, thus corresponding to 100% survival from day 0 to 13 p.i, within directly-infected, contact 1 and contact 2 groups (Table 5.1). Birds directly infected with the filamentous mutant showed similar symptoms to WT-infected birds with 100% survival, however, contact group 1 showed a slightly exacerbation of the symptoms previously described with more anti-social behaviours observed up until day 9 p.i., but still 100% survival. By contrast, contact group 2 birds infected with the filamentous mutant were severely affected by respiratory distress, diarrhoea, depression, reduced activity and loss of appetite, and 2/6 birds were humanely culled at day 10 p.i. and the other 4 birds had to be culled at day 11 p.i.. As mentioned, up to 50% mortality was observed previously with WT Ck/Pakistan avian strain, however that was not the case presented here. The WT-infected birds survived throughout the experiment displaying only minor symptoms, while the mutant-infected birds showed exacerbated symptoms with the highest mortality in the contact group 2, corresponding to the group where the shedding profile was more accentuated. Therefore, these data suggested that a filamentous budding morphology could enhance pathogenicity.

Table 5.1 Symptoms and survival rate of birds infected with the spherical WT or the filamentous mutant of Ck/Pakistan. A description of the symptoms observed is presented.

Virus	Group	Symptoms observed	Fatalities	Live birds at the end of the study (accouting for tissue extraction)	Survival (%)
Ck/Pakistan WT	Directly-infected	Ruffled feathers, snicking and huddle together	0	3	100
	Contact group 1	Ruffling of feathers, snicking and huddle together	0	4	100
	Contact group 2	Ruffling of feathers, snicking and huddle together	0	6	100
Ck/Pakistan mutant	Directly-infected	Ruffling of feathers, snicking and huddle together	0	6	100
	Contact group 1	Ruffling of feathers and snicking and huddle together	0	4	100
	Contact group 2	Ruffling of feathers, snicking, diarrhoea, respiratory distress, depression and isolation behaviour.	2 (day 10 p.i.); 4 (day 11 p.i.) (humane end point)	0	0

5.2.2. Environmental sampling

In order to examine the environmental contamination with virus from the infected birds, water and food samples were collected daily over the course of the experiment and titrated by plaque assay. Water and food samples collected from the housing of mock-infected birds were negative for infectious virus, to a detection limit of 4 PFU (data not shown). Food samples collected from the isolators housing spherical WT- or filamentous mutant-infected birds also showed no detectable levels of infectious particles throughout the course of the experiment (Figure 5.3 A). However, the isolator with WT-infected birds showed water contamination with virus from days 1 to 3 p.i. and at days 7 and 8 p.i., with a peak titre of 10^3 PFU/ml detected at day 1 p.i. which decreased to 10 PFU/ml at later times p.i. (Figure 5.3 B), correlating with the days where buccal shedding was the highest. By contrast, AIV was detected in the water of the isolator containing the mutant-infected birds at days 2 to 5 p.i. and days 7 to 9 p.i., in both instances with an average peak titre of 10^2 PFU/ml. Therefore, the filamentous mutant virus was present in the environment for longer period of time than the spherical WT virus, which could be a direct result of the prolonged buccal shedding observed with the mutant-infected birds.

5.2.3. Spherical and filamentous virus spread within the host and histopathology of respiratory tissues

Since birds infected with the filamentous-mutant virus showed significantly increased viral shedding over a longer period of time, the next step was to examine whether spread within the host differed between the two viruses. For this, tissues representative of the respiratory and gastrointestinal tracts were collected at day 3 p.i. from directly infected and contact group 1-infected birds, homogenised and titrated by plaque assay for the detection of infectious virus. As expected, mock-infected birds showed no detectable levels of infectious virus (< 4 PFU/ml in 50 mg of tissue) nor viral genome (< 10 copies/30 mg tissue) (data not shown). In the nasal tissue of birds infected with either the spherical WT or filamentous mutant, both viruses

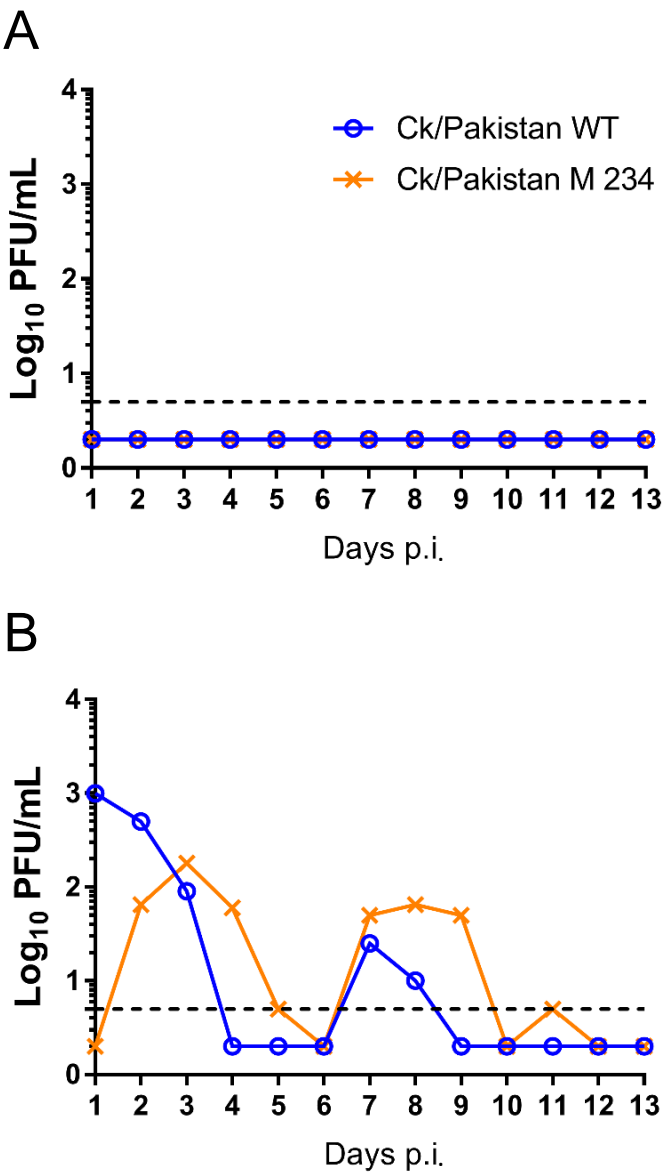

Figure 5.3 Environmental sampling of isolator units containing the infected chickens. Following daily collection (except at day 12) of 1 g of food (A) and 1 ml of water (B), these samples were processed and titrated by plaque assay (see chapter 7, section 7.2.6.6). The detection limit of the plaque assay is indicated (4 PFU/ml).

reached similar titres of between 10^4 and 10^5 PFU/ml. By contrast, in the tracheal tissue, the filamentous mutant replicated significantly more than the spherical WT virus, by almost 100-fold (Figure 5.4 A). Infectious virus was detected sporadically in all other respiratory and gastrointestinal tissues, but at generally low titres (mostly < 100 PFU/ml in a single animal) with no significant differences between the spherical WT and the filamentous mutant. However, the WT virus was detected in the brain at approximately 10^3 PFU/ml in four birds while the filamentous mutant was only detected in the brain of one bird, at 10 PFU/ml. RNA samples extracted from the same tissues were examined by qRT-PCR to quantify the presence of viral genome (measured by the amount of M segment) present in each of the organs tested. Within the respiratory and gastrointestinal tissues, no significant differences were detected in the amounts of viral genome from WT or mutant virus in any of the tissues analysed. Nonetheless, higher amounts of M segment were detected in the nasal and tracheal tissues, correlating with the higher amounts of infectious virus present in these samples (Figure 5.4 B). Overall, these data showed that both morphologies of the virus were detected within the host in the same respiratory and gastrointestinal organs, mostly in similar quantities, thus suggesting that Ck/Pakistan virus spread within the host was morphology-independent. However, in the tracheal tissues the filamentous mutant virus produced a higher number of infectious virions when compared with the spherical WT, suggesting a fitness advantage of the filamentous mutant in this tissue.

Given that both morphologies of Ck/Pakistan virus spread within the host to similar extents, the next step was to determine whether pathology signs associated with infection were strain-dependent. The tissues which were the main focus of this section were from the upper and lower respiratory tract, as it is well established that IAV in domestic poultry mainly replicates in these locations (discussed in chapter 1). Thus, tracheal and lung tissues of directly infected and contact group 1 birds harvested at day 3 p.i. were sectioned and H&E stained. Mock-infected trachea showed no signs of lesions, characterised by the presence of an organised structure of ciliated epithelial cells and goblet cells with an intact lamina propria underneath and normal size capillaries (see chapter 1, figure 1.7). Trachea from WT-infected chickens typically presented disruption of the ciliated epithelium with reduced number of

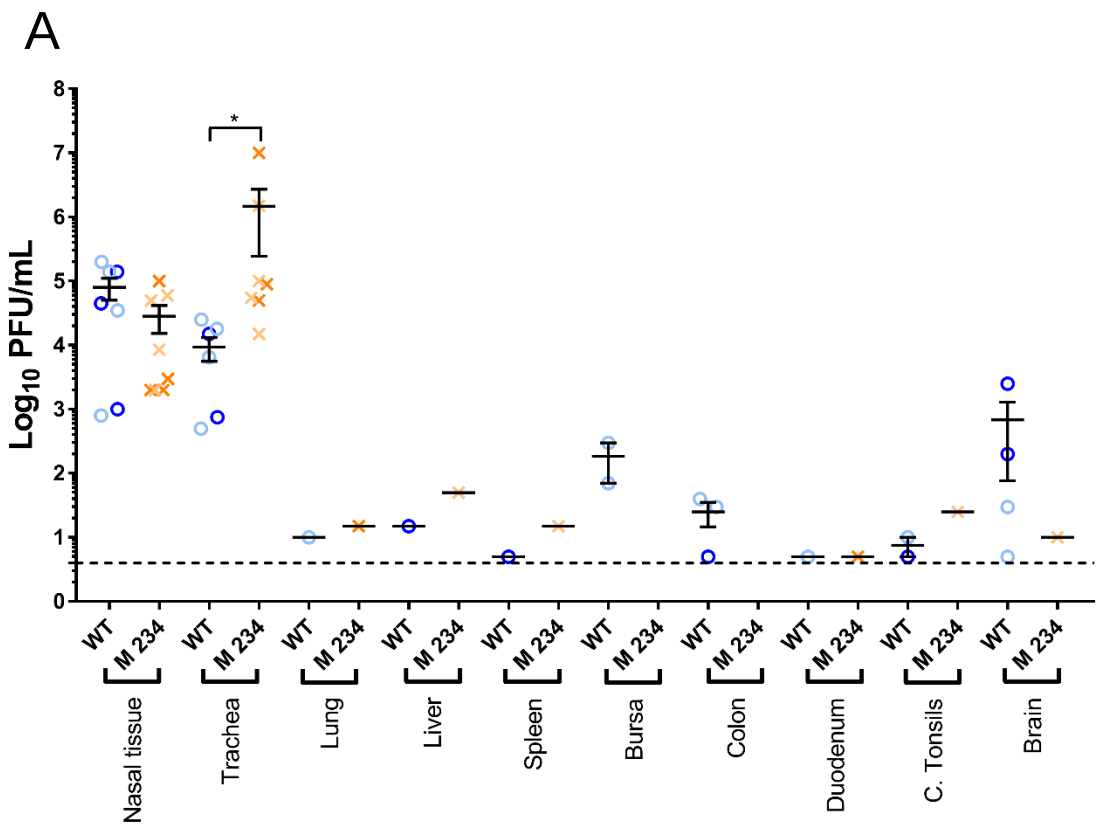
A
Log10 PFU/mL
0
1
2
3
4
5
6
7
8
*
WT
M 234
Nasal tissue
Trachea
Lung
Liver
Spleen
Bursa
Colon
Duodenum
C. Tonsils
Brain

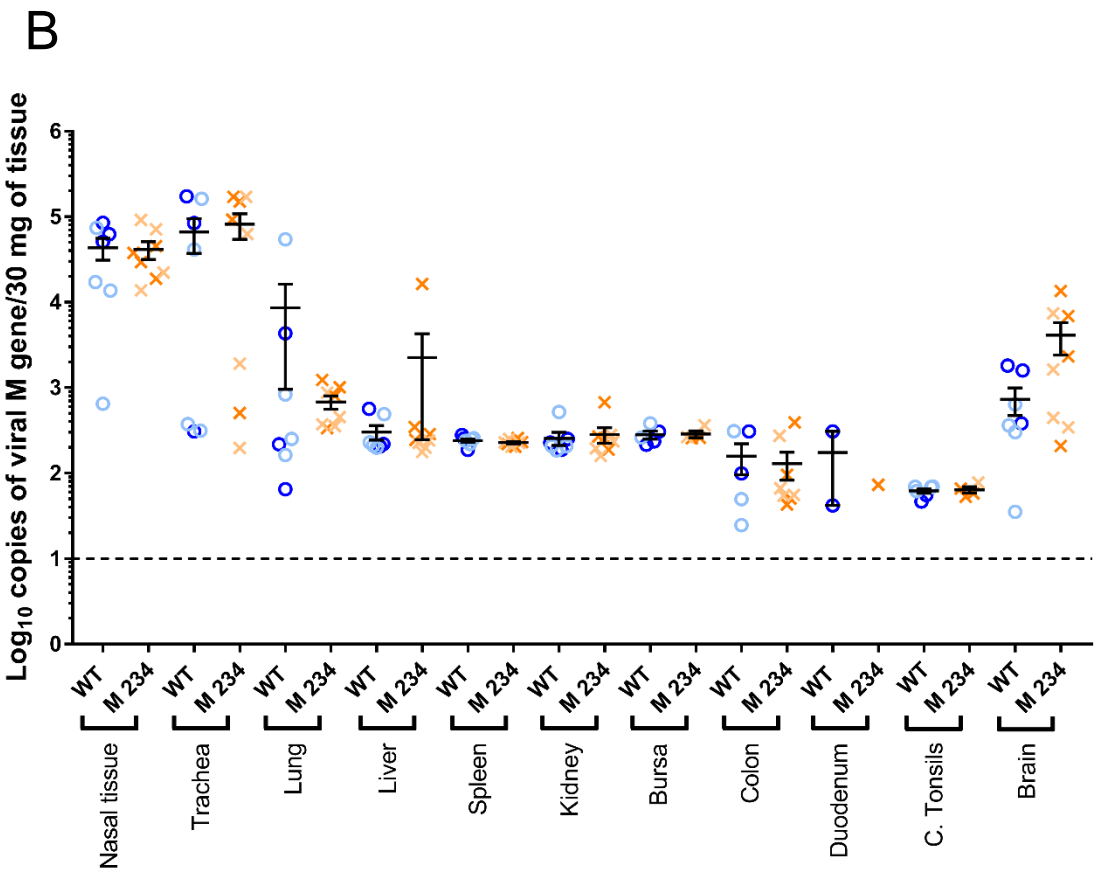
B
Log10 copies of viral M gene/30 mg of tissue
0
1
2
3
4
5
6
WT
M 234
Nasal tissue
Trachea
Lung
Liver
Spleen
Kidney
Bursa
Colon
Duodenum
C. Tonsils
Brain

Figure 5.4 Detection of infectious virus and viral genome in tissues of chickens infected with WT or M1-mutant Ck/Pakistan viruses. The indicated tissues were extracted at day 3 p.i. of directly infected birds or contact-infected birds and titrated by plaque assay for the detection of infectious virus (A) or RNA extracted and quantified by RT-qPCR for the presence of viral M segment (B). Directly infected birds are represented in a darker colour while contact birds are represented in a lighter shade. Blue circles represented birds infected with the spherical WT virus while orange crosses represent filamentous mutant-infected birds. (A) 50 mg of each tissue was used for the detection of infectious virus. (B) Total RNA was extracted from 30 mg of tissue and used for the detection of M segment in the indicated tissue. Non-parametric Mann-Whitney tests were performed to compare WT and mutant for each tissue. Data represent mean +/- SEM (n = 3 directly infected WT and n=4 for all other groups). * $p < 0.05$.

goblet cells and considerate loss of cilia in some occasions. Furthermore, leakage of blood cells and/or infiltration of immune cells into the lamina propria was also observed, disrupting its structure (Figure 5.5). Comparison of the tracheal tissues between WT and mutant-infected birds did not reveal obvious differences in pathology, suggesting that the damage observed was a result of IAV infection rather than virus budding morphology-dependent. Looking at the lung tissue, mock-infected birds showed no signs of disease, characterised by the lack of haemorrhages or infiltration of immune cells into the area within or surrounding the bronchioles. By contrast, WT- or mutant virus-infected birds displayed moderate haemorrhages in the lung with severe congestion around and, in some instances, within the bronchioles with red blood cells and/or immune cells. Yet once again, there were no obvious differences between the two virus strains. Therefore, these data suggested that the pathology signs presented in the tracheal and lung tissues were the result of IAV infection, regardless of virion morphology.

5.3. Discussion

The aim of this part of the study was to determine the biological function of filamentous forms of IAV *in vivo* using the Ck/Pakistan avian strain. The filamentous mutant of Ck/Pakistan was designed and built in chapter 3 based on bioinformatics and statistical analyses. Since this virus presented a virion morphology able to be controlled via one single amino acid mutation (I234L) in M1, it provided an appropriate tool to test the biological function of filaments *in vivo*. Therefore, Ck/Pakistan viruses with spherical or filamentous budding morphologies were used to infect chickens and contact groups were added to test for differences in transmission between the two forms. Directly infected birds with the spherical or filamentous virus showed no significant differences, however contact-infected birds shed the filamentous mutant virus at higher titres and for longer periods of time than WT contact-infected birds (Figure 5.2). Remarkably, contact birds added at day 5 p.i. showed more pronounced buccal and cloacal shedding than the equivalent-WT infected birds,

A

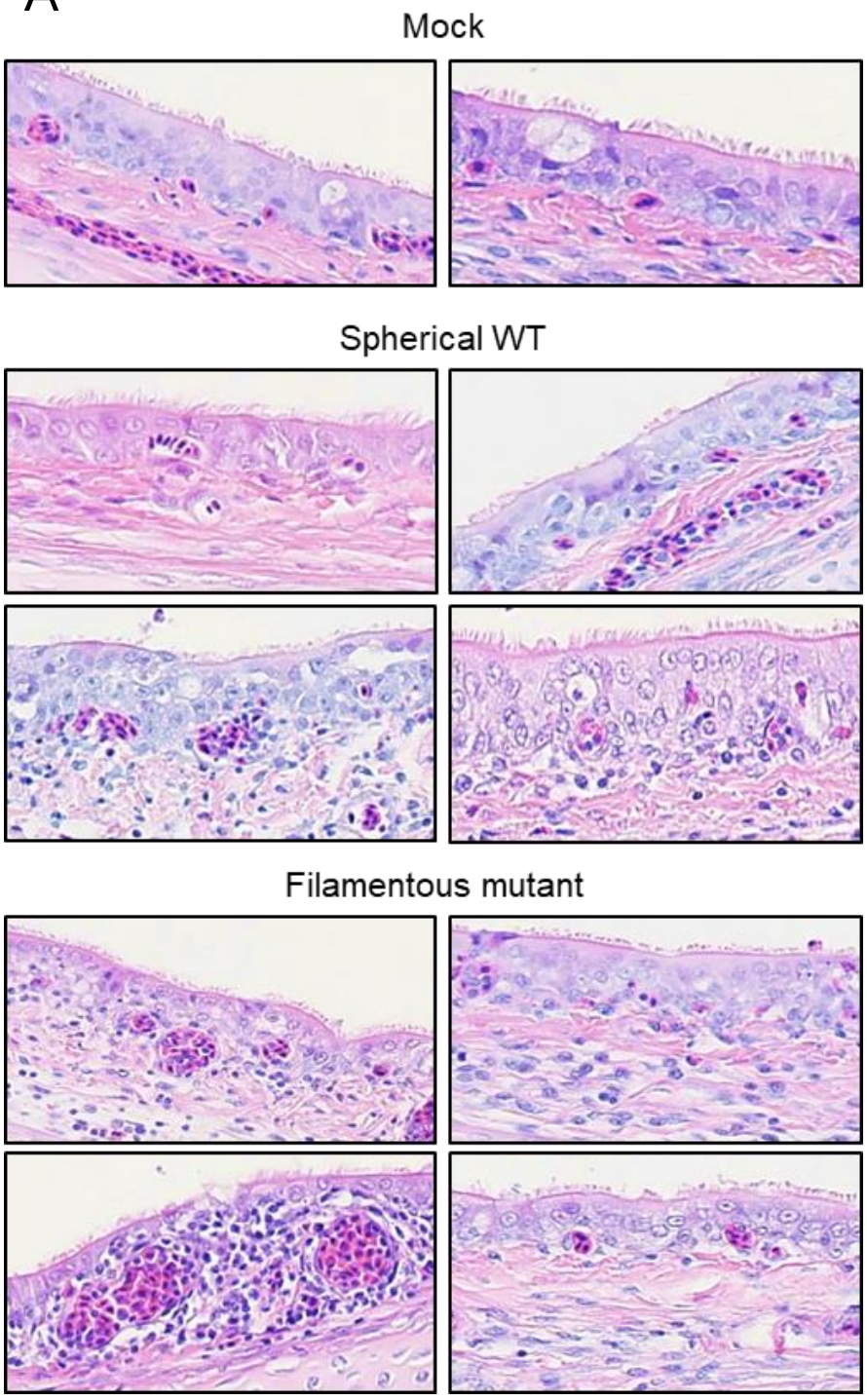

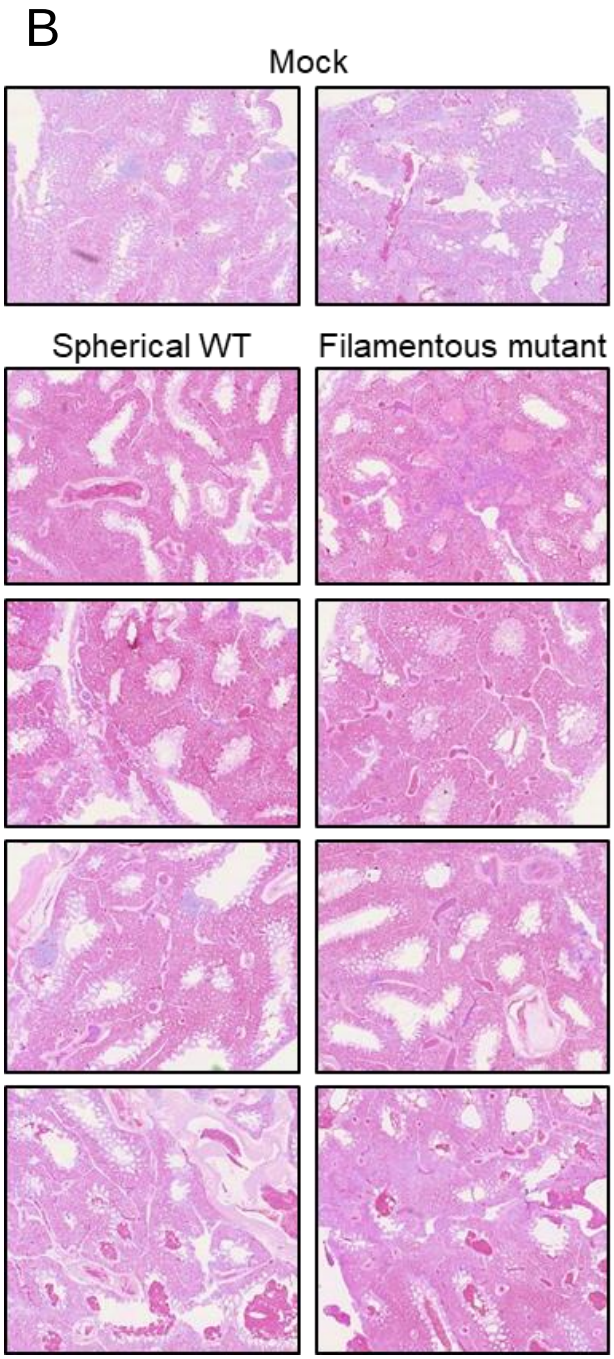

Figure 5.5 Representative histopathology of tracheal and lung tissues infected with the spherical WT or filamentous mutant of Ck/Pakistan. Tracheal (A) and lung (B) tissues were harvested at day 3 p.i. from 3 or 4 directly infected birds and 4 contact group 1 birds infected with WT or mutant virus. Tissues were fixed in 10% formalin and prepared for H&E staining by the histopathology team at the Pathology unit of the Royal (Dick) Veterinary School (University of Edinburgh). Slides were scanned using the Nanozoomer at 20X magnification and visualised with the NDP software. Represented are the H&E sections from 2 directly infected birds and 2 contact group 1 infected with the spherical WT or filamentous mutant.

suggesting that the filamentous mutant of Ck/Pakistan was transmitted more efficiently than the spherical WT virus. This agrees with previous reports for filamentous mammalian strains. Lakdawala et al. reported that ferrets infected with a filamentous human strain released respiratory droplets more consistently than WT-infected ferrets, therefore resulting in an enhanced transmissibility of the filamentous virus between ferrets (Lakdawala et al., 2011). More recently, Campbell et al also showed that insertion of the viral glycoproteins and the M segment of a filamentous human strain into the poorly transmissible PR8 strain increased its transmissibility in guinea pigs (Campbell et al., 2014).

Regarding pathogenicity, filamentous virus-infected chickens dropped to approximately 40% survival rate by the end of the experiment (Table 5.1). It has been reported that infections with WT Ck/Pakistan can reach a mortality rate of 50%, however in this experiment, the mortality rate of WT was 0% while the filamentous mutant was 60%. This raises the question whether this increased mortality rate was a result of virion morphology. However, as shown in chapter 4, the death rate of the filamentous form of Ck/Pakistan *in ovo* was 12 h delayed in comparison with WT-infected eggs. Therefore, the high mortality rate observed with the filamentous mutant in hatched birds was unexpected; to further address this problem whole virus deep sequencing and analysis of the cytokine response would be needed to compare WT and mutant-infected chickens but there was not enough time to perform this.

Environmental sampling of the isolator units with WT or mutant-infected chickens showed that the filamentous virus persisted for longer periods of time in the water and to higher titres than the WT virus (Figure 5.4). This could either correlate with the fact that filamentous mutant-infected chickens were also shedding more virus via the buccal cavity than WT-infected birds, or that the filamentous form of Ck/Pakistan is more stable in water than the spherical WT counterpart. It was shown by Lowen et al. that a human strain of IAV transmitted better in guinea pigs exposed to lower temperatures and relative humidity levels lower than 50% (Lowen et al., 2007). Outside these parameters, virus particles tended to be less stable; therefore it is possible that the filamentous mutant virus is more stable at temperatures between 22 – 25°C with high relative humidity (50% - 80%) (the conditions of the isolator units).

Stability assays would be the next step to address this question but there was insufficient time to finalise these.

Infectious spherical or filamentous forms of Ck/Pakistan were detected in all the tissues of directly-infected or contact group 1 birds, with the exception of the kidney, for which only viral genome was detected. Thus these data showed that both viruses spread similarly within the host (Figure 5.5). Of importance, the main difference was observed in the respiratory tissues. Although spherical and filamentous forms of Ck/Pakistan replicated similarly in the nasal tissue, in the tracheal tissue the filamentous form replicated to a higher titre than the spherical WT virus. The trachea is composed of a mucous layer that overlays the respiratory epithelium, which is coated by a less viscous layer of about 7 μm in depth with the epithelial cells underneath (see chapter 1, section 1.7.1 and figure 1.7). Therefore, Roberts and Compans hypothesised that a filamentous virus that can be up to 30 μm in length would have an advantage when crossing this barrier in comparison to spherical particles of ~ 100 nm in diameter (Roberts & Compans, 1998). The data described here corroborates the hypothesis that filamentous viruses show a fitness advantage when crossing the mucus barrier of the trachea. For instance, a filamentous virus could more readily cross the mucous barrier and reach the epithelial cells where it replicates and its elongated form might also enhance release from the surrounding mucous barrier, allowing virus release into the upper mucous layer and into the lumen of the trachea. Furthermore, Sakai et al. recently showed that filamentous ICV particles showed movement in one direction on a sugar-coated surface in contrast with the random movement of spherical IAV particles (Sakai et al., 2018). Therefore, this property of filamentous particles could facilitate virus travel within the respiratory mucosa to more readily reach the epithelial cells.

Lastly, we also wanted to test whether viral pathogenesis was virion morphology-dependent, thus tissues were collected at day 3 p.i. and the respiratory tissues were analysed. Similarly to what was observed in chapter 4, the mild clinical manifestations detected in these tissues were virion morphology-independent and were simply typical of those associated with a LPAI infection (Spickler et al., 2008). Therefore, these data demonstrated that viral pathogenesis could be independent of virion morphology; however immunohistochemistry

against viral proteins would be needed to ensure the clinical manifestations in the tissues were associated with sites of viral infection.

Overall, these data demonstrated that contact-infected birds with the filamentous mutant of Ck/Pakistan shed the virus via the buccal cavity to a similar titre but for longer periods of time than the WT virus. The filamentous mutant of Ck/Pakistan was also detected in water samples for longer periods of time than the spherical WT. Within the chicken host, even though both forms spread similarly and reached the same organs, the filamentous mutant replicated to a higher titre than the spherical WT in tracheal tissues. Lastly, as observed in chapter 4, spherical or filamentous forms of Ck/Pakistan showed similar levels of pathogenesis in H&E section, which could suggest that pathology is budding morphology-independent. By contrast, the *in vivo* data described in this chapter support the hypothesis that filamentous morphology plays a role in transmission, similar to what has been observed with filamentous mammalian strains.

Chapter 6: Concluding remarks and future directions

6.1. Concluding remarks

The aim of this study was to determine the predominant budding morphology presented by avian strains of IAV and, if filaments were shown to be a common occurrence, then determine their biological significance. In chapter 2, it was shown that avian isolates can be as pleomorphic as mammalian strains. Furthermore, segment 7 was also identified as the major morphology determinant for avian strains of IAV, thus PR8-based 7:1 reassortant virus with segments of avian strains were built and their budding phenotype characterised. Characterisation of these viruses revealed that filamentous 'avian' strains induced filament formation in over 40% of infected cells and the filamentous bundles were as long as 10 μm, comparable with previous results seen with mammalian strains of IAV. Next, it was asked whether avian strains also followed the "filamentous signature rules" previously identified within M1 of mammalian strains. The data described in chapter 3 suggested that was not the case; in fact, the budding morphology of specific avian strains was shown to depend on the amino acid identities at positions 59, 169 and 234 of M1. From this, it was hypothesised that positions 59, 169 and 234 of M1 could be budding morphology determinants for a wider range of avian strains. Bioinformatics coupled with statistical analysis revealed that the amino acid identity at position 234 of M1 was a strong predictor of budding morphology, as chicken viruses with isoleucine at this position tended to show a spherical budding morphology whereas duck viruses with leucine were filamentous. This hypothesis was experimentally corroborated as changing position 234 of M1 in a spherical chicken virus Ck/Pakistan induced the formation of filaments. In chapter 4 the growth of WT and M1-mutant viruses with opposing budding phenotypes was characterised, which showed that in an *in vitro* system the avian viruses replicated similarly, regardless of budding morphology. Yet, *in ovo*, a replication advantage was observed with spherical viruses in contrast with their filamentous counterparts, as previously reported (Seladi-Schulman et al., 2013). This chapter also addressed the pathology caused in chicken embryos upon infection with spherical or filamentous counterpart viruses, which indicated that budding morphology did not have a strong phenotypic effect in this

respect. Finally, in chapter 5 the aim was to determine the biological significance of filaments, thus the Ck/Pakistan chicken viruses built in chapter 3 were used. This virus pair had either a spherical (M1 234 Ile) or filamentous (M1 234 Leu) budding morphology and therefore provided a tool to test the role of filaments *in vivo* in the natural virus host (chicken). The data described in this chapter suggested that filamentous structures could play a role in shedding as the filamentous virus persisted in the respiratory tract of birds for longer periods of time and to higher titres than the spherical WT counterpart, and was shed in greater amounts

A further outcome of the work presented here is the observation that chicken viruses were more likely to be non-filamentous while duck viruses were predominantly filamentous. This suggests that avian IAVs present in wild aquatic birds could be predominantly filamentous and, following adaptation to domestic poultry, lose this trait. This adaptation could be a result of the way domestic poultry is raised, as in a poultry shed filled with hundreds of chickens the virus is under lower selective pressure to transmit efficient as the chances of infecting a new host are very high, while in the wild aquatic birds, not kept in close contact, this pressure is maintained.

6.2. Future directions

6.2.1. *In vitro* analysis

Like with every PhD project, time is always a limiting step and many things are left undone and questions left unanswered, yet it is still a bulk of work that improves the current knowledge on the topic. In chapter 5, it was addressed the biological function of filamentous particles, which suggested a role in enhancing transmission of IAV particles. In addition, it would have been interesting to measure NA activity of the filamentous mutant of Ck/Pakistan, since several studies have reported that filamentous viruses transmitted better and had higher NA activities in comparison to their spherical counterparts, suggesting that M1 and NA activities could have a cumulative effect in enhancing transmission of filamentous viruses (Campbell et al., 2014; Seladi-Schulman et al., 2014). Furthermore, even though the

Ck/Pakistan filamentous virus showed a replication advantage in the tracheal tissue of chickens, it would be good to repeat this observation *in vitro* or *ex vivo*. For instance, Yang et al. developed an in-capsule-mucous penetration system to determine the role of NA during movement of swine IAV through a mucous layer (Yang *et al.*, 2014). The system comprises of inserting a portion of mucous from the host of interest in a plastic capsule, overlaid with a certain amount of virus and allow for vertical dissemination of the virus through the mucus. To measure the distance travelled by the virus from the top of the mucus layer, the authors used cryo-sectioning and immunofluorescence assays. In fact, using a labelled virus and staining for mucins (to delineate the start of the mucus barrier), the authors showed that the virus reached a depth of 30 μm in just 2 min. Therefore, this could be an important system to determine how fast the two budding morphologies of IAV can penetrate the mucous barrier. Although this would provide information about speed, it does not provide information about replication fitness of filamentous and spherical viruses. Thus, another option would be to use cultures of tracheal organ rings (TOCs). Initial efforts at establishing this system in the laboratory showed that PR8 or PR8-based 7:1 avian reassortant viruses replicated well in TOCs and preliminary results showed a tendency for filamentous virus to replicate better in TOCs where the mucous barrier had not been cleared before infection (data not shown).

6.2.2. *In ovo* and *in vivo* studies

Even though it is well established that M1 is the major IAV morphology determinant, it is undeniable that the host also plays some role in determining particle shape as described before. Therefore, *in ovo* studies with duck eggs would be the next step to determine if a virus with a spherical morphology has the advantage in any embryonated egg or if morphology fitness is host-dependent, i.e., would a filamentous virus show an advantage in embryonated duck eggs in comparison with its spherical counterpart. Lastly, it would be interesting to perform the same animal experiment described in chapter 5 but with ducks instead of chickens. For instance, use a filamentous duck virus and its spherical counterpart and assess differences

in transmission, mortality rates and pathogenesis to determine if virion morphology is truly a host adaptation factor from wild aquatic birds to domestic poultry.

Chapter 7: Materials and methods

7.1. Materials

7.1.1. Antibodies and dyes

Table 7.1 Primary antibodies and antisera raised against IAV and cellular proteins.

Antibody	Application	Source
Rabbit polyclonal anti-PR8	IF (1:500)	(Amorim et al., 2007)
Mouse monoclonal anti-NP (AA5H)	IF (1:1000)	Abcam (ab20343)
Rabbit polyclonal anti-PR8 M1 (A2917)	WB (1:500)	(Amorim et al., 2007)
Rabbit polyclonal anti-MBP-NP (A2915)	WB (1:500), plaque immunostaining (1:1000)	(Noton et al., 2007)
Rat monoclonal anti-alpha-tubulin	WB (1:1000)	Serotec (MCA77G)

Table 7.2 Plant lectins.

Lectin	Application	Source
Concanavalin A Alexa Fluor® 488 conjugate	IF (1:50)	Life Technologies
Wheat germ agglutinin biotinylated	IF (1:50)	Sigma
Lycopersicon esculentum agglutinin biotinylated	IF (1:50)	Sigma

Table 7.3 Secondary antibodies.

Antibody	Application	Source
Donkey anti-rabbit IgG (H+L) secondary antibody, Alexa Fluor® 488 conjugate	IF (1:1000)	Thermo Fisher (A-21206)
Donkey anti-mouse IgG (H+L) secondary antibody, Alexa Fluor® 488 conjugate	IF (1:1000)	Thermo Fisher (A-21202)
Streptavidin Alexa Fluor® 488 conjugate	1:200	Thermo Fisher (S11223)
IRDye®800LT Donkey anti-rabbit IgG (H+L)	WB (1:10000)	Li-Cor 926-32213

IRDye®680LT Goat anti-rat IgG (H+L)	WB (1:10000)	Li-Cor 925-68076
Goat anti-rabbit IgG (H+L)-HRP conjugate	plaque assay (1:1000)	Bio-Rad 1721019

Table 7.4 Fluorescent dyes.

Dye	Application	Source
ProLong Gold Antifade Mountant with DAPI	IF (neat)	Invitrogen
DAPI	IF (1:10000)	Invitrogen

7.1.2. Oligonucleotides

DNA oligonucleotides were synthesised by and purchased from Sigma.

Table 7.5 Sequencing primers.

Primer name	Sequence (5' to 3')
Uni12	AGCAAAAGCAGG
pDUAL FWD	ATGTCGTAACAACTCCGCCC
pDUAL REV	TTTTTGGGGACAGGTGTCCG
PR8 HA internal FWD	ACGGAGAAGGAGGGCTCATA
PR8 HA internal REV	TCCAGAGTCCTTTCATTTTCCAGT
PR8 NA internal FWD	TCTTTGTCCCATCCGTGGGT
PR8 NA internal REV	AAGCACGGCCTCATACAGTC
PR8 NP internal FWD	TGCGGGGAAGGATCCTAAGA
PR8 NP internal REV	CATCCTGGGATCCATTCCGG
Dk/Netherlands HA internal FWD	TGCTTTGGGGAGTGCATCAT
Dk/Netherlands HA internal REV	GTTGAACTCCTTGCTCACTGC
Dk/Netherlands NA internal FWD	GGTTTCAGTGACATTAGCGGG
Dk/Netherlands NA internal REV	GTCAGTTCTGGATGCTGGACA
Dk/Netherlands NP internal FWD	GGAGAGGCGAAAATGGACGA

Dk/Netherlands NP internal REV	AGTCCGTACACACAAGCAGG
M segment FWD (MF1)	AGCAAAAGCAGGTAGATATTGAAAGA
M segment REV (MR1027)	AGTAGAAACAAGGTAGTTTTTTACTC

Table 7.6 Site-directed mutagenesis primers.

Primer name	Sequence (5' to 3')
Dk/India M1-A225G (aa 37) FWD	CTTTGCAGGAAAGAACGCCGATCTCGAGGCTCT
Dk/India M1-A225G (aa 37) REV	AGAGCCTCGAGATCGGCGTTCTTTCCTGCAAAG
Dk/India M1-T293G (aa 59) FWD	CTGTCACCTCTGACTAAAGGGATGTTGGGATTTG TATTCA
Dk/India M1-T293G (aa 59) REV	TGAATACAAATCCCAACATCCCTTTAGTCAGAGGT GACAG
Dk/India M1-A729G (aa 205) FWD	CTAGCCTGATTAGCAACCTCCATGGCTTCCGCT
Dk/India M1- A729G (aa 205) REV	AGCGGAAGCCATGGAGGTTGCTAATCAGGCTAG
Dk/Tripura M1-G230A (aa 37) FWD	TCTTTGCAGGAAAGAACACCGATCTTGAGGCTCT C
Dk/Tripura M1-G230A (aa 37) REV	GTGAATACAAATCCCAAAATCCCTTTAGTCAAAGG TGACAGG
Dk/Tripura M1-G298T (aa 59) FWD	CCTGTCACCTTTGACTAAAGGGATTTTGGGATTT GTATTCAC
Dk/Tripura M1-G298T (aa 59) REV	GTGAATACAAATCCCAAAATCCCTTTAGTCAAAGG TGACAGG
Dk/Tripura M1-G734A (aa 205) FWD	TAGCCTGATTAGCGATCTCCATGGCTTCCGC
Dk/Tripura M1-G734A (aa 205) REV	GCGGAAGCCATGGAGATCGCTAATCAGGCTA
Ck/Penn/1 M1-T550C (aa 169) FWD	GCCTGATTAGTGGGTTGGTTGTTGTCACCATCTG T
Ck/Penn/1 M1-T550C (aa 169) REV	ACAGATGGTGACAACAACCAACCCACTAATCAGG C
Ck/Penn/1370 M1-C659T (aa 169) FWD	GCCTGATTAGTGGGTTGATTGTTGTCACCATCTG T

Ck/Penn/1370 M1-C659T (aa 169) REV	ACAGATGGTGACAACAATCAACCCACTAATCAGGC
Ck/Italy M1-A725C (aa 234) FWD	GTGCCGGTCTGAAAGATGATCTTCTTGAAAATTTGCAGG
Ck/Italy M1-A725C (aa 234) REV	CCTGCAAATTTTCAAGAAGATCATCTTTCAGACCGGCAC
Dk/Netherlands M1-C700A (aa 234) FWD	GTGCCGGTCTGAAAGATGATCTTATTGAAAATTTGCAGG
Dk/Netherlands M1-C700A (aa 234) REV	CCTGCAAATTTTCAATAAGATCATCTTTCAGACCGGCAC
Ck/Pakistan M1-A700C (aa 234) FWD	CTCAAGTGCAGGTCTAAAAGATGATCTTCTTGAAAATTTGCAGGC
Ck/Pakistan M1-A700C (aa 234) REV	GCCTGCAAATTTTCAAGAAGATCATCTTTTAGACCTGCACTTGAG

Table 7.7 Primer and probe for RT-qPCR.

Target gene	Sequence (5' to 3')	Probe
IAV M FWD	AGATGAGTCTTCTAACCGAGGTCG	(FAM)TCAGGCCCCCTCAAAGCCGA(TAMRA)

Table 7.8 Primers for cloning avian segment 7s into pDUAL.

Strain	Primer	Sequence (5' to 3')
Ck/Italy	pDUAL + BsmBI site FWD	GTATCGTCTCTGGGGAGCAAAAGCAGGTAGA
	pDUAL + BsmBI site REV	GCGGCGTCTCTTTATTAGTAGAAACAAGGTAGT
Ck/Zhejiang	pDUAL + BsmBI site FWD	GTATCGTCTCTGGGGAGCAAAAGCAGGTAGA
	pDUAL + BsmBI site REV	GCGGCGTCTCTTTATTAGTAGAAACAAGCTATT

Dk/Mongolia	pDUAL + BsmBI site FWD	GTATCGTCTCTGGGGAGCGAAAGCAGGTAGA
	pDUAL + BsmBI site REV	GCGGCGTCTCTTATTAGTAGAAACAGGTAGTT

In blue is represented the BsmBI recognition site with a few nucleotides (underlined) as a spacer since the enzyme cuts upstream of the recognition site. In purple is represented the 5' and 3' UTR of the segment 7s. The nucleotides before the indicated in blue correspond to pDUAL sequences.

7.1.3. Plasmids

Table 7.9 Plasmids used throughout the study.

Name	Description	Source
pDUAL	Reverse genetics plasmid system. RNA pol I and pol II promoters on either side of the insert for mRNA and vRNA-like synthesis.	Prof Ron Fouchier (Erasmus University Medical centre, Rotterdam, Netherlands)
pHH21	Reverse genetics plasmid with a pol I promoter for the synthesis of vRNA-like.	Prof Robert Lamb (Department of Molecular Biosciences, North-Western)
pcDNA 3.1	CMV pol II promoter upstream of the insert for constitutive protein expression.	Invitrogen
pCAGGS	AG promoter (chicken β-actin linked to rabbit β globin) with a CMV enhancer, rabbit globin polyadenylation site and terminator for constitutive protein expression.	Prof Munir Iqbal (The Pirbright Institute, Surrey, UK)
pPol I Luc	Reporter for minigenome reconstitution assays. Contains firefly luciferase reporter gene under the control of pPol I promotor. It is in the reverse orientation flanked by UTRs of PR8 segment 8.	Dr Laurence Tiley (University of Cambridge, Department of Veterinary medicine, Cambridge)

7.1.4. Viruses and reverse genetics system

7.1.4.1. A/Puerto Rico/8/1934 (H1N1)

Table 7.10 Reverse genetics system for PR8.

Plasmid backbone	Segment	Accession number	Reference/Source
pDUAL	PB2	EF467818	(de Wit et al., 2004) Kindly provided by Prof Ron Fouchier (Erasmus University Medical centre, Rotterdam, Netherlands).
	PB1	EF467819	
	PA	EF467820	
	HA	EF467821	
	NP	EF467822	
	NA	EF467823	
	M	EF467824	
	NS	EF467817	

Table 7.11 Avian strains from which segment 7s were used in this study.

Strain	Origin of segment 7 (source and citation)	Accession no.
A/duck/Korea/GJ54/2004	Synthesised from NCBI sequence	GU351861
A/duck/India/02CA10/2011	Provided by Drs Ashwin Raut and Anika Mishra, ICAR, India (Kumar et al., 2017)	CY089416
A/duck/Tripura/103597/2008	Provided by Drs Ashwin Raut and Anika Mishra, ICAR, India (Kumar et al., 2017)	GU252825
A/duck/Shandong/Q1/2013	Synthesised from NCBI sequence	KM504104
A/duck/Dongguan/2685/2013	Synthesised from NCBI sequence	KP285008
A/Duck/Shantou/1588/2000	Synthesised from NCBI sequence	AF523499
A/chicken/Pakistan/UDL-01/2008	Provided by Prof Munir Iqbal, The Pirbright Institute (Iqbal et al., 2013)	CY038461
A/Zhejiang/DTID-ZJU01/2013	Provided by Prof Chen Honglin, The University of Hong Kong	KC885959

A/chicken/Italy/1067/1999	Provided by Prof Lonneke Vervelde, The Roslin Institute, University of Edinburgh (Molesti et al., 2013)	AJ416630
A/duck/Mongolia/200/2015	Provided by Prof Pablo Murcia, Centre for Virus Research, Glasgow	-
A/mallard/Netherlands/10-Cam/1999	Provided by Prof Laurence Tiley, University of Cambridge (Bourret et al., 2013)	KC209518
A/mallard/Wisconsin/1719/1983	Synthesised from NCBI sequence	CY179300
A/mallard/New York/170/1982	Synthesised from NCBI sequence	CY014902
A/chicken/Pennsylvania/1/1983	Provided by Dr Darrell kapczynski (USDA)	CY015074
A/chicken/Pennsylvania/1370/1983	Provided by Dr Darrell kapczynski (USDA)	CY015109
A/gull/Maryland/1824/1978	Synthesised from NCBI sequence	JX982948
A/turkey/South Dakota/7034/1986	Synthesised from NCBI sequence	EU743168

Table 7.12 Avian isolates used in this study.

Strain	Source
A/duck/England/1962	Prof Wendy Barclay, University College London, UK
A/duck/Singapore/5/1997	Prof Lonneke Vervelde, The Roslin Institute, University of Edinburgh
A/chicken/Israel/215/2007	Prof Lonneke Vervelde, The Roslin Institute, University of Edinburgh (Wang et al., 2016)
A/chicken/Saudi Arabia/SP02525/3AAV/2000	Prof Lonneke Vervelde, The Roslin Institute, University of Edinburgh (de Geus et al., 2011)
A/chicken/Italy/1067/1999	Prof Lonneke Vervelde, The Roslin Institute, University of Edinburgh (Molesti et al., 2013)
A/turkey/Canada/1965	Prof Wendy Barclay, University College London, UK

7.1.4.2. A/Udorn/1972 (H3N2)

Table 7.13 Reverse genetics system for Udorn.

Plasmid backbone	Segment	Accession number	Reference/Source
pcDNA 3.1	PB2	CY009643	(Chen et al., 2007) Kindly provided by Prof Robert Lamb (The Northwestern University, USA)
	PB1	CY009642	
	PA	CY009641	
	NP	CY009639	
pHH21	PB2	CY009643	
	PB1	CY009642	
	PA	CY009641	
	HA	CY009636	
	NP	CY009639	
	NA	CY009638	
	M	CY009637	
	NS	CY009640	

7.1.4.3. A/mallard/Netherlands/10-Cam/1999 (H1N1)

Table 7.14 Reverse genetics system for Dk/Netherlands.

Plasmid backbone	Segment	Accession number	Reference/Source
pDUAL	PB2	KC209512	(Bourret et al., 2013) Kindly provided by Prof. Laurence Tiley (Universty of Cambridge, UK)
	PB1	KC209513	
	PA	KC209514	
	HA	KC209515	
	NP	KC209516	
	NA	KC209517	
	M	KC209518	
	NS	KC209519	

7.1.4.4. A/chicken/Pakistan/UDL-01/2008 (H9N2)

Table 7.15 Reverse genetics system for Ck/Pakistan.

Plasmid backbone	Segment	Accession number	Reference/Source
pCAGGs	PB1	CY038456	(Iqbal et al., 2013) Kindly provided by Prof Munir Iqbal (The Pirbright Institute)
pDUAL	PB2	CY038455	
	PB1	CY038456	
	PA	CY038457	
	HA	CY038458	
	NP	CY038459	
	NA	CY038460	
	M	CY038461	
	NS	CY038462	

7.1.5. Eukaryotic cells

Table 7.16 Eukaryotic cell lines.

Cell	Description	Source
MDCK	Madin-Darby Canine kidney cells	Prof Bernadette Dutia, The Roslin Institute
293T	Human embryonic kidney cells	ATCC
QT-35	Japanese quail fibrosarcoma cells	Dr Laurence Tiley, University of Cambridge
DF-1	Chicken fibroblast cells	Dr Lita Murphy, The Roslin Institute
CEF	Chicken embryo fibroblasts	Prepared as detailed in 7.2.1.1
CKC	Chicken kidney cells	Dr Inga Dry, The Roslin Institute
DEF	Duck embryo fibroblasts	Dr Janet Daly, The University of Nottingham

7.1.6. Bacterial culture

Table 7.17 Bacterial culture media.

Medium name	Composition	Source
Luria Broth (LB)	10 g/L tryptone, 5 g/L yeast extract, 5 g/L NaCl (pH 7.0)	Central Service Unit (CSU) at the Roslin Institute
LB agar	15 g/L agar, 10 g/L tryptone, 5 g/L yeast extract, 10 g/L NaCl (pH 7.0)	CSU
CCMB	10 mM potassium acetate (pH 7.0), 10% Glycerol (w/v), 80 mM $CaCl_2.2H_2O$, 20 mM $MnCl_2.4H_2O$, 10 mM $MgCl_2.6H_2O$	Made as necessary with communal laboratory reagents generally provided by Sigma
Super Optimal Broth (SOB)	5 g/L yeast extract, 20 g/L tryptone, 0.5 g/L NaCl, 2.5 mM KCl, 10 mM $MgCl_2$, 10 mM $MgSO_4$	CSU

7.2. Methods

7.2.1. Cell culture

MDCK, 293T, QT-35 and DF-1 cells (Table 7.16) were passaged and maintained in Dulbecco's Modified Eagle's Medium (DMEM, GIBCO), supplemented with 10% (v/v) Foetal Bovine Serum (FBS), 200 mM L-Glutamine (Life technologies), penicillin and streptomycin both at 100 U/ml (Life technologies), also referred to as complete DMEM, in tissue culture flasks (Corning, USA). Before passaging, cells were detached from the flask using 0.25% trypsin-EDTA solution (Life Technologies) for 5 to 15 min, resuspended 1:10 to 1:20 in complete DMEM and left to incubate at 37°C, 5% CO_2.

7.2.1.1. Isolation of CEF cells

CEF cells were prepared from 10-day old embryonated hens' eggs (Henry Stewart and Co Ltd, UK). Embryos were killed by membrane disruption, removed from the egg and placed in a petri dish with sterile PBS for confirmation of death by decapitation. The head and viscera were removed and the bodies washed at least twice in PBS (138 mM NaCl, 2.7 mM KCl, 8 mM Na_2HPO_4, pH 6.7). The bodies were then chopped up using a sterile scalpel and scissors, passed through a 20 ml syringe (Fisher scientific) and loaded onto a 50 ml centrifuge tube (VWR). This was followed by at least three washes in PBS or until bodies were well homogenised using serially smaller syringes (ending with 10 ml ones). Between each wash, the cells were spun at 1500 rpm for 5 min and the supernatant discarded. Following this, 0.25% trypsin-EDTA solution was added to the homogenate (5 ml per embryo) and left to incubate for 30 min at 37°C, 5% CO_2. This solution was filtered with a small metal mesh filter and pelleted at 1500 rpm for 10 min. To the solid parts, it was added more 0.25% trypsin-EDTA solution and left to incubate as before. The supernatants recovered after these steps were passed through a 100 µm nylon filter and pelleted at 1500 rpm for 10 min. This step was repeated until no cells were recovered. The resulting cells were resuspended in 1 ml of M199 (Sigma) supplemented with 4% FBS and penicillin and streptomycin (Pen/Strep) both at 100 U/ml. The cells were then counted and seeded at a density of $1x10^6$ cells/ml and incubated until confluency. Once this point was reached, cells were washed twice in PBS and dissociated using 0.25% trypsin-EDTA:HBSS (1:4). Medium as described above was added to neutralise the trypsin and cells were spun at 1500 rpm for 5 min. Following this, cells were resuspended in 6 ml (for a confluent T175 flask) of freezing medium (containing 10% DMSO and M199 supplemented as before) and stored at -120ºC. When needed, cells were revived in M199 supplemented with 10% FBS and penicillin and streptomycin (Pen/Strep) both at 100 U/ml, followed by passage in M199 supplemented with 7% FBS also with Pen/Strep and kept in M199 supplemented with 4% FBS containing Pen/Strep. Between each passage, cells were washed and trypsinized as described before.

7.2.1.2. Culture of other primary cell types

CKC cells were maintained in Eagle's Minimum Essential Media (EMEM) (Sigma), supplemented with 10% (v/v) FBS, 10% (v/v) tryptose phosphate broth and penicillin and streptomycin both at 100 U/ml. CEF cells were maintained in M199, supplemented with 4% (v/v) FBS, 200mM L-Glutamine, penicillin and streptomycin both at 100 U/ml. DEF cells were maintained in DMEM, supplemented with 10% (v/v) FBS, 200 mM L-Glutamine, penicillin and streptomycin both at 100 U/ml. DEF cells were kept at 37°C and CKC cells at 38°C, both with 5% CO_2. When the cells were confluent, the media was removed, the cell monolayer washed with PBS and trypsin-EDTA solution was added to the flasks and incubated at 37°C. When the monolayer started to detach, the cells were resuspended in complete medium and counted when necessary to seed in fresh flasks, multi-well plates or coverslips at the appropriate density.

7.2.2. Molecular techniques

7.2.2.1. Preparation of competent DH5α bacterial cells

Stocks of *Escherichia coli* bacteria (strain DH5α) were used to produce competent cells. Briefly, at least 10 µl of a starter culture was propagated overnight in 5 ml of SOB medium at 37ºC on an orbital shaker. The next day, the culture was diluted 1:100 in 60 ml of SOB and incubated at 37ºC for 3 h on an orbital shaker until the optical density at 550 nm (OD_{550}) was approximately 0.3. Spectrophotometry was performed using 1 ml of the bacterial culture using blank SOB medium only as a reference. For the first two hours, the OD_{550} was measured once every hour, however in the last hour measurements were taken every 15-30 min. Once the desired OD_{550} was reached, the bacteria were incubated on ice for 10 min followed by centrifugation at 3000 rpm at 4ºC for 10 min. The supernatant was removed and the pellet resuspended in 0.25X of the starting volume (15 ml) of cold CCMB media and left on ice for 4 h. Bacteria were pelleted as before, resuspended in 1/12th of the starting volume (5 ml) of cold CCMB medium, and100 µl aliquots snap frozen on dry ice and stored at -80ºC.

7.2.2.4. Preparation of agar plates

Briefly, 250 ml of LB agar (Table 7.17) was heated in a microwave or boiling water bath until all agar had dissolved. The LB agar was left for a minimum of 30 min at room temperature to cool before the appropriate selection antibiotic was added and the solution mixed. The liquid LB agar was poured into 100 mm x 20 mm petri dishes on a clean bench under the flame of a Bunsen burner. The agar plates were then left at room temperature for a minimum of 1 h to set and stored at 4ºC until further use.

7.2.2.3. Transformation of competent DH5α bacterial cells

The competent DH5α *E. coli* cells prepared before were used to amplify plasmid DNA. The bacterial cells (10-20 µl) were transformed with 20 to 50 ng of the plasmid DNA or mock-transformed with Milli-Q water. This bacteria-DNA mixture was gently mixed and left on ice for a maximum of 30 min. Transformation was then performed by a 45 sec to 1 min heat shock at 42ºC immediately followed by 5 min incubation on ice. After incubation, 750 µl of LB was added and the cells were placed in a shaker (180-200 rpm) for 1 h at 37ºC to recover. 100 µl of bacterial cells were spread onto agar plates containing the appropriate antibiotic using a sterile spreader whilst working under a flame. Agar plates were incubated in an inverted position overnight at 37ºC. The remaining volume of the transformation reaction was stored at 4ºC until confirmation of successfully transformed colonies along with the absence of colonies in the water-transformed bacteria under antibiotic selection. To amplify plasmid DNA from the transformed bacteria, single colonies were picked with a P200 tip and incubated in 5 ml of LB (mini-prep) or 50-100 ml of LB (midi-prep) with antibiotic selection at 37ºC in a shaker. Following overnight incubation, the bacterial cells were pelleted at 4300 rpm at 4ºC for 15 min and the supernatant discarded. Cells were then used to prepare the plasmid DNA or stored at -20ºC.

7.2.2.4. Preparation of plasmid DNA

Small preparations of plasmid DNA were isolated from overnight *E. coli* cultures using a QIAprep miniprep kit (Qiagen), while larger preparations used a QIAprep midiprep kit, as per

the manufacturer's instructions. DNA was dissolved in Milli-Q water and the final concentration was determined by measuring the absorbance at 260 nm using a NanoDrop spectrophotometer. Plasmid integrity was also checked by agarose gel electrophoresis.

7.2.2.5. Isolation of total RNA from allantoic fluid, cells, tissues and swabs

RNA was extracted from virus-containing allantoic fluid of chicken eggs with average titres between $1x10^5$ and $1x10^9$ PFU/ml and cell culture supernatants with a minimum titre of $1x10^4$ PFU/ml. Extractions were performed using a QIAmp viral RNA mini kit (Qiagen), following the manufacturer's instructions. Isolated RNA was dissolved in 30µl of Milli-Q water and quantified using a NanoDrop spectrophotometer.

The chicken tissues collected (described in 7.7.5) were dissected using a sterile scalpel and scissors into appropriate size sections and added to safe-lock microcentrifuge tubes (Fisher scientific) with 700 µl of TRizol reagent (Life technologies) and one 5 mm stainless steel bead (Qiagen). The tissue was then homogenised in a TissueLyser II (Qiagen) for 4 to 12 min at 25 Hz. Following this, 300 µl of chloroform (Sigma) was mixed with the homogenate followed by centrifugation at 13,000 for 30 min at 4ºC. The upper aqueous phase was carefully collected, mixed with one volume of 70 % ethanol (typically 200 µl) and the RNA extracted using an RNeasy mini kit (Qiagen) according to the manufacturer's instructions. Total RNA was extracted from buccal swab samples collected at days 8 and 10 p.i... Briefly, 100 µl of sample was mixed with 100 µl of acidic phenol:chloroform (Thermo Scientific) and vortexed vigorously for 5 sec. The mix was separated by centrifugation at 14,000 rpm for 5 min at 4ºC and the upper aqueous phase was transferred to a new tube. Another 100 µl of acidic phenol:chloroform was added and processed as before. Following this, the aqueous phase was collected and mixed with 1 µl of 3M sodium acetate (Invitrogen) and 250 µl of ice-cold 100% ethanol (EtOH) (Sigma). This mix was incubated at -20ºC for 20 min and spun at 14,000 rpm for 20 min at 4ºC. The supernatant was removed and the pellet washed with 500 µl of ice-cold 70% EtOH before re-pelleted by centrifugation at 14,000 rpm for 10 min at 4ºC. The supernatant was removed and the RNA resuspended in 20 µl of nuclease free water and stored at -80ºC.

7.2.2.6 Reverse transcription (RT)

Single-stranded cDNA was generated from IAV vRNA using a Verso cDNA synthesis kit (Thermo Scientific) and the Uni12 primer (Table 7.5), which anneals to the 12 conserved nucleotides present on the 3' end of all IAV negative sense segments. Each RT reaction contained 1 µg of vRNA, 0.5 µM of Uni12 primer, 20% (v/v) cDNA synthesis buffer, 0.5 mM of each dNTP and 1 µl of reverse transcriptase up to a final volume of 20 µl. This was incubated at 65ºC for 10 min followed by 1 h at 42ºC and for RT enzyme inactivation, a step at 95ºC for 2 min was performed. No template controls (Milli-Q water) were included separately.

7.2.2.7. Polymerase chain reaction (PCR)

Amplification of IAV segment cDNAs was carried out by *Taq* DNA polymerase (Invitrogen). Forward and reverse oligonucleotides were designed to complement conserved regions of segment 7 of the viruses in study (Table 7.5). To validate the sequence of reassortant or fully avian viruses, forward and reverse primers were designed for segments 4 and 6 of A/PR/8/34 (H1N1) and A/mallard/Netherlands/10-Cam/1999 (H1N1). Each reaction contained: 5 mM of each dNTP, 1.5 mM $MgCl_2$, 10 µM each primer and 20% (v/v) of the manufacturer's 5X reaction buffer (*Taq* DNA polymerase, Invitrogen), up to a final volume of 25 µl. The cycle used was as follows: 94ºC for 2 min, followed by 30 cycles at 94ºC for 1.5 min, 55ºC for 1 min and 72ºC for 3 min, with a final step at 72ºC for 10 min.

Selected avian segment 7s (Table 2.1) were synthesised, flanked by the BsmBI (New England Biolabs) site and a few more nucleotides to stabilise the restriction enzyme near the recognition site (Table 7.8). Thereafter, the segment 7s were amplified from their original plasmid using forward and reverse primers containing the BsmBI site as seen in table 7.8. The PCR reaction was prepared as before.

7.2.2.8. Quantitative reverse transcription PCR (RT-qPCR)

Tissues collected from the *in vivo* experiment were placed in RNA later and used for RT-qPCR reactions that were performed in MicroAmp optical 96-well reaction plates (Applied

Bioscience) using a 7500 Fast & Real-Time PCR system (Applied Biosystems). Samples were loaded in technical duplicate and no reverse transcriptase and no template (nuclease free water) controls were included. The output CT values and dissociation curves were analysed using 7500 software v2.3 (Applied Biosystems), Microsoft Excel and GraphPad Prism v7.00. Quantification of vRNA was done using a SuperScript III one-step reverse transcription PCR (RT-PCR) system with platinum Taq DNA Polymerase kit (Invitrogen) following the manufacturer's instructions. Primers and a Taqman probe specific for a conserved region of IAV M1 protein were used as described previously (Spackman et al., 2002) (see table 7.7). The PCR program ran as follows: 50ºC for 5 min, 95ºC for 2 min and 40 cycles of 95ºC for 3 seconds and 60ºC for 30 seconds. For the standard curve, a T7 transcribed RNA standard of the M gene from PR8 strain was used (provided by Dr Anabel Clements). The CT values were then extrapolated against this curve and the results expressed as M gene copy numbers.

7.2.2.9. Agarose gel electrophoresis

Agarose gel electrophoresis was carried out using 0.8-2% (w/v) agarose (Sigma-Aldrich) gels depending on the size of DNA fragments to be separated, stained with SYBRSafe DNA gel stain (1:10,000) (Invitrogen). 1X DNA loading buffer (stock at 6X, New England Biolabs) was added to each sample prior to loading the gel and separation was performed at 80-100 V for 45-60 min in 1X TAE running buffer, made with 0.04 M Tris-acetate and 1 mM EDTA and supplied by the central service unit (CSU) at the Roslin Institute. All agarose gel electrophoresis was carried out in a horizontal electrophoresis tank (Bio-Rad).

7.2.2.10. Isolation of DNA fragments from agarose gels

The vector used for cloning throughout this study (pDUAL) was enzymatically cut and linearized and agarose gel electrophoresis was performed in 2% (w/v) agarose gels to ensure efficient separation of cut and uncut vector. The DNA fragments were visualized on a UV transilluminator and the fragments of interest (linearized plasmid) excised from the gel using a sterile scalpel. The agarose slices containing DNA were transferred to a 1.5 ml centrifuge tube and DNA was isolated using QIAquick gel extraction kit (Qiagen) following the manufacturer's instructions.

7.2.2.11. Purification of DNA segments

DNA inserts containing the restriction site of BsmBI derived from PCR were purified to remove salts, nucleotides, primers and enzymes using a QIAquick PCR purification kit (Qiagen) as per the manufacturer's instructions. DNA inserts were diluted in 30 µl of Milli-Q water. The vector to be used was isolated from agarose gels (see above) and purified using a QIAquick gel extraction kit (Qiagen) as per the manufacturer's instructions. Vector DNA was diluted in 50 µl of Milli-Q water.

7.2.2.12. Restriction enzyme digestion

To clone DNA segments from one plasmid to another, inserts and vector (normally pDUAL unless otherwise indicated) were digested with BsmBI (New England Biolabs) for 2 h at 55ºC. Each reaction contained 10% (v/v) of the manufacturer's 10X reaction buffer, 1-2 µg of DNA and 5-10 units of enzyme to a final volume of 50 µl in Milli-Q water. A water control was added to ensure that there was no other DNA contaminants present.

7.2.2.13. Ligation of DNA fragments

Prior to ligation, the vector DNA 5' and 3' ends were dephosphorylated to prevent self-ligation of the plasmid, using rSAP phosphatase (New England Biolabs) according to the manufacturer's instructions. Reactions with rSAP were prepared as follows: 1 µg of vector DNA, 2 µl of the 10X CutSmart buffer, 1 unit of rSAP and Milli-Q water up to a final volume of 20 µl. This reaction was incubated at room temperature for a maximum of 30 min as indicated in the protocol for ligations involving sticky ends within the vector. rSAP was then inactivated at 65ºC for 5 min.

For ligation of DNA inserts and plasmid vector, reactions were prepared with the following: 10% (v/v) of the ligation buffer (New England Biolabs), 40-50 ng of vector DNA, insert DNA (1:5 or 1:7 ratio (w/w)) and 1 µl of T4 DNA ligase in Milli-Q water to a final volume of 20 µl. The reaction was left at room temperature for between 30 min and 1 h. As a negative control, a ligation reaction was prepared containing only vector DNA. 5 µl of each ligation mix

were used to transform 25 µl of competent *E.coli*. Plasmid DNA was extracted from the resulting individual colonies as described before (section 7.3.4) and to check for the presence of DNA insert, DNA plasmids were digested for 1 h with Apa I (New England Biolabs) at 37ºC. Each reaction contained 10% (v/v) of the manufacturer's 10X reaction buffer, 1 µg of DNA and 5 U of enzyme to a final volume of 50 µl in Milli-Q water.

7.2.2.14. Sanger sequencing

Sequencing of purified DNA segments (plasmids or PCR amplicons) was performed by GATC biotech. A reaction mix was prepared as follows: 2.5 µM of the appropriate primer and 500 ng of plasmid DNA or 80 ng of PCR amplicon to a final volume of 10 µl in Milli-Q water. Sequencing results were analysed using BioEdit Sequence Alignment Editor V7.1.3.0, BLAST (https://blast.ncbi.nlm.nih.gov/Blast.cgi) to confirm the identity of the IAV segment and ExPASy (https://web.expasy.org/translate/) to determine amino acid sequence.

RNA extracted from the buccal swab samples (as described in 7.3.5) was converted to cDNA and the M segment amplified by PCR. Prior to sequencing 10 µl of the PCR product was mixed with 4 µl of ExoSap-It enzyme to digest the primers and dephosphorylate nucleotides (Life technologies), as per the manufacturer's instructions. Then, 9.5 µl of this mix with 0.5 µl of primer (at 10 µM/µl) were sent for sequencing.

7.2.2.15. SDS-PAGE and Western blotting

SDS-PAGE was performed using a resolving gel of 12% (v/v) stacked with a 4% (v/v) gel, which were prepared using reagents supplied by Protogel according to the manufacturer's instructions. All electrophoresis was performed in a Bio-Rad tank (Mini-protean tetra system) at 80 V for 30 min to cross the stacking gel, followed by 140 V for 60 min.

For western blotting analysis, SDS-PAGE gels were transferred to a 0.45 µm nitrocellulose membrane (GE healthcare) with the Trans-blot Turbo blotting system (Bio-Rad), according to the manufacturer's instructions (7 min at 25V). Following semi-dry transfer, membranes were incubated in PBS with 0.1% Tween-20 (Sigma-Aldrich) (PBST) and 5% (w/v)

dried milk (from local supermarkets) for 60 min at room temperature on a rocking platform. Primary antibody was diluted at the desired ratio (see table 7.1) in PBST with 5% (w/v) dried milk and left for 1 h at room temperature or overnight at 4ºC, with rocking. The membrane was then washed 3 times for 5 min in PBST and incubated with secondary antibody diluted (Table 7.3) in PBST with 5% (w/v) dried milk for 45-60 min at room temperature on a rocking platform. The membrane was again washed 3 times for 5 min in PBST and placed in PBS prior to imaging on an infrared scanner (LiCor).

7.2.3. Virus work

7.2.3.1. Generation of P0 stocks

Recombinant viruses were rescued using eight- or twelve-plasmid transfection systems based on the pDUAL RNA Polymerase I/II promoter vector (Tables 7.10 and 7.11). 293T cells at 70-80% confluency were transfected with 250 ng of each plasmid for each segment with 4 µl of Lipofectamine 2000 and Optimem to a final volume of 300 µl. The Lipofectamine/DNA/Optimem mix was left to incubate at room temperature for 30 min. In the meantime, complete medium was removed from the cells and 750 µl of DMEM supplemented with 10% (v/v) FBS and 200 mM L-Glutamine was added. The Lipofectamine/DNA/Optimem mix was then dripped over the cells and left overnight at 37ºC, 5% CO_2. The following day, transfection medium was replaced by 1 ml of DMEM containing 200 mM L-Glutamine, penicillin and streptomycin both at 100 U/ml, 0.14% (v/v) Bovine Serum Albumin (BSA) (Sigma) and 1 µg/ml of TPCK treated trypsin (Sigma) (Viral Growth Medium – VGM). The cells with VGM were left for 48 h at 37ºC, 5% CO_2. After that, the supernatant containing the virus was harvested and cleared by low-speed centrifugation (5 min at 1500 rpm), giving a “passage zero” (P0) viral stock. The 7:1 reassortant virus with WT segment 7 of Ck/Penn/83 was rescued once as previously described. However, the counterpart reassortant virus with a mutated M1 gene was not possible to rescue this way. Instead, co-cultures of 293T and DF-1 or QT-35 cells were used in ratios of 1:1, 1:2, 1:3 and 1:4 with the reaction mixed described before, but still with no success.

The avian 8-plasmid transfection system for A/mallard/Netherlands/10-Cam/1999 (Table 7.14) used with Lipofectamine 2000 reagent only rescued virus with low efficiency (1 in 5 attempts would be positive for viral rescue). Therefore, the transfection reagent XFect (Takara) and higher amounts of the reverse genetics plasmids were used. Briefly, 625 ng of each plasmid of the 8 plasmids was added to 80 µl of XFect reaction buffer and 1.5 µl of XFect polymer solution to a total of 100 µl. Following a 10 sec vortex, this mix was left to incubate at room temperature for 30 min before being dripped over 70-80% confluent 293T cells and left overnight at 37°C, 5% CO_2. The following day, the medium was replaced by 1 ml of VGM and the cells were left for 48 h at 37°C, 5% CO_2. The supernatant was harvested as described before. Xfect provided a 1:1 ratio of positive viral rescues for A/mallard/Netherlands/10-Cam/1999. However, this methodology did not work for other hard-to-rescue viruses such as the PR8-based 7:1 reassortant virus with segment 7 of Ck/Penn/1.

7.2.3.2. Generation of P1 stocks

To generate P1 stocks, MDCK cells were seeded at $4x10^6$ cells/ml in T25 flasks to reach confluency the next day. Cells were washed twice with PBS, inoculated with 100 µl of the P0 stock diluted in 1 ml of serum free DMEM (see above) and incubated for 1 h at 37°C with gentle mixing every 30 min. After this, 5 ml of VGM (see above) was added and the cells were once again incubated at 37°C for 48 h or until CPE was observed by comparison with cells inoculated with supernatants from mock transfected cells (Lipofectamine only control) or cells transfected with 7 instead of 8 RG plasmids (*e.g.* lacking PB1 segment). Following this, the supernatant of the cells was harvested and spun at 4500 rpm for 5 min at 4°C, aliquoted in 200-500 µl aliquots and stored at -80°C until further use. For attempted rescues of the PR8-based Ck/Penn/1 WT or M1-mutant viruses, 1 ml of the P0 stock (neat) was used to inoculate MDCK cells but with no success. Another method tried was to scrape off the 293T cells along with the supernatant (P0 stock) from the 6-well plate using a P1000 pipette and inoculate this in a suspension of MDCK cells in a T25 flask; however this proved not to be fruitful either.

7.2.3.3. Minigenome reconstitution assays

To determine if the failed rescues of Ck/Penn/1 were due to incompatibility of the avian segment 7 with the PR8 polymerase, minigenome reconstitution assays were performed with the polymerase, NP and NS segments of PR8 and the WT or mutated segment 7 of Ck/Penn/1. NS segment was added because it was reported to aid in the nuclear export of M segment mRNA (Pereira et al., 2017). In this instance, NS1 was tagged with GFP for easier distinction between this protein and M1 by western blotting (Pereira et al., 2017). To reach approximately 80-90% confluency on the day of use, 293T cells were seeded at $2x10^5$ cells per well of a 24-well plate. The following day, 50 ng of the plasmids mentioned above and 20 ng of the firefly reporter plasmid (pPol I luciferase) were diluted in 50 µl of Opti-MEM (GIBCO). Per reaction, 1 µl of Lipofectamine 2000 was added to 50 µl of Opti-MEM and left at room temperature for 5-10 min. This last mixture was added to the plasmid-Opti-MEM solution and incubated at room temperature for a minimum of 30 min. At this point, the complete DMEM of 293T cells was removed and 500 µl of Opti-MEM was added per well. Following the incubation period, the transfection mix was dripped over the 293T cells and these were incubated for 48 h at 37ºC, 5% CO_2. Next, the medium was removed and the cells lysed with 120 µl of 1X reporter lysis buffer (Promega). Following scraping and mixing of the cells, the lysates were pelleted at 13,000 rpm for 2 min at 4ºC and the supernatants collected into new tubes and placed on ice. 60 µl of the cell lysate was added to a white-bottom 96-well plate (Corning) and kept on ice. To add the luciferase substrate, the promega GloMax multi detection reader was used to infect 25 µl of 0.6 mM beetle luciferin (Promega) per well and to measure luciferase activity (200 µl/sec injection speed, 0.5 sec gap and 5 sec integration time). The reconstitution assay showed that the PR8 RNPs were actively transcribing the luciferase reporter gene (figure 7.1 A.)

7.2.3.4. Protein electrophoresis and western blotting analyses for the detection of M1 from Ck/Penn/1

While the luciferase expression data from the minigenome reconstitution assays proved that the system was generating active PR8 RNPs, it remained unknown at this point

whether M1 was being expressed. Therefore, aliquots of cell lysate from the reconstitution assays were analysed by western blotting (see section 7.2.2.15). Cells transfected in 24-well plates were washed once in PBS and lysed in 2X laemmli's buffer (final volume of 200 µl). The lysates were boiled at 100ºC for 10 min and 15 µl were loaded onto a polyacrylamide gel and the proteins separated as described before followed by western blotting (see section 7.2.2.15). In addition to the detection of M1 and NP viral proteins, the host protein tubulin was used as a loading control. Virus-infected cells with PR8 and mock transfected cells were used as positive and negative controls, respectively. As expected, mock-transfected cells or cells incubated only with lipofectamine and Opti-mem showed no detectable levels of the viral proteins. All cells were transfected with NP and two (2PNP) or three (3PNP) components of the RdRp. Only in the presence of 3PNP (i.e., active RNP) it was possible to detect the expression of M1 with Ck/Penn/1370 but not Ck/Penn/1 (Figure 7.1 B). NS1 expression was detected in all 3PNP transfected cells, thus the lack of M1 expression was not due to the lack of NS1 (data not shown). Therefore, these results suggest that the segment 7 of Ck/Penn/1 might be incompatible with the PR8 RdRp, but Ck/Penn/1 was not available to use. This may explain the difficulty in rescuing Ck/Penn/1 7:1 in a PR8 backbone and the unsuccessful tries at rescuing Ck/Penn/1 M1 mutant virus.

7.2.3.5. Generation of mutant viruses by site-directed mutagenesis of RG plasmids

Specific segment 7s were mutated with the primers indicated in table 7.6. Mutagenesis was performed using the QuickChange lightning site-directed mutagenesis kit as per the manufacturer's instructions (Agilent technologies). The PCR to introduce point mutations on the specific segment 7s contained: 2.5 µl of the kit's Ta10X reaction buffer, 30 ng of plasmid DNA (with segment 7 inserted), 62.5 ng of each forward and reverse primer, 0.5 µl of dNTP mix, 0.5 µl of *Pfu Turbo* DNA polymerase and the appropriate volume of Milli-Q water to make up to 25 µl of reaction. After the PCR reaction, DpnI enzyme was added (10 U/reaction) to digest methylated parental DNA that did not possess the desired mutation. Next, 5 µl of the PCR reactions were used to transform XL-10 gold competent *E. coli* bacterial cells with a heat shock at 42ºC for 30 sec. Bacterial cells were left to recover for 1 h in 500 µl of SOB medium complemented with 20 mM of glucose (CSU) at 37ºC in an orbital shaker.

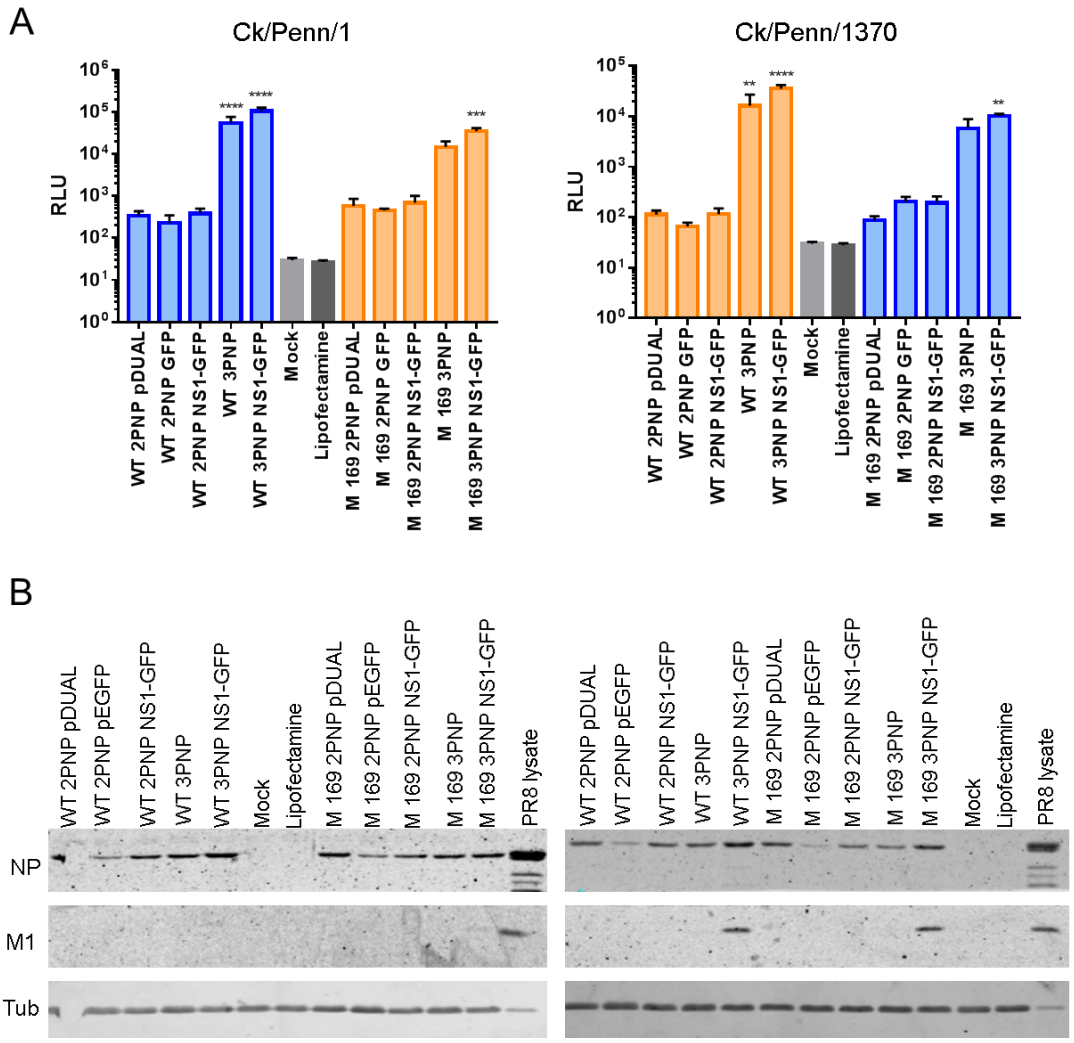

Figure 7.1 Minigenome reconstitution assay with Ck/Penn/1 and Ck/Penn/1370 M segment and PR8 RNP. (A) Minigenome reconstitution assays were performed in 293T cells transfected with 50 ng of the indicated plasmids and 20 ng of luciferase plasmid reporter. Cells were lysed at 48 h post transfection. Luciferin was added and relative light units (RLU) were measured. One way ANOVA analysis was performed to compare all samples to mock-transfected cells. Data represent mean +/- SD (n = 2 biological replicates with 2 technical replicates each). ** $p < 0.01$; *** $p < 0.001$; **** $p < 0.0001$. Spherical viruses are represented in blue and filamentous in orange. (B) WB analysis was performed to detect the expression of M1 from Ck/Pennsylvania segment 7s. NP expression levels were used as a positive control for the detection of viral proteins and tubulin was used as a loading control. A sample of PR8-infected lysed cells was also included as a positive control for the detection of M1. All cells were transfected with PB2, PA and NP (2PNP) and PB1 (3PNP). WT indicates WT segment 7 of Ck/Penn/1 or Ck/Penn/1370, while M1 169 represents the mutant segment 7 of these strains.

Following recovery, the bacterial cells were spun for 1 min at 8,000 rpm and resuspended in 100 µl of the medium, which were used to plate the bacteria into LB agar plates with ampicillin selection overnight at 37ºC in an inverted position. A minimum of 5 colonies were picked, amplified in LB overnight and DNA plasmid extraction was performed as described before (section 7.3.1). The plasmid DNA was then used to generate P0 and P1 viral stocks with the mutated segment 7s in the PR8 or avian background as described previously.

7.2.3.6 Growth of virus in embryonated chicken eggs

P0 viral stocks were obtained as described in section 7.4.1.1 and 100 µl used to infect 10-day old embryonated chicken eggs via the allantoic fluid cavity. Eggs were incubated for 48 h at 37.5ºC with 40-50% humidity. Mock-infected eggs were inoculated with 100 µl of DMEM containing 200 mM of L-Glutamine and penicillin and streptomycin both at 100 U/ml. Infection was performed by puncturing the shell at the top of the egg and just below the line of the air sac, where inoculation was carried out. These small holes were then sealed with Scotch Magic tape and the eggs incubated as above. After infection, eggs were chilled at 4ºC overnight and the allantoic fluid harvested after disruption of the top of the shell and air sac membrane with forceps. Allantoic fluid was clarified by centrifugation at 4500 rpm for 10 minutes at 4ºC and this P1 stock was stored at -80ºC until further use.

7.2.3.7. Haemagglutination assays (HA spot)

To confirm the presence of virus in allantoic fluid from infected eggs, HA spot tests were performed. Briefly, 50 µl of allantoic fluid was mixed with 50 µl of 1% (v/v) of chicken red blood cells (TCS Biosciences) in a V-bottom 96-well plate (Fisher Scientific) and left for 30 min at room temperature. A sample with PBS and blood mixed at a 1:1 ratio was added to check blood cell integrity.

7.2.3.8. Haemagglutination inhibition (HAI) assays

HAI assays were performed to assess the presence of reactive antibodies against influenza virus in pre-infected chicken sera. Chicken serum (50 µl) was serially diluted in a 2-

fold dilution in a 96-well v-bottom plate and mixed with 25 µl of Ck/Pakistan and the plate incubated at 37ºC for 1 h to allow the neutralisation of the virus by the neutralising antibodies. Following this incubation, 50 µl of 1% (v/v) chicken red blood cells was added to each well and the plates incubated at room temperature for 30 to 45 min.

7.2.3.9. Quantification of viral load by plaque assay

Viral titre determination was performed on monolayers of MDCK cells, which were seeded in a 6-well plate at a density of $4x10^6$ cells per well on the day prior to infection to reach a 100% confluency the next day. On the day of infection, cells were washed once with PBS, infected with 450 µl of 10-fold dilutions (in serum free DMEM) of viral stocks (10^{-2} to 10^{-7}) and incubated for 1 h at 37ºC, 5% CO_2. Following incubation, cells were overlaid with 1:1 of VGM and 2.4% (w/v) Avicel (FMC Biopolymer) in H_2O and left for 48 h at 37ºC, 5% CO_2. Cells were then fixed with 2 ml of 10% neutralised buffered formalin (NBF) for at least 20 min and either stained with toluidine blue or immunostained for viral NP. For NP staining, cells were permeabilised with 0.2% Triton X-100 in PBS for 10 min at room temperature on a rocking platform and washed twice with PBS. Following permeabilisation, cells were incubated with rabbit anti-NP diluted 1:1000 in 2% BSA in PBS for 1 h at room temperature on a rocking platform. Cells were then washed twice with PBS and incubated with anti-rabbit-Horse Radish Peroxidase (HRP) antibody (diluted as above) for 1 h at room temperature on a rocking platform. Cells were washed three times with PBS and NP viral protein was detected with a TrueBlue kit (Kirkegaard & Perry Labs), as per the manufacturer's instructions.

Viral load quantification of the tissues collected from *in vivo* studies (section 7.2.6.4) was performed with 50 mg of tissue processed as described in 7.3.5. For this, MDCK cells were washed, infected as before but overlaid with agarose overlay medium and left for 72 h. This medium contained: 0.6% (w/v) low-melting point agarose (Oxoid), 10% (v/v) of EMEM, 0.21% (w/v) of BSA, 1 mM of L-Glutamine, 0.15% (v/v) of sodium bicarbonate (Sigma), 10 mM of HEPES (Sigma), 1X Penicillin-Streptomycin, 0.01% (v/v) Dextran DEAE (Sigma) and 2 µg/ml TPCK treated trypsin. Following 72 h, solid overlay media was removed and the cells

fixed and stained with a solution of 1:1 methanol:acetone containing crystal violet stain (Sigma).

7.2.3.10. Embryonic lethality assays

To measure embryo viability following infection, 10-day old embryonated chicken eggs were mock-infected (serum free DMEM) or infected (as described before) with increasing quantities of virus ranging from 0.001 to 1 PFU in 10-fold increments. The viruses were diluted in serum free DMEM to reach the desired PFU dose. The eggs were then incubated at 37.5ºC with 40-50% humidity and embryo viability was checked every 12 hrs by candling the eggs for at least 60 sec followed by record of embryo movement. This was performed over a period of 96 hrs and when a loss of embryo viability was detected, eggs were chilled overnight at 4ºC followed by confirmation of death by membrane disruption. Following the infection period, 1 ml of allantoic fluid from each egg was harvested and used to test for the presence of infectious virus by HA spot tests (described above).

7.2.3.11. Viral infections

The cells used for these studies were typically seeded the day prior to infection to reach approximately 70-80% confluency on the day of infection. Cells were washed once with PBS and incubated with virus stock (diluted in serum free DMEM to achieve the desired MOI) for 1 h at 37ºC, 5% CO_2.

7.2.3.12. Multicycle infections

Multicycle infections were typically performed in monolayers of cells in 12-well plates infected with 300 µl of virus stock diluted in serum free DMEM to a MOI of 0.01 and kept for 1 h at 37ºC with 5% CO_2. Following virus adsorption, the cells were overlaid with VGM and the supernatants harvested at 48 h p.i., cleared by centrifugation at 4,500 rpm for 5 min and stored at -80ºC until further use.

7.2.3.13. Single cycle infections

Single cycle infections were typically performed in monolayers of cells in 24-well plates incubated for 1 h with 200 µl of virus stock diluted in serum free medium. To test the best conditions to study the filamentous budding morphology of IAV, cells were infected at MOI of 3 for 8, 12, 16, 20 or 24 hrs at 37ºC. Representative images from each time point at different MOI are shown in figure 7.2. Based on this, infections were performed in complete DMEM at a MOI of 3 for a period of 16 h and kept at 37ºC with 5% CO_2.

7.2.4. Fluorescent imaging

7.2.4.1. Antibody staining

Virus-infected cells seeded on glass coverslips following single cycle infections were washed once in PBS and fixed in 4% formaldehyde for a maximum of 20 min at room temperature. Following fixation, cells were washed three times for 5 min each time with PBS/1% FBS on a rocking platform. For staining of cytoplasmic or nuclear proteins, cells were permeabilised for 5 min with 0.2% TX-100 in PBS, followed by PBS/1% FBS washes as described before. At this point, the primary antibody was added to the cells at the appropriate dilution (see table 7.1) for 1 h at room temperature or overnight at 4ºC on a rocking platform. Following primary antibody incubation, cells were washed three times with PBS/1% FBS as described before. The secondary antibody was then added at the appropriate dilution (see table 7.3) and the cells were kept in the dark for 45 min at room temperature on a rocking platform. The secondary antibody incubation also included DAPI (Table 7.4) to delineate nuclei. Coverslips were mounted on microscope slides using ~10 µl drops of ProLong Gold antifade reagent (Life technologies) and stored in the dark at 4ºC before imaging.

7.2.4.2. Lectin staining

Cells infected with avian IAV isolates had to be surface-stained with plant lectins, as specific antibodies were not available for all the avian HA subtypes. As before, following single

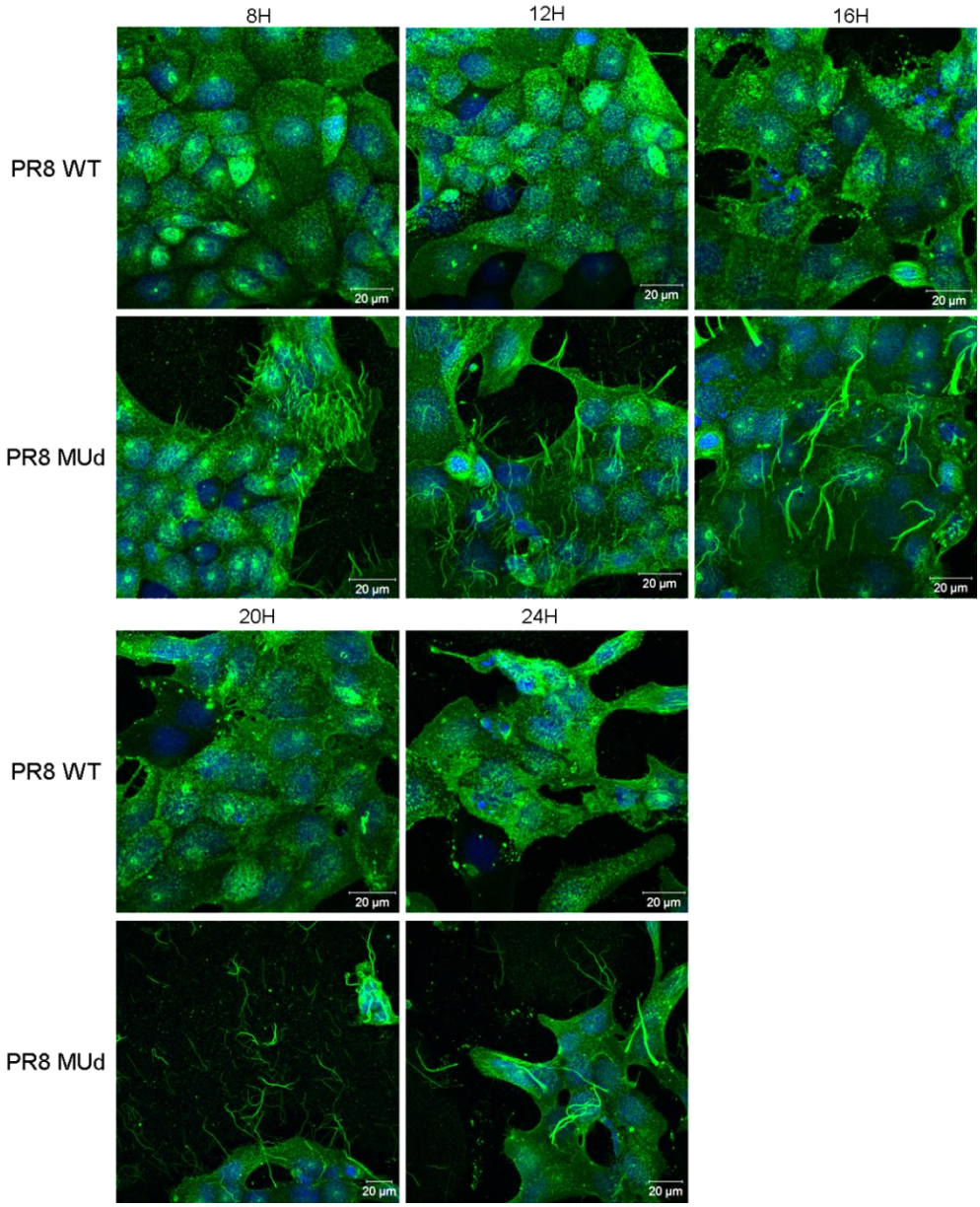

Figure 7.2 IF assays at different time points. MDCK cells were infected with PR8 WT or PR8 MUd at MOI of 3 and fixed at the times indicated. Cells were stained with antibody against whole PR8 virus that on unpermeabilised cells mainly detects HA (green) and DAPI for nuclei (blue). At 8 h and 12 h p.i., filamentous bundles were just starting to appear on the surface of the cells, whereas at 16 h p.i. it seemed that the bundles had reached a maximum length. At 20h and 24h p.i. it was possible to see bundles of filaments detaching from the cells. It was also noted that at 20 and 24 h p.i. the cells started to round up and detach, especially with PR8 WT-infected cells. Therefore, MOI of 3 at 16 h p.i. was selected for use throughout the study. Scale bar (20 µm) indicated. Z-stack images were collected using a LSM710 confocal microscope and maximum intensity projections are represented.

cycle infection, cells were washed once with PBS and fixed with 4% formaldehyde for a maximum of 20 min at room temperature. Cells were then washed three times with PBS, 5 min each, on a rocking platform at room temperature. Lectin was added (see table 7.2) for 1 h at room temperature on a rocking platform. Three 5 min washes with PBS were then performed and the avidin-FITC complex was added to biotin-conjugated lectins (Table 7.3) along with DAPI (Table 7.4) and left at room temperature for 45 min on a rocking platform. Following this incubation, cells were washed in PBS as before and mounted on microscope slides as previously.

7.2.4.3. Imaging

Once the cells in glass coverslips were mounted and dried on microscope slides, these were imaged on a LEICA DMLB epifluorescence microscope (using 20X or 40X lenses) or a Zeiss LSM710 confocal microscope (40X or 63X lenses). These images were collected as stacking files and tif files. The stacking files were further processed in ImageJ. For the confocal microscope, all the images presented in this study are maximum intensity projections of Z-stacks taken across the depth of the plasma membrane at approximately 0.30-0.45 µm increments. The excitation wavelengths typically used were410-467 m for cells stained with 488-Alexa fluorophore and 493-586 m for the detection of DAPI staining. The
pinhole size was of 51 µm for the detection of 493-586 m wavelengths and of 41 µm for wavelengths within 410-467 m. The scanning was done in frame mode with an average of 0.03 ms per line, 0.64 µs per pixel and 1.56 sec per frame with a kalman averaging of two to improve signal to noise ratio and prevent bleaching of the sample. The image size was of 1024x1024 pixels with an 8-bit depth. The scanner zoom was generally kept at 1 in the x and y axis. Images were then processed in the ZEN software black edition (Zeiss).

7.2.5. Study of *in ovo* pathology

To study the gross and tissue pathology of virus- or mock-infected chicken embryos, these were killed by membrane disruption followed by decapitation. For photographic record, the embryos were pulled from the egg and placed in a petri dish with PBS. Embryos were photographed along with a ruler for scale purposes, on the day of harvesting. Following this, embryos were decapitated with a scalpel and placed in 10% neutralised buffered formalin (NBF) for a minimum of 24 h. Embryos to be stained for H&E were sent to the pathology department at the Royal (Dick) School of Veterinary Studies at the Easter Bush Campus in Edinburgh, where they were paraffin-embedded, sectioned and stained for H&E.

Embryos to be used for titre determination were killed as described above and washed in PBS twice. Embryos were macerated through a 50 ml syringe and then through a 20 ml syringe inside a 50 ml falcon tube which contained 2 ml of serum free DMEM. This homogenate was vortexed for 30 sec to 1 min and centrifuged at 4500 rpm for 10 min at 4ºC to remove the solid debris. 1 ml aliquots were harvested and stored at -80ºC until further use.

7.2.6. *In vivo* experiments

7.2.6.1. Ethics statement

All animal procedures were performed as instructed by the United Kingdom Home Office Guidelines under the Animals (Scientific procedures) Act 1986, and the protocols approved by the Home Office of the United Kingdom. All chicken experimentation was carried out under an approved project license (Numbers: P68D44CF4X and PPL3002952) and by licensed personnel. Individual studies were performed after a study request protocol had been submitted to and approved by the Pirbright Institute Animal Welfare and Ethics Review Board.

7.2.6.2. Biosecurity

All chicken animal work with IAV was performed in self-contained BioFlex B50 Rigid Body Poultry isolators (Bell Isolation systems) at the Pirbright Institute Containment level 2 + facility.

7.2.6.3. *In vivo* viral infections

Mixed sex 3-week old specific pathogen free Rhode Island Red chickens bred at the Pirbright Institute poultry production unit were used. Pre-infection sera were obtained from all chickens and were all negative for antibodies reactive against A/chicken/Pakistan/UDL-01/2008 through HAI assays performed by Dr Jean-Remy Sadeyen (data not shown). Chickens were separated into groups: Mock, WT and mutant. The WT and mutant groups were housed in self-contained poultry isolators, while the mock group was kept in the Pen floor. Chickens were infected with 50 µl per nostril of 10^5 PFU/ml of virus or mock-infected with the same volume of PBS using a P200 Gilson pipette, performed by Dr Jean-Remy Sadeyen at the Pirbright Institute. At day 1 or 5 p.i., naïve sentinel birds were introduced into the isolators with the infected birds in order to determine if transmission occurred. At 13 days p.i., birds were humanely culled using 1 ml of pentobarbital and sera samples collected for analysis of virus specific antibodies.

All birds were tested for the presence of virus daily by swabbing both buccal and cloacal cavities with sterile polyester tipped swabs (Fisher Scientific), which were submerged in 1 ml of viral transport media (WHO, 2006), vortexed for 10 sec, clarified by centrifugation at 1500 rpm for 10 min at 4ºC, aliquoted in 400 µl aliquots and stored at -80ºC until further use.

7.2.6.4. Tissue collection

At days 3 and 13 p.i. four birds from each group (only 3 birds for WT at day 3) were humanely culled as described above and organs (nasal tissue, trachea, lungs, liver, duodenum, spleen, kidney, bursa, cecal tonsils, colon and brain) were snap frozen for infectious titre determination, for viral genome quantification by RT-qPCR of M segment in

RNA later, or were placed in 10% NBF for histopathology analysis. Where possible, the tissues were harvested from the same region (e.g. upper trachea)

7.2.6.5. Infectious virus isolation from infected tissues

At days 3 p.i., the snap frozen tissues were thawed on ice and 50 mg of each tissue was cut up using sterile scalpels and forceps. The tissue was placed in a 1.5 ml centrifuge tube with 250 µl of PBS with 1% (v/v) Pen/Strep and nystatin (Sigma) and a 5 mm stainless steel bead. The tissues were then homogenised in a tissue lyser II for 4 min at 28 Hz. The homogenate was centrifuged at 13,000 rpm for 10 min at 4ºC and the supernatant harvested and kept on ice to proceed with plaque assays for the detection of infectious virus.

7.2.6.6. Environmental sampling of food and water

Food and water samples were collected daily from the isolators with infected chickens (WT or mutant) and from the pen floor where mock-infected chickens were kept. 1.5 ml centrifuges were used to collect approximately 1 g of food and 1 ml of water. The food samples were dissolved in 1 ml of serum free DMEM and vortexed until homogeneous. The samples were centrifuged at 13,000 rpm for 20 min at 4ºC and the supernatant stored at -80ºC until further use. To the water samples, 250 µl of Pen/Strep and nystatin (100U/ml) were added and these were stored as above.

7.2.7. Bioinformatics analysis

To select the segment 7 nucleotide sequences, just over 8000 complete sequences were collected from the Influenza Research Database (www.fludb.org) on May 2016. A random subsample of 2000+ sequences was selected, aligned in MEGA6 and grouped into a phylogenetic tree with the help of Dr Sam Lycett. This tree was divided into clades based on the oldest identified branches within the tree, as it would guarantee more distinction between clades. The sequences that composed the clades were copied into an Excel spreadsheet and a random number generator was used to decide which segment 7s to synthesise.

The sequences used in figure 3.12 were collected in June 2017 from the Influenza Research Database, grouped into avian hosts using Excel and aligned with MEGA6. A script from Dr Sam Lycett was adapted to identify the amino acids present at the desired positions. Then, the amino acid prevalence overall was calculated as: $\left(\frac{\#\text{ sequences with specific amino at specific position}}{\#\text{ total sequences}}\right) \times 100$. For the amino acid prevalence within chicken and duck sequences, the denominator was replaced for the number of chicken or duck sequences.

7.2.7.1. Structural modelling

Predicted tertiary structures of M1 were obtained using the online programme I-TASSER (https://zhanglab.ccmb.med.umich.edu/I-TASSER/) (Yang et al., 2015) using the programme's default settings. All protein models were further processed using PyMOL molecular graphics system (https://pymol.org/2/).

7.2.7.2. Filamentous phenotype quantification

To quantify the filamentous budding phenotype two measurements were collected: % of infected cells producing filamentous bundles and the average length of these bundles. Virus-infected cells were imaged and a total of 6 pictures portraying different fields of view were collected per virus over a total of three independent experiments. The % of infected cells was calculated as indicated: $\frac{\#\text{ cells producing filaments}}{\#\text{ infected cells}} \times 100$. To determine the length of the filamentous bundles produced, 15 filamentous bundles were randomly selected per field of view (or picture), as illustrated in figure 7.3. These bundles were measured in ImageJ (Schneider et al., 2012) in pixels and converted to μm as indicated: $\frac{\text{bundle length (pixels)} \times \text{scale bar (μm)}}{\text{20 μm scale bar (pixels)}}$.

7.2.8. Statistical analysis

Most statistical analyses were performed in GraphPad prism v7.00 or Microsoft Excel. In chapter 3, the statistical analysis with the Fisher's exact test was performed in R, for which Dr Sam Lycett designed a script to fit the research questions of the project (see table 3.2). In chapter 5, the data from the *in vivo* studies was tested for normality in GraphPad using D'Agostino-Pearson normality test, which revealed that the data did not follow a normal distribution.

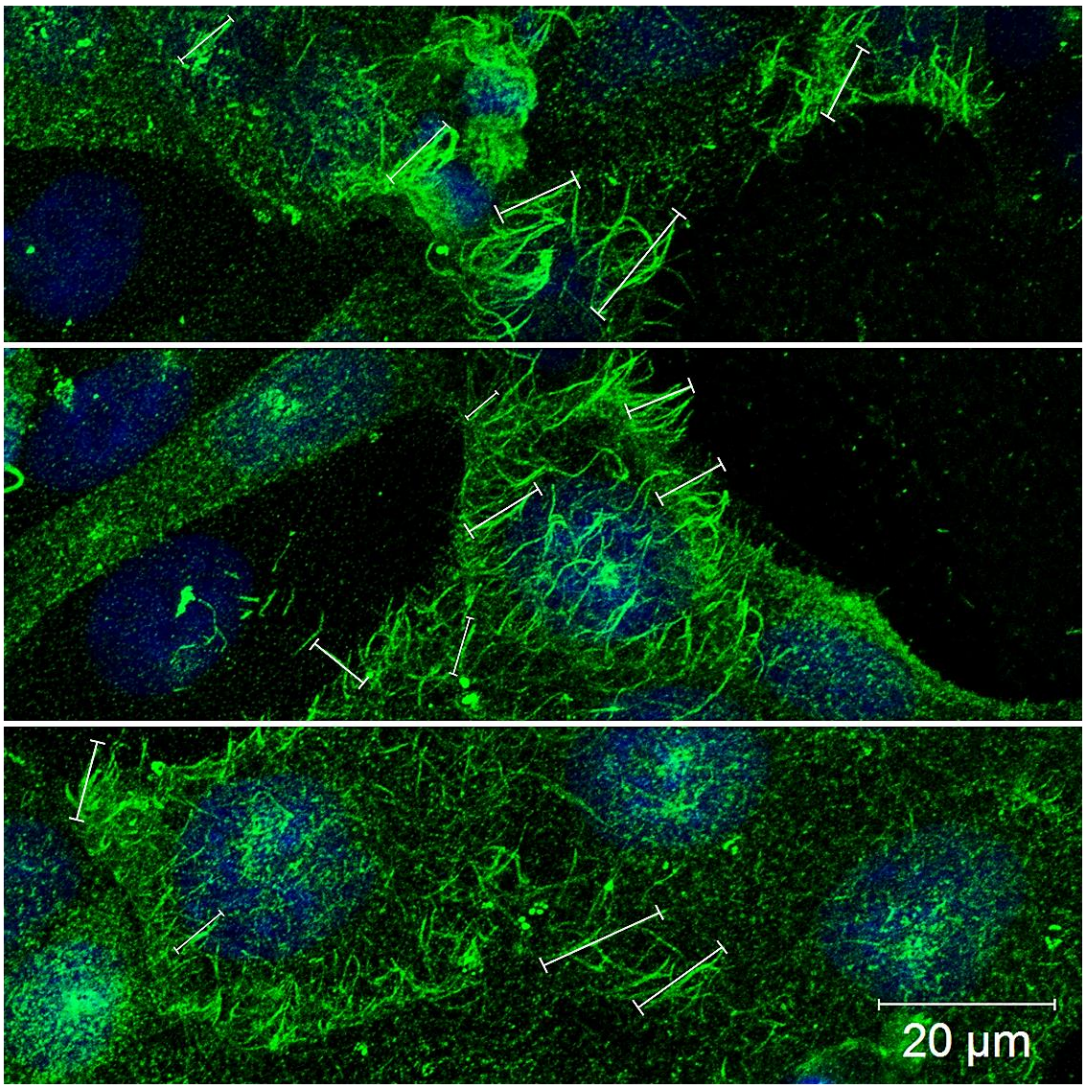

Figure 7.3 Example length measurements for filamentous bundles. MDCK cells were infected with PR8-based 7:1 reassortant virus with segment 7 from Dk/Netherlands at an MOI of 3 and fixed 16 h p.i.. Cells were stained with antibody against whole PR8 virus that mainly detects HA (green) and DAPI to delineate the nuclei (blue) before imaging by confocal microscopy. Filamentous bundles present on the surface of the cells were measured as indicated by the white scale bars. Scale bars were fitted to the image that were measured in ImageJ in pixel units, which were then used to convert the pixel size of the bundles into µm. The filamentous bundles were selected as randomly as possible to represent the overall population. Per experiment, 2 pictures were collected and used as described.

References:

Akarsu, H., Burmeister, W. P., Petosa, C., Petit, I., Muller, C. W., Ruigrok, R. W. & Baudin, F. (2003). Crystal structure of the M1 protein-binding domain of the influenza A virus nuclear export protein (NEP/NS2). EMBO J, 22(18), 4646-4655. doi:10.1093/emboj/cdg449

Alame, M. M., Massaad, E. & Zaraket, H. (2016). Peramivir: A Novel Intravenous Neuraminidase Inhibitor for Treatment of Acute Influenza Infections. Front Microbiol, 7, 450. doi:10.3389/fmicb.2016.00450

Ali, A., Avalos, R. T., Ponimaskin, E. & Nayak, D. P. (2000). Influenza virus assembly: effect of influenza virus glycoproteins on the membrane association of M1 protein. J Virol, 74(18), 8709-8719.

Al-Mubarak, F., Daly, J., Christie, D., Fountain, D. & Dunham, S. P. (2015). Identification of morphological differences between avian influenza A viruses grown in chicken and duck cells. Virus Res, 199, 9-19.

Amorim, M. J., Read, E. K., Dalton, R. M., Medcalf, L. & Digard, P. (2007). Nuclear export of influenza A virus mRNAs requires ongoing RNA polymerase II activity. Traffic, 8(1), 1-11. doi:10.1111/j.1600-0854.2006.00507.x

Andrewes & Glover. (1941). Spread of infection from the respiratory tract of the ferret. I. Transmission of influenza A virus. The British Journal of Experimental Biology, 22, 91-97.

Avalos, R. T., Yu, Z. & Nayak, D. P. (1997). Association of influenza virus NP and M1 proteins with cellular cytoskeletal elements in influenza virus-infected cells. J Virol, 71(4), 2947-2958.

Barman, S. & Nayak, D. P. (2000). Analysis of the transmembrane domain of influenza virus neuraminidase, a type II transmembrane glycoprotein, for apical sorting and raft association. J Virol, 74(14), 6538-6545.

Baudin, F., Bach, C., Cusack, S., & Ruigrok, R. W. (1994). Structure of influenza virus RNP. I. Influenza virus nucleoprotein melts secondary structure in panhandle RNA and exposes the bases to the solvent. EMBO J, 13(13), 3158-3165.

Beale, R., Wise, H., Stuart, A., Ravenhill, B. J., Digard, P. & Randow, F. (2014). A LC3-interacting motif in the influenza A virus M2 protein is required to subvert autophagy and maintain virion stability. Cell Host Microbe, 15(2), 239-247.

Beigel, J. H., Farrar, J., Han, A. M., Hayden, F. G., Hyer, R., de Jong, M. D. Writing Committee of the World Health Organization Consultation on Human Influenza, A. H. (2005). Avian influenza A (H5N1) infection in humans. N Engl J Med, 353(13), 1374-1385. doi:10.1056/NEJMra052211

Berri, F., Haffar, G., Le, V. B., Sadewasser, A., Paki, K., Lina, B., Riteau, B. (2014). Annexin V incorporated into influenza virus particles inhibits gamma interferon signaling and promotes viral replication. J Virol, 88(19), 11215-11228. doi:10.1128/JVI.01405-14

Bialas, K. M., Bussey, K. A., Stone, R. L. & Takimoto, T. (2014). Specific nucleoprotein residues affect influenza virus morphology. J Virol, 88(4), 2227-2234.

Bialas, K. M., Desmet, E. A. & Takimoto, T. (2012). Specific residues in the 2009 H1N1 swine-origin influenza matrix protein influence virion morphology and efficiency of viral spread in vitro. PLoS One, 7(11), e50595.

Blaas, D., Patzelt, E. & Kuechler, E. (1982). Identification of the cap binding protein of influenza virus. Nucleic Acids Res, 10(15), 4803-4812.

Blumenkrantz, D., Roberts, K. L., Shelton, H., Lycett, S. & Barclay, W. S. (2013). The short stalk length of highly pathogenic avian influenza H5N1 virus neuraminidase limits transmission of pandemic H1N1 virus in ferrets. J Virol, 87(19), 10539-10551. doi:10.1128/JVI.00967-13

Bouchet, J., McCaffrey, M. W., Graziani, A. & Alcover, A. (2018). The functional interplay of Rab11, FIP3 and Rho proteins on the endosomal recycling pathway controls cell shape and symmetry. Small GTPases, 9(4), 310-315. doi:10.1080/21541248.2016.1224288

Bourmakina, S. V. & Garcia-Sastre, A. (2003). Reverse genetics studies on the filamentous morphology of influenza A virus. J Gen Virol, 84(Pt 3), 517-527. doi: 10.1099/vir.0.18803-0

Bourret, V., Croville, G., Mariette, J., Klopp, C., Bouchez, O., Tiley, L. & Guerin, J. L. (2013). Whole-genome, deep pyrosequencing analysis of a duck influenza A virus evolution in swine cells. Infect Genet Evol, 18, 31-41.

Boycott, R., Klenk, H. D. & Ohuchi, M. (1994). Cell tropism of influenza virus mediated by hemagglutinin activation at the stage of virus entry. Virology, 203(2), 313-319. doi:10.1006/viro.1994.1489

Braam, J., Ulmanen, I. & Krug, R. M. (1983). Molecular model of a eucaryotic transcription complex: functions and movements of influenza P proteins during capped RNA-primed transcription. Cell, 34(2), 609-618.

Brankston, G., Gitterman, L., Hirji, Z., Lemieux, C. & Gardam, M. (2007). Transmission of influenza A in human beings. Lancet Infect Dis, 7(4), 257-265. doi:10.1016/S1473-3099(07)70029-4

Bruce, E. A., Digard, P. & Stuart, A. D. (2010). The Rab11 pathway is required for influenza A virus budding and filament formation. J Virol, 84(12), 5848-5859.

Bruce, E. A., Medcalf, L., Crump, C. M., Noton, S. L., Stuart, A. D., Wise, H. M., Elton, D., Bowers, K. & Digard, P. (2009). Budding of filamentous and non-filamentous influenza A virus occurs via a VPS4 and VPS28-independent pathway. Virology, 390(2), 268-278.

Bui, M., Whittaker, G. & Helenius, A. (1996). Effect of M1 protein and low pH on nuclear transport of influenza virus ribonucleoproteins. J Virol, 70(12), 8391-8401.

Burleigh, L. M., Calder, L. J., Skehel, J. J. & Steinhauer, D. A. (2005). Influenza A viruses with mutations in the M1 helix six domain display a wide variety of morphological phenotypes. J Virol, 79(2), 1262-1270. doi:10.1128/JVI.79.2.1262-1270.2005

Burnet, F. & Lind, P. (1957). Studies on filamentary forms of influenza virus with special reference to the use of dark-ground-microscopy. Arch. Ges. Virusforsh, 7.

Burnet, F. L., P. (1957). Studies on filamentary forms of influenza virus with special reference to the use of dark-ground-microscopy. Arch. Ges. Virusforsh, 7.

Burnet, F. M. (1941). Growth of influenza virus in the allantoic cavity of the chick embryo. Austral. J. Exp. Bio. MedSci., 19, 291. doi: 10.1038/icb.1941.44

Bussey, K. A., Desmet, E. A., Mattiacio, J. L., Hamilton, A., Bradel-Tretheway, B., Bussey, H. E. & Takimoto, T. (2011). PA residues in the 2009 H1N1 pandemic influenza virus enhance avian influenza virus polymerase activity in mammalian cells. J Virol, 85(14), 7020-7028. doi:10.1128/JVI.00522-11

Cady, S. D., Schmidt-Rohr, K., Wang, J., Soto, C. S., Degrado, W. F. & Hong, M. (2010). Structure of the amantadine binding site of influenza M2 proton channels in lipid bilayers. Nature, 463(7281), 689-692. doi:10.1038/nature08722

Calder, L. J., Wasilewski, S., Berriman, J. A. & Rosenthal, P. B. (2010). Structural organization of a filamentous influenza A virus. Proc Natl Acad Sci U S A, 107(23), 10685-10690. doi:10.1073/pnas.1002123107

Campbell, P. J., Danzy, S., Kyriakis, C. S., Deymier, M. J., Lowen, A. C. & Steel, J. (2014). The M segment of the 2009 pandemic influenza virus confers increased neuraminidase activity, filamentous morphology, and efficient contact transmissibility to A/Puerto Rico/8/1934-based reassortant viruses. J Virol, 88(7), 3802-3814.

Campbell, P. J., Kyriakis, C. S., Marshall, N., Suppiah, S., Seladi-Schulman, J., Danzy, S., Lowen, A. C. & Steel, J. (2014). Residue 41 of the Eurasian avian-like swine influenza a virus matrix protein modulates virion filament length and efficiency of contact transmission. J Virol, 88(13), 7569-7577. doi:10.1128/JVI.00119-14

Campitelli, L., Donatelli, I., Foni, E., Castrucci, M. R., Fabiani, C., Kawaoka, Y. & Webster, R. G. (1997). Continued evolution of H1N1 and H3N2 influenza viruses in pigs in Italy. Virology, 232(2), 310-318. doi:10.1006/viro.1997.8514

Cao, S., Liu, X., Yu, M., Li, J., Jia, X., Bi, Y. & Liu, W. (2012). A nuclear export signal in the matrix protein of Influenza A virus is required for efficient virus replication. J Virol, 86(9), 4883-4891. doi:10.1128/JVI.06586-11

Capua, I., & Marangon, S. (2006). Control of avian influenza in poultry. Emerg Infect Dis, 12(9), 1319-1324. doi:10.3201/eid1209.060430

Cauldwell, A. V., Long, J. S., Moncorge, O., & Barclay, W. S. (2014). Viral determinants of influenza A virus host range. J Gen Virol, 95(Pt 6), 1193-1210. doi:10.1099/vir.0.062836-0

Chan, P. K. (2002). Outbreak of avian influenza A(H5N1) virus infection in Hong Kong in 1997. Clin Infect Dis, 34(2), 58-64. doi: 10.1086/338820

Chase, G. P., Rameix-Welti, M. A., Zvirbliene, A., Zvirblis, G., Gotz, V., Wolff, T., Schwemmle, M. (2011). Influenza virus ribonucleoprotein complexes gain preferential access to cellular export machinery through chromatin targeting. PLoS Pathog, 7(9), e1002187. doi:10.1371/journal.ppat.1002187

Chen, B. J., Leser, G. P., Jackson, D., & Lamb, R. A. (2008). The influenza virus M2 protein cytoplasmic tail interacts with the M1 protein and influences virus assembly at the site of virus budding. J Virol, 82(20), 10059-10070. doi:10.1128/JVI.01184-08

Chen, B. J., Leser, G. P., Morita, E. & Lamb, R. A. (2007). Influenza virus hemagglutinin and neuraminidase, but not the matrix protein, are required for assembly and budding of plasmid-derived virus-like particles. J Virol, 81(13), 7111-7123. doi:10.1128/JVI.00361-07

Chen, Y., Liang, W., Yang, S., Wu, N., Gao, H., Sheng, J., Yao, X., Zhang, Y., Wu, H., Zheng, S., Diao, H., Xia, S., Zhang, Y., Chan, K., Tsoi, H., Teng, J., Song, W., Wang, P., Lau, S. & other authors (2013). Human infections with the emerging avian influenza A H7N9 virus from wet market poultry: clinical analysis and characterisation of viral genome. The Lancet, 381(9881), 1916-1925

Chlanda, P., Schraidt, O., Kummer, S., Riches, J., Oberwinkler, H., Prinz, S., Briggs, J. A. (2015). Structural Analysis of the Roles of Influenza A Virus Membrane-Associated Proteins in Assembly and Morphology. J Virol, 89(17), 8957-8966. doi:10.1128/JVI.00592-15

Choppin, P. W. & Tamm, I. (1960). Studies of two kinds of virus particles which comprise influenza A2 virus strains. Journal of experimental medicine, 112(5), 895-920.

Chou, Y. Y., Albrecht, R. A., Pica, N., Lowen, A. C., Richt, J. A., Garcia-Sastre, A., Hai, R. (2011). The M segment of the 2009 new pandemic H1N1 influenza virus is critical for its high transmission efficiency in the guinea pig model. J Virol, 85(21), 11235-11241. doi: 10.1128/JVI.05794-11

Chou, Y. Y., Vafabakhsh, R., Doganay, S., Gao, Q., Ha, T., & Palese, P. (2012). One influenza virus particle packages eight unique viral RNAs as shown by FISH analysis. Proc Natl Acad Sci U S A, 109(23), 9101-9106. doi:10.1073/pnas.1206069109

Chu, M. C. Dawson, M. I. & Elford, W. J. (1949). Filamentous forms associated with newly isolated Influenza virus. Lancet, 603.

Cohen, M., Zhang, X. Q., Senaati, H. P., Chen, H. W., Varki, N. M., Schooley, R. T., & Gagneux, P. (2013). Influenza A penetrates host mucus by cleaving sialic acids with neuraminidase. Virol J, 10, 321. doi:10.1186/1743-422X-10-321

Colman, P. M. (1994). Influenza virus neuraminidase: structure, antibodies, and inhibitors. Protein Sci, 3(10), 1687-1696. doi:10.1002/pro.5560031007

Connor, R. J., Kawaoka, Y., Webster, R. G., & Paulson, J. C. (1994). Receptor specificity in human, avian, and equine H2 and H3 influenza virus isolates. Virology, 205(1), 17-23. doi:10.1006/viro.1994.1615

Cox, J., Hampson, A. & Hamilton, R. (1980). An immunofluorescence study of infleunza virus filament formation. Arch Virol, 63.

Crawford, P. C., Dubovi, E. J., Castleman, W. L., Stephenson, I., Gibbs, E. P., Chen, L., . . . Donis, R. O. (2005). Transmission of equine influenza virus to dogs. Science, 310(5747), 482-485. doi:10.1126/science.1117950

Dadonaite, B., Vijayakrishnan, S., Fodor, E., Bhella, D., & Hutchinson, E. C. (2016). Filamentous influenza viruses. J Gen Virol, 97(8), 1755-1764. doi:10.1099/jgv.0.000535

de Castro Martin, I. F., Fournier, G., Sachse, M., Pizarro-Cerda, J., Risco, C., & Naffakh, N. (2017). Influenza virus genome reaches the plasma membrane via a modified endoplasmic reticulum and Rab11-dependent vesicles. Nat Commun, 8(1), 1396. doi:10.1038/s41467-017-01557-6

de Geus, E. D., van Haarlem, D. A., Poetri, O. N., de Wit, J. J. & Vervelde, L. (2011). A lack of antibody formation against inactivated influenza virus after aerosol vaccination in presence or absence of adjuvantia. Vet Immunol Immunopathol, 143(1-2), 143-147.

de Vries, E., Tscherne, D. M., Wienholts, M. J., Cobos-Jimenez, V., Scholte, F., Garcia-Sastre, A., de Haan, C. A. (2011). Dissection of the influenza A virus endocytic routes reveals macropinocytosis as an alternative entry pathway. PLoS Pathog, 7(3), e1001329. doi:10.1371/journal.ppat.1001329

de Wit, E., Munster, V. J., van Riel, D., Beyer, W. E., Rimmelzwaan, G. F., Kuiken, T., Fouchier, R. A. (2010). Molecular determinants of adaptation of highly pathogenic avian influenza H7N7 viruses to efficient replication in the human host. J Virol, 84(3), 1597-1606. doi:10.1128/JVI.01783-09

de Wit, E., Spronken, M. I., Bestebroer, T. M., Rimmelzwaan, G. F., Osterhaus, A. D., & Fouchier, R. A. (2004). Efficient generation and growth of influenza virus A/PR/8/34 from eight cDNA fragments. Virus Res, 103(1-2), 155-161. doi:10.1016/j.virusres.2004.02.028

Dias, A., Bouvier, D., Crepin, T., McCarthy, A. A., Hart, D. J., Baudin, F., Ruigrok, R. W. (2009). The cap-snatching endonuclease of influenza virus polymerase resides in the PA subunit. Nature, 458(7240), 914-918. doi:10.1038/nature07745

Digard, P., Elton, D., Bishop, K., Medcalf, E., Weeds, A. & Pope, B. (1999). Modulation of nuclear localization of the influenza virus nucleoprotein through interaction with actin filaments. J Virol, 73(3), 2222-2231.

Doms, R. W., Lamb, R. A., Rose, J. K. & Helenius, A. (1993). Folding and assembly of viral membrane proteins. Virology, 193(2), 545-562. doi:10.1006/viro.1993.1164

Dorscheid, R. D. Conforti, E. A., Hamann, J. K., Rabe, F. K. & White, R. S. (1999). Characterization of cell surface lectin-binding patterns of human airway epithelium. The Histochemical Journal, 31, 145-151.

Dubois, J., Terrier, O., & Rosa-Calatrava, M. (2014). Influenza viruses and mRNA splicing: doing more with less. MBio, 5(3), e00070-00014. doi:10.1128/mBio.00070-14

Edinger, T. O., Pohl, M. O. & Stertz, S. (2014). Entry of influenza A virus: host factors and antiviral targets. J Gen Virol, 95(Pt 2), 263-277. doi:10.1099/vir.0.059477-0

Eisfeld, A. J., Neumann, G. & Kawaoka, Y. (2015). At the centre: influenza A virus ribonucleoproteins. Nat Rev Microbiol, 13(1), 28-41. doi:10.1038/nrmicro3367

Elleman, C. J. & Barclay, W. S. (2004). The M1 matrix protein controls the filamentous phenotype of influenza A virus. Virology, 321(1), 144-153. doi: 10.1016/j.virol.2003.12.009

Els, M., Laver, W. & Air, G. (1989). Sialic acid is cleaved from glycoconjugates at the cell surface when influenza virus neuraminidase are expressed from recombinant vaccinia viruses. Virology, 170.

Elton, D., Bruce, E. A., Bryant, N., Wise, H. M., MacRae, S., Rash, A., Smith, N., Turnbull, M. L., Medcalf, L., Daly, J. M. & Digard, P. (2013). The genetics of virus particle shape in equine influenza A virus. Influenza Other Respir Viruses, 7 Suppl 4, 81-89.

Elton, D., Simpson-Holley, M., Archer, K., Medcalf, L., Hallam, R., McCauley, J. & Digard, P. (2001). Interaction of the influenza virus nucleoprotein with the cellular CRM1-mediated nuclear export pathway. J Virol, 75(1), 408-419. doi:10.1128/JVI.75.1.408-419.2001

England, R. J., Homer, J. J., Knight, L. C., & Ell, S. R. (1999). Nasal pH measurement: a reliable and repeatable parameter. Clin Otolaryngol Allied Sci, 24(1), 67-68.

Fahy, J. V., & Dickey, B. F. (2010). Airway mucus function and dysfunction. N Engl J Med, 363(23), 2233-2247. doi:10.1056/NEJMra0910061

FAO. (2018). H7N9 situation update. www.fao.org/ag/againfo/programmes/en/empres/H7N9/situation_update.html. Accessed on 20/09/2018

Firth, A. E., Jagger, B. W., Wise, H. M., Nelson, C. C., Parsawar, K., Wills, N. M., … Atkins, J. F. (2012). Ribosomal frameshifting used in influenza A virus expression occurs within the sequence UCC_UUU_CGU and is in the +1 direction. Open Biol, 2(10), 120109. doi:10.1098/rsob.120109

Fodor, E. (2013). The RNA polymerase of influenza a virus: mechanisms of viral transcription and replication. Acta Virol, 57(2), 113-122.

Fodor, E. & Smith, M. (2004). The PA subunit is required for efficient nuclear accumulation of the PB1 subunit of the influenza A virus RNA polymerase complex. J Virol, 78(17), 9144-9153. doi:10.1128/JVI.78.17.9144-9153.2004

Francis, T. (1934). Transmission of influenza by a filterable virus. Science.

Fraser, C., Donnelly, C. A., Cauchemez, S., Hanage, W. P., Van Kerkhove, M. D., Hollingsworth, T. D. Collaboration, W. H. O. R. P. A. (2009). Pandemic potential of a strain of influenza A (H1N1): early findings. Science, 324(5934), 1557-1561. doi:10.1126/science.1176062

Furuse, Y., Suzuki, A., Kamigaki, T. & Oshitani, H. (2009). Evolution of the M gene of the influenza A virus in different host species: large-scale sequence analysis. Virol J, 6, 67. doi:10.1186/1743-422X-6-67

Galloway, S. E., Reed, M. L., Russell, C. J. & Steinhauer, D. A. (2013). Influenza HA subtypes demonstrate divergent phenotypes for cleavage activation and pH of fusion: implications for host range and adaptation. PLoS Pathog, 9(2), e1003151. doi:10.1371/journal.ppat.1003151

Garten, R. J., Davis, C. T., Russell, C. A., Shu, B., Lindstrom, S., Balish, A., Cox, N. J. (2009). Antigenic and genetic characteristics of swine-origin 2009 A(H1N1) influenza viruses circulating in humans. Science, 325(5937), 197-201. doi:10.1126/science.1176225

Gaush, C. R., & Smith, T. F. (1968). Replication and plaque assay of influenza virus in an established line of canine kidney cells. Appl Microbiol, 16(4), 588-594.

Gog, J. R., Afonso Edos, S., Dalton, R. M., Leclercq, I., Tiley, L., Elton, D., von Kirchbach J.C., Naffakh N., Escriou N. & Digard, P. (2007). Codon conservation in the influenza A virus genome defines RNA packaging signals. Nucleic Acids Res, 35(6), 1897-1907. doi:10.1093/nar/gkm087

Gomez-Puertas, P. Albo, C., Perez-Pastrana, E., Vivo, A. & Portela, A. (2000). Influenza Virus Matrix Protein Is the Major Driving force in virus budding. J Virol, 74, 11538-11547.
Goswami, D., Gowrishankar, K., Bilgrami, S., Ghosh, S., Raghupathy, R., Chadda, R., . . . Mayor, S. (2008). Nanoclusters of GPI-anchored proteins are formed by cortical actin-driven activity. Cell, 135(6), 1085-1097. doi:10.1016/j.cell.2008.11.032
Grgic, H., Hunter, D. B., Hunton, P. & Nagy, E. (2008). Pathogenicity of infectious bronchitis virus isolates from Ontario chickens. Can J Vet Res, 72(5), 403-410.
Hale, B. G., Randall, R. E., Ortin, J. & Jackson, D. (2008). The multifunctional NS1 protein of influenza A viruses. J Gen Virol, 89(Pt 10), 2359-2376. doi:10.1099/vir.0.2008/004606-0
Halvorson, D. A., Karunakaran, D. & Newman, J. A. (1979). Avian influenza in caged laying. Avian Diseases, 24.
Hay, A. J., Lomniczi, B., Bellamy, A. R. & Skehel, J. J. (1977). Transcription of the influenza virus genome. Virology, 83(2), 337-355.
Hay, A. J., Skehel, J. J. & McCauley, J. (1982). Characterization of influenza virus RNA complete transcripts. Virology, 116(2), 517-522.
Henikoff, S. & Henikoff, J. G. (1992). Amino acid substitution matrices from protein blocks. Proc Natl Acad Sci U S A, 89.
Herfst, S., Schrauwen, E. J., Linster, M., Chutinimitkul, S., de Wit, E., Munster, V. J., Sorrell E.M., Bestebroer T.M., Burke D.F., Smith D.J., Rimmelzwaan G.F., Osterhaus A.D. & Fouchier, R. A. (2012). Airborne transmission of influenza A/H5N1 virus between ferrets. Science, 336(6088), 1534-1541. doi:10.1126/science.1213362
Hickman, H. D., Mays, J. W., Gibbs, J., Kosik, I., Magadan, J. G., Takeda, K., Das S., Reynoso, G.V., Ngudiankama, B.F., Wei, J., Shannon, J.P., McManus, D. & Yewdell, J. W. (2018). Influenza A Virus Negative Strand RNA Is Translated for CD8(+) T Cell Immunosurveillance. J Immunol, 201(4), 1222-1228. doi:10.4049/jimmunol.1800586
Hillis, M. D. & Bull, J. J. (1993). An empirical test of bootstrapping as a method for assessing confidence in phylogenetic analysis. Syst. Biol., 42(2), 182-192.
Horimoto, T. & Kawaoka, Y. (2005). Influenza: lessons from past pandemics, warnings from current incidents. Nat Rev Microbiol, 3(8), 591-600. doi:10.1038/nrmicro1208
Hsu, M. T., Parvin, J. D., Gupta, S., Krystal, M. & Palese, P. (1987). Genomic RNAs of influenza viruses are held in a circular conformation in virions and in infected cells by a terminal panhandle. Proc Natl Acad Sci U S A, 84(22), 8140-8144.
Huang, X., Liu, T., Muller, J., Levandowski, R. A. & Ye, Z. (2001). Effect of influenza virus matrix protein and viral RNA on ribonucleoprotein formation and nuclear export. Virology, 287(2), 405-416. doi:10.1006/viro.2001.1067
Hutchinson, E. C., Charles, P. D., Hester, S. S., Thomas, B., Trudgian, D., Martinez-Alonso, M. & Fodor, E. (2014). Conserved and host-specific features of influenza virion architecture. Nat Commun, 5, 4816. doi:10.1038/ncomms5816
Hutchinson, E. C., von Kirchbach, J. C., Gog, J. R. & Digard, P. (2010). Genome packaging in influenza A virus. J Gen Virol, 91(Pt 2), 313-328. doi:10.1099/vir.0.017608-0
Hutten, S. & Kehlenbach, R. H. (2007). CRM1-mediated nuclear export: to the pore and beyond. Trends Cell Biol, 17(4), 193-201. doi:10.1016/j.tcb.2007.02.003
ICTV. (2017). International committee on Taxonomy of Viruses. Retrieved 15/08/2018 https://talk.ictvonline.org/
Imai, M., Watanabe, T., Hatta, M., Das, S. C., Ozawa, M., Shinya, K., Zhong, G., Hanson, A., Katsura, H., Watanabe, S., Li, C., Kawakami, E., Yamada, S., Kiso, M., Suzuki, Y., Maher, E.A., Neumann, G. & Kawaoka, Y. (2012). Experimental adaptation of an influenza H5 HA confers respiratory droplet transmission to a reassortant H5 HA/H1N1 virus in ferrets. Nature, 486(7403), 420-428. doi:10.1038/nature10831

Iqbal, M., Yagub, T., Mukhtar, N., Shabbir, M. Z. & McCauley, J. (2013). Infectivity and transmissibility of H9N2 avian influenza virus in chickens and wild terrestrial birds. Veterinary Research, 44.

I-TASSER. (2017). Zhang Lab. https://zhanglab.ccmb.med.umich.edu/I-TASSER/

Iuliano, A. D., Roguski, K. M., Chang, H. H., Muscatello, D. J., Palekar, R., Tempia, S., Mustaquim, D. (2018). Estimates of global seasonal influenza-associated respiratory mortality: a modelling study. The Lancet, 391(10127), 1285-1300. doi:10.1016/s0140-6736(17)33293-2

Iwasaki, A. & Pillai, P. S. (2014). Innate immunity to influenza virus infection. Nat Rev Immunol, 14(5), 315-328. doi:10.1038/nri3665

Jagger, B. W., Wise, H. M., Kash, J. C., Walters, K. A., Wills, N. M., Xiao, Y. L., Dunfee, R.L., Schwartzman, L.M., Ozinsky, A., Bell, G.L., Dalton, R.M., Lo, A., Efstathiou, S., Atkins, J.F., Firth, A.E., Taubenberger, J.K. & Digard, P. (2012). An overlapping protein-coding region in influenza A virus segment 3 modulates the host response. Science, 337(6091), 199-204. doi:10.1126/science.1222213

Jin, H., Leser, G. P., Zhang, J. & Lamb, R. A. (1997). Influenza virus hemagglutinin and neuraminidase cytoplasmic tails control particle shape. EMBO J, 16(6), 1236-1247. doi:10.1093/emboj/16.6.1236

Johnson, C. A., Pekas, D. J. & Winzler, R. J. (1964). Neuraminidases and Influenza Virus Infection in Embryonated Eggs. Science, 143(3610), 1051-1052.

Johnson, D. C. & Maxfield, B. G. (1976). An occurrence of avian influenza virus infection in laying chickens. Avian Diseases, 20.

Kabachinski, G. & Schwartz, T. U. (2015). The nuclear pore complex--structure and function at a glance. J Cell Sci, 128(3), 423-429.

Kanehira, K., Uchida, Y. & Saito, T. (2016). Visualization of avian influenza virus infected cells using self-assembling fragments of green fluorescent protein. Electronic Journal of Biotechnology, 19, 61-64. doi: 10.1016/j.ejbt.2015.08.008

Kawaguchi, A., Matsumoto, K. & Nagata, K. (2012). YB-1 functions as a porter to lead influenza virus ribonucleoprotein complexes to microtubules. J Virol, 86(20), 11086-11095. doi:10.1128/JVI.00453-12

Kawaoka, Y. & Webster, R. (1985). Evolution of the A/Chicken/Pennsylvania/83 (H5N2) infleunza virus. Virology, 146.

Kilbourne, E. D. & Murphy, J. S. (1960). Genetic studies of influenza virus. Journal of experimental medicine, 11.

Kilbourne, E. D. (2006). Influenza pandemics of the 20th century. Emerg Infect Dis, 12(1), 9-14. doi:10.3201/eid1201.051254

Kolesnikova, L., Heck, S., Matrosovich, T., Klenk, H. D., Becker, S. & Matrosovich, M. (2013). Influenza virus budding from the tips of cellular microvilli in differentiated human airway epithelial cells. J Gen Virol, 94(Pt 5), 971-976. doi:10.1099/vir.0.049239-0

Krammer, F., Smith, G. J. D., Fouchier, R. A. M., Peiris, M., Kedzierska, K., Doherty, P. C., Palese, P., Shaw, M.L., Treanor, J., Webster, R.G. & Garcia-Sastre, A. (2018). Influenza. Nat Rev Dis Primers, 4(1), 3. doi:10.1038/s41572-018-0002-y

Kumar, A., Vijayakumar, P., Gandhale, P., Ranaware, P., Kumar, D., Kulkarni, D., Raut, A. & Mishra, A. (2017). Genome-wide gene expression pattern underlying differential host response to high or low pathogenic H5N1 avian influenza virus in ducks. Acta Virologica, 61, 66-76.

Kuo, R. L., Li, L. H., Lin, S. J., Li, Z. H., Chen, G. W., Chang, C. K., . . . Shih, S. R. (2016). Role of N Terminus-Truncated NS1 Proteins of Influenza A Virus in Inhibiting IRF3 Activation. J Virol, 90(9), 4696-4705. doi:10.1128/JVI.02843-15

Lagarda-Diaz, I., Guzman-Partida, A. M. & Vazquez-Moreno, L. (2017). Legume Lectins: Proteins with Diverse Applications. Int J Mol Sci, 18(6).

Lakdawala, S. S., Lamirande, E. W., Suguitan, A. L., Jr., Wang, W., Santos, C. P., Vogel, L., Matsuoka, Y., Lindsley, W.G., Jin, H. & Subbarao, K. (2011). Eurasian-origin gene segments contribute to the transmissibility, aerosol release, and morphology of the 2009 pandemic H1N1 influenza virus. PLoS Pathog, 7(12), e1002443. doi:10.1371/journal.ppat.1002443

Lamb, R. A. & Choppin, P. W. (1979). Segment 8 of the influenza virus genome is unique in coding for two polypeptides. Proc Natl Acad Sci U S A, 76(10), 4908-4912.

Lee, M. T., Klumpp, K., Digard, P. & Tiley, L. (2003). Activation of influenza virus RNA polymerase by the 5' and 3' terminal duplex of genomic RNA. Nucleic Acids Res, 31(6), 1624-1632.

Leser, G. P. & Lamb, R. A. (2005). Influenza virus assembly and budding in raft-derived microdomains: a quantitative analysis of the surface distribution of HA, NA and M2 proteins. Virology, 342(2), 215-227. doi:10.1016/j.virol.2005.09.049

Leser, G. P. & Lamb, R. A. (2017). Lateral Organization of Influenza Virus Proteins in the Budozone Region of the Plasma Membrane. J Virol, 91(9). doi:10.1128/JVI.02104-16

Li, C., Li, C., Zhang, A. J., To, K. K., Lee, A. C., Zhu, H., Wu, H. W., Chan, J. F., Chen, H., Hung, I. F., Li, L. & Yuen, K. Y. (2014). Avian influenza A H7N9 virus induces severe pneumonia in mice without prior adaptation and responds to a combination of zanamivir and COX-2 inhibitor. PLoS One, 9(9), e107966.

Liang, Y., Hong, Y. & Parslow, T. G. (2005). cis-Acting packaging signals in the influenza virus PB1, PB2, and PA genomic RNA segments. J Virol, 79(16), 10348-10355. doi:10.1128/JVI.79.16.10348-10355.2005

Lin, S., Naim, H. Y., Rodriguez, A. C. & Roth, M. G. (1998). Mutations in the middle of the transmembrane domain reverse the polarity of transport of the influenza virus hemagglutinin in MDCK epithelial cells. J cell biol, 142(1), 51-57.

Liu, D., Shi, W., Shi, Y., Wang, D., Xiao, H., Li, W., Bi, Y., Wu, Y., Li, X., Yan, J., Liu, W., Zhao, G., Yang, W., Wang, Y., Ma, J., Shu, Y., Lei, F. & Gao, G. F. (2013). Origin and diversity of novel avian influenza A H7N9 viruses causing human infection: phylogenetic, structural, and coalescent analyses. Lancet, 381(9881), 1926-1932. doi:10.1016/S0140-6736(13)60938-1

Liu, T., Muller, J. & Ye, Z. (2002). Association of Influenza Virus Matrix Protein with Ribonucleoproteins May Control Viral Growth and Morphology. Virology, 304(1), 89-96.

Long, J. S., Giotis, E. S., Moncorge, O., Frise, R., Mistry, B., James, J., Morisson, M., Iqbal, M., Vignal, A., Skinner, M.A. & Barclay, W. S. (2016). Species difference in ANP32A underlies influenza A virus polymerase host restriction. Nature, 529(7584), 101-104. doi:10.1038/nature16474

Lourisirirotchanakul, S., Rojanasang, P., Thakerngpol, K., Choosrichom, N., Chaichoune, K., Pooruk, P., Namsai, A., Webster, R. & Puthavathana, P. (2013). Electron micrographs of human and avian influenza viruses with high and low pathogenicity. Asian Biomedicine, 7, 155-167.

Lowen, A. C., Mubareka, S., Steel, J. & Palese, P. (2007). Influenza virus transmission is dependent on relative humidity and temperature. PLoS Pathog, 3(10), 1470-1476. doi: 10.1371/journal.ppat.0030151

Luytjes, W., Krystal, M., Enami, M., Parvin, J. D. & Palese, P. (1989). Amplification, expression, and packaging of foreign gene by influenza virus. Cell, 59(6), 1107-1113.

Ma, W., Liu, Q., Bawa, B., Qiao, C., Qi, W., Shen, H., Chen, Y., Ma, J., Li, X., Webby, R.J., García-Sastre, A. & Richt, J. A. (2012). The neuraminidase and matrix genes of the 2009 pandemic influenza H1N1 virus cooperate functionally to facilitate efficient replication and transmissibility in pigs. J Gen Virol, 93(Pt 6), 1261-1268. doi: 10.1099/vir.0.040535-0

Mänz, B., Brunotte, L., Reuther, P. & Schwemmle, M. (2012). Adaptive mutations in NEP compensate for defective H5N1 RNA replication in cultured human cells. Nature Communications, 3(1). doi:10.1038/ncomms1804

Marsh, G. A., Hatami, R. & Palese, P. (2007). Specific residues of the influenza A virus hemagglutinin viral RNA are important for efficient packaging into budding virions. J Virol, 81(18), 9727-9736. doi:10.1128/JVI.01144-07

Martin, K. & Helenius, A. (1991). Nuclear transport of influenza virus ribonucleoproteins: the viral matrix protein (M1) promotes export and inhibits import. Cell, 67(1), 117-130.

Martyna, A., Bahsoun, B., Badham, M. D., Srinivasan, S., Howard, M. J. & Rossman, J. S. (2017). Membrane remodeling by the M2 amphipathic helix drives influenza virus membrane scission. Sci Rep, 7, 44695. doi:10.1038/srep44695

Matlin, K. S., Reggio, H., Helenius, A. & Simons, K. (1981). Infectious entry pathway of influenza virus in a canine kidney cell line. J cell biol, 91(3 Pt 1), 601-613.

Matrosovich, M. N., Matrosovich, T. Y., Gray, T., Roberts, N. A. & Klenk, H. D. (2004). Human and avian influenza viruses target different cell types in cultures of human airway epithelium. Proc Natl Acad Sci U S A, 101(13), 4620-4624. doi:10.1073/pnas.0308001101

Matrosovich, M., Tuzikov, A., Bovin, N., Gambaryan, A., Klimov, A., Castrucci, M. R., Donatelli, I. & Kawaoka, Y. (2000). Early alterations of the receptor-binding properties of H1, H2, and H3 avian influenza virus hemagglutinins after their introduction into mammals. J Virol, 74(18), 8502-8512.

McCown, M. F. & Pekosz, A. (2006). Distinct domains of the influenza a virus M2 protein cytoplasmic tail mediate binding to the M1 protein and facilitate infectious virus production. J Virol, 80(16), 8178-8189. doi: 10.1128/JVI.00627-06

McKimm-Breschkin, J. L. (2013). Influenza neuraminidase inhibitors: antiviral action and mechanisms of resistance. Influenza Other Respir Viruses, 7 Suppl 1, 25-36. doi:10.1111/irv.12047

Medvedeva, T., Alexandrova, G. & Smorodintsev, A. (1968). Differentiation of temperature variants of inlfuenza A2 vivurses on the basis of plaque formation. Journal of Virology, 2.

Mintaev, R. R., Alexeevski, A. V. & Kordyukova, L. V. (2014). Co-evolution analysis to predict protein-protein interactions within influenza virus envelope. J Bioinform Comput Biol, 12(2), 1441008. doi:10.1142/S021972001441008X

Misek, D. E., Bard, E. & Rodriguez-Boulan, E. (1984). Biogenesis of epithelial cell polarity: intracellular sorting and vectorial exocytosis of an apical plasma membrane glycoprotein. Cell, 39(3 Pt 2), 537-546.

Mitnaul, L. J., Matrosovich, M. N., Castrucci, M. R., Tuzikov, A. B., Bovin, N. V., Kobasa, D. & Kawaoka, Y. (2000). Balanced hemagglutinin and neuraminidase activities are critical for efficient replication of influenza A virus. J Virol, 74(13), 6015-6020.

Moeller, A., Kirchdoerfer, R. N., Potter, C. S., Carragher, B. & Wilson, I. A. (2012). Organization of the influenza virus replication machinery. Science, 338(6114), 1631-1634. doi:10.1126/science.1227270

Molesti, E., Cattoli, E., Ferrara, F., Bottcher-Friebershauser, E., Terregino, C. & Temperton, N. (2013). The production and development of H7 infleunza virus pseudotypes for the study of humoral responses against avian viruses. J. Mol. Gen. Med., 7.

Momose, F., Sekimoto, T., Ohkura, T., Jo, S., Kawaguchi, A., Nagata, K. & Morikawa, Y. (2011). Apical transport of influenza A virus ribonucleoprotein requires Rab11-positive recycling endosome. PLoS One, 6(6), e21123. doi:10.1371/journal.pone.0021123

Morgan, C., Rose, H. & Moore, D. (1956). Structure and development of viruses observed in the electron microscope. J. Exp. Med, 104(2).

Morgan, C., Rose, H., & Moore, D. H. (1956). Structure and development of viruses observed in the electron microscope. III. Influenza virus. J Exp Med, 104(2), 171-182.

Mosley, V. M. & Wyckoff, R. W. G. (1946). Electron Micrography of the Virus of Influenza. Nature, 3983, 263.

Mukaigawa, J. & Nayak, D. P. (1991). Two signals mediate nuclear localization of influenza virus (A/WSN/33) polymerase basic protein 2. J Virol, 65(1), 245-253.

Muramoto, Y., Noda, T., Kawakami, E., Akkina, R. & Kawaoka, Y. (2013). Identification of novel influenza A virus proteins translated from PA mRNA. J Virol, 87(5), 2455-2462. doi:10.1128/JVI.02656-12

Muramoto, Y., Takada, A., Fujii, K., Noda, T., Iwatsuki-Horimoto, K., Watanabe, S., Horimoto, T., Kida, H. & Kawaoka, Y. (2006). Hierarchy among viral RNA (vRNA) segments in their role in vRNA incorporation into influenza A virions. J Virol, 80(5), 2318-2325. doi:10.1128/JVI.80.5.2318-2325.2006

Naffakh, N., Tomoiu, A., Rameix-Welti, M. A. & van der Werf, S. (2008). Host restriction of avian influenza viruses at the level of the ribonucleoproteins. Annu Rev Microbiol, 62, 403-424. doi:10.1146/annurev.micro.62.081307.162746

Nakajima, K., Desselberger, U. & Palese, P. (1978). Recent human influenza A (H1N1) viruses are closely related genetically to strains isolated in 1950. Nature, 274(5669), 334-339.

Nakajima, N., Hata, S., Sato, Y., Tobiume, M., Katano, H., Kaneko, K., Nagata, N., Kataoka, M., Ainai, A., Hasegawa, H., Tashiro, M., Kuroda, M., Odai, T., Urasawa, N., Ogino, T., Hanaoka, H., Watanabe, M. & Sata, T. (2010). The first autopsy case of pandemic influenza (A/H1N1pdm) virus infection in Japan: detection of a high copy number of the virus in type II alveolar epithelial cells by pathological and virological examination. Jpn J Infect Dis, 63(1), 67-71.

Nath, S. T. & Nayak, D. P. (1990). Function of two discrete regions is required for nuclear localization of polymerase basic protein 1 of A/WSN/33 influenza virus (H1 N1). Mol Cell Biol, 10(8), 4139-4145.

Neumann, G., Hughes, M. T. & Kawaoka, Y. (2000). Influenza A virus NS2 protein mediates vRNP nuclear export through NES-independent interaction with hCRM1. EMBO J, 19(24), 6751-6758. doi:10.1093/emboj/19.24.6751

Nieto, A., de la Luna, S., Barcena, J., Portela, A., Valcarcel, J., Melero, J. A. & Ortin, J. (1992). Nuclear transport of influenza virus polymerase PA protein. Virus Res, 24(1), 65-75.

Nishimura, H., Hara, M., Sugawara, K., Kitame, F., Takiguchi, K., Umetsu, Y., Tonosaki, A. & Nakamura, K. (1990). Characterization of the cord-like structures emerging from the surface of influenza C virus-infected cells. Virology, 179(1), 179-188.

Noda, T. (2012). Native morphology of influenza virions. Front Microbiol, 2, 269. doi:10.3389/fmicb.2011.00269

Noda, T., Sagara, H., Yen, A., Takada, A., Kida, H., Cheng, R. H. & Kawaoka, Y. (2006). Architecture of ribonucleoprotein complexes in influenza A virus particles. Nature, 439(7075), 490-492. doi:10.1038/nature04378

Noton, S. L., Medcalf, E., Fisher, D., Mullin, A. E., Elton, D. & Digard, P. (2007). Identification of the domains of the influenza A virus M1 matrix protein required for NP binding, oligomerization and incorporation into virions. J Gen Virol, 88(Pt 8), 2280-2290. doi:10.1099/vir.0.82809-0

Nturibi, E., Bhagwat, A. R., Coburn, S., Myerburg, M. M. & Lakdawala, S. S. (2017). Intracellular Colocalization of Influenza Viral RNA and Rab11A Is Dependent upon Microtubule Filaments. J Virol, 91(19). doi:10.1128/JVI.01179-17

Ohuchi, M., Ohuchi, R., Feldmann, A. & Klenk, H. D. (1997). Regulation of receptor binding affinity of influenza virus hemagglutinin by its carbohydrate moiety. J Virol, 71(11), 8377-8384.

Olsen, C. W., Karasin, A. I., Carman, S., Li, Y., Bastien, N., Ojkic, D., Alves, D., Charbonneau, G., Henning, B. M., Low, D. E., Burton, L. & Broukhanski, G. (2006). Triple reassortant H3N2 influenza A viruses, Canada, 2005. Emerg Infect Dis, 12(7), 1132-1135. doi:10.3201/eid1207.060268

O'Neill, R. E., Jaskunas, R., Blobel, G., Palese, P. & Moroianu, J. (1995). Nuclear import of influenza virus RNA can be mediated by viral nucleoprotein and transport factors required for protein import. J Biol Chem, 270(39), 22701-22704.

O'Neill, R. E., Talon, J. & Palese, P. (1998). The influenza virus NEP (NS2 protein) mediates the nuclear export of viral ribonucleoproteins. EMBO J, 17(1), 288-296. doi:10.1093/emboj/17.1.288

Ortega, J., Martin-Benito, J., Zurcher, T., Valpuesta, J. M., Carrascosa, J. L. & Ortin, J. (2000). Ultrastructural and functional analyses of recombinant influenza virus ribonucleoproteins suggest dimerization of nucleoprotein during virus amplification. J Virol, 74(1), 156-163.

Osterholm, M. T., Kelley, N. S., Sommer, A. & Belongia, E. A. (2012). Efficacy and effectiveness of influenza vaccines: a systematic review and meta-analysis. Lancet Infect Dis, 12(1), 36-44. doi:10.1016/S1473-3099(11)70295-X

Palese, P. & Shaw, M. L. (2007). Orthomyxoviridae: the viruses and their replication. In D. M. K. a. P. M. Howley (Ed.), Fields Virology (5th ed., pp. 1647-1689). Philadelphia, PA. : Wolters Kluwer; Lippincott Williams and Wilkins.

Palese, P., Tobita, K., Ueda, M. & Compans R. W. (1974). Characterization of Temperature Sensitive Influenza Virus Mutants Defective in Neuraminidase. Virology, 61, 397-410.

Park, E. K., Castrucci, M. R., Portner, A. & Kawaoka, Y. (1998). The M2 ectodomain is important for its incorporation into influenza A virions. J Virol, 72(3), 2449-2455.

Pereira, C. F., Read, E. K. C., Wise, H. M., Amorim, M. J. & Digard, P. (2017). Influenza A Virus NS1 Protein Promotes Efficient Nuclear Export of Unspliced Viral M1 mRNA. Journal of Virology, 91(e00528-17). doi:10.1128/JVI

Petrova, V. N. & Russell, C. A. (2018). The evolution of seasonal influenza viruses. Nat Rev Microbiol, 16(1), 60. doi:10.1038/nrmicro.2017.146

Pica, N. & Palese, P. (2013). Toward a universal influenza virus vaccine: prospects and challenges. Annu Rev Med, 64, 189-202. doi:10.1146/annurev-med-120611-145115

Pinto, L. H., Holsinger, L. J. & Lamb, R. A. (1992). Influenza virus M2 protein has ion channel activity. Cell, 69(3), 517-528.

Plotch, S. J., Bouloy, M., Ulmanen, I. & Krug, R. M. (1981). A unique cap(m7GpppXm)-dependent influenza virion endonuclease cleaves capped RNAs to generate the primers that initiate viral RNA transcription. Cell, 23(3), 847-858.

Pu, J., Sun, H., Qu, Y., Wang, C., Gao, W., Zhu, J., Sun, Y., Bi, Y., Huang, Y., Chang, K., Cul, J. & Liu J. (2017). M gene reassortment in H9N2 influenza virus promotes early infection and replication: contribution to rising virus prevalence in chickens in china. Journal of Virology, 91(8). doi:e02055-16

Roberts, K. L., Leser, G. P., Ma, C. & Lamb, R. A. (2013). The amphipathic helix of influenza A virus M2 protein is required for filamentous bud formation and scission of filamentous and spherical particles. J Virol, 87(18), 9973-9982. doi:10.1128/JVI.01363-13

Roberts, K. L., Manicassamy, B. & Lamb, R. A. (2015). Influenza A virus uses intercellular connections to spread to neighboring cells. J Virol, 89(3), 1537-1549. doi:10.1128/JVI.03306-14

Roberts, P. C. & Compans, R. W. (1998). Host cell dependence of viral morphology. Proc Natl Acad Sci U S A, 95, 5746-5751.

Roberts, P. C., Lamb, R. A. & Compans, R. W. (1998). The M1 and M2 proteins of influenza A virus are important determinants in filamentous particle formation. Virology, 240, 127-137.

Robertson, J. S., Schubert, M. & Lazzarini, R. A. (1981). Polyadenylation sites for influenza virus mRNA. J Virol, 38(1), 157-163.

Rodriguez-Boulan, E., Paskiet, K. T. & Sabatini, D. D. (1983). Assembly of enveloped viruses in Madin-Darby canine kidney cells: polarized budding from single attached cells and from clusters of cells in suspension. J cell biol, 96(3), 866-874.

Rossman, J. S. & Lamb, R. A. (2011). Influenza virus assembly and budding. Virology, 411(2), 229-236. doi:10.1016/j.virol.2010.12.003

Rossman, J. S., Jing, X., Leser, G. P. & Lamb, R. A. (2010). Influenza virus M2 protein mediates ESCRT-independent membrane scission. Cell, 142(6), 902-913. doi: 10.1016/j.cell.2010.08.029

Rossman, J. S., Jing, X., Leser, G. P., Balannik, V., Pinto, L. H. & Lamb, R. A. (2010). Influenza virus M2 ion channel protein is necessary for filamentous virion formation. J Virol, 84(10), 5078-5088. doi:10.1128/JVI.00119-10

Rossman, J. S., Leser, G. P. & Lamb, R. A. (2012). Filamentous influenza virus enters cells via macropinocytosis. J Virol, 86(20), 10950-10960. doi:10.1128/JVI.05992-11

Sakai, T., Nishimura, S. I., Naito, T. & Saito, M. (2017). Influenza A virus hemagglutinin and neuraminidase act as novel motile machinery. Sci Rep, 7, 45043. doi:10.1038/srep45043

Sakai, T., Takagi, H., Muraki, Y. & Saito, M. (2018). Unique Directional Motility of Influenza C Virus Controlled by Its Filamentous Morphology and Short-Range Motions. J Virol, 92(2). doi:10.1128/JVI.01522-17

Sauter, N. K., Bednarski, M. D., Wurzburg, B. A., Hanson, J. E., Whitesides, G. M., Skehel, J. J. & Wiley, D. C. (1989). Hemagglutinins from two influenza virus variants bind to sialic acid derivatives with millimolar dissociation constants: a 500-MHz proton nuclear magnetic resonance study. Biochemistry, 28(21), 8388-8396.

Schaffer, F. L., Soergel, M. E. & Straube, D. C. (1976). Survival of airborne influenza virus: effects of propagating host, relative humidity, and composition of spray fluids. Arch Virol, 51(4), 263-273.

Scheiffele, P., Rietveld, A., Wilk, T. & Simons, K. (1999). Influenza viruses select ordered lipid domains during budding from the plasma membrane. J Biol Chem, 274(4), 2038-2044.

Schneider, C. A., Rasband, W. S. & Eliceiri, K. W. (2012). NIH Image to ImageJ: 25 years of image analysis. Nat Methods, 9(7), 671-675.

Scholtissek, C., von Hoyningen, V. & Rott, R. (1978). Genetic relatedness between the new 1977 epidemic strains (H1N1) of influenza and human influenza strains isolated between 1947 and 1957 (H1N1). Virology, 89(2), 613-617.

Schwarz, F. & Aebi, M. (2011). Mechanisms and principles of N-linked protein glycosylation. Curr Opin Struct Biol, 21(5), 576-582.

Seladi-Schulman, J., Campbell, P. J., Suppiah, S., Steel, J. & Lowen, A. C. (2014). Filament-producing mutants of influenza A/Puerto Rico/8/1934 (H1N1) virus have higher neuraminidase activities than the spherical wild-type. PLoS One, 9(11), e112462. doi:10.1371/journal.pone.0112462

Seladi-Schulman, J., Steel, J. & Lowen, A. C. (2013). Spherical influenza viruses have a fitness advantage in embryonated eggs, while filament-producing strains are selected in vivo. J Virol, 87(24), 13343-13353. doi: 10.1128/JVI.02004-13

Selman, M., Dankar, S. K., Forbes, N. E., Jia, J. J. & Brown, E. G. (2012). Adaptive mutation in influenza A virus non-structural gene is linked to host switching and induces a novel protein by alternative splicing. Emerg Microbes Infect, 1(11), e42. doi:10.1038/emi.2012.38

Seo, S. H., Hoffmann, E. & Webster, R. G. (2002). Lethal H5N1 influenza viruses escape host anti-viral cytokine responses. Nat Med, 8(9), 950-954. doi:10.1038/nm757

Sha, B. Luo, M. (1997). Structure of a bifunctional membrane-RNA binding protein, influenza virus matrix protein M1. Nature Structural Biology, 4, 239-244.

Shaw, M. L., Stone, K. L., Colangelo, C. M., Gulcicek, E. E. & Palese, P. (2008). Cellular proteins in influenza virus particles. PLoS Pathog, 4(6), e1000085. doi:10.1371/journal.ppat.1000085

Shih, S. R., Nemeroff, M. E. & Krug, R. M. (1995). The choice of alternative 5' splice sites in influenza virus M1 mRNA is regulated by the viral polymerase complex. Proc Natl Acad Sci U S A, 92(14), 6324-6328.

Shih, S. R., Suen, P. C., Chen, Y. S. & Chang, S. C. (1998). A novel spliced transcript of influenza A/WSN/33 virus. Virus Genes, 17(2), 179-183.

Short, K. R., Richard, M., Verhagen, J. H., van Riel, D., Schrauwen, E. J., van den Brand, J. M., Mänz, B., Bodewes, R. & Herfst, S. (2015). One health, multiple challenges: The inter-species transmission of influenza A virus. One Health, 1, 1-13. doi:10.1016/j.onehlt.2015.03.001

Shtykova, E. V., Dadinova, L. A., Fedorova, N. V., Golanikov, A. E., Bogacheva, E. N., Ksenofontov, A. L., Baratova, L.A., Shilova, L.A., Tashkin, V.Y., Galimzyanov, T.R., Jeffries, C.M., Svergun, D.I. & Batishchev, O. V. (2017). Influenza virus Matrix Protein M1 preserves its conformation with pH, changing multimerization state at the priming stage due to electrostatics. Sci Rep, 7(1), 16793. doi:10.1038/s41598-017-16986-y

Sieczkarski, S. B. & Whittaker, G. R. (2002). Influenza virus can enter and infect cells in the absence of clathrin-mediated endocytosis. J Virol, 76(20), 10455-10464.

Simonsen, L., Spreeuwenberg, P., Lustig, R., Taylor, R. J., Fleming, D. M., Kroneman, M., Van Kerkhove M.D., Mounts A. W, Paget, J. Teams, G. L. C. (2013). Global mortality estimates for the 2009 Influenza Pandemic from the GLaMOR project: a modeling study. PLoS Med, 10(11), e1001558. doi:10.1371/journal.pmed.1001558

Simpson-Holley, M., Ellis, D., Fisher, D., Elton, D., McCauley, J. & Digard, P. (2002). A Functional Link between the Actin Cytoskeleton and Lipid Rafts during Budding of Filamentous Influenza Virions. Virology, 301(2), 212-225. doi:10.1006/viro.2002.1595 Skehel, J. J. & Wiley, D. C. (2000). Receptor binding and membrane fusion in virus entry: the influenza hemagglutinin. Annu Rev Biochem, 69, 531-569. doi:10.1146/annurev.biochem.69.1.531

Smirnov Yu, A., Kuznetsova, M. A. & Kaverin, N. V. (1991). The genetic aspects of influenza virus filamentous particle formation. Arch Virol, 118(3-4), 279-284.

Sorrell, E. M., Song, H., Pena, L. & Perez, D. R. (2010). A 27-amino-acid deletion in the neuraminidase stalk supports replication of an avian H2N2 influenza A virus in the respiratory tract of chickens. J Virol, 84(22), 11831-11840. doi:10.1128/JVI.01460-10

Spackman, E., Senne, D. A., Myers, T. J., Bulaga, L. L., Garber, L. P., Perdue, M. L., Lohman, K., Daum, L.T. & Suarez, D. L. (2002). Development of a Real-Time Reverse Transcriptase PCR Assay for Type A Influenza Virus and the Avian H5 and H7 Hemagglutinin Subtypes. Journal of Clinical Microbiology, 40(9), 3256-3260. doi:10.1128/jcm.40.9.3256-3260.2002

Spickler, A. R., Trampel, D. W. & Roth, J. A. (2008). The onset of virus shedding and clinical signs in chickens infected with high-pathogenicity and low-pathogenicity avian influenza viruses. Avian Pathol, 37(6), 555-577. doi: 10.1080/03079450802499118

Stewart, M. (2007). Molecular mechanism of the nuclear protein import cycle. Nat Rev Mol Cell Biol, 8(3), 195-208. doi:10.1038/nrm2114

Su, S., Gu, M., Liu, D., Cui, J., Gao, G. F., Zhou, J. & Liu, X. (2017). Epidemiology, Evolution, and Pathogenesis of H7N9 Influenza Viruses in Five Epidemic Waves since 2013 in China. Trends Microbiol, 25(9), 713-728. doi:10.1016/j.tim.2017.06.008

Subbarao, E. K., London, W. & Murphy, B. R. (1993). A single amino acid in the PB2 gene of influenza A virus is a determinant of host range. J Virol, 67(4), 1761-1764.

Swayne, D. E. & Alexander, D. J. (1994). Confirmation of nephrotropism and nephropathogenicity of three low-pathogenic chicken-origin influenza viruses for chickens. Avian Pathol, 23(2), 345-352. doi: 10.1080/03079459408419002

Swayne, D. E. (2006). Microassay for measuring thermal inactivation of H5N1 high pathogenicity avian influenza virus in naturally infected chicken meat. Int J Food Microbiol, 108(2), 268-271.

Swayne, D. E. (2008). Avian Infleunza Control Strategies. In D. E. Swayne (Ed.), Avian Influenza (1 ed.). Iowa, USA: Blackwell publishing.

Swayne, D. E., Radin, M. J., Hoepf, T. M. & Slemons, R. D. (1994). Acute renal failure as the cause of death in chickens following intravenous inoculation with avian influenza virus a/chicken/alabama/7395/75 (h4n8). Avian Diseases, 38.

Swayne, D. E., Spackman, E. & Pantin-Jackwood, M. (2014). Success factors for avian influenza vaccine use in poultry and potential impact at the wild bird-agricultural interface. Ecohealth, 11(1), 94-108. doi:10.1007/s10393-013-0861-3

Takeda, M., Leser, G. P., Russell, C. J. & Lamb, R. A. (2003). Influenza virus hemagglutinin concentrates in lipid raft microdomains for efficient viral fusion. Proc Natl Acad Sci U S A, 100(25), 14610-14617. doi:10.1073/pnas.2235620100

Taubenberger, J. K. & Morens, D. M. (2006). 1918 Influenza: the mother of all pandemics. Emerg Infect Dis, 12(1), 15-22. doi:10.3201/eid1201.050979

Taubenberger, J. K., Reid, A. H., Lourens, R. M., Wang, R., Jin, G. & Fanning, T. G. (2005). Characterization of the 1918 influenza virus polymerase genes. Nature, 437(7060), 889-893. doi:10.1038/nature04230

Tellier, R. (2009). Aerosol transmission of influenza A virus: a review of new studies. J R Soc Interface, 6 Suppl 6, S783-790. doi:10.1098/rsif.2009.0302.focus

Thaa, B., Herrmann, A. & Veit, M. (2010). Intrinsic cytoskeleton-dependent clustering of influenza virus M2 protein with hemagglutinin assessed by FLIM-FRET. J Virol, 84(23), 12445-12449. doi:10.1128/JVI.01322-10

Tong, S., Li, Y., Rivailler, P., Conrardy, C., Castillo, D. A., Chen, L. M., Recuenco, S., Ellison, J.A., Davis, C.T., York, I.A., Turmelle, A.S., Moran, D., Rogers, S., Shi, M., Tao, Y., Weil, M. R. & other authors (2012). A distinct lineage of influenza A virus from bats. Proc Natl Acad Sci U S A, 109(11), 4269-4274. doi:10.1073/pnas.1116200109

Tong, S., Zhu, X., Li, Y., Shi, M., Zhang, J., Bourgeois, M., Yang, H., Chen, X., Recuenco, S., Gomez, J., Chen, L.M., Johnson, A., Tao, Y., Dreyfus, C., Yu, W., McBride, R. & other authors (2013). New world bats harbor diverse influenza A viruses. PLoS Pathog, 9(10), e1003657. doi:10.1371/journal.ppat.1003657

Valentine, R. C. & Isaacs, A. (1957). The Structure of Influenza Virus Filaments and Spheres. J. Gen. Microbiol, 16, 195-204.

Vandegrift, K. J., Sokolow, S. H., Daszak, P. & Kilpatrick, A. M. (2010). Ecology of avian influenza viruses in a changing world. Ann N Y Acad Sci, 1195, 113-128. doi:10.1111/j.1749-6632.2010.05451.x

Varga, Z. T., Grant, A., Manicassamy, B. & Palese, P. (2012). Influenza virus protein PB1-F2 inhibits the induction of type I interferon by binding to MAVS and decreasing mitochondrial membrane potential. J Virol, 86(16), 8359-8366. doi:10.1128/JVI.01122-12

Verhagen, J. H., van der Jeugd, H. P., Nolet, B. A., Slaterus, R., Kharitonov, S. P., de Vries, P. P., Vuong, O., Majoor, F., Kuiken, T. & Fouchier, R. A. (2015). Wild bird surveillance around outbreaks of highly pathogenic avian influenza A(H5N8) virus in the Netherlands, 2014, within the context of global flyways. Euro Surveill, 20(12).

Vijayakrishnan, S., Loney, C., Jackson, D., Suphamungmee, W., Rixon, F. J. & Bhella, D. (2013). Cryotomography of budding influenza A virus reveals filaments with diverse morphologies that mostly do not bear a genome at their distal end. PLoS Pathog, 9(6), e1003413. doi:10.1371/journal.ppat.1003413

Wang, Y., Davidson, I., Fouchier, R. & Spackman, E. (2016). Antigenic Cartography of H9 Avian Influenza Virus and Its Application to Vaccine Selection. Avian Diseases, 60(1s), 218-225.

Ward, A. C., Castelli, L. A., Lucantoni, A. C., White, J. F., Azad, A. A. & Macreadie, I. G. (1995). Expression and analysis of the NS2 protein of influenza A virus. Arch Virol, 140(11), 2067-2073.

Watanabe, K., Takizawa, N., Katoh, M., Hoshida, K., Kobayashi, N. & Nagata, K. (2001). Inhibition of nuclear export of ribonucleoprotein complexes of influenza virus by leptomycin B. Virus Res, 77(1), 31-42.

Watanabe, T., Watanabe, S., Noda, T., Fujii, Y. & Kawaoka, Y. (2003). Exploitation of nucleic acid packaging signals to generate a novel influenza virus-based vector stably expressing two foreign genes. J Virol, 77(19), 10575-10583.

Webster, R. G. Bean, W. J., Owen, G. T., Chambers, T. M., & Kawaoka, Y. (1992). Evolution and ecology of influenza A viruses. Microbiological Reviews, 56, 152-179.

Weinheimer, V. K., Becher, A., Tonnies, M., Holland, G., Knepper, J., Bauer, T. T., Schneider, P., Neudecker, J., Rückert, J.C., Szymanski, K., Temmesfeld-Wollbrueck, B., Gruber, A.D., Bannert, N., Suttorp, N., Hippenstiel, S., Wolff, T. & Hocke, A. C. (2012). Influenza A viruses target type II pneumocytes in the human lung. J Infect Dis, 206(11), 1685-1694. doi:10.1093/infdis/jis455

Westwood, J. C. N. (1952). A study of chick embryo lesions produced by influenza viruses. British Journal of Experimental Pathology, 33(6).

WHO. (2006). Annex 8. Viral transport media (VTM).

WHO. (2018a). Fact sheet: Avian Influenza. https://www.who.int/en/news-room/fact-sheets/detail/influenza-(avian-and-other-zoonotic) Acessed on 20/08/2018

WHO. (2018b). Fact Sheet: Influenza (Seasonal). https://www.who.int/news-room/fact-sheets/detail/influenza-(seasonal) Acessed on 20/08/2018

Wise, H. M., Barbezange, C., Jagger, B. W., Dalton, R. M., Gog, J. R., Curran, M. D., Taubenberger, J.K., Anderson, E.C. & Digard, P. (2011). Overlapping signals for translational regulation and packaging of influenza A virus segment 2. Nucleic Acids Res, 39(17), 7775-7790. doi:10.1093/nar/gkr487

Wise, H. M., Foeglein, A., Sun, J., Dalton, R. M., Patel, S., Howard, W., Anderson, E.C., Barclay, W.S. & Digard, P. (2009). A complicated message: Identification of a novel PB1-related protein translated from influenza A virus segment 2 mRNA. J Virol, 83(16), 8021-8031. doi:10.1128/JVI.00826-09

Wise, H. M., Hutchinson, E. C., Jagger, B. W., Stuart, A. D., Kang, Z. H., Robb, N., Schwartzman, L.M., Kash, J.C., Fodor, E., Firth, A.E., Gog, J.R., Taubenberger, J.K. & Digard, P. (2012). Identification of a novel splice variant form of the influenza A virus M2 ion channel with an antigenically distinct ectodomain. PLoS Pathog, 8(11), e1002998. doi:10.1371/journal.ppat.1002998

Worobey, M., Han, G. Z. & Rambaut, A. (2014). A synchronized global sweep of the internal genes of modern avian influenza virus. Nature, 508(7495), 254-257. doi:10.1038/nature13016

Wright, P. F., Neumann, G. & Kawaoka, Y. (2007). Orthomyxoviridae. In W. K. L. W. a. Wilkins (Ed.), Fields Virology. Philadelphia, PA.

Xu, C. & Ng, D. T. (2015). Glycosylation-directed quality control of protein folding. Nat Rev Mol Cell Biol, 16(12), 742-752.

Yamanaka, K., Nagata, K. & Ishihama, A. (1991). Temporal control for translation of influenza virus mRNAs. Arch Virol, 120(1-2), 33-42.
Yamayoshi, S., Watanabe, M., Goto, H. & Kawaoka, Y. (2016). Identification of a Novel Viral Protein Expressed from the PB2 Segment of Influenza A Virus. J Virol, 90(1), 444-456. doi:10.1128/JVI.02175-15
Yang, J., Yan, R., Roy, A., Xu, D., Poisson, J. & Zhang, Y. (2015). The I-TASSER Suite: protein structure and function prediction. Nat Methods, 12(1), 7-8. doi:10.1038/nmeth.3213
Yang, X., Steukers, L., Forier, K., Xiong, R., Braeckmans, K., Van Reeth, K. & Nauwynck, H. (2014). A beneficiary role for neuraminidase in influenza virus penetration through the respiratory mucus. PLoS One, 9(10), e110026. doi:10.1371/journal.pone.0110026
Yasuda, J., Nakada, S., Kato, A., Toyoda, T. & Ishihama, A. (1993). Molecular assembly of influenza virus: association of the NS2 protein with virion matrix. Virology, 196(1), 249-255. doi:10.1006/viro.1993.1473
Ye, Z. P., Baylor, N. W. & Wagner, R. R. (1989). Transcription-inhibition and RNA-binding domains of influenza A virus matrix protein mapped with anti-idiotypic antibodies and synthetic peptides. J Virol, 63(9), 3586-3594.
Ye, Z., Robinson, D. & Wagner, R. R. (1995). Nucleus-targeting domain of the matrix protein (M1) of influenza virus. J Virol, 69(3), 1964-1970.
Yen, H. L. (2016). Current and novel antiviral strategies for influenza infection. Curr Opin Virol, 18, 126-134. doi:10.1016/j.coviro.2016.05.004
Yi, S. M. P., Harson, R. E., Zabner, J. & Welsh, M. J. (2001). Lectin binding and endocytosis at the apical surface of human airway epithelia. Gene Therapy, 8, 1826-1832.
Yoon, S. W., Webby, R. J. & Webster, R. G. (2014). Evolution and ecology of influenza A viruses. Curr Top Microbiol Immunol, 385, 359-375. doi:10.1007/82_2014_396
Zeng, X., Tian, G., Shi, J., Deng, G., Li, C. & Chen, H. (2018). Vaccination of poultry successfully eliminated human infection with H7N9 virus in China. Sci China Life Sci. doi:10.1007/s11427-018-9420-1
Zhang, J., Leser, G. P., Pekosz, A. & Lamb, R. A. (2000). The cytoplasmic tails of the influenza virus spike glycoproteins are required for normal genome packaging. Virology, 269(2), 325-334. doi:10.1006/viro.2000.0228
Zhang, J., Pekosz, A. & Lamb, R. A. (2000). Influenza virus assembly and lipid raft microdomains: a role for the cytoplasmic tails of the spike glycoproteins. J Virol, 74(10), 4634-4644.
Zhang, K., Wang, Z., Fan, G. Z., Wang, J., Gao, S., Li, Y., Sun, L., Yin, C.C. & Liu, W. J. (2015). Two polar residues within C-terminal domain of M1 are critical for the formation of influenza A Virions. Cell Microbiol, 17(11), 1583-1593. doi:10.1111/cmi.12457
Zhang, W., Zheng, W., Toh, Y., Betancourt-Solis, M. A., Tu, J., Fan, Y., Vakharia, V.N., Liu, J., McNew, J.A., Jin, M. & Tao, Y. J. (2017). Crystal structure of an orthomyxovirus matrix protein reveals mechanisms for self-polymerization and membrane association. Proc Natl Acad Sci U S A, 114(32), 8550-8555. doi: 10.1073/pnas.1701747114
Zhang, Y., Guo, X., Qi, J., Liu, L., Wang, J., Xu, S., W, J. & Yin, Y. (2014). Complete Genome Sequence of an H9N2 Influenza Virus Lethal to Chickens. Genome Announc, 2(6). doi: 10.1128/genomeA.00929-14
Zheng, H., Lee, H. A., Palese, P. & Garcia-Sastre, A. (1999). Influenza A virus RNA polymerase has the ability to stutter at the polyadenylation site of a viral RNA template during RNA replication. J Virol, 73(6), 5240-5243.
Zhirnov, O. P., Poyarkov, S. V., Vorob'eva, I. V., Safonova, O. A., Malyshev, N. A. & Klenk, H. D. (2007). Segment NS of influenza a virus contains an additional gene NSP in positive-sense orientation. Doklady Biochemistry and Biophysics, 414(1), 127-133. doi:10.1134/s1607672907030106